General Distribution
OCDE/GD(97)16
GRS - 137

NEA/CSNI/R(96)26

International Standard Problem ISP37

VANAM M3 - A Multi Compartment Aerosol Depletion Test with Hygroscopic Aerosol Material

Comparison Report

M. Firnhaber, T.F. Kanzleiter, S. Schwarz, G. Weber

December 1996

COMMITTEE ON THE SAFETY OF NUCLEAR INSTALLATIONS
OECD NUCLEAR ENERGY AGENCY
Le Seine Saint-Germain – 12, boulevard des Îles
F-92130 Issy-les-Moulineaux (France)
Tel. (33-1) 45 24 82 00 Fax (33-1) 45 24 11 10

Gesellschaft für Anlagen- und Reaktorsicherheit (GRS) mbH

OECD/NEA-CSNI International Standard Problem ISP37

VANAM M3 - A Multi Compartment Aerosol Depletion Test with Hygroscopic Aerosol Material

Manfred Firnhaber [1]
Teja Fritz Kanzleiter [2]
Siegfried Schwarz [1]
Gunter Weber [1]

1) Gesellschaft für Anlagen- und Reaktorsicherheit (GRS) mbH
Köln, Germany

2) Battelle Ingenieurtechnik GmbH
Eschborn, Germany

Dezember 1996

GRS - 137
OCDE/GD (97) 16
ISBN 3-923875-90-8

Descriptors:

Light Water Reactor, International Standard Problem No. ISP37, VANAM, Containment, Multi-compartment Geometry, Severe Accident Analysis, Thermal-hydraulics, Hygroscopic Aerosol Behavior

ORGANISATION FOR ECONOMIC CO-OPERATION AND DEVELOPMENT

Pursuant to Article 1 of the Convention signed in Paris on 14th December 1960, and which came into force on 30th September 1961, the Organisation for Economic Co-operation and Development (OECD) shall promote policies designed:

- to achieve the highest sustainable economic growth and employment and a rising standard of living in Member countries, while maintaining financial stability, and thus to contribute to the development of the world economy;
- to contribute to sound economic expansion in Member as well as non-member countries in the process of economic development; and
- to contribute to the expansion of world trade on a multilateral, non-discriminatory basis in accordance with international obligations.

The original Member countries of the OECD are Austria, Belgium,Canada, Denmark, France, Germany, Greece, Iceland, Ireland, Italy, Luxembourg, the Netherlands, Norway, Portugal, Spain, Sweden, Switzerland, Turkey, the United Kingdom and the United States. The following countries became Members subsequently through accession at the dates indicated hereafter: Japan (28th April 1964), Finland (28th January 1969), Australia (7th June 1971), New Zealand (29th May 1973), Mexico (18th May 1994) and the Czech Republic (21st December 1995). The Commission of the European Communities takes part in the work of the OECD (Article 13 of the OECD Convention).

NUCLEAR ENERGY AGENCY

The OECD Nuclear Energy Agency (NEA) was established on 1st February 1958 under the name of the OEEC European Nuclear Energy Agency. It received its present designation on 20th April 1972, when Japan became its first non-European full Member. NEA membership today consists of all European Member countries of OECD as well as Australia, Canada, Japan, Republic of Korea, Mexico and the United States. The Commission of the European Communities takes part in the work of the Agency.

The primary objective of NEA is to promote co-operation among the governments of its participating countries in furthering the development of nuclear power as a safe, environmentally acceptable and economic energy source.

This is achieved by:

- *encouraging harmonization of national regulatory policies and practices, with particular reference to the safety of nuclear installations, protection of man against ionising radiation and preservation of the environment, radioactive waste management, and nuclear third party liability and insurance;*
- *assessing the contribution of nuclear power to the overall energy supply by keeping under review the technical and economic aspects of nuclear power growth and forecasting demand and supply for the different phases of the nuclear fuel cycle;*
- *developing exchanges of scientific and technical information particularly through participation in common services;*
- *setting up international research and development programmes and joint undertakings.*

In these and related tasks, NEA works in close collaboration with the International Atomic Energy Agency in Vienna, with which it has concluded a Co-operation Agreement, as well as with other international organisations in the nuclear field.

COMMITTEE ON THE SAFETY OF NUCLEAR INSTALLATIONS

The Committee on the Safety of Nuclear Installations (CSNI) of the OECD Nuclear Energy Agency (NEA), is an international committee made up of senior scientists and engineers. It was set up in 1973 to develop and coordinate the activities of the Nuclear Energy Agency concerning the technical aspects of the design, construction and operation of nuclear installations insofar as they affect the safety of such installations. The Committee's purpose is to foster international cooperation in nuclear safety among the OECD Member countries.

The CSNI constitutes a forum for the exchange of technical information and for collaboration between organisations which can contribute, from their respective backgrounds in research, development, engineering or regulation, to these activities and to the definition of its programme of work. It also reviews the state of knowledge on selected topics of nuclear safety technology and safety assessment, including operating experience. It initiates and conducts programmes identified by these reviews and assessments in order to overcome discrepancies, develop improvements and reach international consensus on technical issues of common interest. It promotes the coordination of work in different Member countries including the establishment of cooperative research projects and assists in the feedback of the results to participating organisations. Full use is also made of traditional methods of cooperation, such as information exchanges, establishment of working groups, and organisation of conferences and specialist meetings.

The greater part of the CSNI's current programme of work is concerned with safety technology of water reactors. The principal areas covered are operating experience and the human factor, reactor coolant system behaviour, various aspects of reactor component integrity, the phenomenology of radioactive releases in reactor accidents and their confinement, containment performance, risk assessment, and severe accidents. The Committee also studies the safety of the nuclear fuel cycle, conducts periodic surveys of the reactor safety research programmes and operates an international mechanism for exchanging reports on safety related nuclear power plant accidents.

In implementing its programme, the CSNI establishes cooperative mechanisms with NEA's Committee of Nuclear Regulatory Activities (CNRA), responsible for the activities of the Agency concerning the regulation, licensing and inspection of nuclear installations with regard to safety. It also cooperates with NEA's Committee on Radiation Protection and Public Health and NEA's Radioactive Waste Management Committee on matters of common interest.

* * * * * * * * * * *

Requests for additional copies of this report should be addressed to:

Nuclear Safety Division
OECD Nuclear Energy Agency
12 Boulevard des Iles
92130 Issy les Moulineaux
France

Abstract

International Standard Problems (ISP) organized by the OECD are defined as comparative exercises in which predictions with different computer codes for a given physical problem are compared with each other and with a carefully controlled experimental study. The main goal of ISPs is to increase confidence in the validity and accuracy of analytical tools used in assessing the safety of nuclear installations. In addition, it enables the code user to gain experience and to improve his competence.

This paper presents the results and assessment of the "open" International Standard Problem No. 37 (ISP37), which deals with the containment thermal-hydraulics and aerosol behavior during an unmitigated severe LWR accident with core melt-down and steam and aerosol release into the containment. The ISP attracted wide support, representatives of 22 organizations participated using the codes CONTAIN, FIPLOC, MELCOR, RALOC, FUMO, MACRES, REMOVAL etc. Some participants performed several calculations with different codes. The containment and aerosol behavior experiment VANAM M3 was selected as experimental comparison basis. The main phenomena investigated are the thermal behavior of a multicompartment containment, e.g. pressure, temperature and the distribution and depletion of a soluble aerosol.

The ISP37 has demonstrated that the codes used could calculate the thermal-hydraulic containment behavior in general with sufficient accuracy. But with respect to the needs of aerosol behavior analysis the accuracies, both analytical and experimental as well, for specific thermal-hydraulic variables should be improved.

Although large progress has been made in the simulation of aerosol behavior in multicompartment geometries the calculated local aerosol concentrations scatter widely. However, the aerosol source term to the environment is overestimated in general. The largest uncertainty concerning the aerosol results is caused by a limited number of thermal hydraulic variables like relative humidity, volume condensation rate and atmospheric flow rate. In some codes also a solubility model is missing.

Studies such as ISP37 serve to illuminate code modeling assumptions or simplifications, such as when solubility effects are not treated, and give rise to code improvements, as reported for MACRES and MELCOR after the evaluation of ISP37. In MELCOR for instance improved models like aerosol growth due to condensation on the particles, enhanced the results of the aerosol behavior, especially the aerosol depletion in the "dry" phase of the test, as could be seen in post ISP37 calculation done by the code developer.

Contents

1 Introduction

A standard problem is defined as a comparison between experimental and analytical results, in this case out of the field of reactor safety research. The detailed comparison of the data permits conclusions for the reliability and precision of computer simulations of postulated accidents and contributes to the development and improvement of reactor safety computer codes [1].

Following a suggestion of the Federal Republic of Germany, the OECD-CSNI[1] agreed to offer the experiment VANAM M3 at the Battelle Model Containment (BMC) [2], an experiment on thermohydraulic and aerosol behavior in a containment, as International Standard Problem No. 37 (ISP37) to its member countries[2]. The experiment VANAM M3 has already been performed by Battelle Eschborn. The experiment and the execution of the ISP are sponsored by the German Ministry for Education, Science, Research and Technology. The ISP has been conducted as an open standard problem, i.e. besides initial and boundary conditions, all experimental results are delivered to the participants in the ISP prior to performing the calculation.

After the preparatory meeting [3], held at Battelle Eschborn on May 30-31, 1995, 22 organizations from 12 countries including 2 non OECD countries, submitted their results for comparison and evaluation.

ISP37 follows a series of former ISP in this area. The most related ones are ISP29 [4] (Thermal-Hydraulics and Hydrogen Distribution in the HDR Facility) and CEC benchmark problems (Benchmark on FIPLOC Verification Experiment F2: Thermal-Hydraulics in the Battelle Model Containment BMC [5] and Benchmark on DEMONA B3 Experiment: Thermal-Hydraulics and Aerosol in the BMC [6]).

Compared to previous ISPs, the main difference is the use of a multi compartment geometry and of a soluble aerosol.

---

[1] Organization for Economic Cooperation and Development - Committee on the Safety of Nuclear Installations

[2] As in previous ISPs some non-OECD countries were also invited.

2 Objectives of the Standard Problem

During an unmitigated severe LWR accident with core melt-down radioactive fission and activation products are being released into the containment as gas, vapor or, to a great extent, adsorbed on aerosols, while the containment building serves as a final barrier to the environment. Since the containment pressure and temperature, time dependence and distribution of fission products and aerosols are very important with respect to mitigate the accident, e.g. by venting, a detailed knowledge of thermal-hydraulics, of fission products and aerosol behavior and an appropriate analytical prediction capability are of great importance. Experimental results and code predictions can be used to quantify the safety margins presently existing in the safety systems of operating reactors, and to explore possibilities of mitigating the severe accident consequences. In order to demonstrate the capability of current computer codes to model and to calculate the thermal-hydraulics and the aerosol distribution and settlement in a containment with sufficient accuracy, the OECD-CSNI decided to propose a containment thermal-hydraulic and aerosol behavior standard problem.

The general objectives of the International Standard Problem No. 37 (ISP37) are to analyze the thermal-hydraulics of a containment atmosphere and the distribution and settlement of aerosols after a severe accident with pressurizer relief valve discharge. (low pressure path LP* according to the German Risk Study Phase B [7])

In more detail the objectives of ISP37 are the comparison and investigation of the following physical variables and phenomena:

- State-of-the-art status review on computer codes for containment analysis, i.e. thermal-hydraulic and aerosol behavior
- Phenomena to be investigated
  - multi compartment geometry
  - stratified atmosphere
  - atmosphere mixing by natural convection loops
  - thermal energy balance
  - structural heat transfer

- wall condensation
- volume condensation
- aerosol distribution and settling
- hygroscopic aerosol component
- steam condensation on aerosols
- identification of experimental accuracy and problems etc.

3 Description and Results of Experiment VANAM M3

A detailed description of the VANAM test facility and the results of test M3 are given in [2]. This chapter concentrates on the main characteristics of the test facility and the main features of the results for the convenience of the reader.

3.1 VANAM Test Facility

3.1.1 Model Containment, Fluid and Aerosol Injection

The VANAM tests are performed in the Battelle model containment (Fig. 3.1 to 3.3). Its free volume of 626 m^3 is subdivided into several compartments which are interconnected by vent openings, thus forming a geometry similar to that of a PWR containment. Outer and inner walls of the model containment are built of reinforced concrete, some smaller parts are made of steel.

The following locations are provided for fluid and aerosol release:

- in outer compartment R5 at an elevated position for steam and aerosol injection,
- in inner compartment R3 for steam and air injection,
- at bottom of the annulus R9.4 for air removal and re-injection during the heat-up phase

Steam is injected to preheat the containment structures and to provide a defined steam concentration in the atmosphere for the aerosol depletion test period. Most of the steam condenses at the structures and the condensate is collected in the individual compartment sumps. In the beginning of the heat-up period a part of the initial air mass is drained (from the bottom of R9) to enhance structure heat-up by steam condensation. Later on a similar mass of air is re-injected into R3 and R9.

NaOH aerosol is produced by evaporating an aqueous high-concentration NaOH solution in a plasma torch and by subsequent rapid vapor condensation. The generated NaOH aerosol, suspended in steam and air, is transported from the aerosol generator via a approximately 4 m long channel to the release site in compartment R5.

3.1.2 Thermal-Hydraulic Instrumentation and Measurement Error

Containment pressure is almost uniform within the model containment volume. It is measured by two (redundant) strain-gauge-type pressure transducers with an accuracy of ± 0.02 bar.

Temperatures of containment atmosphere, concrete structures, and compartment sumps are measured by thermocouples with an accuracy of ± 1.4 K, the major part of this value being attributed to systematic errors.

The structural temperature gauges, in general, are located ca. 1 cm below the concrete surface.

Atmospheric flow velocities within the vent openings are rated by bi-directional turbine flow meters. The minimum measurable value (threshold) amounts to 0.2 m/s, the accuracy is ± 0.15 m/s.

Relative atmospheric humidity (RH): Over long periods of the experiment the containment atmosphere is saturated (100 % RH) or even supersaturated. For some test periods, however, containment atmosphere can be locally superheated (RH <100 %) and RH data are needed to calculate the partial steam pressures. For this purpose some capacitive humidity sensors are installed to measure the local relative humidity with an accuracy of ± 10 % RH. Unfortunately, those sensors are not very reliable, in some cases the error band may be larger. If an humidity sensor becomes wet by

condensate for a certain period of time its signal surpasses the 100 % limit up to the value of its upper electric threshold (115 - 120 % RH).

Compartment sump water levels are measured by capacitive level meters installed outside of the containment and connected to the drain lines of the individual compartment sumps and to the containment dome. Since water and air is drained or reinjected through this line, the measurements are erroneous during these periods, e.g. between 14.37 h and 16.61 h. For regular periods the measuring accuracy is estimated to be ± 0.01 m.

Steam injection: Steam mass flow is determined by orifice obstruction meters. Typical accuracies are ± 0.01 kg/s for steam flow to R5, and ± 0.006 kg/s for steam flow to R3. No redundant measuring system is available to verify the steam flow data obtained.

Air removal and re-injection: Air mass flow is evaluated from swing whirl measurements with typical inaccuracies of ± 0.6 l/s (for air removal) or ± 0.3 g/s (for air reinjection), respectively. The measured air flow data can be verified by balancing the air masses in the containment (obtained from pressure, local temperature and humidity data) before and after the air removal or injection periods.

Condensation rate: At the inner surface of the concrete shell of the model containment three areas of 1 m^2 each are defined for continuous condensate collecting. The condensate level rise in small collecting cylinders is continuously measured and evaluated to obtain the condensation rates at the respective sites.

3.1.3 Aerosol Instrumentation and Measurement Error

Aerosol concentration and particle size distribution are determined by remote-controlled filter stations installed at seven locations in the model containment. Each filter station can be successively charged with twelve filter samples for later laboratory evaluation, eight filters being used to determine aerosol concentration over time, four more filters to evaluate particle size distributions.

Aerosol concentration is determined by weighing the filter deposits and measuring the fluid volumes sucked through the filters. Typical measuring errors range between 12 and 30 % of the measured concentration values.

To obtain particle size distributions the respective four filters have to be charged with only a small amount of aerosol material (deposits of less than one monolayer of particles). Scanning electron microscope pictures are taken of the filter samples and evaluated by a semi-automatic optical method assuming spherical particle shapes to compute particle size number distributions and particle size mass distributions.

The aerosol material on the filters has been dried prior to evaluation. Therefore the measured aerosol concentration and particle size distribution data refer to solid NaOH material, while in the containment atmosphere NaOH was dissolved in larger water droplets.

Airborne water concentration: Extinction photometers are installed at eight locations within the model containment to rate local fog droplet (and aerosol) concentrations in the containment atmosphere. The photometers assess light extinction which is a function of (1) concentration and (2) size distribution of the airborne droplets (or dry particles, respectively), and (3) their optical properties as well. As (2) and (3) are not exactly known the photometers can yield only qualitative or semi-quantitative results for the time-dependent airborne water concentration.

3.2 Test Performance and Initial Boundary Conditions

The VANAM experimental procedure is oriented to the PWR core melt scenario with pressure relief of the German Risk Study Phase B [7]. The tests results serve for investigation of the phenomena involved and code verification.

During the first test periods steam is released at an elevated position in R5, representing the blowdown of the primary circuit over the pressurizer quench tank. After a phase without release, steam is released into the lower central compartment R3, corresponding to a contact of core melt with sump water.

The steam injection rate and the air leak rate are shown in the Fig. 3.4 to 3.5.

3.2.1 Test Phase I: Facility Heat-up, t = 1.13 to 17.2 h

Starting at 25 °C initial temperature of the test facility, steam is released into R5 to heat up the facility, the steam release rate being controlled to get a constant containment pressure of 1.25 bar.

In the beginning of phase I 225 kg air are drained out of R9.4. As a result steam can enter also the lower regions of the model containment and heat up the structures there. To the end of phase I air is re-injected into R9.4 (221 kg) and R3 (97 kg) to adjust the desired air content.

3.2.2 Test Phase II: First Aerosol Release, t = 17.2 to 18.23 h

2.21 kg NaOH aerosol, suspended in a hot steam-air mixture, is released into R5. The containment pressure is no longer controlled and rises from 1.25 to 2.05 bar.

3.2.3 Test Phase III: "Dry" Aerosol Depletion, t = 18.23 to 22.7 h

No fluid is released into the containment. Since steam condensation at the containment structures is no longer compensated by steam injection the containment pressure decreases to 1.25 bar. Due to the heat flowing back from the inner structures to the atmosphere, aerosol depletes under slightly superheated "dry" atmosphere conditions.

3.2.4 Test Phase IV: Second Aerosol Release, t = 22.7 to 23.14 h

0.719 kg NaOH aerosol, suspended in a hot steam-air mixture, is released into R5. The containment pressure increases to 1.7 bar.

3.2.5 Test Phase V: "Wet" Aerosol Depletion, t = 23.14 to 25.26 h

During the first 10 min of phase V no fluid is released into the containment and the pressure drops to 1.6 bar. Then steam is released into the lower central compartment R3. An overall loop convection develops and homogenizes the containment

atmosphere (except the dead-end area in the R9 annulus). Aerosol depletes under (super-) saturated "wet" conditions. The containment pressure re-increases to 1.7 bar.

3.2.6 Test Phase VI: Further "Wet" Aerosol Depletion, t = 25.26 to 30 h

Again, steam is released into R5. Aerosol depletion continues. The containment pressure stabilizes around 1.7 bar.

3.3 Experimental Thermal-Hydraulic Results

3.3.1 Containment Pressure

The total pressure of the containment atmosphere is directly measured. It is the sum of the partial pressures of steam and air which can be determined from temperature, humidity and total pressure data. Due to inhomogeneous atmosphere distribution the partial pressures of steam and air may locally differ, the total pressure, however, is almost uniform over the entire containment volume (local differences between the individual compartments due to hydrostatics or flow phenomena are in the order of a mbar).

Fig. 3.7a depicts the time history of the total pressure measured in test M3 and the averaged partial air pressure as given by a FIPLOC calculation simulating the containment by a single node and using otherwise proposed input data. As a sample, Fig. 3.7b shows the measured total pressure and some local air pressures derived from locally measured data to demonstrate the actual inhomogeneity of the steam-air containment atmosphere in VANAM test M3.

The averaged partial air pressure depends on the mass of air enclosed in the containment and its temperature. Over the test periods the initial air mass within the containment was reduced by

- air removal during test phase I (t = 1.75 - 4.05 h)
- containment leakage over all test phases

and increased by

- air re-injection at the end of test phase I (t= 14.37 - 15.45 h)
- air portion of the aerosol carrier gas in test phases II (t = 17.2 - 18.23 h) and IV (t = 22.72 - 23.14 h).

The averaged partial air pressure follows this time history.

The partial steam pressure, which is the difference of the total and the partial air pressure, is a result of the steam injection rate and steam condensation at structures.

In test phase I steam injection rate is controlled to keep the total pressure constant at 1.25 bar. Almost all of the injected steam condenses on the structures to heat them up by its condensation heat. Only a few percent of the injected steam remains in the atmosphere. It increases the containment pressure and replaces the leaked and removed air.

Starting at phase II, the total pressure depends on the steam and air injections:

- During phase II the pressure rises due to aerosol injection (with a steam-air carrier gas).
- During phase III (no injection, proceeding condensation) the partial steam pressure reaches its minimum of 0.45 bar and the total pressure drops to 1.25 bar.
- In Phase IV (second aerosol injection) the total pressure increases again, becomes stabilized in Phases V and VI (steam injection) and reaches its final value of 1.67 bar.

3.3.2 Atmosphere Temperature Distribution, Internal Flow Phenomena

As stated in the previous chapter, atmosphere temperature distribution within the containment is governed by the steam distribution which results from steam injection, condensation, and internal flow phenomena. For that reason, atmosphere exchange effects (with the tendency to mixing) or stagnation (stable stratification) can be detected also by monitoring the development of the atmospheric temperatures.

Temperatures of dome and annulus of compartment R9:

The development of the atmospheric temperatures in the dome and the annulus (R9) at different elevations are shown in Fig. 3.8a The successive temperature rises in the first hours of test phase I indicate a downward steam front progression in the annulus, mainly due to the air drain from the bottom of the annulus. At t = 7.5 h, for example, the steam front has reached the 1.6 m level and at the end of test phase I re-injection of air leads to a temperature drop in the lower annulus region due to steam replaced by air and ongoing heat absorption by structures. In the further course of the experiment, a stable annulus atmosphere stratification develops.

From 5 to 15 h during phase I the dome atmosphere consists of almost pure steam, because the dome temperature (TATMR9D) corresponds to the containment pressure.

Temperatures of the inner (R3) and outer compartments (R5, R6):

Fig. 3.8b shows a selection of atmospheric temperatures in the inner and outer compartments in comparison to the dome temperature. In general, the injection compartment R5 and the dome R9 have almost the same temperatures. This suggests an intense atmosphere mixing in the two compartments. In some periods the temperature is in R5 somewhat higher than in the R9 dome, due to local superheating.

Within the lower compartment R6 and R3 a strong stratification develops (TATMR628 > TATMR6 > TATMR605). During test phases I to IV the temperature TATMR3 in R3 is as low as the lower temperature in R6.

In test phase V steam is injected into the lower compartment R3. This leads to a rapid temperature rise in the lower compartments R3 and R6 to the temperature level of R5 and R9 dome, which suggests an overall convection involving the inner and outer compartments and the dome. Only the temperature TATMR605, which is located below the vent flow between R6 and R3 stays behind this general trend.

In test phase VI again, steam is injected into the upper outer compartment R5 and the lower compartments are not longer involved in the convection. Their temperatures decrease due to steam condensation at structures and subsequent air accumulation.

Temperatures in the Centers of the Calculation Nodes:

Fig. 3.9a and 3.9b show a selection of measured temperatures to which the calculated temperatures are to be compared. They correspond to the centers of the proposed calculation nodes.

An interesting behavior is to be seen for R1: As soon as the steam front has entered the upper regions of R8 and R6 (t =4.5 h) the temperature in R1 starts to rise, indicating that steam enters R1 and replaces the air present.

3.3.3 Condensation Rate

Maximum condensation occurs in the beginning of the heat-up phase. At the end of test phase I, at about t = 15 h, in the periods of air re-injection and almost no steam injection, the condensation rates drop to zero. During the first aerosol release phase (t = 17.5 h) condensation reincreases, and decreases again during the subsequent test phase III with no steam injection. Again, a minor condensation rate maximum is detected during the second aerosol release (t = 23 h), and a substantial increase occurs in the final test phase VI with steam injection into R5.

3.3.4 Air Mass in the Containment, Leak Rate

Fig. 3.10 shows the air mass inventory in the model containment during the course of the experiment, as determined from measured pressure, local temperature and humidity data. An independent evaluation of the air mass by GRS [8] deviates only by 30 to 45 kg. This corresponds to a partial air pressure of 0.05 to 0.075 bar. From the time dependent air mass, the air injection and and removal rate the air leak rate was estimated.

3.3.5 Humidity

Experimental humidities are given in Fig. 3.11.

The dome atmosphere has a humidity of or close to 100% except for phase III from 20 to 23 h when no steam is injected into the containment.

Although the containment atmosphere cannot exceed 100% humdity the signal in R9.3 is for longer time periods above this value due to measurement errors. Taking this into account the humidity in R9.3 is 100% in phase I up to 15 h. The low humidity measured between 12 and 14 h is not explainable. Arround 15 h when air was reinjected into the annulus the humidity falls below 100%. It is generally less than 100% from phase III up to 23 h in phase VI.

3.4 Experimental Aerosol Results

3.4.1 Mass and Particle Size Distribution of the Released NaOH Aerosol

The NaOH masses generated and released can be determined from the NaOH consumptions of the aerosol generator:

- Test phase II (1st aerosol release): 2.21 kg NaOH
- Test phase IV (2nd aerosol release): 0.719 kg NaOH

Only minor NaOH deposits within the aerosol generator had been observed after completion of the test.

Measurements of aerosol size distribution at the aerosol generator exit or in the aerosol release channel could not be obtained. As a replacement the particle size distributions measured in the release compartment R5 a few minutes prior to completion of the first aerosol release phase, is proposed. Approximated by a log-normal distribution the following parameters have been obtained:

- Test phase II (1st aerosol release; t = 18.14 h):
  Mass median diameter of dried NaOH aerosol MMDTR5 = 0.86 µm
  Geometric standard deviation GSDTR3 = 1.8

3.4.2 Fog Formation and Airborne Water Concentration

Volume condensation in the steam-air containment atmosphere generates fine airborne water droplets which are expected to dissolve the NaOH aerosol particles and, due to their larger diameters, enhance aerosol depletion by gravitational settling.

The existing inhomogeneities of steam-air and temperature distribution in the containment lead to locally different volume condensation effects. Semi-quantitative information on local volume condensation (fog formation) can be obtained from the extinction photometer and humidity measurements, and, to a smaller extent, from calorimeter and spectral photometer measurements.

The respective data measured are compiled in Fig. 3.11. The main periods of fog droplet formation are:

- In test phase I (facility heat-up; irrelevant for aerosol behavior),
- during and after the two aerosol release periods,
- during test period V (steam injection into the cold compartment R3),
- in the final phase of test period VI (in the annulus of R9 only, due the specific local conditions)

3.4.3 Aerosol Concentration

Filter stations are used to measure dry NaOH aerosol mass concentration at seven locations for eight different time intervals by filter sampling. An interpretation of the data points obtained leads to the aerosol concentration curves depicted in Fig. 3.12, e. g.

- for the dome of R9 and the aerosol release compartment R5 (3 filter stations),
- for the annulus of R9 (2 filter stations),
- for the inner compartments R3 and R8 (each with 1 filter station).

During test phases V and VI the aerosol concentration differences between dome and inner compartments disappear. This is attributed to the intense mixing, connected with strong fog formation, during test phase V (steam injection into lower, cold compartment R3). Only the dead-end annulus compartment shows an independent local aerosol depletion history in this period. Remarkably large aerosol concentration differences (almost up to 2 orders of magnitude) develop between the annulus and the other compartments.

As a sample, Fig. 3.12 displays also the error band of the concentration data points measured in the dome compartment of R9.

3.4.4 Aerosol Particle Size Distribution

Another four filter samples of each filter station are used for evaluation of dry NaOH particle size distributions for different time intervals at different locations. All samples consist of compact, almost spherical particles. Some of the results obtained agree well with the expected log-normal size distribution, others do not. The mass median diameters vary between 0.35 and 2.5 μm, the geometric standard deviations between 1.38 and 2.12. During aerosol depletion the particle size median values decrease, as expected, at almost all locations.

4 Calculations by the Participants

4.1 Participants and Codes

Representatives of 22 organizations from 12 countries, including 2 non OECD countries, participated in the International Standard Problem No. 37 (ISP37) based on the VANAM M3 experiment on thermal-hydraulics and aerosol behavior in a containment [9-33]. They submitted a total of 27 contributions, most of them both for the thermal-hydraulic and aerosol part as well, using the codes CONTAIN, MELCOR, FIPLOC, RALOC, GOTHIC, FUMO, ECART, MACRES, MOSAIC and REMOVAL [34-43]. Tab. 4.1 summarizes the participating organizations and the codes used. All codes uses lumped parameter assumptions.

4.2 Selection of Variables to be Calculated

The selection of variables to be calculated by the participants was done in order to meet the objectives of the ISP [8]. Special attention was given to the correct representation of the overall thermal-hydraulic and aerosol behavior of the containment, to suitable location of a measurement device and to an acceptable measurement error. Only those variables which meet these criteria have been chosen for comparison.

The main thermal-hydraulic variables are pressure and temperature. From the temperature distribution a picture of atmospheric stratification in each compartment can be obtained. Due to relatively large measurement errors for the humidity and heat transfer to the structures only general results are given.

The selected aerosol variables are aerosol and airborne water concentration, geometric standard deviation and particle size distribution.

For representing the spatial distribution in the containment the variables for temperature and aerosol concentration are selected for different compartments.

A detailed lists of all variables are given in [8].

4.3 Codes and Computational Models Used for ISP37 Calculations

4.3.1 General Code Descriptions

The following part contains short general code descriptions as far as available from the participants. The relevant thermal hydraulic and aerosol features used in ISP37 are described in 4.3.2 and 4.3.3.

CONTAIN

CONTAIN has been developed by the Sandia National Laboratories and is the US Nuclear Regulatory Commission's principal best-estimate, mechanistic containment analysis tool for severe accidents [34]. CONTAIN is an integrated analysis tool used for predicting the physical, chemical, and radiological conditions inside a containment building following the release of radioactive material from the primary system. The interactions among thermal-hydraulic phenomena, aerosol behavior and fission product behavior are taken into account. The code includes atmospheric models for steam/air thermal-hydraulics, intercell flows, condensation/evaporation on structures and aerosols, aerosol behavior, fission product transport, effect of fission product decay, and gas combustion. It also includes models for reactor cavity phenomena such as core-concrete interactions and coolant pool scrubbing.

MELCOR

The code MELCOR is being developed by the Sandia National Laboratories for the US Nuclear Regulatory Commission [35]. It is a fully integrated, engineering-level computer code that models the progression of severe accidents in LWR nuclear power plants. A spectrum of severe accident phenomena, including reactor coolant system and containment thermal hydraulic response, core heat up, degradation and relocation, and fission product release and transport, is treated in MELCOR in a unified framework for both boiling water reactors and pressurized water reactors.

FIPLOC

The code FIPLOC (Fission Product Localization) has been developed by the Gesellschaft für Anlagen- und Reaktorsicherheit (GRS) mbH, Germany, with the support

of the Ministry for Education, Science, Research and Technology [36]. FIPLOC is a computer code for the integrated analysis of thermal hydraulics, aerosol behavior including pool scrubbing, and iodine behavior in a multi-compartment containment geometry. The main purpose of FIPLOC is to calculate the distribution and retention of airborne fission products in a LWR containment and to predict the radioactive source term to the environment. FIPLOC makes use of the lumped parameter technique. Tight couplings are accomplished between the thermal hydraulic model (extended RALOC Mod 2.1 code), the aerosol models (MAEROS, MGA, MONAM, and SPARC), and the iodine model (IMPAIR) in order to simulate the interaction processes. Effects of fission product decay heat on thermal-hydraulics are comprehended.

RALOC

The code RALOC is used to calculate the thermal-hydraulic behavior and combustion phenomena in a multi compartment containment [37].

Calculations can be performed for single and multi-compartment containments and closed buildings of nuclear power plants, as well as for compartmentalized systems with more or less large openings to the environment. For the description of the physical processes during an accident propagation arbitrary compartment systems and -geometries can be simulated by specified volumes. The conditional changes related to location and time are reduced to a purely time dependent behavior within the control volumes. These volumes are connected by junctions. For the simulation of heat transfer and heat conduction via walls and internal components specified structures can be coupled to the volumes. The heat conduction is described in one dimension, for the simulation of heat transfer processes (heat- and mass transfer) different models and correlations are available.

RALOC does not calculate aerosol phenomena.

MACRES

The stand alone aerosol code MACRES developed by NUPEC is a mechanistic computer code of aerosol and gaseous radioactive material behavior in LWR systems for realistic estimation of the source term [38]. It models the phenomena in the gaseous phase and interactions among vapors, particles and structural surfaces.

The initial and boundary thermal hydraulic conditions have to be provided such as: wall and gas temperatures or inter-cell flow rates.

MOSAIC

The aerosol code MOSAIC (Monte Carlo Simulation of the Aerosol Dynamic) has been developed by the Institute for Nuclear Technology and Energy Systems (IKE) at the University of Stuttgart [39]. It uses the Monte Carlo method to solve the general dynamic equations of a multi-component aerosol. Arbitrary size distributions of aerosols can be calculated. Numerical problems like numerical diffusion are avoided. All mechanisms are treated interactively.

REMOVAL

The aerosol code REMOVAL has been developed by the Japan Atomic Research Institute (JAERI) [40] . It analyzes the fission product behavior in an LWR containment during a severe accident. REMOVAL can analyze the behavior of multi-component aerosols, inorganic iodine, organic iodide and other gaseous fission products in multi-compartment geometries.

ECART

ECART (ENEL Code for Analysis of Radionuclide Transport) has been developed with the support of Synthesis, Themas, University of Pisa and Politecnico of Milano [41].

ECART contains three modules witch are linked together. The thermal hydraulic module basing on FUMO [42] provides boundary conditions to the other two modules throughout the pathway of the fission product. The vapor and aerosol transport module bases on TRAP-MELT [46], NAUA [47] and SPARC [48] calculates the amount of fission products in each compartment that are retained or released. The chemical equilibrium model evaluates the chemical reactions occurring between the components in the system.

Tab. 4.1: Participants and Codes

Code	Participating Institution	ISP 37 Abbreviation		Thermal Hydraulic Results	Aerosol Results
CONTAIN	CIEMAT	CIEMAT	Spain	x	x
	ECN	ECN	Netherlands	x	x
	Kurchatov Inst.	KI-CON	Russia	x	x
	VUJE	VUJE-CON	Slovakia	x	x
	FZK	FZK	Germany	x	x
MELCOR	CTN-UPM	CTN	Spain	x	x
	ENEA	ENEA	Italy	x	x
	KAERI	KAER	Korea	x	x
	Kurchatov Inst.	KI-MEL	Russia	x	x
	NUPEC	NUP-MEL	Japan	x	x
	Russ. Acad. of Sci.	RAS	Russia	x	x
	Sandia Nat. Lab.	SNL	USA	x	x
	Studsvik Eco Safe	STU	Sweden	x	x
	VUJE	VUJE-MEL	Slovakia	x	x
	Russian Institute of Atomic Reactor	RIAR	Russia	x	
FIPLOC	IPSN/GRS	IPSN/GRS-Fs	France/ Germany	x	x
	GRS/IPSN	GRS/IPSN-Fe	Germany/ France	x	x
	IFE	IFE-1	Germany	x	x
	IFE	IFE-2	Germany		
	JRC	JRC	European Community	x	x
RALOC	GRS/IPSN	GRS/IPSN-Re	Germany/ France	x	
GOTHIC	Battelle	Battelle	Germany	x	
FUMO	Uni Pisa	UPIS	Italy	x	
ECART	Uni Pisa/ENEL	ENEL	Italy	x	x
MACRES	NUPEC	NUP-Ma	Japan		x
MOSAIC	IKE	IKE	Germany		x
REMOVAL	JAERI	JAERI	Japan		x

4.3.2 Computational Models Used for the TH-Calculations

The following code options and modelling features as far as they are delivered by the participants are discussed here:

- coupling between atmosphere and water,
- flow equation,
- maximum water content in a node and drainage,
- sump simulation,
- heat transfer

CONTAIN

An atmospheric node can contain water as airborne droplets and condensate film on the wall. When the film thickness exceeds a limiting value, water is drained into a specified sump. Optionally a film tracking model can be used.

The atmosphere is in thermal equilibrium with the airborne water, but the water film can have a lower temperature (nonequilibrium).

Pool or sumps can be modelled by a specific option, which simulates the pool with an atmospheric layer above and a structure with a fixed temperature boundary at the bottom. Heat and mass exchange (condensation and evaporation) is calculated between the pool and the atmosphere.

The CONTAIN flow equation is similar to the one used in FIPLOC.

FIPLOC

- Under saturated conditions the steam and the water in a node are in thermal equilibrium. They have the saturation temperature. If the temperature changes either water evaporates or steam condenses in order to conserve the thermal equilibrium. When in a node all water is evaporated or drained out, the atmosphere can become superheated.

- The maximum water content in the individual nodes is an input value. For the atmosphere nodes the recommended value of 0.1 kg per m^3 node volume was used by all participants. This is an estimated value representing a water film on the walls and the floor. When the water mass in a node exceeds the input maximum value, it is drained into a specified node below (no flow equation). The drainage can be distributed to several nodes.
- The thermal non-equilibrium between the atmosphere and larger amounts of water is modelled by defining separate sump nodes. Water can drain from the atmosphere node to a sump node, but atmospheric flow is not allowed. The heat exchange between the sump and the atmosphere node is modelled by a heat conductor. The recommanded simulation of the heat conductor, which represents a 10 cm water layer on the top of the sump node, was used by all participants.

In the atmospheric flow equation the derivative of mass flow rate with respect to time is calculated using the boundary term, the pressure balancing term, and the unrecoverable pressure loss.

FUMO

Atmospheric nodes contain air and water droplets, which are in thermal equilibrium. Condensate is immediately drained to a specified pool. It can be distributed to several pools.

If a pool is specified in a node thermal non-equilibrium is simulated. The energy and mass transfer between the atmosphere and the pool is calculated.

In contrast to all other codes FUMO does not calculate the derivatives in respect to time of the thermal hydraulic variables. It uses a quasi steady approach.

In the FUMO calculation submitted to the ISP37 the mass flow rate between the nodes is calculated by an orifice equation. In case convection loops are possible they have to be defined by the user. Than the convection loops are simulated using an electrical analogy of capacity-resistance networks. The natural circulation flow is obtained by solving a set of linear algebraic equations along the branches of the loops, the pressure balancing term of the orifice equation is superimposed.

GOTHIC

GOTHIC has in the addressed features similar models as MELCOR:

Each node can contain airborne water and a pool. (A water film as in MELCOR is not simulated.) Thermal nonequilibrium is modelled between the pool and the atmosphere.

The flow equation simulates two phase flow (atmosphere and water) similar to MELCOR. Therefore the pool formation and drainage is handled in a similar way.

In the GOTHIC lumped parameter nodes, water is simulated as a pool and a dispersed droplet field. Thermal nonequilibrium with heat and mass exchanges between atmosphere, droplets and water pool is modelled, resulting in three temperatures per node.

Non-stationary equations of motion are solved for each junction, resulting in three flow velocities for atmosphere, droplets and pool water; momentum exchange between the three fields is taken into account. Drainage is influenced by the elevations of node bottoms and connected junctions, similar to the MELCOR treatment.

Heat conductors can exchange heat with the atmosphere or the pool water, depending on the height of the water level; also, heat and mass exchange between atmosphere and the pool surface is calculated.

Droplet generation in the atmosphere under superheated conditions is modelled either by a homogeneous or a heterogeneous nucleation model.

In addition to the lumped-parameter approach, GOTHIC can simulate multidimensional flow distributions. This option was not used in the present ISP37 model, however.

MELCOR

Each node can contain airborne water, a water film on the wall and a pool.

When equilibrium thermodynamics is used in a control volume, mass and energy transfer between the pool and the atmosphere is implicitly determined by the assumption that the pool and the atmosphere are in thermal and evaporative equilibrium.

If a volume, in which non-equilibrium thermodynamics is specified, contains both a pool and an atmosphere, the mass and energy transfer between both is calculated by condensation, convection and evaporation.

The flow equation simulates two phase flow (atmosphere and water), e. g. atmospheric flow and drainage are simulated with the same equation in the same flow path. Similar to the codes above the derivative of the velocities in respect to time is calculated using the buoyancy term, the pressure balancing term and the unrecoverable pressure loss. But in addition the following terms are simulated:

- momentum through the flow path by area changes
- interface force between atmosphere and water

The following flow regimes are possible:

- pure atmospheric flow
- two phase flow, same direction or counter current
- pure liquid flow

Water content and drainage:

Under the slow transient conditions of VANAM M3 a remarkable pool can be formed only if the junction elevation is higher than the bottom elevation of the node. No pool can form if these elevations are equal.

If the film thickness exceeds a maximum value (default 0.5 mm) the excess water is transferred into the pool. By activating an optional film tracking model, networks of

connected structures can be defined and film drainage from higher to lower structures are simulated.

RALOC

In the RALOC calculations the thermal equilibrium option was used. The above addressed simulations are the same as in FIPLOC. An exception is the drainage which is simulated by the weir equation and a pipe flow equation.

4.3.3 Computational Methods Used for Aerosol Caculations

The main features of the aerosol models used are summarized in Tab. 4.2

Tab. 4.2: Code Features used in Aerosol Calculations

Code	Version	Coupling with thermal hydraulics	Geometry	Aerosol model based on	Condensation model	Solubility effect
CONTAIN	1.12 1.11 (only KI)	integrated	multi-compartment	MAEROS	fixed and moving grid	yes
MELCOR	1.8.3	integrated	multi-compartment	MAEROS	fixed grid	no (standard version)
FIPLOC	2.O	integrated	multi-compartment	MAEROS	moving grid	yes
ECART	95,3	integrated	multi-compartment	TRAP/MELT2	fixed grid	no
MACRES	-	stand alone	multi-compartment	-	fixed grid	yes
MOSAIC	-	stand alone	single volume	-	-	no
REMOVAL	mod2.H	stand alone	multi-compartment	-	fixed grid	yes

CONTAIN

Within the CONTAIN code the aerosol behavior is simulated by the aerosol model MAEROS. Several enhancements to the original MAEROS [44] have been added applying aerosol processes in a LWR-containment.

MAEROS is am multicomponent aerosol code which evaluates the dynamic particle size distribution of each component in a control volume. The distribution is discretised in a number of particle size classes (sections). All particles within a section have the same composition including the water condensed on the particles. The most important constraint is that the material density is assumed to be the same for all components including the airborne water.

In MAEROS four agglomeration processes are treated: Brownian diffusion, differential gravitational settling, turbulent shear agglomeration, and turbulent inertial agglomeration.

Four natural deposition processes are modelled: sedimentation, diffusion to surfaces, thermophoresis, and diffusiophoresis.

Condensation or evaporation of water on/from the aerosol is calculated either by the fixed grid or the moving grid technique. With the fixed grid technique the Mason equation is solved in a common time step together with the agglomeration and depletion processes. Kelvin and solubility effect are not considered.

By use of the moving grid model MGA [45] the calculations of the particle growth or shrinking by condensation and evaporation respectively are separated from the other aerosol processes. The algorithm is based on the methods of characteristics to calculate the trajectories of the sectional boundaries. The Mason equation is used including the Kelvin and the solubility effects. After each MGA time step the aerosol are remapped onto the MAEROS fixed grid again. In the proceeding MAEROS time step the water component is treated like a solid component. In CONTAIN the fixed grid and the moving grid method are available.

In multi-component geometries the airborne particles are transported by the atmosphere flows between the control volumes.

MELCOR

In MELCOR the aerosol behavior is calculated by the MAEROS model, too, but without direct inclusion of condensation and evaporation in the MAEROS solution framework. A description of MAEROS is given in the chapter for CONTAIN.

The particle growth/shrinking by steam condensation/evaporation is calculated separately by the Control Volume Hydrodynamics (CVH) package. Water droplets are transported as fog by the CVH package and treated as water-class aerosols by the RN package. The difference between CVH fog and RN water-class masses in a control volume at the end of the CVH time step represents net condensation of water onto or evaporation from the aerosol in that volume. The net change in the water mass is imposed on the water-class inventory in the RN package, which then uses the Mason equation to distribute the mass over the aerosol size distribution in the control volume.

Beside the originally implemented conventional Runge-Kutta integration routine an explicit (forward Euler solver) is used to increase the efficiency.

The aerosols are transported between the control volumes by the flow of atmosphere and pool water, assuming zero slip between the aerosol and the host medium. Additionally in absence of bulk flow, aerosols may move by Brownian motion or by gravitational settling through openings between control volumes.

A modification of the code for ISP37 was made by the Sandia National Laboratories. In this none standard version of MELCOR the hygroscopic modelling was added to the existing aerosol physics package.

FIPLOC

In FIPLOC the aerosol behavior is treated by the aerosol model MAEROS. Condensation on or evaporation from the aerosol are calculated by the moving grid model MGA separately from the other aerosol processes. The impact of the hygroscopic aerosols on the thermal hydraulic is modelled. The aerosol equation system is solved by the ODE-solver FEBE [49].

The aerosols is transported between the control volumes by the atmospheric flows. At weak flow conditions the transport by particle settling is considered additionally.

ECART

In ECART the vapor and aerosol transport module is mainly based on the TRAP/MELT2 [46] model and contains some features of the NAUA [47] and SPARC [48] codes. Each control volume in which vapors and aerosols are well mixed is divided into several sub-regions, where local thermal hydraulic conditions can be taken into account. Agglomeration and depletion processes in compartments, the aerosol deposition in pipes, the dry physical resuspension and pool scrubbing are modelled.

MACRES

The aerosol code MACRES models mechanistically chemical reactions in the gaseous phase, homogeneous and heterogeneous nucleation of vapors, adsorption and condensation of vapors on structural surfaces and evaporation from surfaces.

In the MACRES code agglomeration (Brownian, gravitational, turbulent), deposition (sedimentation, diffusion, thermophoresis, diffusiophoresis) and aerosol transport are modelled. Steam condensation on the aerosol particles is modelled under humidity condition less than 100% by use of the Mason equation including Kelvin and the solubility effects, which is solved simultaneously with the transport and deposition processes. Change of the particle density caused by steam condensation is considered. Evaporation from the aerosol is not modelled.

The aerosol is simulated not only to be transported among several control volumes by atmospheric flow but also to settle down from upper volumes to lower volumes. Thermal-hydraulic conditions such as wall and atmospheric temperatures, inter-cell flow rates and relative humidity etc. have to be provided as boundary conditions for MACRES calculations.

MOSAIC

The aerosol code MOSAIC uses the Monte Carlo method to solve the general dynamic equations of a multi-component aerosol. Arbitrary size distributions of aerosols

can be calculated. Numerical problems like numerical diffusion are avoided. All mechanisms are treated interactively. At the moment MOSAIC is a single volume code. The thermal hydraulic data has to be given in the input.

REMOVAL

The REMOVAL code includes models for agglomeration (Brownian, gravitational, and turbulent), steam condensation, evaporation, hygroscopicity, deposition (sedimentation, diffusion, thermophoresis, and diffusiophoresis), and transport of aerosol particles.

Steam condensation/evaporation are calculated by the Mason equation which was extended for the Kelvin and solubility effects. Between the compartments aerosol is transported by the atmospheric flows. The additional transport by gravitation from upper into lower compartments is considered.

Agglomeration and deposition processes are integrated by a Runge-Kutta solver. The particle growth by condensation is calculated by an Euler method. For large time steps equilibrium droplet sizes are assumed.

4.3.4 Modelling Features Proposed

In the ISP37 specification data and guidance for modelling the experiment is given. This includes the following topics:

- The nodalization (Fig. 4.1) including nodes, atmospheric flow paths, drainage flow paths and distribution, containment structures with material properties,
- the initial and boundary thermal-hydraulic conditions (pressure, temperatures, the steam injection rates, the air removal and injection rates and the air leakage rate out of the entire containment etc.),
- boundary aerosol conditions (injection rate, particle size distribution, density, solubility and shape of the particle, etc.)

4.3.4.1 Nodalization

In the specification a nodalization was proposed to be used by all participants with a minimum number of nodes. The aim was:

- to facilitate the comparison,
- to make it as easy as possible for the participants to perform a combined thermal-hydraulic/aerosol calculation,
- to leave enough room for the participants to simulate all important phenomena,
- specifically the dome was proposed to be simulated by one node since its atmosphere is well mixed throughout the whole experiment,
- compartment R4 was proposed also to be modelled by one node due to its small influence on the overall behavior of the containment,
- the sumps on the bottom of the containment were proposed to be modelled either as individual nodes or included in the nodes above according to the code requirements.

4.3.4.2 Leakage

The model containment has an atmospheric and aerosol leakage through small cracks and fissures in the walls. The main leakage is in the outer shell. But also a small part of the atmosphere may be pressed into the base material and the internal structures. Steam and air leakage have a different behavior. Air as an uncondensable gas penetrates through the wall into the environment. Most of the steam however condenses within the first centimeters of the wall.

Since the total containment air leak rate is well known, it was proposed to be used as a boundary condition.

The local air leak distribution however is not known, therefore participants were free to split up the air leakage of the entire containment individually.

The steam leakage was proposed to be neglected, since in the experiment it could not be measured. Also it is rather an enhancement of the heat transfer into and through

the structures than a leakage, since most of the steam condensed inside the first centimeters of the wall.

4.3.4.3 Aerosol Data

The data for the two NaOH aerosol injections and the steam/air carrier gas are listed in Tab. 6, 7 and 10 of [8]. The aerosol mass injection rates are constant for the two injection periods. The losses of aerosol material in the generator and the injection pipe are small (< 10 %) and thus neglected.

The particle size distribution of the primary aerosol injected by the torch generator was estimated from SEM-pictures[3] at the end of the first injection period. A log-normal distribution of the particle size was assumed with MMD = 0.2 µm and GSD = 1.9.

The effective density of the small and compact primary NaOH-particles was not known. The theoretical density of pure NaOH is 2130 kg/m³. In the moist atmosphere the salt solved rapidly and the effective particle density decreased. For models like MAEROS which cannot distinguish between different densities of the aerosol components (NaOH and water) the effective density of the NaOH/water droplets of 1 100 kg/m³ was proposed. 12 Participants used this average density.

A Van't Hoff factor of 2.0 for the solubiltiy of NaOH was commonly used. The dynamic and the agglomeration shape factors of 1.0 were applied by all participants.

4.3.5 Modelling Features Used

Despite the proposed way of modelling features the participants had the possibility to choose their own model, if it appeared to be adequate. The specific deviations are given in Tab. 4.3. Generally the proposed nodalization of Fig. 4.1 was adapted by the participants. Different nodalizations applied are shown in Fig. 4.2a to f

For the stand alone aerosol calculations with MACRES NUPEC used the proposed nodalization with two additional flow pathes between the compartments R5/R6 and R7/R8 respectively in order to simulate counter current flows. JAERI used the nodalisation without modifications.

[3] Scanning Electron Microscope

Tab. 4.3: Deviations from the proposed input

Participant Calculation	Deviation	Effect on the result
CIEMAT	R4 simulated by two nodes	stratification in R4
ECN	areas of flow path between: • R6 -> R3 and R8 -> R3 4 times larger • R5 -> R6 and R7 -> R8 2 times larger	less stability of atm. flow
KI-CON	- air mass from Phase II on 80 to 50 kg lower - structure 45, concrete in between R1 and R9 thickness 0.3 m instead of 0.92 m	containment pressure
VUJE-CON	- leakage modelled by flow path (steam + air) ->* - air mass too high: at 30 h (+ 50 %) - water pumped out of the sump of R94 - material properties of concrete and steel -> CONTAIN values	containment pressure
IPSN/GRS-Fs (FIPLOC)		
GRS/IPSN-Fe (FIPLOC)	extended nodalization: - R6, R8 each 3 levels, 5 nodes - annulus 4 levels, 4 nodes - R4 3 levels, 3 nodes	pressure, stratification
GRS/IPSN-Re (RALOC)	same as Fe (see above)	see above
IFE-2	R4 included into the annulus, R6 and R8 have same sump	minor
IFE-1	- R4 included into the annulus, R6 and R8 have same sump - steam leakage, integral at 30 h 1 700 kg (9.5 % of total steam injection)	pressure
JRC	- the boundary temperatures are exchanged (the building has 10 °C, the environment and the soil have 22 °C)	pressure
CTN	-	
ENEA	-	
FZK 1	as FZK 2 plus: oxygen instead air, cell volume and oxygen injection reduced by factor 1.1	pressure

Participant Calculation	Deviation	Effect on the result
FZK 2	modelling of outer shell structures, for example • coating not simulated • S1, S2 1.884 m concrete instead 0.45 m concrete, 0.02 m air gap, 0.24 m YTONG • S8 1.09 m concrete instead 0.6 m light concrete	pressure
KAERI	- structure 2 and 3 combined, cylindrical geometry, 100 m^2, instead 77 m^2, - structure 4 and 5 combined, cylindrical geometry The combined structures are attached to the environment. Structure 2 and 4 however are in reality attached to the building	slightly lower pressure, 0.03 bar
	- pressure control to experimental pressure in phase I -> different time history of the steam injection, but the integral steam injection is only slightly smaller - steam injection temperature instead of enthalpy	pressure history in phase slightly lower pressure
KI-MEL	nodalisation: - dome: 2 layers, 2 nodes (2 flow paths) - R4: 2 layers, 2 nodes	see (4.1.3.5)
	junction area input: A node 1, l node 1, A junction, l junction, A node 2, l node 2	stability of the flow
NUP-MEL		
RAS	- steam leakage together with air leakage only 10 % of the vapor content integral 520 kg ≙ 3 % - 6244 kg water drawn out during phase I - Structures (often cylindrical geometry instead of slabs) - coarse structure nodalisation - dome 3 layers 2 nodes (but connected by 2 flow paths) - flow resistance U38, U36 5.0 instead 2.7	pressure - 0.03 bar pressure
SNL		
STUD	- coating and air gap not simulated - some structures are modelled by a cylindrical geometry	pressure

Participant Calculation	Deviation	Effect on the result
VUJE-MEL	nodalisation: - dome 2 layers, 2 nodes (1 flow path!) - R4 2 layers, 2 nodes - structure 47, 4.2 m^2 steel in dome outer shell not simulated - structure 51, 0.4 m^2 steel door in R9.4 not simulated	pressure and stratification
Battelle	coating and steel-liner not simulated	pressure
UPISA FUMO	nodalisation: - R6, R8 each 2 Layers, 2 nodes	stratification
	- Flow area reduction by a factor of 10: RRo, RRu, U29, R6 upper - R6 tower, R8 upper - R8 lower	stability of flow
	- Flow pressure loss coefficient: 2.5 instead of 2.7, 1.5 instead of 1.0	negligible
	- steam leakage modelled at location of air leakage, but very small	pressure (minor)
	- air mass 30 to 40 kg lower	pressure

4.4 Comparison of Analytical and Experimental Results

According to the two sub-problems the comparison is separated into a thermal-hydraulic and an aerosol part.

4.4.1 Comparison of the Thermal-hydraulic Results

4.4.1.1 Consistency Check, Reference Calculation and Evaluation Procedure

Each calculation[4] is checked for consistency with respect to results and selected input data. Most checks are done qualitatively, some quantitatively. With the consistency check, which was especially important due to the complex geometry and test procedure, some unexpected behavior of the results could be explained.

Due to the large number of submitted results a reference calculation was chosen for each code group, which matches the best the following criteria:

- simulation of the atmospheric stratification
- use of the specified input
- agreement with the experimental flow velocities

The selected reference calculations are:

Code	Participant
CONTAIN	CIEMAT
MELCOR	NUP-MEL
FIPLOC/RALOC	GRS/IPSN-Fs
GOTHIC[1]	Battelle
FUMO[1]	UPISA

[1] only one calculation was done with GOTHIC and FUMO

[4] Due to the late delivery no consistency check was performed on the ECART results

The comparison of the data was done in two steps:

- between the experiment and the reference calculations of the different codes,
- comparison between the experiment and those calculations using the same code.

The aim of the comparisons between the calculations using the same code is to identify a code typical behavior and to explain deviations between the calculations. This procedure was followed in particular with the pressure data.

4.4.1.2 Containment Pressure

- **Comparison for the reference calculation with experiment**

The containment pressures of the reference calculation of each code are compared to the experiment in Fig. 4.3. The calculated data follow with the same tendency fairly close the experimental curve. The maximal deviation from the experiment of about 0.35 bar is within an uncertainty band given by:

- the uncertainties of the experimental boundary conditions, which are estimated to ± 0.1 bar,
- the systematic overprediction of the pressure by neglecting the "steam leakage", which is roughly estimated at 0.1 to 0.3 bar,
- the systematic underprediction of the pressure by the proposed nodalization, which allows in contrast to the experiment steam condensation on the lower containment structures. The underprediction is estimated to 0.1 bar.

The differences at three selected times are given in Tab. 4.4

Tab. 4.4: Difference between calculated and measured containment pressure for the reference calculations

Participant Code	$p_{cal} - p_{exp}$ (bar)		
	Phase I t = 12.5 h	End of Phase III	End of Exp. t = 30 h
GRS/IPSN-FS FIPLOC	+ 0.15	- 0.02	+ 0.21
Battelle GOTHIC	0	+ 0.05	+ 0.08
NUP-MEL MELCOR	+ 0.03	0	+ 0.14
UPISA FUMO	+ 0.09	- 0.02	+ 0.21
CIEMAT CONTAIN	+ 0.2	+ 0.1	+ 0.35

The deviations between the pressure of the reference calculations themselves are even smaller. The largest is with 0.2 bar at 12.5 h and 0.26 bar at 30 h between CONTAIN (CIEMAT) and GOTHIC (Battelle).

The deviations between CONTAIN, FIPLOC and MELCOR can be explained by:

- air masses in the containment

- sump temperatures

- heat transfer

The higher pressure of CONTAIN (CIEMAT) compared to FIPLOC (GRS/IPSN-Fs) is mainly the result of the higher air content used by CIEMAT.

The lower pressure of MELCOR (NUP) compared to FIPLOC (GRS/IPSN-Fs) is caused by higher heat flux to the sump and by the condensation heat transfer model.

GOTHIC (Battelle) calculates the lowest pressure and is the closest to the experiment. However it did not simulate the coating in the containment shell, which acts like a

thermal isolator between the containment atmosphere and the containment shell. In addition it has irregularities in the condensation heat transfer.

FUMO (UPISA) uses a small steam leakage and a slightly too small air mass both decreasing the pressure towards the experimental value.

A detailed description of the results of the reference calculations is given in appendix 7.2.

- **FIPLOC/RALOC Group**

In the FIPLOC/RALOC group, given in Fig. 4.4a, the maximum deviation between the calculated pressures is 0.2 bar (excluded IFE-1, which simulates compared to the others a large steam leakage).

The reference calculation GRS/IPSN-Fs is nearly equidistant to the experimental pressure. It shows a slight overprediction for example at 12.5 h by 0.15 bar and at 30 h by 0.21 bar. At the end of phase III it is close to the experiment.

All deviations are caused by different modelling input:

- GRS/IPSN-Fe and -Re use a more detailed nodalization and are able to simulate the stratification better than GRS/IPSN-Fs. Therefore less steam gets in contact with the lower structures. This results in a higher pressure.
- JRC uses a different heat transfer option, that gives under high steam content lower heat transfer coefficients compared to the reference calculation. In addition a too high atmospheric boundary temperature was used.
- IFE-2 calculates only a slightly higher pressure than GRS/IPSN-Fs. It uses the same heat transfer option as JRC which works in direction of a higher pressure. However artificial mixing of the atmosphere of the dome and the annulus counterbalances this effect. IFE-1 differs to IFE-2 by simulating a steam leakage (9.5 % of the total injected steam). This results in a pressure close to the experiment.

Tab. 4.5 gives some detailed information.

Tab. 4.5: Experimental containment pressure compared to FIPLOC/RALOC group

Participant	$p_{calculated} - p_{experiment}$ (bar)			Reason for deviation from
Calculation	Phase I 12.5 h	End of Phase III	End exp. 30 h	reference calculation
GRS/IPSN-Fs	+ 0.15	- 0.02	+ 0.21	FIPLOC reference calculation
IFE-2	+ 0.18	0.	+ 0.23	- smaller heat transfer coefficients -> higher pressure - less detailed nodalisation in R4 (minor) - mixing of dome and R93 -> lower pressure
GRS/IPSN-Fe	+ 0.23	0.	+ 0.32	detailed nodalisation prevents steam condensation on the lower structures -> higher pressure
GRS/IPSN Re	+ 0.23	0.	+ 0.32	same as GRS/IPSN-Fe
JRC	+ 0.3	0.	+ 0.39	smaller heat transfer coefficients and exchange of the boundary temperatures -> higher pressure
IFE-1	+ 0.04	0.	0.	steam leakage modelled (9.5 % of the total steam injection) -> lower pressure mixing of dome and R93

- **CONTAIN Group**

The results for the CONTAIN group are given in Fig 4.4b. Within the CONTAIN group the pressure deviations are larger than in the FIPLOC/RALOC group. They reach at the end of the experiment (30 h) a maximum of 0.84 bar between VUJE-CON and ECN.

The pressure curve of reference calculation CIEMAT is nearly equidistant to the experimental curve with an overprediction of 0.2 bar at 12.5 h, 0.1 bar at the end of phase III and 0.34 bar at 30 h.

The pressure difference between VUJE-CON and CIEMAT increases during the experiment. At the end VUJE-CON has a 0.18 bar higher pressure. The main reason is the difference of the air content, resulting at the end in a 0.13 bar higher average

partial air pressure of VUJE-CON (VUJE-CON did not simulate the air leakage as proposed).

ECN underpredicts in contrast to CIEMAT the experimental pressure. The main reason for this different behavior is caused by the different coupling to the boundaries. While CIEMAT calculated the heat flux from the outer surfaces of the outer shell to the environment and the outside building using heat transfer coefficients (as done generally by all other calculations), ECN fixed the outer surface temperatures of the outer shell to the boundary temperatures, thus causing a higher heat loss out of the containment. This is confirmed by a corrected study done by ECN, which gets a pressure close to CIEMAT

The pressure calculated by KI-CON decreases during the experiment more and more below CIEMAT. This has two reasons: At the beginning of phase II the air content is 50 to 80 kg too low, and the lower cell option was applied in disagreement with the CONTAIN manual causing a distortion of the water balance. A corrected study done by KI-CON resulted in a pressure history very similar to CIEMAT. The remaining small difference might be explained by the coarse heat slab nodalization used by KI-CON.

FZK2 is very close to the experiment and gets a lower pressure than CIEMAT. The reason is a deviation of the structure input from the proposal and therefore from the real geometry: The coating on the outer shell is not simulated and the wall thickness of the outer shell structures which have together 50 % of the outer shell surface area are increased to an improper value. A corrected study done by FZK using the proposed input shows a pressure closer to CIEMAT but still somewhat lower: 0.1 bar in phase I and 0.2 bar at the end of the calculation. FZK1 has a higher pressure than FZK2. The reason might be that FZK1 uses oxygen instead of air and has reduced the free volumes by a factor of 1.1 without reducing the air injection.

Tab. 4.6 gives some detailed information about the deviations and the reasons.

Tab. 4.6: Experimental containment pressure compared to CONTAIN group

Participant Calculation	$p_{calculated} - p_{experiment}$ (bar) Phase I 12.5 h	End of Phase III	End exp. 30 h	Reason for deviation from reference calculation
CIEMAT	+ 0.2	+ 0.1	+ 0.34	reference calculation
KI-CON	+ 0.09	- 0.3	- 0.135	(1) air mass starting phase II 50 to 80 kg too low (2) wrong application of the lower cell option results in a wrong water balance
VUJE-CON	+ 0.23	+ 0.21	+ 0.52	too high air-content
ECN	- 0.23	- 0.2	- 0.31	- fixed outer shell outside surface temperatures -> lower pressure (see ENEA ,MELCOR))
FZK2	+ 0.03	- 0.04	- 0.05	deviation from the proposed heat slab input
FZK1	+ 0.17	- 0.04	+ 0.04	as FZK2 (plus other reasons see text above)

- **MELCOR Group**

The pressure results of the MELCOR group are given in Fig. 4.4c and 4.4d. For most of the MELCOR calculations (VUJE-MEL, RAS and ENEA excluded) the differences of the containment pressures are very small (less than 0.1 bar) and therefore not further investigated.

The reference calculation NUP-MEL has at the beginning a typical pressure behavior, as it is observed with the MELCOR calculation in the ISP: At the first hour after the start of the steam injection the containment pressure is overpredicted, from 2.5 to 5 h it is underpredicted, then it is close to the experiment. Only with the start of phase VI a more significant deviation develops with 0.14 bar at the end of the experiment.

The results of the other MELCOR calculation show generally the same behavior. The differences between the results is mainly caused by differences in the input (e. g. structure modelling or structure temperature) or whether the stratification in the inner compartments is simulated.

KAERI controlled the steam injection rate during phase I in order to get the experimental pressure. Therefore it does not have the "typical MELCOR pressure behavior". The pressure control changes the steam injection rate especially up to 5 h, however the integral steam injection at the end of phase I is nearly equal to the experiment .

ENEA underpredicts the containment pressure because the outer surface temperatures of the outer shell are fixed to the boundary temperatures, thus causing a higher heat loss out of the containment (see ECN in the CONTAIN group). A calculation corrected in this respect gives the results closer to the experiment like the majority of the other MELCOR calculations.

The pressure calculated by RAS is lower than the pressure of the experiment and the reference calculation, although most reasons given in Tab. 4.5 leads to a higher pressure. The following modelling features cause the lower pressure: (1) The simulation of 510 kg steam leakage decrease the pressure (approximately 0.03 bar). (2) The individual heat conductors are subdivided into few layers only. This enhances the heat flow through the structures and causes a higher heat loss out of the containment atmosphere compared to a finer heat slab nodalization. (3) The artificial mixing of the atmosphere in compartment R9.3 and R9.4 by two parallel flow paths gets steam into R9.4. This condenses on the cold walls lowering the pressure. A corrected study done by RAS, with a single flow path between R9.3 and R9.4 and more detailed structure nodalization especially of structure 6, confirmed the statement above and resulted in a higher pressure history.

Tab. 4.7 gives some detailed information about the deviations and the reasons.

Tab. 4.7: Experimental containment pressure compared to MELCOR group

Participant	$p_{calculated} - p_{experiment}$ (bar)			Reasons for deviation from
Calculation	Phase I 12.5 h	End of Phase III	End exp. 30 h	reference calculation
NUP-MEL	+ 0.03	0.	+ 0.14	reference calculation
RIAR	+ 0.05	0.	+ 0.2	
KI-MEL	+ 0.03	0.	+ 0.1	dome 2 layers but mixed (minor) R4 2 layers (minor)
KAERI	0.	- 0.02	+ 0.1	- structure input - 0.03 bar - slightly lower steam injection/lower pressure, due to pressure control phase I
SNL	+ 0.03	0.	+ 0.13	
STUD	+ 0.08	+ 0.06	+ 0.15	- structure input - uniform initial temperature in outer shell (slightly higher pressure)
CTN	+ 0.08	0.	+ 0.16	
VUJE-MEL	- 0.08	- 0.12	+ 0.04	1. dome 2 layers, 1 flow paths -> inversely stratified 2. R4 2 layers 3. outer shell steel structures not simulated 1 to 3 should result in a higher pressure! 4. coarse heat slab nodalisation
RAS	- 0.13	+ 0.1	0.	1. steam leakage 510 kg - 0.03 bar 2. coarse heat slab nodalisation ($T_{structure}$ 6 first too low) 3. $T_{structure}$ 2 building too low 4. mixing R9.3 and R9.4 1 to 4 result in a lower pressure 5. cylinder geometry
ENEA	- 0.2	- 0.13	- 0.16	fixed outer shell outside surface temperatures

- **ECART, FUMO and GOTHIC**

The comparison for ECART (ENEL), FUMO (UPISA) and GOTHIC (Battelle) is given in Fig. 4.4e. All calculations show a very good agreement with the experimental

results. In the case of GOTHIC and FUMO the agreement is caused by some modelling deficiencies[5].

4.4.1.3 Atmospheric Temperatures

The local atmospheric temperature depends mainly from the local steam content (partial steam pressure), which determines the saturation temperature, e. g. it depends from the steam air distribution within the containment. Steam air distribution is basically influenced by a correct calculation of stratification and convection in the containment (see below).

To give an impression about the accuracy of the calculated temperature in the containment, the temperature of the dome R9, and of the lower inner compartment R3 are discussed here. Additional information is given in the chapter about atmospheric stratification and mixing.

With a few exceptions all calculated temperatures in the dome, which are plotted in Fig. 4.5a to 4.5e, agree fairly well with the experimental value, because with the relatively high partial steam pressure in the dome deviations of the steam content have only a small effect on the temperatures.

The lower temperatures calculated by KI-CON, ECN and ENEA correspond to their lower total containment pressures (lower steam contents). The lower temperature calculated by VUJE-MEL is related to the nodalization of the dome with two nodes.

Measured and calculated temperatures of the lower inner compartment R3 are compared in Fig. 4.6a to 4.6e. During the course of the experiment in R3 either stratification or mixing takes place (see below), which can be seen from the results. If the temperature stays low at approximately 40 °C, e. g. in phase I through III, or decreases, e. g. in phase V stratification occurs in the compartment. In phase IV the temperature increase up to 100 °C. This is an indication of mixing in and convection between the compartments. It can be seen that some calculations follow the experiment fairly close, other deviate significantly.

[5] ECART was not investigated in detail

4.4.1.4 Atmospheric Stratification and Mixing

From the temperature plots, given in Fig. 3.8 and 3.9 for the experiment and Fig. 4.8a to 4.8y and Fig. 4.9a to 4.9y for the different calculations, the occurrence of stratification and mixing can be derived. Two dominant atmospheric convection loops have been observed in the experiment:

- The steam injection into R5 in the phases I, II, IV and VI induces the upper convection loop mixing the atmosphere of the upper outer compartments (R5, R7) and the dome. Meanwhile the atmosphere stays stratified in the lower outer compartments (R6 and R8) and the inner compartment (R3).
- The steam injection into R3 in the phase V induces the overall convection which mixes the atmosphere of the lower and upper inner and outer compartments with the dome.

The atmosphere in the dead end annulus stays always stratified.

Almost all calculations simulate the atmospheric stratification between the dome and the annulus (see Fig. 4.8a to Fig. 4.8y). By adopting the proposed nodalization this result can be expected. The calculations which show deviating results use an unfavorable nodalization.

All calculations simulate the convection loops observed in the experiment:

- The upper convection loop (see TATMR5, TATMR7 and TATMR9D in Fig. 4.9a to 4.9y).
- The overall convection loop (see phase V in Fig. 4.9a to 4.9y).

The simulation of the stratification the inner compartments is more difficult than for the annulus, since the proposed nodalization gives the codes the freedom to calculate either convection loops or stagnation between the inner compartments depending on the atmospheric conditions.

The following calculations show a stratification between the inner compartments:

- all FIPLOC calculations (see TATMR6, TATMR8 and TATMR3 in Fig. 4.9a to Fig. 4.9f),

- the RALOC calculation,
- all CONTAIN calculations (see Fig. 4.9g to Fig. 4.9l and comments in Tab. 4.4 for FZK and ECN),
- the MELCOR calculations NUP-MEL and RAS (see Fig. 4.9q and 4.9r),
- the GOTHIC calculation (see Fig. 4.9w),

The others show almost no stratification in the inner compartments or an intermediate behavior.

- **Deviation from the general behavior**

a) Dome and annulus

- RAS simulates parallel flow paths between the dome and R9.3 and between R9.3 and R9.4. The latter flow paths have a countercurrent flow and mix the atmosphere of R9.3 and R9.4.
- IFE-1,2 use parallel flow paths connecting the dome and R9.3. A countercurrent flow mixes the atmosphere of these nodes.
- VUJE-MEL calculates an physically unrealistic stratification because the temperature in the dome is lower than in the annulus (see below).

b) Lower outer compartments

The reason that most MELCOR calculations do not simulate the stratification in the inner compartments is related to too large maximum time steps and/or unfavorable simulations.

In the two MELCOR calculations which simulate the stratification the following measures to get stable results are applied:

- NUP-MEL reduced the maximum time step to 1 s,
- RAS reduced the maximum time step to 2 s and increased in addition the flow resistance coefficients by a factor of 2.

In a parametric study done by NUPEC with a maximum time step of 10 s the stratification was not simulated.

The other MELCOR calculations used larger maximum time steps than 2 s except for KI-MEL (2 s).

KI-MEL uses two unfavorable simulations: (1) The flow path inertias are smaller than the proposed values, which are applied by NUP-MEL . (2) Parallel flow paths connecting e. g. R7 and R8 cause a slight atmosphere mixing of these compartments.

- **Effects of nodalization on stratification**

GRS/IPSN-Fe and GRS/IPSN-Re use an extended nodalization. Compared to the proposed nodalization used by GRS/IPSN-Fs the number of nodes simulating the atmosphere is extended from 11 to 23:

- R6 and R8 are each split up into 5 nodes which form 3 levels. The flow areas of the junctions connecting these nodes are the full geometric areas. The codes are free to calculate either convection or stratification between the nodes simulating R6 and R8.
- The annulus is simulated by four levels, splitting up R9.4 and R9.3.
- R4 is simulated by 3 levels.

In addition nodes situated at the same level are connected by horizontal parallel flow paths simulating the upper and the lower half of the geometric openings. This allows the code to calculate a countercurrent flow in case of small density differences between the nodes.

By this the experimental stratification in R6 and R8 is simulated and the simulation of the stratification in the annulus is improved. Also the temperature rise of R1 during phase I caused by steam inflow is simulated. The calculated temperatures are generally in a good agreement with the measurement except for slight overprediction in general and larger overprediction in R9.4 caused by a too high steam content (too high pressure) in the calculation. The results of GRS/IPSN-Fe and -Re are almost identical.

In the FUMO nodalization of UPISA R6 and R8 are splitted up into two nodes each, which form two levels. For flow stability reasons the areas of the junctions connecting these nodes are reduced to 10% of the geometric areas. Convection within R6 and R8 is not possible. A slight stratification is calculated within R6 and R8 and steam enters R1.

In the CIEMAT calculation R4 is splitted up into two nodes forming two levels. This should create a stratification within R4 but have only a minor effect on the rest of the containment.

VUJE-MEL simulates the dome by two nodes forming the two levels R9.1 and R9.2. Since they are connected by one flow path only the atmosphere of R9.1 and R9.2 cannot be mixed by convection as in the experiment. This results in a too low steam content in R9.1. Therefore the dome temperature, which is the average value fo the temperatures in R9.1 and R9.2, is too low.

KI-MEL simulates also the dome by two nodes R9.1 and R9.2, but they are connected by two parallel flow paths at the same elevation with slightly different flow areas. Up to 2.5 h the flow in these paths is small and seems to have the same direction. While the temperature rise of R9.2 follows closely the temperature of R5, the temperature of R9.1 rises only slowly. Then countercurrent flow starts in the parallel junctions mixing fast the atmosphere of R9.1 and R9.2 almost completely. Parallel flow paths are modelled between R7 and R8, R8 and R3 and between R3 and R6, too. This contributes to the fact, that the stratification in the inner compartments occurs only intermediately. A parametric study done by KI with single instead of parallel flow paths improved the simulation of the stratification slightly by calculating up to 20 °C lower temperatures in R3. Another unfavorable simulation of KI-MEL in respect to stratification are the small flow path inertias, which are a result of splitting up the paths into three sections with different areas and lengths.

The nodalization used by RAS contains parallel flow paths between the dome and R9.3 and between R9.3 and R9.4, each pair with different junction elevations. This results in slight countercurrent flow and mixing between R9.3 and R9.4, but in no countercurrent flow and stratification between the dome and R9.3. A parametric study done by RAS without these parallel flow paths showed the thermal stratification between R9.3 and R9.4.

The nodalization of IFE-1 and -2 contains parallel flow paths between the dome and R9.3. Their junction elevations differ by 0.05m. This causes a countercurrent flow, which mixes the atmosphere of R9.3 and the dome. A parametric study done by IFE setting the elevations of the parallel paths to the same value resulted in a thermal stratification between the dome and R9.

An overview of the different modelling with respect to stratification gives Tab. 4.8.

Tab. 4.8: Simulation of the atmospheric stratifications

Code	Participant	Stratification		Comment
		Dome-Annulus	**Dome-Inner Compartments**	
CONTAIN	CIEMAT	yes	yes	
	ECN	yes	yes temp. R3 higher than CIEMAT	oscillations in R3 probably caused by 2 to 4 times larger flow areas
	KI-CON	yes	yes	
	VUJE-CON	yes	yes temp. R3 higher than CIEMAT	
	FZK1,2	yes	yes	- weak internal loop in the inner compartments R8 -> R1 -> R6 -> R3 -> R8
MELCOR	NUP-MEL	yes	yes	
	CTN	yes	intermediate	
	ENEA	yes	no	
	SNL	yes	no	
	STUD	yes	no	
	VUJE-MEL	temperatures dome - annulus are inverse	intermediate	dome nodalisation: 2 layers (R9.1, R 9.2) one flow paths -> temp R9.1 > temp R9.3
	KAERI	yes	no	
	RIAR	yes	no	
	RAS	temperatures of R93 and R94 almost equal *	yes	* nodalisation: counter current flow in parallel flow paths between R93 and R94

Code	Participant	Stratification		Comment
		Dome-Annulus	Dome-Inner Compartments	
	KI-MEL	yes	intermediate **	** artificial mixing by parallel flow paths between R7 and R8, and lower flow path inertia than specified
FIPLOC	IPSN/GRS-Fs	yes	yes	
	IFE1,2	temperatures of R93 and dome are almost equal *	yes	* nodalization: counter-current flow in parallel flow paths in between R93 and R94
	JRC	yes	yes	
	GRS/IPSN-Fe	yes	yes	detailed nodalisation and horizontal parallel flow paths -> better simulation of the temperatures of R1, R6 and R8
RALOC	GRS/IPSN-Re	yes	yes	detailed nodalisation and horizontal parallel flow paths -> better simulation of the temperatures of R1, R6 and R8
GOTHIC	Battelle	yes	yes	
FUMO	UPISA	yes	intermediate	

4.4.1.5 Atmospheric Flow Velocities

The calculated and experimental atmospheric flow velocities in the openings between the dome and R5 (U59), between R7 and R8 (U78), and as an example between dome and annulus (RRo, RRu) are shown in Fig. 4.10a to 4.10h and 4.11 for representative calculations of each code. Comparing the experimental and calculated velocities larger measurement uncertainties has to be considered, e. g. the experimental flow is not uniform over the openings and the initial velocity of 0.2 m/s is necessary to initiate the turbine flow meter.

For U59 the calculations generally reproduce the tendency of the experimental behavior. All calculations simulate the upper convection loop. The velocity is high during the

first hours of phase I, then it decreases and increases again with the restart of the steam injection in phase V.

The magnitude of the velocities is generally in the order of the experimental values with following exceptions:

- The CONTAIN calculations FZK-1, FZK-2 and VUJE-CON have a higher velocity up to a factor of 2.
- FUMO calculates a lower velocities (about 30% of the experimental value).

U78 - lower outer compartment R8 to upper outer compartment R7

Due to the stratification the flow in U78 is, with the exception of phase V very low. The calculations, which simulate the stratification between the upper and the lower outer compartments, generally show very small flow velocities during the corresponding phases of the experiment. Only in phase V when the stratification is destroyed the flow velocity increases sharply. The calculations which do not simulate the stratification generally have an oscillatory and or higher flow velocity in U78.

GOTHIC simulates also the stratification in the outer compartments but its velocity in U78 is from 3 to 10 h higher and sometimes oscillating. This picture however does not reflect the really calculated velocity since too few data points are plotted. The oscillations are triggered by oscillations in the heat flow to the dome structures. They do not occur anymore in a parametric study done by Battelle with a reduction of the maximum time step to 0.75 s (originally 5 s).

VUJE-MEL and UPISA simulate the stratification intermediately. Their velocities in U78 seem to correspond to this behavior.

The calculated atmospheric flow velocities from the dome to R9.3 (RRo) and from R9.3 to R9.4 (RRu) are qualitatively similar. As an example the results of CIEMAT are shown in Fig. 4.11. During the heat up phase they reflect the steam flow into the annulus. About a quarter of the injected steam condenses in the annulus.

4.4.1.6 Atmospheric Humidity

A comparison between measured and calculated humidities for the dome and the upper annulus (R9.3) is given in Fig. 3.11 and Fig. 4.12a to 4.12j. Since the humidity measurements are very uncertain, only qualitative conclusions are possible.

- **Reference calculations**

The dome atmosphere is at or close to saturation. This is proved by the fact that the atmospheric and the structural surface temperature (Fig. 4.12a) are very close together and steam condenses on the dome structures almost through the entire experiment. Only from 20 to 22.7 h during phase III a larger superheating has occurred.

The atmosphere in the upper annulus is at or close to saturation up to 15 h (Fig 4.12g). This is indicated by the smooth temperature history. A short time before 15 h air is injected into the annulus decreasing the partial steam pressure and resulting in a superheating of the annulus. This is indicated by the unregular temperature history. After 28 h it becomes saturated again.

FIPLOC (GRS/IPSN-Fs), MELCOR (NUP-MEL) and UPISA (FUMO) calculate well the saturated conditions in the dome, however underpredict the superheating during phase III. For the annulus also the saturation from 1.13 to 15 h is simulated well. NUP-MEL and FUMO however show after 15 h too short time spans of superheating. Generally these calculations have the tendency to underpredict the superheating.

CONTAIN (CIEMAT) and GOTHIC calculate superheated instead of saturated conditions in the dome. The conditions in R9.3 from 1.13 to 15 h are simulated well, the superheating after 15 h in R9.3 is overpredicted. In summary these calculations overpredict the superheating.

With respect to thermal non equilibrium no important improvement could be detected between the results from the codes with non equilibrium (CONTAIN, GOTHIC, MELCOR) and those with equilibrium (FIPLOC, FUMO).

- **FIPLOC/RALOC Group**

All FIPLOC/RALOC are similar to the reference calculation. They reflect well the experimental data with a tendency of underprediction of the superheating in the dome during phase III (Fig. 4.12b/h).

- **CONTAIN Group**

VUJE and FZK have results similar to the reference calculation, ECN is close to the experiment. Parametric studies done by ECN and CIEMAT show that this difference is caused by the choice of the convection and radiation heat transfer ("dry heat transfer") coefficients. ECN has a larger "dry heat" transfer coefficient since it uses natural convection plus radiation, while CIEMAT uses natural convection only (Fig. 4.12c/i).

- **MELCOR Group**

The MELCOR calculations can be classified in three categories:

- ENEA, KAERI and VUJE calculate always saturation,
- NUP, RIAR, KI and RAS are in agreement with the experiment when saturation occurred. But they tend to be close to saturation by either underpredicting the time spans of saturation or calculating too low superheating,
- SNL, STUD and CTN overpredict the superheating.

4.4.1.7 Sump Levels and Temperatures

Fig. 4.13a and 4.13b show the sump water levels in the lower inner compartment R8 and in the annulus for the reference calculations. The experimental values can be used only for orientation since until 4 h water was drained out in order to allow the controlled air removal from the bottom of the annulus. The deviations between calculated levels, which can be discussed only qualitatively, have the following reasons:

- The codes use different drain models, this results in a different distribution of drain flow throughout the containment, especially for condensate draining out of in the dome,

- the steam condensation in the individual compartments varies between the calculations,
- in some calculations part of the condensate stays in the upper containment compartments, e. g. CIEMAT (CONTAIN) 9%, mainly water film on the walls, Battelle (GOTHIC) 13%, in the outer compartments, upper annulus, dome, R2 and NUPMEL (MELCOR) 16%, mainly in pools modelled in R2, upper outer compartments,
- FIPLOC and FUMO have almost all condensate in the sumps.

Since most of the water is collected in the sumps of the annulus and lower outer compartments, sump water temperatures of these compartments are shown in Fig. 4.14a and 4.14b for the reference calculations. The experimental value can only be used for orientation, because the sump has a temperature gradient from the warm atmosphere to the cold bottom and the thermocouple is 0.1 m above the sump bottom. With respect to the atmosphere and sump bottom temperature it can be concluded that all calculations overpredict the energy flow into the sump.

GRS/IPSN (FIPLOC) and GRS/IPSN(RALOC) are the closest to the measurement. From 10 h on the FIPLOC temperature is about 20 °C higher than the experiment. The others calculate generally higher temperatures, up to 50 °C.

The differences in the calculated sump temperatures can be explained by the following modelling features:

- The energy exchange of the condensate with the walls and the atmosphere on its way to the sumps,
- Coupling with the atmosphere above the sump,
- Heat flow from the sump water to the bottom.

MELCOR and GOTHIC calculate a coupling between atmosphere and sump, which is close to thermal equilibrium. This increases the sump temperatures towards the atmospheric temperature, as can be seen during phase V when the sump temperature follows the rapid increase of the atmospheric temperature. CONTAIN does not show this rapid sump temperature increase during phase V. This is an indication of a more realistic coupling. FIPLOC and FUMO show also a more realistic coupling. The

FIPLOC results are achieved by modelling the sumps as extra nodes only thermally connected to the atmosphere by heat conductors.

The results of the other calculations show basically the same behavior of the sump temperature as the relevant reference calculation. Only the sump temperatures of the MELCOR calculations which do not simulate the stratification in the inner compartments are higher in the lower outer compartment and lower in the annulus compared to the reference calculation.

The effect of sump temperature on the pressure is quantified in the appendix.

4.4.1.8 Heat Transfer

The heat flux from the containment atmosphere to the structures is nearly proportional to the steam injection rate, since almost all injected steam condenses on the structures. In principle the variables, which have been submitted by the participants, can be compared with data estimated from measurements, but some only with a large degree of uncertainty. Therefore a comparison will be given for some selected variables only like structure temperature, temperature differences between atmosphere and structure and wall condensation rate.

- **Structure Temperature and Temperature Difference**

Fig. 4.15a to 4.15f show the atmospheric temperature in the dome and the surface temperature on the containment side of structure 8 both for the experiment and the reference calculations. In the experiment the differences between these temperatures are generally very small. Since almost during the entire experiment steam condenses on structure 8 indicating a large heat transfer coefficient and atmospheric conditions at or very close to saturation. An exception is phase III when superheating occurred. In addition the temperature 1 cm inside the structure is shown for the calculations.

NUP-MEL (MELCOR) and UPISA (FUMO) (Fig. 4.15d and 4.15f) calculate always saturated atmosphere conditions and generally a very small temperature difference between wall and atmosphere, showing a high heat transfer coefficient. This is in good agreement with the experiment, except for phase III.

IPSN/GRS-Fs (FIPLOC) (Fig. 4.15b) calculates generally saturated atmospheric conditions. From 5 to 15 h, when the dome atmosphere consists almost completely of steam, the calculated temperature difference between atmosphere and wall surface is like the experiment very small. Afterwards with a steam - air mixture in the containment the temperature difference is about 4 °C higher.

CIEMAT (CONTAIN) and Battelle (GOTHIC) (Fig. 4.15c and Fig. 4.15e) calculate generally a too high temperature difference between atmosphere and surface, because superheated instead of saturated conditions are simulated.

Fig. 4.16a to 4.16f show the atmospheric temperature in upper annulus and the temperature 1 cm inside of structure 3 again for both the experiment and for the reference calculations. The smooth temperature history of the experimental atmospheric temperature up to 15 h indicates conditions at or very close to saturation (Fig. 4.16a). The following unregular behavior up to 28 h indicates superheating. During the strong heat up of the wall from 3 to 6 h the temperature difference between the atmosphere and 1 cm in the concrete is large (at 5 h around 20 °C), indicating the large heat flow. Towards the end of the heat up phase (10 h) it is only 10 °C.

IPSN/GRS-Fs (FIPLOC), CIEMAT (CONTAIN), NUP-MEL (MELCOR) (Fig. 4.16b to 4.16d) calculate the same temperature behavior and approximately the same temperature differences between atmosphere and 1 cm inside the structures as in the experiment.

Battelle (GOTHIC) (Fig. 4.16e) calculates temperature data similar to the experiment, however the temperature differences between the atmosphere and 1 cm inside the wall are much smaller. The reason is that the 2 mm thick coating is not simulated. This affects also the calculated pressure.

UPISA (FUMO) (Fig. 4.16f) calculates a slower temperature increase, since it does not simulate the stratification in the inner compartments. Therefore more steam condenses in the inner compartments and less in R9.3. The temperature differences between the atmosphere and 1 cm inside the wall are therefore first somewhat lower, at 10 h however similar to the experiment.

- **Wall Condensation Rates**

The measured wall condensation rates can only be used for orientation, i.e. the results are more qualitatively than quantitatively. The calculations are compared to the measurement in the annulus for structure 2 at 5 m elevation (Fig. 4.17a to 4.17e). The experimental behavior is matched quite well by the calculations which simulate the stratification in the inner compartments. The calculations, which do not simulate this stratification however get more steam into the inner compartments and less into the annulus and have therefore a lower wall condensation rate.

- **Heat Flow**

Fig. 4.18a shows the heat flow to structure 3 calculated by the reference calculations of the different codes. They reflect the wall condensation rates.

Fig. 4.18b shows the heat flow densities (KW/m^2) at different locations calculated by IPSN/GRS-Fs. They are typical for the codes calculating the stratification in the inner compartments. First the maximal heat flux takes place in the dome then it is shifted more into the annulus R9.3 and R9.4 and for a smaller part into the outer compartment R6.

Fig. 4.18c shows the heat flow densities calculated by UPISA, which calculates an intermediate stratification in the inner compartments. Here the condensation in the outer compartment R6 is greater compared to IPSN/GRS-Fs.

4.4.2 Comparison of Aerosol Results

The NaOH concentrations in the lower inner compartment R3, the dome and the annulus (see also Fig. 3.12) are depicted for each participant in order to investigate the aerosol distribution within the multicompartment geometry. Additionally in the overlay plots the aerosol parameters of different codes are plotted in five groups: CONTAIN, MELCOR part 1 and 2, FIPLOC, and the stand alone codes plus ECART.

In all compartments except the annulus measured aerosol concentrations for $t > 26$ h are unrealistically high. This behavior can only be explained by assuming an additional aerosol source e. g. rust aerosols from the steam generator or resuspended

NaOH from the common part of the steam-aerosol-injection system. Therefore, all NaOH-concentrations being less than $2 \cdot 10^{-6}$ kg/m^3 are indicated in the plots by brackets and not regarded in the evaluation.

4.4.2.1 NaOH Concentration and Depletion in the Dome

The two filter stations installed in the dome at the elevations of 6 m and 7.6 m measured NaOH aerosol concentration differences up to a factor of 3.7 due to temporary inhomogenities. In the plots an average value is drawn. However, at the end of the first injection phase this average value is too high. The theoretical maximal concentration is 7 g/m^3 assuming the 2.21 kg NaOH are well mixed in the upper outer compartments R5, R7, and the dome zones R9.1 and R9.2 without any deposition. Thus it is correct that nearly all calculations predict the maximum NaOH concentration of about 4 g/m^3.

- **CONTAIN (Fig. 4.19a)**

The CONTAIN results show in the experimental phases III, V and VI a wide spread of the NaOH concentrations. Only CIEMAT matched the experimental data fairly well in all phases. VUJE overestimates significantly the concentrations in all depletion phases. The ECN calculation agrees with the experiment in phase III but underestimates strongly the aerosol concentrations in phase V. Heat transfer by radiation was considered in the CONTAIN calculation of ECN only. But there are indications that the heat transfer by radiation is overestimated effecting a too large volume condensation rate.

KI and VUJE did not use the solubility option available in CONTAIN. This explains the rather dry NaOH behavior of the VUJE calculation in phase III but not that in phase V in which intensive volume condensation was detected (see Tab. 4.8).

- **MELCOR (Fig. 4.19b and 4.19c)**

The NaOH aerosol concentrations in the dome calculated by MELCOR show in general a more uniform behavior compared to the CONTAIN calculations. In phase III all aerosol depletion curves are significantly flatter than measured and the aerosol concentrations at the end of this phase lie about one order of magnitude over the experimental ones. This is due to the fact that the solubility effect is not modelled in the

MELCOR standard version. With the non-standard version of MELCOR used by SNL which includes the solubility effect this discrepancy is slightly reduced but not eliminated.

- **FIPLOC (Fig. 4.19d)**

In phase III all FIPLOC calculations reproduce the measured NaOH concentrations in the dome fairly well and the spread of the different calculations is small. In phases V and VI the two GRS/ISPN calculations and the JRC calculation have a similar depletion behavior. In agreement with the measurement the slope of the decay curves in phase V increases in time indicating a growth of the droplets. The water condensing in the volume is distributed on a rapidly decreasing number of particles. The fast aerosol decay is somewhat overestimated by GRS/IPSN and more by JRC. JRC uses a temperature boundary on the outer side of the containment wall of 10 ^{0}C instead of 22 ^{0}C and a different heat transfer option compared to GRS/IPSN (see Tab. 4.3).

The two IFE curves deviate from the other FIPLOC calculations and have greater aerosol concentration than measured. This deviation is caused by an artificial mixing of the dome and the upper annulus. Two parallel flow paths with different junction hights were installed by mistake. Water loaded particles are dried in the slightly superheated annulus. That reduces the aerosol decay in the dome.

- **ECART, MACRES, MOSAIC, and REMOVAL (Fig. 4.19e)**

The measured NaOH concentrations in the dome are closely matched in phases III, IV and V by the NUPEC calculation with MACRES. But in phase VI the concentrations are overestimated while the calculated amount of airborne water decreases (see Fig. 4.21e and chapter 4.4.2.4).

The NaOH concentrations calculated by JAERI with REMOVAL are underestimated by about one order of magnitude in phase III. This deviation is partly caused by a too early termination (20 min) of the first aerosol injection. In phases V and VI the aerosol concentrations are simulated considerably larger than the experimental data.

The results of the single volume calculation by IKE with MOSAIC are compared to the experimental value of the dome. In phase III the NaOH concentrations are quite well

predicted. In phase V greater values are attained and at the beginning of phase VI the concentration curve drops suddenly. The calculation ends at t = 26 h.

In the ECART calculation the measured NaOH concentration is matched quite well in phase III although the solubility effect is not modelled. This is achieved by unrealistically large primary particles (see chapter 4.4.2.5). The determined aerosol decay is in the first half of phase V similar to the measured one but in the second half and in phase VI it is much too slow because nearly no volume condensation is calculated.

4.4.2.2 NaOH Concentration and Depletion in the Upper Annulus

The aerosol behavior in the dead ended annulus is almost independent from that in the inner compartments and the dome. In phases V and VI the NaOH concentrations in R9.3 are significantly higher than in all other compartments in the containment because of the temporarely superheated conditions (see chapter 3.3.5). For each participant the data for the annulus are plotted together with the data for the dome and lower inner compartment R3 in Fig. 20a to 20w.

- **CONTAIN**

In phase III all CONTAIN calculations, except VUJE track the measured concentrations well. The VUJE concentrations are too high because of the dry character of the calculation.

In the phases V and VI ECN strongly underpredicts the NaOH concentrations. The KI results show a similar behavior to those of the FIPLOC calculations by GRS/IPSN and JRC. The measured values are matched fairly well up to t = 27 h then they drop fast due to the onset of volume condensation, which occurs in the experiment later.

- **MELCOR**

Because of the mostly 'dry' conditions in R9.3 the agreement between the MELCOR results and the experiment is better than in the other compartments.

In phase III the aerosol decay rate is underestimated by all MELCOR calculations causing an overprediction of the NaOH concentration by more than one order of magnitude. Only RAS agrees well.

In phases V and VI most concentrations calculated with MELCOR are somewhat higher than the measured values. RAS, SNL, and partly VUJE, are in a quite good agreement with the measurement.

- **FIPLOC**

The five FIPLOC calculations match the measured NaOH concentrations in the upper annulus R9.3 in phase III fairly well. Partly in phase III and in phases V and VI the IFE calculations have a deviating behavior because of the artificial mixing between the dome and the upper annulus. It effects an earlier beginning of the volume condensation in the annulus.

At t = 27 h the GRS/IPSN calculation and the JRC calculation give a rapid drop of the calculated NaOH concentrations reflecting a noticeable increase of the aerosol removal rate. Droplet size and airborne water concentration increase after the onset of volume condensation, which is ealier than in the test (see Tab. 4.8).

- **ECART, MACRES and REMOVAL**

The NaOH depletion rate calculated by JAERI with REMOVAL for the annulus is much smaller than measured. But the calculated particle sizes are very large (phase III: MMD = 15 - 20 µm and in phases V and VI: MMD = 5 - 12 µm). The NaOH concentration in the dome is temporarily lower than in R9.3. A reason for this discrepancy could not be determined.

The NaOH concentration history calculated by NUPEC with MACRES has the same shape as the measured points but all values lie about 2 orders of magnitude below them except at the beginning of phase III and at the end of VI.

The NaOH concentration in the upper annulus calculated by ENEL with ECART is in good agreement with the measurement.

4.4.2.3 Spatial NaOH Aerosol Distribution

The NaOH aerosol was distributed by atmospheric flows in different compartments of the model containments. Considerable aerosol concentration differences between adjacent compartments were established in stagnant, stratified atmospheres. In

compartments mixed by atmospheric flows the NaOH concentration differences were rather small and the thermal hydraulic conditions were similar.

- **CONTAIN (Fig. 4.20a to 4.20d)**

In the CIEMAT and the KI calculations the measured NaOH aerosol distribution is reproduced fairly well. But contrary to the experiment the concentration in R3 exceeds that of the dome in phase III.

With the beginning of phase VI when steam is injected into R5 the NaOH concentrations calculated by CIEMAT split up. In the upper compartments R7, R8, and the dome they drop faster because of the fog formation. The calculated concentrations are about one order of magnitude higher than measured. In the experiment the splitting is not detected.

The ECN calculation qualitatively shows the measured NaOH distribution. However, it is effected by the too strong aerosol depletion in phase V.

The VUJE prediction also qualitatively reflects the experimental distribution. In this calculation the distribution is effected by the nearly 'dry' aerosol behavior.

- **MELCOR (Fig. 4.20e to 4.20m)**

In most of the MELCOR calculations (CTN, ENEA, KAERI, KI, SNL, and STUD) the differences between the calculated NaOH concentrations in all compartments without the annulus are very small or disappear in phase III. This behavior is in strong contradiction to the measured inhomogenous aerosol distribution. In the calculation the atmospheric stratification is not established (see Tab. 4.8). The reason is a too intensive atmospheric mixing in this stagnant phase III. This unrealistic mixing occurs again in phase VI when the stratification is reestablished.

The stratification between the dome and the dead ended annulus is correctly calculated.

The NUP, RAS and VUJE calculations simulate in phase III temporary aerosol concentration differences. A concentration splitting in phase VI is comparable to that of CIEMAT with CONTAIN.

The largest aerosol concentration differences in phase III are given by the RAS calculation and have therefore the best agreement with the measured distribution of all MELCOR calculations. In phase VI a splitting of the NaOH concentrations is predicted. But the higher concentrations are in the upper compartments. RAS is the only calculation with an aerosol leakage simulated.

- **FIPLOC (Fig. 4.20n to Fig. 4.20r)**

The aerosol distribution is fairly well predicted by GRS/IPSN and JRC with FIPLOC. In the annulus the concentrations drop at t = 27 h to small values caused by the onset of the volume condensation in the calculation. In the experiment this sudden NaOH concentration decrease was not detected. But in the upper annulus fog formation was detected in the second half of phase VI.

The aerosol distribution obtained by IFE diverge from the experiment. The concentrations in the dome and the annulus are nearly equal because of an artificial mixing. Two parallel flow paths with different junction hights were used by mistake.

IFE calculates a splitting of the NaOH concentrations similar to that of RAS with MELCOR at the beginning of phase VI. Droplets coming from the dome are dried in the upper annulus. The second IFE-calculation, in which the steam leakage was modelled, has the same over all behavior.

- **ECART, MACRES and REMOVAL (Fig. 4.20s to 4.20v)**

The concentration differences simulated with REMOVAL by JAERI are in parts much larger than the measured ones. Contrary to the experiment no mixing is achieved in the mixing phase V. The dry character of the calculation enlarged this discrepancy.

In the MACRES calculation made by NUPEC the calculated concentration differences are in parts considerably larger than in the experiment.

In the ECART calculation by ENEL the aerosol concentration difference between the dome and the annulus is well predicted. But in contradiction to the experiment the aerosol concentration in the inner compartment R3 exceeds significantly the concentration in the dome during the phases III and VI.

4.4.2.4 Airborne Water Concentration

The calculated airborne water concentrations are depicted in Fig. 4.21a to 4.21e.

Between the CONTAIN calculations the predicted airborne water concentrations (Fig. 4.21a) differ widely reflecting the spread of the NaOH concentrations.

KI and VUJE did not use the solubility option available in CONTAIN. This explains the rather dry NaOH behavior of the VUJE calculation in phase III but not that in phase VI in which intensive volume condensation was detected (Tab. 4.8).

Tab. 4.8: Detected Fog and Measured Humidities

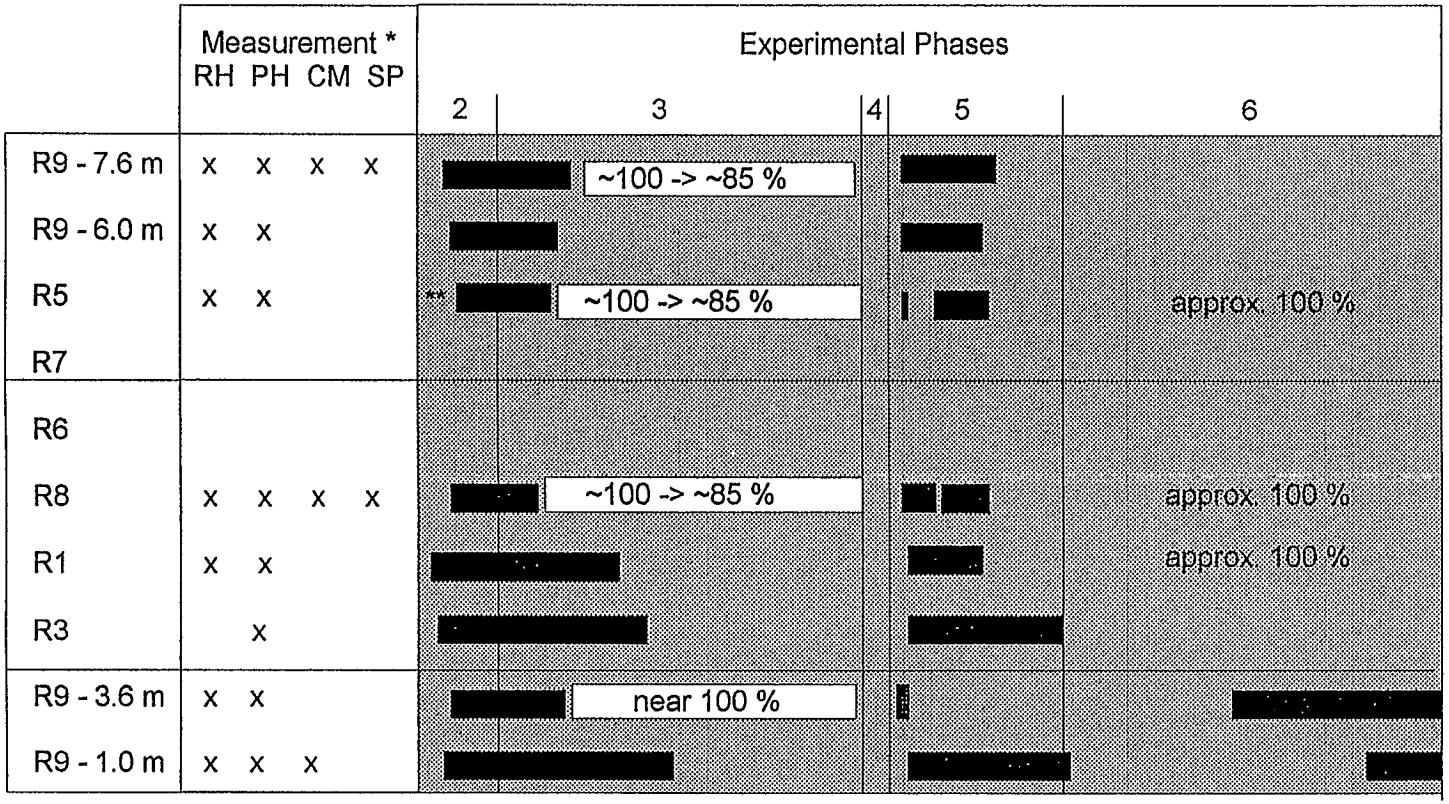

*) measurement errors see chapter 3.1.2

**) stratified, upper part superheated in ph. 2

Legend:
RH humidity sensor
PH extinction photometer
CM calorimeter
SP spectral photometer

fog on hygroscopic NaOH particles detected (rh ⩽ 100%)

85 % superheated conditions (rh < 100%) measured

Although the solubility effect is not considered by KI there is much water on the particles. In the KI simulation this airborne water (fog) was produced in the heat up phase I (40 g/m³) and did not disappear during the first aerosol injection. This behavior is contrary to all other calculations and to the experiment. Only very little fog was detected in the dome at the beginning of the first injection period.

SNL and RAS calculate a significant amount of airborne water in phase III, which leads to the fastest drop of the aerosol concentration of all MELCOR calculations in this period. As in phase III also in the phases V and VI the aerosol decay is generally underpredicted by MELCOR. Only the KAERI and NUPEC calculations give a stronger decay in phase V matching the experimental NaOH data much better than the others. But in phase VI the KAERI and NUPEC concentrations are also too high. The too slowly dropping aerosol concentrations are in correspondence with the low airborne water content. In phase V only SNL, RAS and KAERI calculate noticeable amounts of water. In the experiment fog was detected in all parts of the containment in phase V.

In none of the FIPLOC calculations fog was simulated in the heat-up phase I. In the phases II to V there is nearly no spread of the calculated airborne water concentrations (Fig. 4.21d).

4.4.2.5 NaOH Particle Size

- **Mass Median Diameter (MMD)**

In the experiment the NaOH droplets were sampled on filters. The filters were dried and then evaluated with a scanning electron microscope, which caused a shrinkage of the droplets. This shrinkage depends on the H_2O and NaOH mass fractions in the droplets. The theoretical ratio of the dry particle to the wet particle diameter is 0.68, 0.35 and 0.17 for the ratios m_{H2O}/m_{NaOH} = 1, 10 and 100. Therefore the calculated MMDs of the NaOH + H_2O droplets and the measured MMDs of the dry NaOH particles cannot be compared directly. In the plots (Fig. 4.22a to 4.22e) the measured dry particle sizes are put into brackets. Calculated MMDs showing a good agreement with the measured MMDs (e. g. for most MELCOR calculations) belong to calculations with unrealistically small airborne water concentrations.

The calculations with solubility effect (CIEMAT and ECN with CONTAIN, and all FIPLOC calculations) give a strong increase of the MMD with a maximum of about 6 µm at the beginning of phase III. After approximately one hour the MMDs are reduced as a consequence of decreasing humidities and the sedimentation of the larger particles. The MELCOR calculations predict dry particle sizes. In the SNL simulation with the non-standard version including the solubility effect the MMD is not significantly increased.

In phases V and VI the tendencies are the same: A strong increase of the particle sizes in the calculations of GRS/IPSN and JRC; differing but remarkable increase in the IFE, CIEMAT and ECN calculations; relatively small particles (MMD < 3 µm) in all MELCOR calculations, KI and NUPEC predict even MMD < 1.5 µm.

The mass median diameters predicted by JAERI with REMOVAL and NUPEC with MACRES in phases III and V are higher than those predicted by all other codes. Maximum MMDs of 25 µm in the JAERI calculation and 15 µm in the NUPEC calculation are reached.

The MMD in the IKE simulation with MOSAIC is about 0.5 µm and nearly constant throughout the experiment. It corresponds with the aerosol depletion rate only because the plate out by diffusiophoresis is in this calculation much higher than the deposition by sedimentation. This result is unrealistic.

- **Geometric Standard Deviation**

Geometric Standard Deviations (GSD) for the total aerosol in the dome are plotted in Fig. 4.23a to 4.23d. All submitted GSD lie near 2.0 and match the measured values derived from the dried NaOH samples quite well. In phase VI only the MELCOR calculations by STUD and NUPEC produced broader aerosol size distributions with GSD > 4.0. Both calculations have oscillating airborne water concentrations in this period.

- **Particle Size Distribution**

The measured and calculated particle size distributions of the NaOH component in the dome at t = 18.14 h (end of first aerosol injection) are depicted in Fig. 4.24a to Fig. 4.24e. The droplet size distributions are normalized by dividing the mass concentrations in each size class by the particle size range of this class.

A direct comparison of the measured with the calculated particle size distribution is not possible due to the drying process in the measurement procedure.

In calculations without Kelvin effect the condensing water distributes uniformly on all particles. Only JAERI considered in the calculation with REMOVAL the Kelvin effect. But the results are not strongly effected.

4.4.2.6 Mass Balance

The mass balance for the NaOH and the airborne water include the airborne state, the settled masses on the floor and the masses plated out by diffusion and diffusiophoresis onto all surfaces in the containment. The NaOH and water respectively deposited on the containment surfaces could not be measured.

- **NaOH mass balance at t = 30 h**

Tab. 4.9 gives the aerosol mass balance at t = 30 h provided by the participants. Most of the calculations determine a total NaOH inventory equal or close to the injected 2.93 kg NaOH.

Tab. 4.9: Mass Balance NaOH Calculated

Code	Participant	Airborne NaOH [kg]	Settled NaOH [kg]	Diffused NaOH [kg]	Total NaOH [kg]
CONTAIN	CIEMAT	$1.46\ 10^{-02}$	2.39	$5.39\ 10^{-01}$	2.94
	ECN	$2.58\ 10^{-03}$	2.63	$4.32\ 10^{-01}$	3.06
	KI-CON	$2.04\ 10^{-03}$	2.30	$6.25\ 10^{-01}$	2.93
	VUJE-CON	$2.25\ 10^{-03}$	2.12	$6.85\ 10^{-01}$	2.81
MELCOR	CTN	$2.46\ 10^{-02}$	2.02	$8.97\ 10^{-01}$	2.94
	ENEA	$2.53\ 10^{-02}$	2.91	$4.09\ 10^{-03}$	2.94
	KAERI	$1.40\ 10^{-02}$	3.02	$1.17\ 10^{-03}$	3.04
	KI-MEL	$2.55\ 10^{-02}$	2.52	$3.78\ 10^{-01}$	2.92
	NUPEC	$1.51\ 10^{-02}$	2.04	$8.06\ 10^{-01}$	2.86
	RAS	$3.64\ 10^{-05}$	2.73	$1.95\ 10^{-01}$	2.93
	SNL	$2.49\ 10^{-03}$	2.59	$3.35\ 10^{-01}$	2.92
	STUD	$2.70\ 10^{-01}$	2.86	$4.20\ 10^{-02}$	3.17
	VUJE-MEL	$1.36\ 10^{-02}$	2.92	$6.07\ 10^{-03}$	2.93
FIPLOC	IPSN/GRS-Fs	$7.13\ 10^{-12}$	2.62	$9.35\ 10^{-02}$	2.71
	GRS/IPSN-Fe	$2.54\ 10^{-05}$	2.58	$2.00\ 10^{-01}$	2.78
	IFE-1	$5.05\ 10^{-04}$	2.81	$2.42\ 10^{-01}$	3.05
	IFE-2	$2.66\ 10^{-04}$	2.86	$1.88\ 10^{-01}$	3.05
	JRC	$2.08\ 10^{-05}$	2.34	$1.26\ 10^{-01}$	2.40
ECART	ENEL				
MACRES	NUPEC	$1.76\ 10^{-04}$	2.90	$3.58\ 10^{-02}$	2.93
MOSAIC	IKE				
REMOVAL	JAERI	$1.37\ 10^{-02}$	2.68	$1.52\ 10^{-03}$	2.69
	EXPERIMENT	$4.44\ 10^{-04}$			2.93

At the end of the VANAM M3 test 0.044 g of the injected NaOH was still airborne most of it in the annulus. The CONTAIN calculations overestimate this airborne mass noticeably and the MELCOR calculations without RAS considerably. The FIPLOC results lie in the same order of magnitude with experimental value or underestimate it. Only the GRS/IPSN calculation with the standard nodalization predicts almost no airborne NaOH.

The diffused mass calculated with FIPLOC (0.09 - 0.24 kg) is smaller than that calculated with CONTAIN (0.54 - 0.68 kg). The MELCOR values spread widely (0.006 - 0.9 kg). MACRES (0.03 kg) and REMOVAL (0.0015) determined considerably smaller diffused masses.

- **Airborne Water Balance at t = 30 h**

Table 4.10 gives the distribution of the airborne water (fog) at t = 30 h.

Tab. 4.10: Mass Balance Fog Calculated

Code	Participant	Airborne fog [kg]	Settled fog [kg]	Diffused fog [kg]	Total fog at t = 30 h [kg]	Total fog at t = 22,6 h [kg]	Fog formed in ph. 4,5,6 [kg]	Remarks
CONTAIN	CIEMAT	2.09E+00	1.24E+02	5.49E+01	1.81E+02	1.66E+02	1.51E+01	
	ECN	1.47E+01	1.41E+03	4.03E+02	1.83E+03	1.49E+03	3.38E+02	
	KI-CON	8.30E+00	2.45E+03	6.98E+02	3.16E+03	2.69E+03	4.70E+02	much fog in phase 1
	VUJE-CON	5.04E+00	1.58E+02	2.15E+02	3.78E+02	3.26E+02	5.18E+01	
MELCOR	CTN	4.96E+00			4.96E+00	1.56E-04		only airborne data
	ENEA	2.94E+00	1.51E+04	7.31E+01				includes wall condensate
	KAERI	3.04E+00			3.04E+00			only airborne data
	KI-MEL	1.19E+00	5.66E+01	7.76E+01	1.35E+02	6.08E+01	7.45E+01	
	NUPEC	1.37E+00	1.57E+02	6.41E+01	2.22E+02	1.73E+02	4.94E+01	
	RAS	3.80E+02	1.74E+04	1.34E+02				includes wall condensate
	SNL	3.16E+00			3.16E+00	7.85E-01		only airborne data
	STUD	5.50E-01	1.68E+04	5.41E+02				includes wall condensate
	VUJE-MEL	1.63E+00	4.36E+01	1.16E+02	1.61E+02	8.94E+01	7.16E+01	
FIPLOC	IPSN/GRS-Fs	2.81E+00	3.20E+02	1.89E+01	3.42E+02	2.42E+02	9.96E+01	
	GRS/IPSN-Fe	5.26E+00	2.73E+02	2.54E+01	3.04E+02	1.27E+02	1.77E+02	
	IFE-1	1.09E+01	3.00E+02	2.46E+01	3.36E+02	7.39E+01	2.62E+02	
	IFE-2	1.60E+01	4.45E+02	3.57E+01	4.97E+02	7.64E+01	4.20E+02	
	JRC	1.65E+01	6.04E+02	2.42E+01	6.45E+02			
ECART	ENEL							almost no fog calculated
MACRES	NUPEC	7.95E-02	4.49E+03	6.67E+00	4.49E+03	1.06E+03	3.43E+03	
MOSAIC	IKE							little fog calculated
REMOVAL	JAERI	3.53E-02	8.26E+02	1.25E-01	8.26E+02	7.95E+02	3.08E+01	

The volumes for the settled fog in the MELCOR calculations by ENEA, RAS, and STUD include also wall condensate and cannot be further evaluated.

The highest amount of total fog formed is calculated by ECN and KI with CONTAIN. The KI values include a relatively high amount of fog during the heat up phase, when no NaOH aerosol was present.

The values for the total fog formed, which are mostly governed by the thermal-hydraulic models, differ both between the results of one code group and the results of different codes as well. The first shows a distinct user influence.

Table 4.11 summarizes the fog generated in phases IV, V and VI in which the solubility effect is of minor importance. Some unrealistically high values (ENEA, RAS and STUD) which probably include condensate from the wall are not considered.

Tab. 4.11: Fog formation in Phases IV, V, and VI

Code	Fog formed in phases IV, V, and VI [kg]	Remarks
CONTAIN	15 - 470	
MELCOR	49 - 74	
FIPLOC	100 - 420	
REMOVAL	31.00	RH from experiment, solubility effect only

The calculated total airborne water masses spread widely reflecting the differences in the NaOH aerosol depletion curves.

4.5 Computational Effort

Tab. 4.12 gives some information about the computational effort of the participants to run their simulations. In order to estimate the relative speed of the different computers, the participants executed a test case "linpackd" that was provided by the ISP organizers and supplied the necessary computing time. From this time, the cpu time for the ISP37 simulation, and the number of atmospheric nodes a normalized effort was calculated which can be used to compare the computational requirements of the

different codes. Highest efforts are associated with MELCOR if small time steps are applied, which is necessary to avoid too much numerical diffusion. An enhanced effort is shown by FIPLOC if the options for hygroscopic aerosol behavior are active. Also MOSAIC and REMOVAL show higher efforts.

Tab. 4.12: Computational Effort for ISP37 Calculations

Organisation	Code/Nodes	Strat.	Computer	linp	cpu	effort	Dt
FZK	CONTAIN/11	y	RISC 6000/370	1.5	10	6.7	1.0
ECN	CONTAIN/11	y	RISC 6000/320H	13.	2.6	0.2	
VÚJE	CONTAIN/11	y	Pentium 90 MHz	5	1.5	0.3	
Kurchatov	CONTAIN/11	y	486DX/100MHz		75		
CIEMAT	CONTAIN/12	y	RISC 6000	3.4	12.5	3.4	< 1.4
ENEL	ECART/15		RISC 6000/250T	1.9	6.1	2.4	0.16
IfE	FIPLOC/10	y	HP715/50MHz	8.3	17.5	2.3	10
GRS/IPSN	FIPLOC/23	y	IBM 9000	3.2	8.2	1.2	
GRS/IPSN	FIPLOC/11	y	IBM 9000	3.2	6.4	2.0	
JRC Ispra	FIPLOC/Th/ 11/Th+Ae/11	y y	Sun SPARC 19 CONVEX 3860	7.7 5.1	0.14	0.02	
GRS/IPSN	RALOC/Th/23	y	RISC 6000/550	1.2	2.2	0.9	
Uni Pisa	FUMO/Th/13	~	RISC 6000/250	2.2	1.6	0.6	0.6
Battelle	GOTHIC/Th/11	y	HP735/99MHz	4.1	1	0.2	1.6
NUPEC	MACRES/Ae/11		Sun SPARC 20	9	24	6.7	3
KAERI	MELCOR/11	n	Sun/670 MP	7.6	12.5	1.6	11
NUPEC	MELCOR/11	y	DEC 3000/900	0.4	5.7	14.3	1
Sandia	MELCOR/11	n	Sun SPARC 10	12.	8.8	0.73	
UPM	MELCOR/17	~	DEC2000 Alpha	0.5	2.9	3.8	15
RIAR	MELCOR/11	n	Pentium 66		7.1		
RAS	MELCOR/11	y	RISC 6000		10		
ENEA	MELCOR/11	n	RISC 6000	5.4	55	10.2	
Kurchatov	MELCOR/13	~	Pentium120MHz	3.8	8	1.8	1.8

Organisation	Code/Nodes	Strat.	Computer	linp	cpu	effort	Dt
Studsvik	MELCOR/11	n	Sun SPARC 630	9.0	3.2	0.4	
VÙJE	MELCOR/13	~	Pentium 90 MHz	5	16	2.7	
IKE	MOSAIC/Ae/1		DEC Alpha	1.6	0.5	3.4	
JAERI	REMOVAL/Ae/11		Sun SPARC 20	3.0	8.5	2.8	4.8

linp: cpu time (s) for linpackd sample case

cpu: cpu time (h) for ISP37 calculation

Th: thermal-hydraulics only calculation

effort: (11*cpu)/(nodes*linp)

Dt: average time step (s)

Ae: aerosol only calculation

Strat: Stratification in inner rooms simulated: y = yes, n = no, ~ = intermediate

5 Summary and Assessment

The objective of the International Standard Problem (ISP) No. 37 on atmosphere and aerosol behavior in a containment, which has been proposed by OECD-CSNI, is to analyze and describe the thermal-hydraulic and the aerosol distribution and settlement in a containment following a severe accident with core meltdown and reactor vessel pressure release through the pressurizer release valve and to examine the reliability and accuracy of containment and aerosol computer codes used in severe accident situations. The experiment selected for this ISP was the VANAM M3 test conducted in the Battelle Model Containment (BMC) at Battelle Ingenieurtechnik, Eschborn. The BMC is a large multi compartment model containment with a free volume of 626 m^3. Therefore it is well suited for investigations regarding thermal stratification, atmospheric mixing or spatial aerosol distributions.

Due to the great complexity of the experiment the ISP was conducted as an open exercise, i.e. not only the initial and boundary conditions were given to the participants for performing the calculations, but also all relevant test results. Thus a better comparison capability was given by eliminating as far as possible erroneous results.

The relatively large containment and great number of different compartments generally give many suitable possibilities to model the test facility. To facilitate the comparison a reference nodalization of the containment, which meets the basic requirements of all codes used in the ISP, was developed and distributed to the participants. Therefore the participants were asked to adhere to this nodalization as far as possible.

The ISP attracted wide support. Representatives of 22 organizations from 9 OECD member countries, two non-OECD countries and the CEC submitted a total of 23 thermal-hydraulic and 22 aerosol calculations. They used the codes CONTAIN, ECART, FIPLOC and MELCOR for both thermal-hydraulic and aerosol calculations as well, FUMO, GOTHIC and RALOC for stand alone thermal-hydraulic and MACRES, MOSAIC and REMOVAL for stand alone aerosol calculations.

Some organizations used more than one code. The great number of calculations made it possible to group the data according to the codes used and to compare the results of the codes in each group with the experiment and with each other.

The main physical variables compared in the report are temperature, pressure, atmospheric velocity and humidity for the thermal hydraulic part and aerosol and airborne water concentrations and particle size for the aerosol part. Most variables have been measured and calculated for different location in the containment.

Since several calculations were done with the same codes (CONTAIN, MELCOR, FIPLOC/RALOC), reference calculations for each code were chosen. They had to match the following criteria: Simulation of the atmospheric stratification observed in the experiment and closest use of the proposed input. This gave the possibility to compare the different codes and to find the reasons for deviations of results obtained with the same code.

At the comparison workshop, held in Cologne [50], the following observations and conclusions have been drawn by the participants and the ISP organizer:

- **Pressure**

The reference calculations predicted the containment pressure quite well with a maximum deviation of approximately 0.35 bar, which is in the range of an error band given by uncertainties of the experimental boundary conditions and the systematic overprediction due to the neglect of the unknown steam leakage. The differences between the reference calculations were only 0.2 bar. FIPLOC and CONTAIN differ mainly due to different containment air contents. The pressure calculated by MELCOR deviates from the results above mainly due to the sump modelling and the condensation heat transfer.

The deviations between the calculations using the same code are caused by modelling differences like steam leakage, environmental temperatures, condensation heat transfer models and nodalization.

The quality of the pressure comparison is reduced by the uncertainties of the experimental boundary conditions.

- **Atmospheric Temperatures**

The local atmospheric temperatures depend from the local air/steam distribution, which in turn is influenced mainly by convection between and stratification in the different compartments.

Dome: Most of the calculated dome temperatures are close to the experimental data. They lie in a band of approximately 10 ^{0}C above the experimental data. Larger deviations have their reasons in specific modelling assumptions, which do not fit the problem well.

Compartment R3: The low temperature in R3 is one indication of thermal stratification (except phase V) between the atmosphere of the upper and lower compartments. Calculations which simulate the stratification (FIPLOC, RALOC, CONTAIN, few MELCOR) follow the experimental temperature behavior, the other have a too high temperature.

- **Atmospheric Stratification and Mixing**

All calculations simulated both the upper convection loop (upper outer compartments, dome) and overall convection loop (inner and outer compartments, dome) as well, but not all calculations simulated the atmospheric stratification between the dome and the annulus. Calculations without stratification in the annulus used unfavorable deviations from the proposed nodalization (e. g. parallel flow path between dome and annulus).

The simulation of the stratification between the upper compartments R5, R7 and the lower compartments R3, R6, R8 is more difficult than in the annulus, since the proposed nodalisation allows both stratification and mixing as well. Stratification is achieved by all FIPLOC, CONTAIN and two MELCOR calculations and by the ones with GOTHIC and RALOC.

The reason for the MELCOR calculations for not calculating stratification are atmospheric oscillations which occured with larger time steps.

- **Atmospheric Flow Velocity**

The tendency of the atmospheric flow velocities is calculated correctly where stratification and mixing is in agreement with the experiment.

- **Atmospheric Humidity**

Only a qualitative comparison was possible since the experimental measurements have a large uncertainty.

FIPLOC and MELCOR reference calculations predict the atmospheric conditions for the dome throughout the complete experiment quite well, however they underpredict the superheating in the dome. CONTAIN reference calculation predicts superheated conditions in the dome instead of saturation.The CONTAIN calculation by ECN matches the humidity much better. This is caused by the use of different dry heat transfer models.

The codes using thermal non equilibrium do not have better humidity results than those using equilibrium.

- **Sump Level and Temperature**

The sump level is influenced by many experimental boundary conditions and analytical assumptions. Therefore a direct comparison of experimental and analytical results with general conclusion is not possible.

The experimental sump temperature, which has a steep gradient from surface to bottom, is measured in the lower part of the sump. All reference calculations have a higher sump temperature than measured. FIPLOC and RALOC results are relatively close to the measurement, MELCOR and CONTAIN are generally somewhat higher. Reasons for the too high analytical temperatures are the coupling between the atmosphere and the sump and the too high condensate temperature. While in the FIPLOC calculations only a connection by heat conductors exists, the coupling in MELCOR leads due to a rough nodalization to a too high heat transfer, which results in a too high sump temperature.

Heat Transfer to Structures

The heat transfer can be judged by structure temperatures, wall condensation rates and heat flow.

Results with correct steam air distributions calculate the wall condensation rates in good agreement with the measured data. The heat flow respectively the heat flow density reflect the wall condensation rate quite well.

This more or less qualitative comparison gives the impression that the heat transfer to the structures is quite well modelled by most of the codes. Differences in modelling the heat transfer, e. g. too rough nodalization or neglecting of wall coating, results in the observed pressure differences.

- **Aerosol Concentration and Depletion**

All calculations with integral codes predict the tendency of the aerosol concentration during the course of the experiment well, e. g. they calculated a correct maximum during the time of injection and a greater depletion rate during "wet" atmospheric condition than during "dry". But the actually calculated NaOH concentrations show a spread of approximately 2 orders of magnitude at the end of the "dry" depletion phase and about 5 orders of magnitude at the end of the "wet" depletion phase. Mostly the NaOH aerosol concentrations are overpredicted due to an underestimation of the droplet growth by steam condensation.

The standard version of MELCOR overestimates the NaOH concentrations in superheated conditions, because of a missing solubility model.

Under saturated conditions all FIPLOC and 2 CONTAIN results are in fairly good agreement with the experimental data, while the MELCOR data show a too low depletion rate. The deviations of the results of the stand alone code are significantly larger than those from the integral codes. Besides model improvements (e. g. modelling of the solubility effect) a more correct consideration of the thermal-hydraulic boundary conditions relevant for the aerosol behavior is necessary.

Spatial Aerosol Distribution

The measured NaOH distribution in the compartments of the model containment is well obtained by CONTAIN, ECART and FIPLOC calculations. In most MELCOR calculations the aerosol concentration differences measured within the inner compartments at atmospheric stratifications are not established because of oscillating atmospheric inter-compartment gas flows.

The stand alone codes MACRES and REMOVAL give considerably larger aerosol concentration differences within the containment than measured, due to insufficient atmospheric flow rates, which are given as input.

- **NaOH Droplet Size**

Calculations with solubility effect, e. g. some CONTAIN, all FIPLOC, MACRES, and REMOVAL results, follow the expected droplet size history, especially the increase during the "dry" depletion phase. MELCOR does not calculate the significant increase shortly after the injection phases and during the "wet" depletion phase due to the missing consideration of the solubility effect and underestimation of the volume condensation. The droplet growth by volume condensation is not sufficiently calculated by ECART. The droplet sizes calculated by MOSAIC are too low.

The calculations could not be compared directly with measurement, since due to the measurement procedure only the diameters of dry droplets have been determined.

- **Mass Balance**

While the total NaOH mass balance at the end of the experiment was calculated fairly well by all codes, the airborne part of the NaOH mass was overestimated considerably by the CONTAIN, MELCOR and REMOVAL calculations.

The calculated total airborne water mass spreads widely reflecting the differences of droplet sizes and the depletion rates.

General Observations

The ISP37 has demonstrated that the codes used could calculate the thermal-hydraulic behavior in general with sufficient accuracy. But with respect to the needs of

aerosol behavior analysis the accuracies, both analytical and experimental as well, for specific thermal-hydraulic variables like humidity, wall condensation and heat transfer should be improved.

Although large progress has been made in the simulation of aerosol behavior in multi-compartment geometries the calculated local aerosol concentrations scatter widely. However, the aerosol source term to the environment is overestimated in general. The largest uncertainty concerning the aerosol results is caused by a limited number of thermal hydraulic variables like relative humidity, volume condensation rate and atmospheric flow rate. In some codes also a solubility model is missing.

By choosing a physically correct nodalization the lumped-parameter concept was found to be basically suited to predict the inhomogenious distributions of gases and aerosols in the containment. But the user has a great influence on the calculated results, both the thermal-hydraulic and the aerosol as well, if specific nodalization features and different code options have been selected unfavorably.

Studies such as ISP37 serve to illuminate code modeling assumptions or simplifications, such as when solubility effects are not treated, and give rise to code improvements, as reported for MACRES and MELCOR after the evaluation of ISP37. In MELCOR for instance improved models like aerosol growth, enhanced the results of the aerosol behavior, especially the aerosol depletion in the "dry" phase of the test, as could be seen in post ISP37 calculation done by the code developer.

Transferring the lessons learned from ISP37 to real reactor plants the scaling and the differences in the conditions of the test investigated and an accident in a real plant have to be considered. Therefor the results of ISP37 have some limitation in the applicability for real plants.

ISP37 demonstrated the importance of assessments of this kind. Like other ISP it provided a forum for the international community enhancing the experience in dealing with thermal-hydraulic and aerosol behavior under severe accident conditions. In a future ISP special attention should be given to reactor applicability and to those thermal-hydraulic variables which have the main influence on aerosol behavior.

6 References

[1] CSNI Standard Problem Procedure
CSNI Report No. 17, November 1989

[2] T. Kanzleiter
VANAM Multi-Compartment Aerosol Depletion Test M3 with Soluble Aerosol Material
Technical Report BleV-R67.098-304 (July 1993) Battelle-Institut e.V. Frankfurt am Main

[3] Summary Record on the Preparatory Workshop on International Standard Problem No. 37 (VANAM M3 Test)
OECD, NEA/SEN/SIN/WG4(95) 7, July 1995

[4] OECD/CSNI International Standard Problem No. 29
Distribution of Hydrogen within the HDR-Containment under Severe Accident Conditions
CSNI Report NEA/CSNI/R(93)4, 1993

[5] K. Fischer, M. Schall, L. Wolf
CEC Thermal-Hydraulic Benchmark Exercise on FIPLOC Verification Experimental Phases 2, 3 and 4 - Results of Comparisons
EUR 14454 EN, 1993

[6] J. Gauvain
Post-Test Calculation of Thermal-Hydraulic Behaviour in DEMONA Experiment B3 with Various Computer Codes Used in EC Member States
Report EUR 12197 EN, 1989

[7] Deutsche Risikostudie Kernkraftwerke Phase B
Gesellschaft für Reaktorsicherheit
Verlag TÜV Rheinland, Köln, 1990

[8] M. Firnhaber, S. Schwarz, G. Weber
Specification of the ISP37, VANAM M3 A Multicompartment Aerosol Depletion Test with Hygroscopic Aerosol Material
GRS, Köln, April 1995

[9] C. Smutek, B. Schwinges
ISP37 VANAM M3 FIPLOC Calculation
IPSN, Note Technique SEMAR 96/37, Cadarache, 1996

[10] W. Klein-Heßling, C. Smutek
ISP37 VANAM M3 Detailed FIPLOC/RALOC Calculations
GRS/IPSN, 1996

[11] J. Klepác
A Brief Report on ISP 37, Vanam M3 A Multicompartment Aerosol Depletion Test with Hygroscopic Aerosol Material, Calculation Using CONTAIN 1.1.2 Code, September 1995
Nuclear Power Plants Research Institute (VÚJE), Trnava, Slovakia

[12] M. Cvan
A Brief Report on ISP 37, Vanam M3 A Multicompartment Aerosol Depletion Test with Hygroscopic Aerosol Material, Calculation Using MELCOR 1.8.3 Code, September 1995
Nuclear Power Plants Research Institute (VÚJE), Trnava, Slovakia

[13] F. Oriolo, S. Paci
Thermal-Hydraulic Simulations of the OECD CSNI ISP-37 on VANAM M3 Test Using the Fumo Code,
Università Degli Studi Di Pisa, DCMN, RL 679(95), 1995

[14] L. Nilsson
ISP37 MELCOR 1.8.3 Calculation of Aerosol Depletion Test VANAM M3, Contribution from Studsvik EcoSafe, Sweden
Studsvik EcoSafe, ES-95/55, 1995

[15] R. C. Smith
ISP37 MELCOR Calculations Using MELCOR: Results with a Simple Hygroscopic Aerosol Model
Sandia National Laboratories, September 1995

[16] A. Moskovchenko, V. Nosatov
ISP37 VANAM M3
Russian Academy of Sciences, Nuclear Safety Institute, October 1995

[17] Y. Kiso
Thermalhydraulics and Aerosol Analysis of ISP37 VANAM M3 with MELCOR Code
Nuclear Power Engineering Corporation, Tokyo, 1995

[18] C. Kröger
ISP37 VANAM M3 Post Test Calculation
JRC Ispra Establishment, October 1995

[19] J. Stuckert, A. Shaikhiev
ISP37 VANAM M3, Accompanying Report
Research Institute of Atomic Reactors, Dimitrovgrad, 1995

[20] M. Boudaev
VANAM M3 A Multi Compartment Aersol Depletion Test with Hydroscopic Aerosol Material
Russian Research Centre 'Kurchatov Institute', Moscow, October 1995

[21] D. Tomachik
VANAM M3 A Multi Compartment Aersol Depletion Test with Hydroscopic Aerosol Material
Russian Research Centre 'Kurchatov Institute', Moscow, October 1995

[22] H. D. Kim, S. W. Cho, J. W. Park
VANAM M3 A Multi Compartment Aersol Depletion Test with Hygroscopic Aerosol Material
Korea Atomic Energy Research Institute, Taejon, September 1995

[23] N. Kourti
International Standard Problem 37 VANAM M3
Institut für Kernenergetik und Energiesysteme, Universität Stuttgart, September 1995

[24] B. Fritsche
VANAM M3 A Multi Compartment Aersol Depletion Test with Hygroskopic Aerosol Material
Institut für Energetik und Umwelt GmbH, Leipzig, November 1995

[25] F. Parozzi, F. Orilio, S. Paci
ECART Results for the VANAM M3 Test
ENEL Nuclear Energy Division, Milano, January 1996

[26] J. A. Fernández-Benítez, I. Martinez Gozalo, F. Spano
ISP37 (VANAM M3 Experiment), Simulation with the MELCOR Code
Universidad Politecnica de Madrid, CTN-58/95, November 1995

[27] E. Hontanón, L.E. Herranz
International Standard Problem No. 37 on VANAM M3 Experiment, An Analysis with CONTAIN 1.12l, TN/TS-18/II-9, November 1995
Madrid

[28] G. Henneges, H. Peter
The International Standard Problem ISP37
Calcualtions with CONTAIN 1.12 for VANAM M3
Forschungszentrum Karlsruhe, FZKA 5795, Juli 1996

[29] Y. Kiso
Aerosol Analysis of VANAM M3 with MACRES Code
Nuclear Power Engineering Corporation, Tokyo, 1995

[30] M. Schall, K. Fischer
International Standard Problem No. 37: VANAM M3 - Multi Compartment Aersol Depletion Test with Hygroscopic Aerosol Material , ISP39 Thermalhydraulic Analysis using the Computer Code GOTHIC
Battelle Ingenieurtechnik, Eschborn, Report BF-V 68.334-1, October 1995

[31] N. B. Siccama
VANAM ISP-37 CONTAIN Assessment
ECN, ECN-R--96-001, April 1996

[32] T. Kudo, N. Yamano, J. Sugimoto
Accompanying Report on JAERI´s Analysis of International Standard Problem (ISP)-37 with REMOVAL Code
JAERI, 1995

[33] F. de Rosa, D. Diamanti, R. Mari
International Standard Problem ISP37: VANAM - M3 A Multi Compartment Aerosol Depletion Test with Hygroscopic Aerosol Material
ENEA, Bologna, 1995

[34] Murata K. K. et al.
User's Manual for CONTAIN 1.1; A Computer Code for Severe Nuclear Reactor Accident Containment Analysis
NUREG/CR-5026; SAND87-2309

[35] R. M. Summers et al.
MELCOR Computer Code Manuals1
NUREG/CR-6119, SAND93-2185 Vol. 2
Sandia National Laboratories(Sept. 1994)

[36] G. Weber, S. Schwarz, F. Ewig, K. Fischer
Benutzerhandbuch für FIPLOC 3.0
Gesellschaft für Anlagen- und Reaktorsicherheit (GRS)mbh
To be published

[37] W. Klein-Heßling
RALOC - MOD 4.0 User Manual
GRS-A-2308,October 1995

[38] MACRES (to be published)

[39] MOSAIC (to be published)

[40] REMOVAL (to be published)

[41] R. Fontana, E. Salina, F. Parozzi
ECART (ENEL Code for Analysis of Radionuclide Transport). Definition of the Code Architecture and Construction of the Aerosol and Vapour Transport Module
ENEL Report No. 1019/2, March 1991 (unpublished work)

[42] A. Manfredi, M. Mazzini, F. Oriolo, S. Paci
FUMO Code Manual Volume 1: System Models
University of Pisa, DCMN Internal Report RL 533 (92)

[43] T. L. George et. al.
Containment Analysis with GOTHIC. Proc. 27th National Heat Transfer Conference,
Minneapolis, MN, U.S.A., 1991

[44] F. Gelbard
MAEROS User Manual
NUREG/CR-1391, December 1991

[45] F. Gelbard
Modeling Multicomponent Aerosol Partical Growth by Vapor Condensation
Aerosol Science and Technology 12, p. 399-412, 1990

[46] H. Jordan, M. R. Kuhlmann
TRAP-MELT2 User´s Manual
USNRC, NUREG/CR-4205, BMI-2124, Washington D. C. May 1985

[47] H. Bunz, M. Koyro, W. Schöck
NAUA Mod5 und MAUA Mod5M
KFK 4278, Karlsruhe, September 1987

[48] P. C. Owczarski, K. W. Burk
SPARC-90: A Code for Calculating Fission Product Capture in Suppression Pools
NUREG/CR-5765, PNL-7723, October 1991

[49] E. Hofer
An A(α)–stable Variable Order ODE-Solver and its Application
Mathematical Methods for Solution of Nuclear Enineering Problems
Munich, 1981

[50] Summary Record on the Comparison Workshop on International Standard Problem No. 37 (VANAM M3 Test)
OECD, NEA/SEN/SIN/WG4(96)6, April 1996

7 Appendix

7.1 Additional Contributions by the Participants

Nuclear Safety Institute RRC

NUPEC

ENEL/ Uni Pisa

ENEA

Forschungszentrum Karlsruhe

NUCLEAR SAFETY INSTITUTE
RUSSIAN RESEARCH CENTRE "KURCHATOV INSTITUTE"

SOME RESULTS OF POST ISP-37 CONTAIN 1.11 CALCULATIONS

M.BOUDAEV

There are some results of post ISP-37 calculations performed in Nuclear Safety Institute RRC "Kurchatov Institute" by CONTAIN 1.11.

The differences between these calculations and the calculations which results were presented at the end of 1995 for Draft Comparison Report are:

- improved air mass in containment (during first calculation there was a mistake in air leak rate in input data);
- all structures were simulated (during first calculation structure 47 was not simulated);
- during first calculation artificial pool was simulated in R9.D. It was made for modeling of condensate drainage distribution according the recomendations of "Specification of International Standard Problem ISP-37" (page 60, fig.6). It was found that modeling of this kind was not possible for CONTAIN 1.11, because it leaded to unphysical results, but in User Manual such modeling was recomended. So new calculation was performed without modeling of artificial pool in R9.D. Condensate was drained from R9.D to R9.4.

Enclosed you will find pictures of pressure, temperatures and aerosol concentrations for this post ISP37 calculation, performed by CONTAIN 1.11.

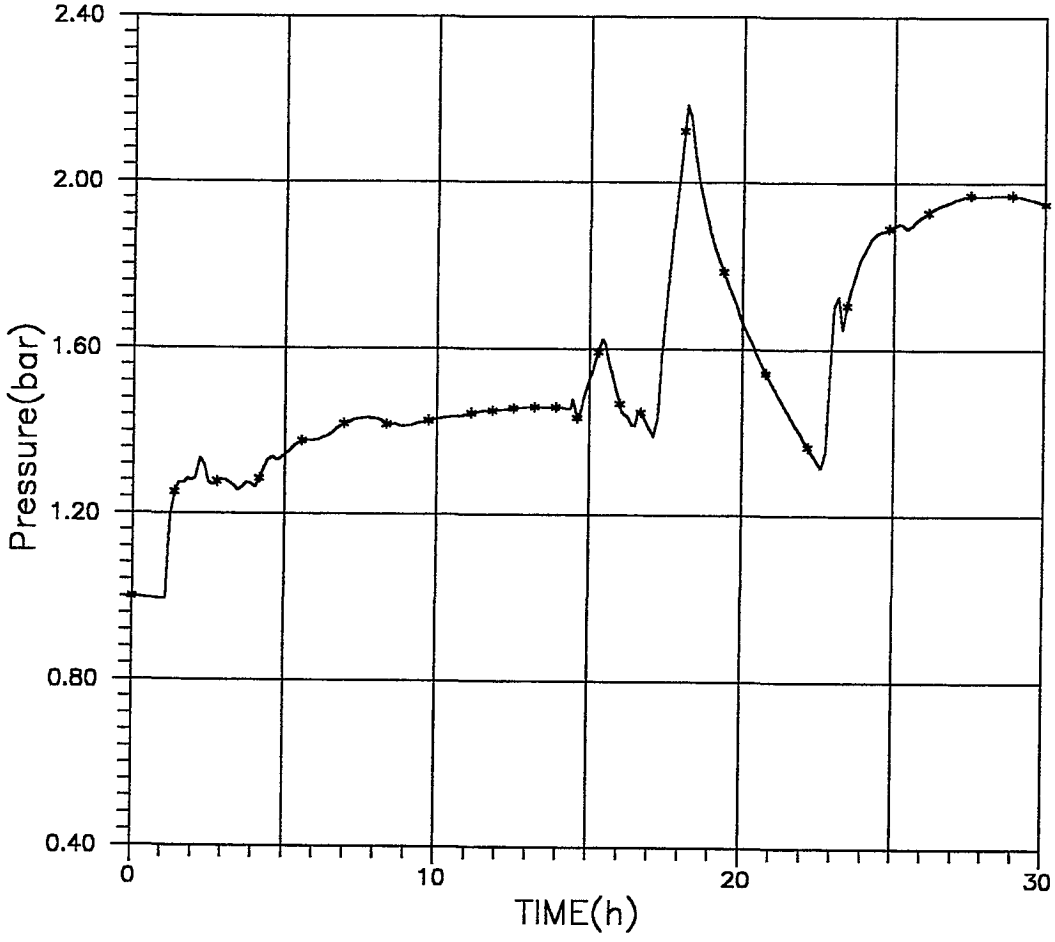

Figure 1. CONTAIN 1.11 Post ISP 37 Calculations. Containment Pressure.

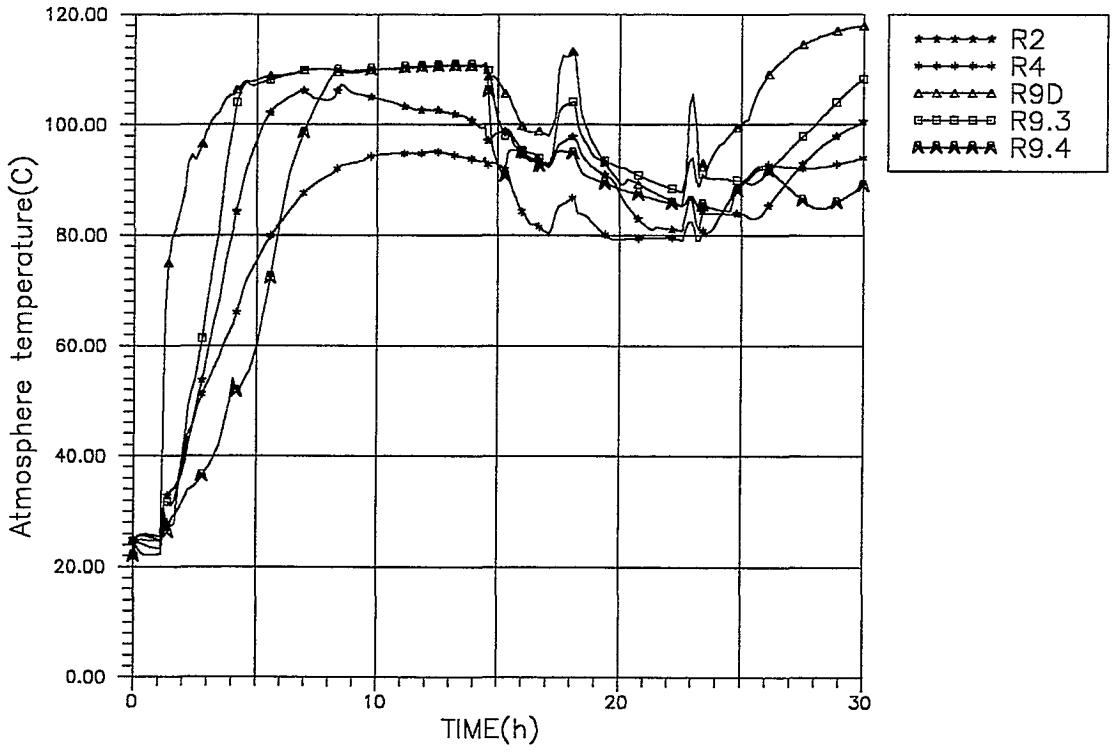

Figure 2. CONTAIN 1.11 Post ISP 37 Calculations. Atmosphere temperatures.

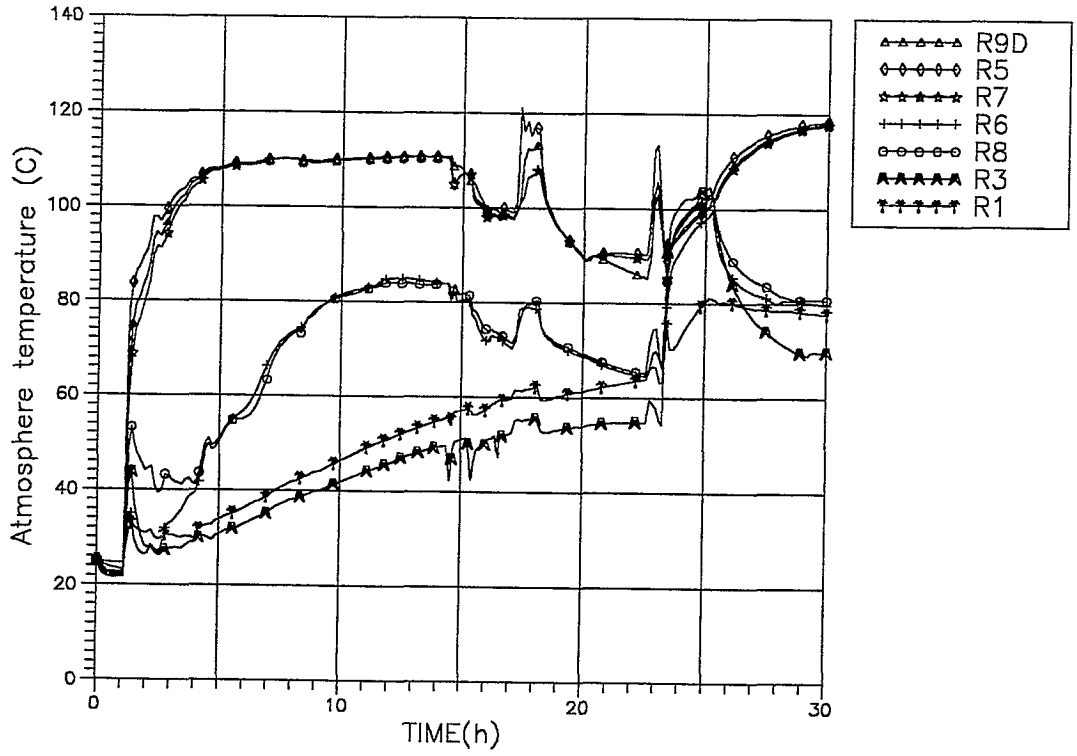

Figure 3. CONTAIN 1.11 Post ISP 37 Calculations. Atmosphere temperatures.

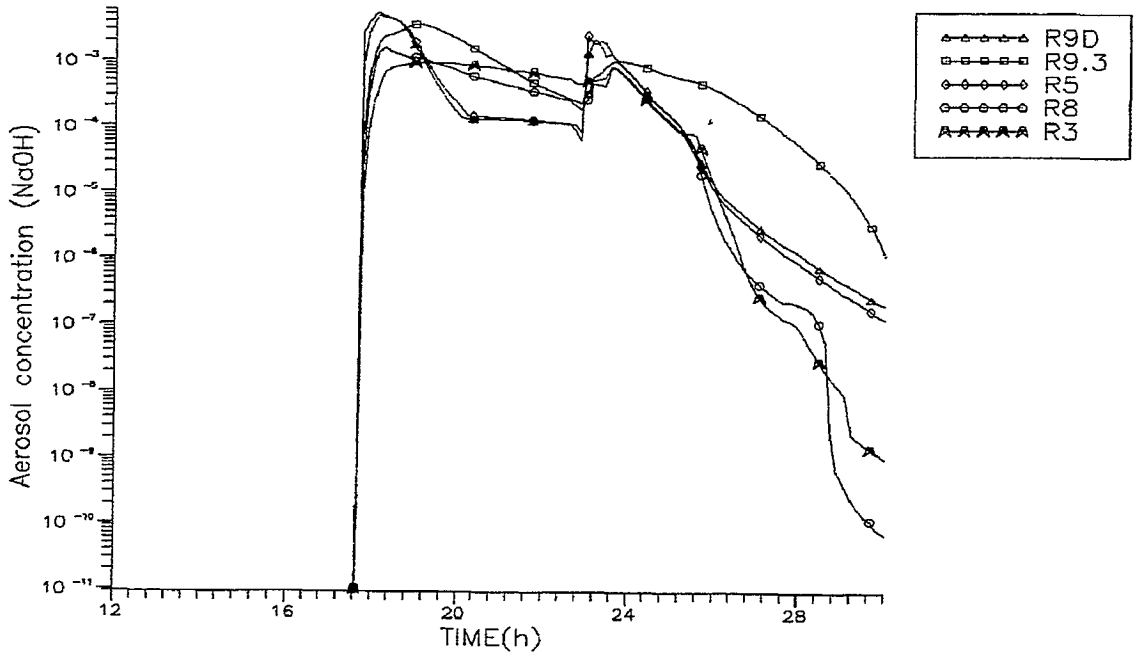

Figure 4. CONTAIN 1.11 Post ISP 37 Calculations. Aerosol /NaOH/ concentration.

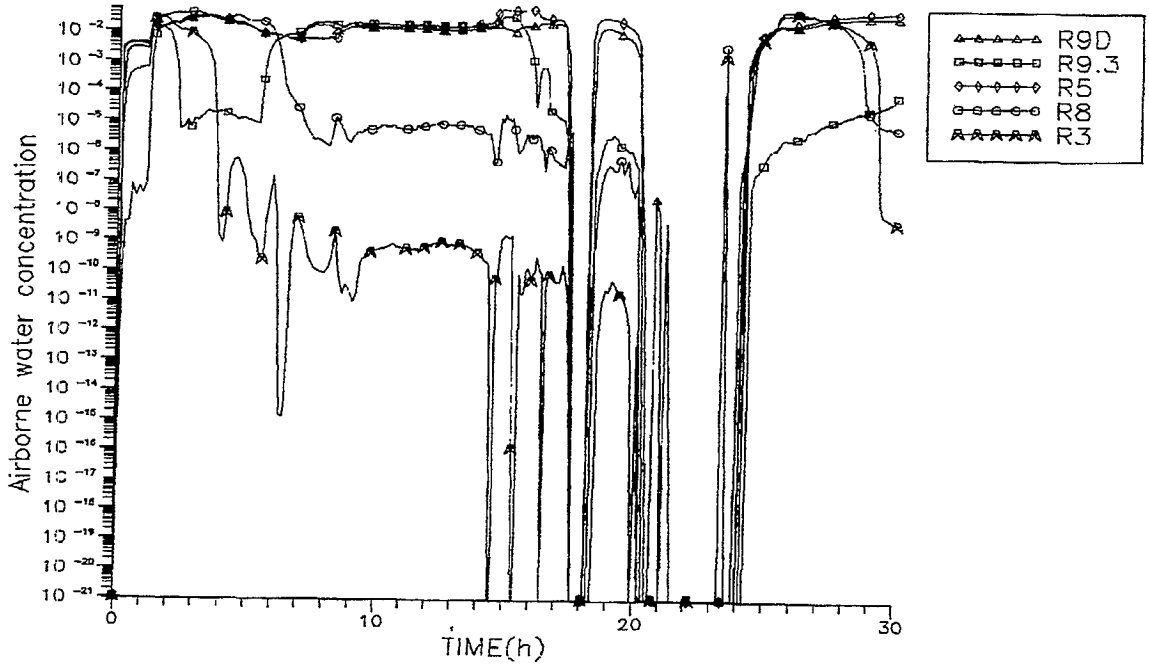

Figure 5. CONTAIN 1.11 Post ISP 37 Calculations. Airborne water concentration.

Post-ISP37 with Aerosol Behavior Stand-Alone Code MACRES (Contribution by NUPEC)

1 Introduction

MACRES code is a mechanistic code for aerosol behavior analysis developed at NUPEC. MACRES code needs thermal hydraulic boundary conditions such as atmospheric temperatures, wall temperatures, relative humidity etc. In this VANAM calculation these date are based on the experimental results read from Kanzleiter report. Flow velocity which was not measured in the experiment is based on the FIPLOC calculation results that were distributed by GRS in ISP37.

Our ISP37 NaOH concentration results showed good agreement in the Dome, however in other rooms the calculated concentrations was much lower than the experimental values.

After ISP37 calculation, MACRES code was slightly revised, boundary condition data were modified and a new calculation was conducted.

This report explains these new calculation results with the revised MACRES code.

2 Revised models and modified boundary conditions

2.1 Revised models

Two models were revised in MACRES code. One was the particle transfer rate calculation among sections due to condensation particle growth. Old model assumed constant particle number density in a section and the new model assumes constant particle mass density in a section.

The other revised model allows for gravitational deposition through open areas between rooms. In old model this phenomena was modeled only between annular rooms R93 and R94. However in new model other gravitational deposition paths such as from the Dome to R93, R4, R5, R7 and R2, from R7 to R8 and from R5 to R6 are modeled.

2.2 Modified boundary conditions

In addition to the model revision, input data was modified. Relative humidity is limited to 97 % on its upper bound considering measurement error and the FIPLOC calculated, relative humidity upper bound, and some data like flow velocities and wall temperatures were corrected from misread values.

3 New calculation results

3.1 NaOH aerosol atmospheric concentration

Figure 1 shows the old (lower) and new (upper) calculation results.

In Dome in phase 3 the analysis results are slightly lower than experimental value however they are in good agreement. Significant improvement over the previous analysis was seen. In Dome in phase 5 the analysis result is improved slightly.

In R93 the result is significantly improved from old results and shows good agreement with the experimental values.

In R3 the result is also significantly improved however is still lower than experimental values.

3.2 Fog amount formed in phase 4, 5 and 6

Fog amount formed in phase 4, 5 and 6 was drastically decreased from 3430 kg of old calculation to 19.4 kg of new calculation and became on the same order as other participants results reported in ISP37.

A parametric calculation with relative humidity upper bound of 99 % showed fog mass formed in phase 4, 5 and 6 of 90 kg. Considering these results 97 % upper bound of relative humidity is believed to have resulted in a reasonable estimate of fog mass in new calculation and results are found to be very sensitive to the relative humidity for values over about 95 %.

Figure 2 shows mass median diameter calculation results of old (lower) and new (upper) calculations.

As can be seen from the figures newly calculated MMD is significantly decreased reflecting the relative humidity upper bound. Considering the measurement of dry particles the result of slightly larger values of MMD than experiment is reasonable.

4 Discussion

There are several different conditions between old and new calculations. Limited relative humidity upper bound and the flows through open areas between rooms had much influence on the new calculation results.

Because stand-alone code MACRES does not calculate steam mass conservation, relative humidity values are given as input at each time. Therefore the values are keys to MACRES code hygroscopicity calculation. In submitted case, measured relative humidity values were obtained by reading it from plots however there's a relatively large measurement error of 10 %. According to our other calculation with the upper bound of relative humidity at 99 %, the NaOH concentration was about 3 to 5 times smaller in Dome, about 2 to 3.5 times smaller in R93 and about 2 times smaller in R3 during phase 3, compared to the results of limited upper bound of 97 %.

The NaOH concentrations in Dome and room 3 are still smaller than experimental results in new calculation. After the 1st aerosol injection the difference already exists. Discrepancies with the experimental results appear at the end of the 1st injection however the results are similar to the experimental data plus this initial offset after this time.

In Dome, detail examination of analysis results shows that the amount of deposition in R2, R5 and Dome and the flow rate to R93, R94 may be the possible causes of the differences. However in R2 and R5, aerosols deposit due to diffusiophoresis in addition to sedimentation.

Diffusiophoresis is directly connected to steam condensation rate i.e. heat and mass transfer coefficients and sometimes it is difficult for a lumped parameter code to estimate those values in a volume modeled with a single node.

In R3 the deposition is relatively small and the cause of the differences at the end of 1st injection is the flow rate into the room from other rooms. The experimental flow distribution review should provide insight into these discrepancies.

5 Summary

New calculation was conducted after the submission of ISP37 results with revised model and modified data. The results was much improved and showed good agreement with experiment.

There are some different conditions between old and new calculations, however limiting the relative humidity upper bound to 97 % and the model addition of flows through open areas between rooms had much influence on the calculation. The value of 97 % is believed to be reasonable judging from newly calculated fog amount.

Because the NaOH concentration in Dome and room 3 is still slightly smaller further investigation of relative humidity and flow distribution review is thought to be necessary.

New calculation

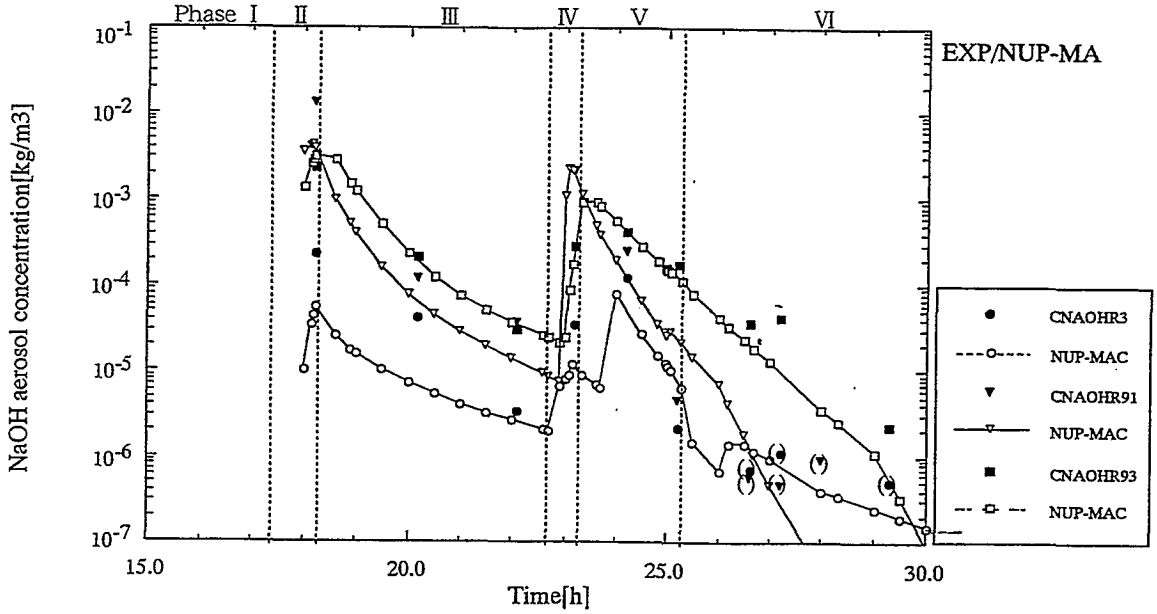

Figure : NaOH aerosol concentration in R3,Dome and R9.3(MACRES-NUPEC)

Old calculation

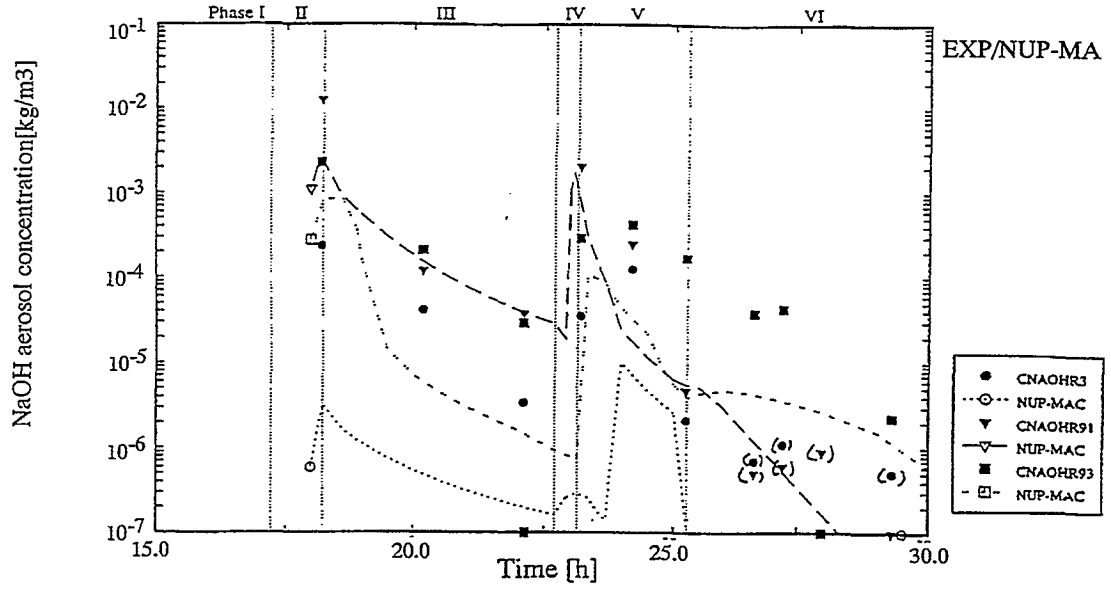

Figure 1 NaOH aerosol concentration in R3, Dome and R93 (MACRES - NUPEC)

New calculation

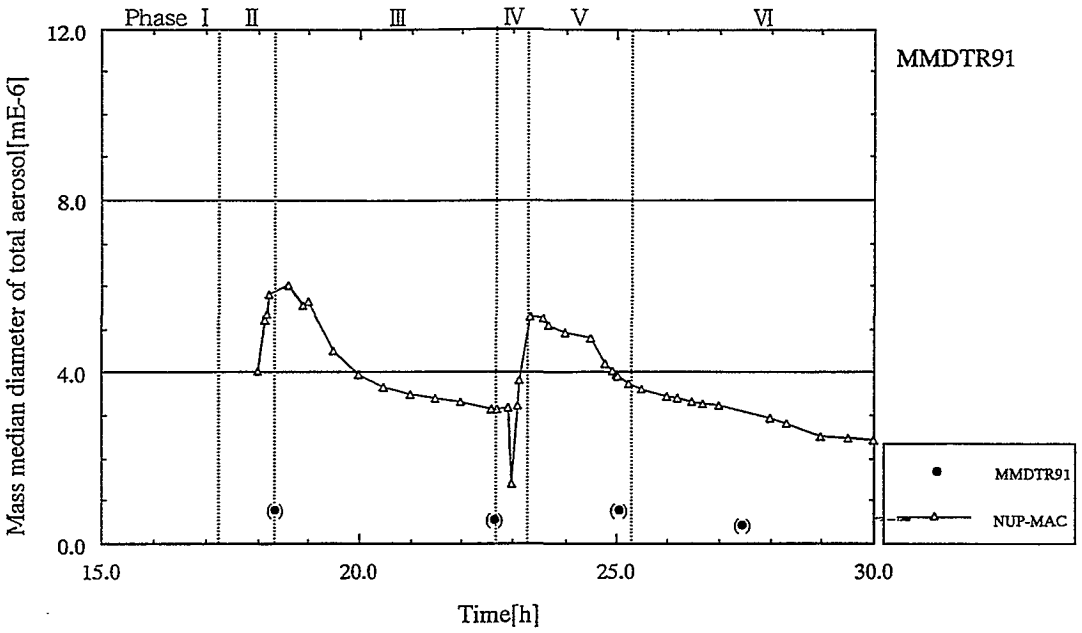

Figure : Mass median diam. of the tot.aeros. in the Dome(MACRES)

Old calculation

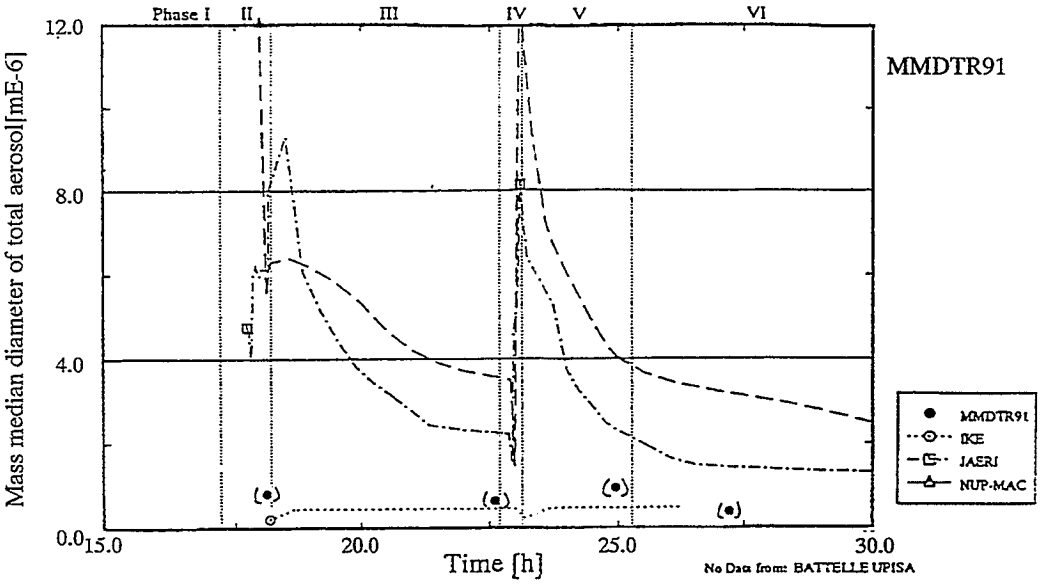

Figure 2 Mass median diameter of the total aerosols in the Dome(MACRES - NUPEC)

Results from the VANAM M3 Test Analysis

F. Parozzi - ENEL Nuclear Energy Division, Milano (Italy)
F. Oriolo, S. Paci - Dipartimento di Costruzioni Meccaniche e Nucleari, Pisa (Italy)

These comments deal with the results obtained from the integrated thermal-hydraulic and aerosol analysis of the VANAM M3 test using the ENEL code ECART [Fontana 1991].

BMC was subdivided into 15 control volumes, 55 heat structures and 19 junctions (13 proposed in the specification plus two connecting the internal subdivisions of R6 and R8 plus the 4 junctions connecting the two drain tubes to sumps). Through vertical junctions also water drain flow is possible if the sump level reaches the height of the junction inlet. This 15 volumes nodalisation has been chosen on the basis of the 11 volumes proposed nodalization, subdividing R6 and R8 into two ECART nodes and simulating the two tubes linking the volumes R2-R8 and R1-R3. The first modification was done to better predict the high temperature vertical stratification inside R6 and R8 and also to predict better the high temperature flow rate in the junctions linked to the upper parts of R8 and R6, towards the central R1. All injections, removals and air leakages are modelled by input tables, no leak flow paths are used. For the steam leakages a volumetric flow derived from the air flow-rate and the mixture composition in the internal volume interested to the leakage is employed. The ECART internal package is adopted to evaluate the heat transfer coefficients.

The aerosol module has been activated after 60,000. s from the beginning of the test, defining two different species: NaOH and H_2O. The last one is used to permit condensation on the dry particles with a flow-rate calculated by the thermal-hydraulic module. A very small injection of water as aerosol has been considered before the first NaOH injection to start the condensation process.

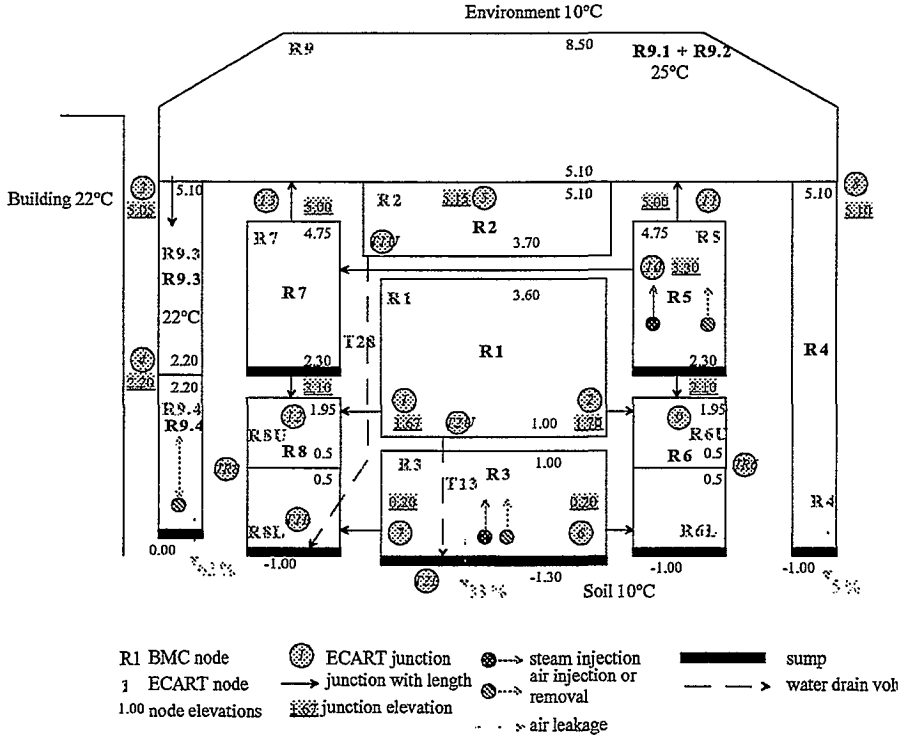

Fig. 1: ECART nodalisation for VANAM M3.

Comparison between aerosol concentrations of M3 and M2* with a no hygroscopic aerosol provides a hint to the increased occurrence of droplets for the NaOH aerosol which cannot be neglected in the code input. Although dried, finely

disperse and having a low density, NaOH aerosol in M3 steam atmosphere degrades more quickly. This can hardly be explained in another way than by ascribing this to an increased formation of droplets owing to NaOH hygroscopic qualities, not modelled inside ECART. For these reasons characteristics of aerosols injected have been changed from reference values [Firnhaber 1995] to the larger values reported in Table 1. On the basis of experimental results [Kanzleiter 1993] also standard deviation has been changed from the constant value 1.9 into two different values 1.72 and 2.34 for the two injections.

	Table 10 [Firnhaber 1995]	**Table A.1** [Firnhaber 1995]	**Estimated** [Kanzleiter 1993]		**ECART Input**	
Phase	**I & II**	**I**	**I**	**II**	**I**	**II**
Geometric mean diameter [μm]	0.058	0.33 ÷ 0.35	0.358	0.404	3.58	4.04
Standard deviation	1.9	1.9 ÷ 1.8			1.72	2.34
density [kg/m^3]	2,130. (dry)				1,000.	1,000.

Table 1: NaOH Aerosol characteristics.

During *phase I* there is a purely saturated steam atmosphere, correctly predicted by ECART, in injection compartment R5 (Fig. 4), in adjacent R7 as well as in dome (Fig. 5) and in the top part of annulus. In R5 there is a slight overheating only near the injection point, that it is not possible to predict with a lumped parameter code. In lower internal compartments R3 (Fig. 3), R6 (Figs. 6 and 7) and R8 there is a high air content during the entire time range, as temperatures show. In R6 (Fig. 8) and R8 upper parts a significant stratification, with a highly steamy layer below the ceiling, is observed. The internal R1 (Fig. 2), "coupled" to R6 and R8 at this level, is influenced hereby and therefore shows significantly high temperatures. This is the reason for which the ISP nodalization [Firnhaber 1995] was changed, splitting R6 and R8. During hot aerosol injection *(phase 2)* increased temperatures are present in R5 (Fig. 4) and, in a minor degree, also in its adjacent zones, which decrease after injection stop under heat absorbing structures influence. Partial shift of atmosphere from hotter zones to previously cooler zones (R1, R3, R6, R8) in the latter leads to a certain temperature increase. R9 temperature increases with the increase of steam pressure. In *phase 3 (no injection)*, together with pressure, atmospheric temperatures in "steamy' zones (e.g. R9, R5, R7) also fall in accordance with steam pressure decreasing by condensation. There is no such effect in zones with steam contents already low (R3, central and lower parts of R6 and R8), and temperatures there largely remains unchanged. During 2nd aerosol injection *(phase 4),* atmospheric temperatures develop in a similar way as in phase 2. By steam injection into R3 (Fig. 3) *(phase 5)* atmospheres of internal rooms and dome (Fig. 5) become very similar. Only in R3 a higher temperature ensues, while in largely closed R1 (Fig. 2) lower temperatures are observed. Annulus central and lower parts are excluded from this mixing. In *phase 6,* steam is injected again into R5 and from there spreads in horizontal and upward directions. Temperatures in lower compartments (R3, R6 and

R8 lower zones) under the influence of still heat absorbing structures slowly fall. In R5 and R7 as well as in dome, temperatures together with pressure steadily increase, i.e. steam content there continuously rises, while a part of air slowly shifts to lower volums. Temperatures in the annulus further stagnate, while a front containing a steamy mixture slowly settles from above.

During injection phases, aerosol concentration, as expected, is highest in R5 (Fig. 8) as well in dome (Fig. 9), where there are intensive exchange processes. After termination of admissions, concentration in these compartments quickly decreases, as aerosol partially spreads in adjacent zones, but partially also because depletion processes become effective (sedimentation after previous agglomeration of small primary particles to larger aggregates, increased by hygroscopic behaviour). In annulus (Fig. 10), concentration decreases more slowly than in remaining zones and, therefore in later phases, it is far below other values (by up to two orders of magnitude). Rapid, uniform decrease of aerosol concentrations during phase 5 is also remarkable, when steam is injected into previously cold R3. This, on one side, leads to an intensive fog formation, on other side, steam and fog formed flow off to lateral and upper compartments, while high density atmosphere can flow downwards at the same time. This causes an intensive mixing and thus an equalisation of concentration in these zones, fog spreading everywhere effectively accelerating aerosol depletion also for hygroscopic NaOH behaviour.

With VANAM M3 an integral, thermohydraulic/aerosol multi-compartment containment experiment for purposes of ECART verification has been analysed for the fist time. ECART simulation for thermal-hydraulic shows a number of deviations that can be caused by:

- deficiencies in the leakage modelling;
- local measurements deviating from the room average values;
- limitations of nodalisation (further subdivisions are required).

The available information is not sufficient to identify the major causes of deviations. However, pressure and temperature distribution are simulated in accordance with measured data, such that thermal-hydraulic basis for aerosol behaviour is given. Thermal stratification is shown and also its break-up by steam injection into R3 and subsequent re-establishment are simulated.

From the point of view of aerosol behaviour, increased steam condensation in the atmosphere, as a consequence of hygroscopic material, is actually not simulated in ECART and will require further studies.

BIBLIOGRAPHY

[Firnhaber 1995] - M Firnhaber, *"Draft Specification of ISP-37: VANAM M3 - A Multi Compartment Aerosol Depletion Test with Hygroscopic Aerosol Material"*, GRS mbH, April 1995.

[Fontana 1991] - R. Fontana et Alii, *"ECART: Definition of the Code Architecture and Construction of the Aerosol and Vapour Transport Module"*, ENEL Report. No. 1019/2, 1991.

[Kanzleiter 1993] - T. Kanzleiter, *"VANAM Multi-compartment Aerosol Depletion Test M3 with Soluble Aerosol Material"*, Battel-Institute e.V. Report BIeV-R67.098-304, July 1993.

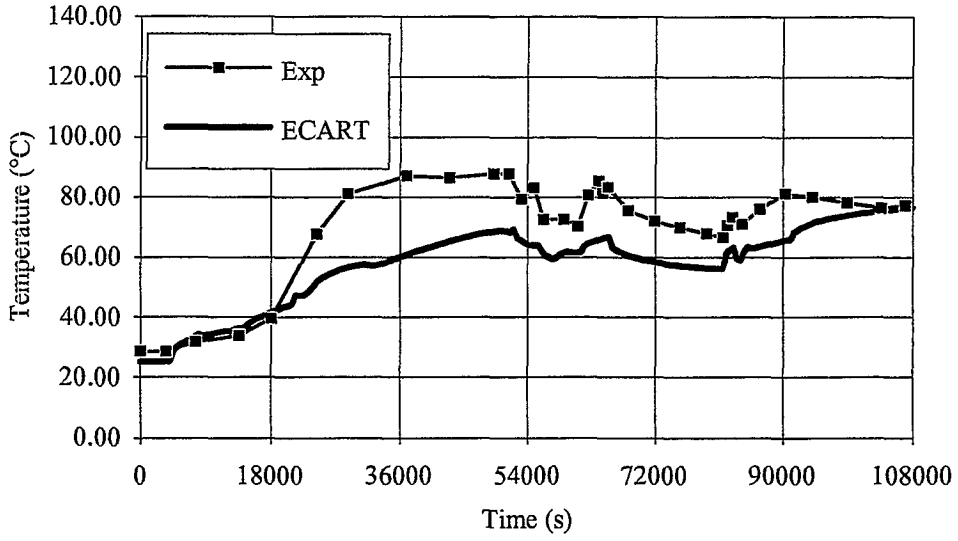

Fig. 2: R1 atmosphere temperature

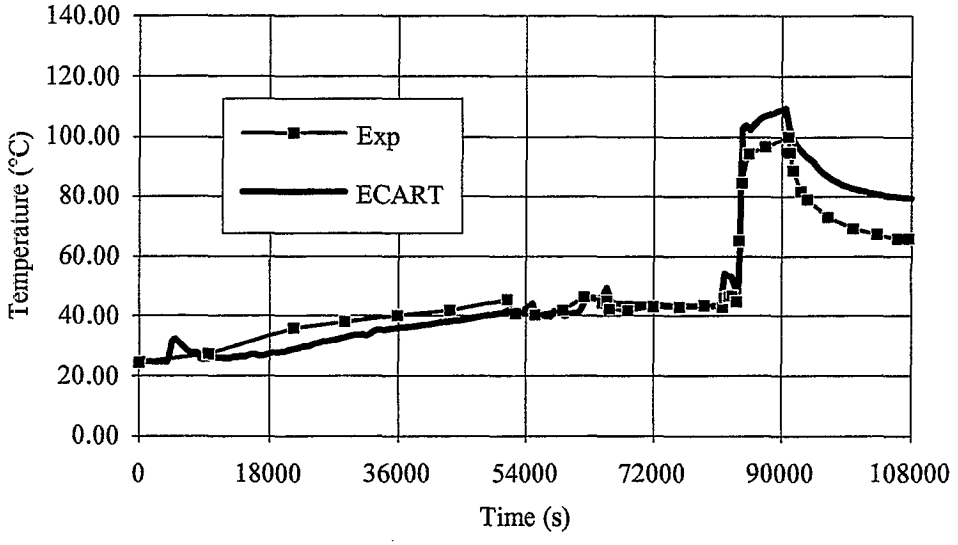

Fig. 3: R3 atmosphere temperature

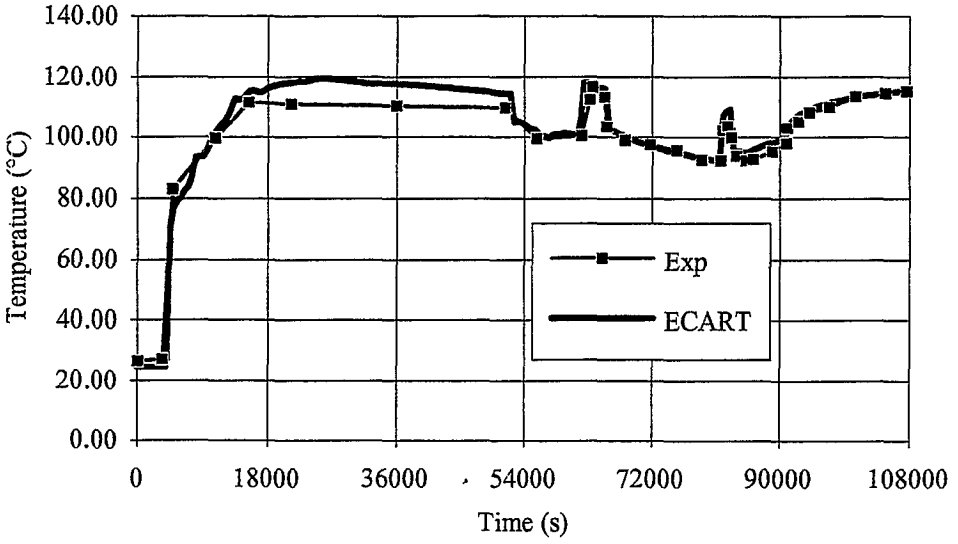

Fig. 4: R5 atmosphere temperature

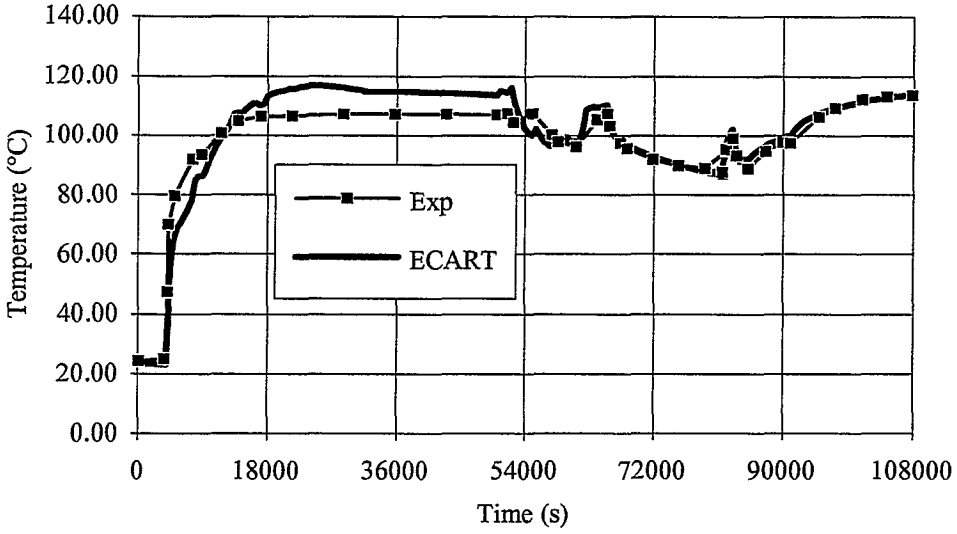

Fig. 5: R9 Dome atmosphere temperature

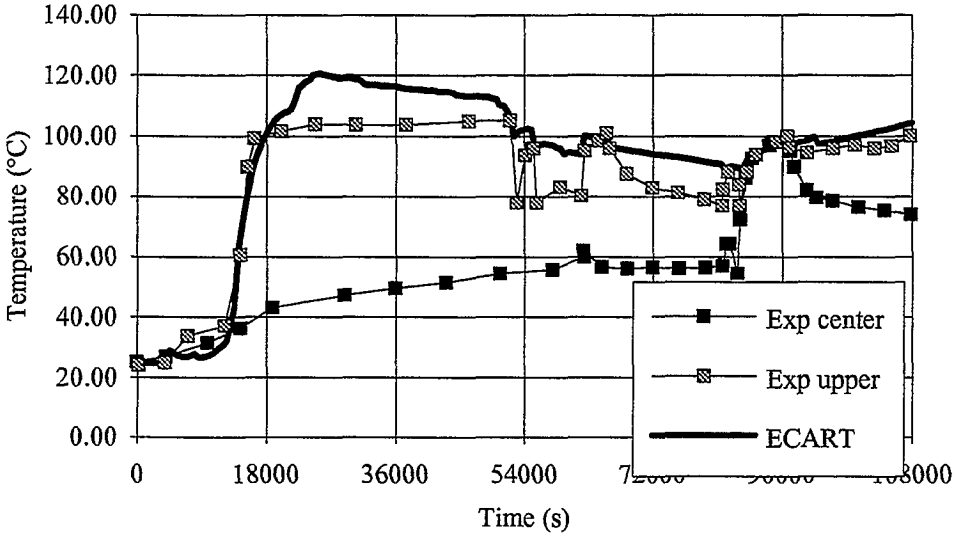

Fig. 6: R6 atmosphere temperature (upper zone)

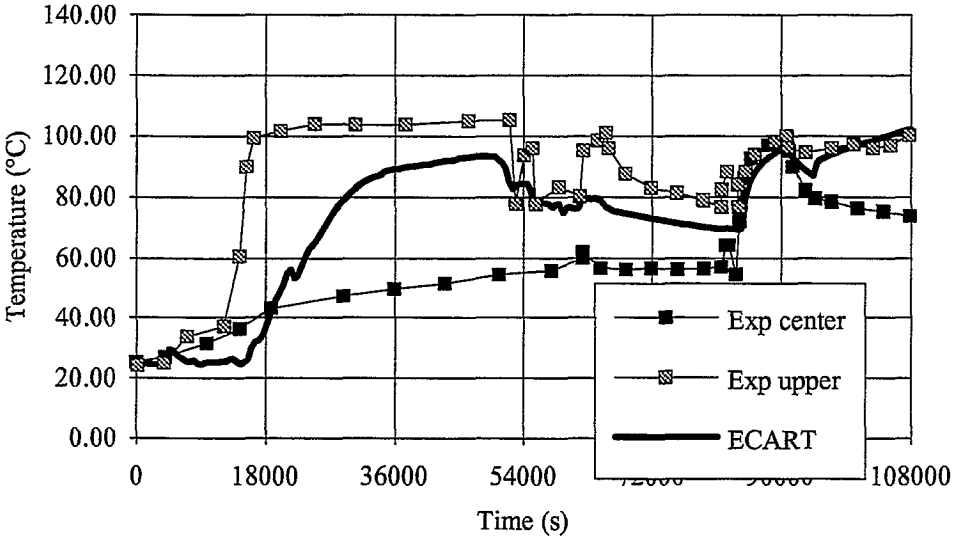

Fig. 7: R6 atmosphere temperature (lower zone)

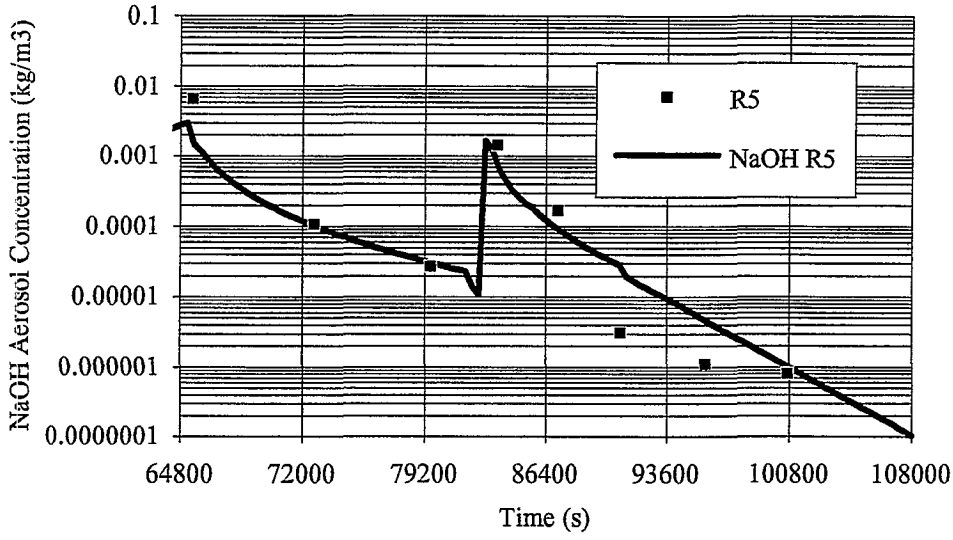

Fig. 8: NaOH aerosol concentration in R5 atmosphere

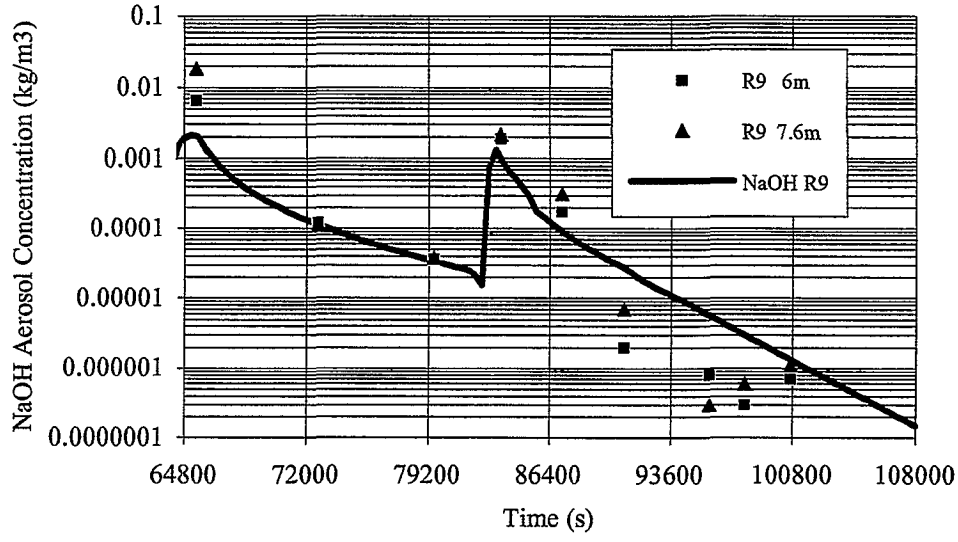

Fig. 9: NaOH aerosol concentration in R9 atmosphere

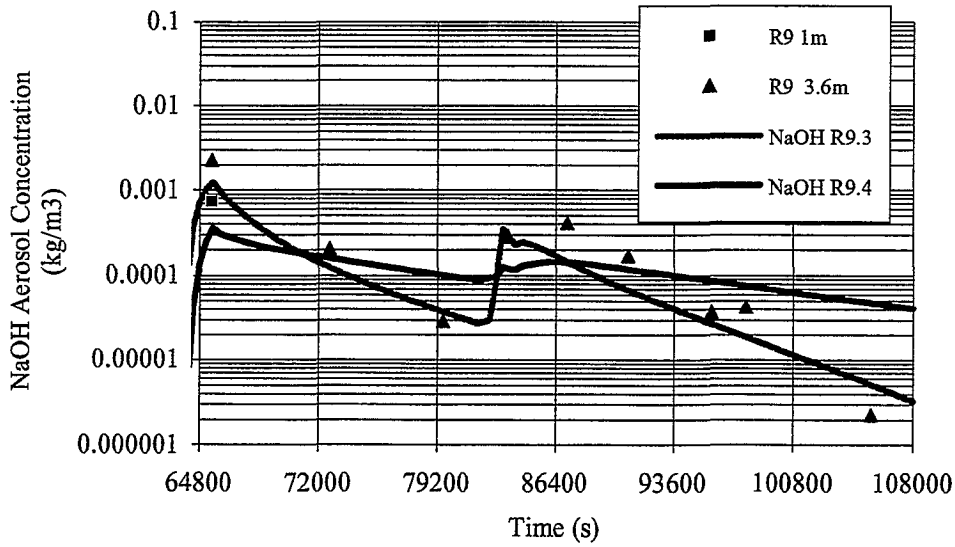

Fig. 10: NaOH aerosol concentration in R9.3 - R9.4 atmosphere

ISP37 VANAM M3

Conclusive Report by ENEA

LIST OF CONTENTS

1. INTRODUCTORY REMARKS

The ENEA of Bologna performed two different calculations for the ISP n.37 on VANAM M3. The second one has been done making some relevant changes to the input used to realise the first one. A short synthesis focusing on the highlights and the reasons why these two calculations have been needed is reported afterwards.

2. SYNTHESIS OF THE ANALYTICAL RESULTS FROM THE FIRST CALCULATION

In our first ISP37 VANAM M3 results, all the required variables were included excepting:

- 81-82 (steam leakrate and integral steam leakrate), because leak paths were not used, but the air leakage has been modelled by mean of negative sources, with the purpose of correctly evaluating the total air mass.
- 99-100 (wall condensation rates) and 101-111 (volume condensation rates), because MELCOR does not supply this kind of output variables.

Moreover, variables A35-A41 (mass median diameter of total aerosol) and A42-A48 (geometric standard deviation) are provided only as plots, accompanied by a listing of the used plot values. As a consequence, in file 1 the above variables have values that are interpolations between the values at the previous and at the following timestep. Therefore only two significant decimal figures have been reported. We are aware that some discrepancies from the actual values are unavoidable with this procedure, but it was the only alternative to not providing these values at all. About variables A49 in file1 (leaked NaOH aerosol mass from containment) and A61-A65 in file3 (NaOH mass leaked-water mass leaked with droplets), they are identically equal to zero, since, as already pointed out, no leak flow path has been used.

In general, the values of thermal-hydraulics variables show a good agreement with the experimental graphics that we received, while those relative to aerosol variables are a little bit less satisfactory. In particular, the maximum of suspended aerosol concentration is, in node R5, about 55% of the experimental value, while in the surrounding nodes it reaches values exceeding the expected ones. Probably this is due to an overestimation of the atmosphere velocity (that is of the mass flow) in the flow paths connecting R5 and the nodes next to it, at the time of the first aerosol injection.

An underestimation is without doubt to be expected in the aerosol deposition velocity, since, in MELCOR, a hygroscopic model has not been introduced yet, thus not properly taking into account the aerosol particles growth due to the linked phenomena. As a consequence, we foresee that the values we obtained for variables A21-A34 should be lower than the actual ones.

3. THE SECOND CALCULATION

A second calculation has been performed on the VANAM M3 test by making a few, but significant, changes in the input that was used to realise the first one. We did this since we

noticed, from the experimental-calculated values comparison plots we received, that the hypothesis we had assumed, regarding a constant temperature of the external faces of the containment outer shell, was not fulfilled.

Thus, the first change has been the introduction of two additional nodes that simulate the environment and the building. They have a very large volume and fixed thermodynamic properties. In particular, the temperatures of these nodes are, respectively, 10 °C and 22 °C (from Specification). Differently from the first calculation, the outer shell structures are not externally isolated, but they are subject to heat exchange also with "environment" or "building", depending on Table 3b. In this way, also the temperature of the outer face of these structures can rise. Another input change has been a different sharing of the air leak among nodes R9.4, R3 and R4. While, in the first case, it was given by, respectively, 61.9 %, 24.6 %, 13.5 %, in the second calculation it has been assumed as follows: 75 % to R9.4, 15 % to R3 and 10 % to R4. The reason of this variation has been that, as a consequence of the altered thermodynamic properties in the single nodes from the first to the second calculation, at a time of about 16 hours a larger air mass would have been removed from R3 than the actual mass present in the node. This new sharing has been chosen in order to reflect the reciprocal ratios of the lateral areas of the considered nodes.

Finally, a further change has been made regarding the lower and upper limits for the aerosol particles diameter: they are now 6 E-9 m and 1.5 E-5 m, in order to obtain a more significant distribution of the suspended aerosol mass among the dimensional sections (still 30 adopted).

4. CONCLUSIONS

As it can be seen from the graphs, the results from our second calculation are finer than those from the first one. In particular it depends on the more realistic assumption on temperatures of outer face, since here the outer shell structures are not simulated as externally isolated.

The International Standard Problem ISP37
Calculations with CONTAIN 1.12 for VANAM M3

G. Henneges
Forschungszentrum Karlsruhe (FZK)
Institut für Neutronenphysik und Reaktortechnik (INR)

This paper deals with results of a series of containment thermalhydraulic and aerosol studies made with the multicompartment code system CONTAIN 1.12 for the VANAM experiment M3.

1. Calculations

The CONTAIN 1.12 Version /2/ with update C110W for use on workstations was used. It was distributed in Sept. 1994 to FZK. All calculations were run on IBM RISC 6000/370 workstation. Optimisation to level 2 of the F77 compiler gave equal results as those calculated with 1.12 version on the IBM main frame computer M3090 and is therefore believed reliable. Higher optimisation to compiler level 3 gave wrong results for aerosols and fission product calculations if the code was not modified.

CONTAIN calculations stop if the timestep size is too coarse. The time intervalls had to be reduced to values of 1.0s which means that the CPU-time is large. Changing the steep slopes of material injections or removals was necessary. For air-leakage only changes from linear interpolation to step functions of the input tables solved convergence problems.

The aerosol calculations made problems if the 'moving grid scheme' was used. This is necessary when the hygroscopic behaviour of NaOH is calculated. Then the calculation stopped around 60000s. A restart at 54068s with a coarser timestep of 2.0s for the next 20000s did work. If radiation heat transfer was included the calculation stopped at 90000s and increasing (Δt up to 10s) or decreasing (Δt down to 0.1s) did not solve the problem.

Five different calculations are compared. The influence of simplifications was studied for example by

- taking only oxygen instead of air as atmospheric gas
- modeling the outer structures only by concrete
- using flow coefficients according to Idel'chick or improved values
- including radiation transport effects.

The differences of the discussed CONTAIN calculations are summarized in the following table. The calculations submitted to the first ISP37 comparision workshop were cases 40 and 42. Both differ only in the composition of the atmospheric gas, which is pure O2 for case 40 and air(0.79 N2 + 0.21 O2 molefractions) for case 42. They used the flux coefficients (cfc) of Tab. 2b from /1/ which are based on Idel'chick evaluations. In both cases a simplified description of the outer structures was used. To separate the effect of only O2 versus air in the atmosphere is possible by comparing case 40 with 42.

Table: Differences of CONTAIN calculations

Case	cfc		Air	O2	Outer Structure		Aerosol	Rad.
	Idel'chick Tab. 2a	/1/ Tab. 2b			Modified	Correct	NaOH	on
40	x			x	x			
42	x		x		x			
44	x		x			x		
45		x	x			x	x	
46		x	x			x	x	x

The influence of the correct modelling of the outer structures can be studied by comparing the results of cases 42 with 44. Which are the better flux coefficients - those of Tab. 2a or Tab. 2b in /1/ was not easy to answer. Therefore with both sets calculations were made (case 44 and 45). No radiative heat transfer is modelled in cases 40 to 45. This effect of radiation heat transfer is studied only in case 46 where the simplified GASWAL block is activated additionally.

2. Pressure

The measured pressure in the dome (cell 11) is shown in Fig. 1. Calculated values and the influence of the above mentioned input modifications can be seen here as well and compared with the measured values. Firstly, it shows the influence of the simplification O2 vrs. air. Case 40 with only oxygen gives up to 0.1bar higher pressures. The peak value is identical for both cases. Comparing case 42 with 44 values reveals the influence of the correct modelling of the outer structures. The simplification reduced the p-values by about 0.05bar in phase 1 and phase 6. For phase 2 to 5 they are nearly identical. Cases 44 and 45 used different flux coefficients. The difference on pressure evolution is very small (< 0.02 bar) till 27h. Then it increases to 0.2 bar at 30h. Case 44 stays closer to the experiment (Δp < 0.1bar). It differs in the heat up phase by only 0.1bar from the experiment; for the other phases the agreement is even better. These differences in pressure evolution can be qualitatively explained if the structure surface temperatures are examined.

3. Structure Temperatures

The temperature profiles at the beginning of the calculation are user input (TUNIF was 22°C = a uniform initial temperature for the whole structure). One calculated temperature profile for outer structure 2 is shown in Fig. 2 for case 42 and 44 at about 10h (36018s) and at 30h(108000s). Structure 2 is located in room 9.3 (9) and part of the outer shell. It was chosen as an example of the outer structures which were modelled differently in cases 40,42 and 44 to 46. The insulation effect of the air gap at 45 cm depth is well shown.

The sharp increase of the temperature of structure 2 near the surface (Fig. 3) for case 44 results from the coating material. It has a much stronger influence on the thermal hydraulics than expected and should therefore not be neglected. The simplifications made for cases 40 and 42 with respect to outer structure modelling results in too small structure temperatures at the surfaces because the coating was not modeled by the proposed method. This leads to lower pressure values which only apparently agree better with the experiment for case 42.

4. Temperatures

Some measured and calculated temperature profiles are shown in Fig. 4 and 5. The bold curves are the experimental values. Fig. 4 summarizes the temperature curves for room 3 and the dome (cell 11). The temperatures in room 9.3 (cell 9) are given in Fig. 5.

It can be seen that after the 'heat up phase' (15h) the measured temperatures of cells 9 and 11 are nearly the same (108°C. Till the end of phase 1 (17.2h) the temperatures drop in both cells. Due to the air/steam injection in phase 2 (till 18.23h) the temperatures increase again by about 10°C. They drop in phase 3 (till 22.7h) by up to 15°C. In phase 4 (till 23.14h) follows again a temperature rise of some degrees because steam/air is injected a second time in cell 5. After a short stop of all injections (10min) steam is injected into the lower room 3. This causes the temperature to rise in the cells 11 and 3 till 25.26h. Then the steam injection is switched back to cell 5 till the end of the experiment (30h). This induces additional temperature increase in the dome (11) but not in cells 3 and 9.

This overall trend holds for each of the calculated temperature curves. The stratification is very well reproduced. The calculation for cell 9 shows no larger temperature differences than those for cell 11 but the shape differs more from the experimental plot. This is even more obvious for cell 3 where the calculated curves differ up to 20°C and the shape is quite different from experiment for cases 40 to 44. Case 45 gives the best results for cells 9 and 3.

Taking all calculated results one may conclude that the overall trend is well predicted, especially in those nodes where major aerosol effects take place (nodes 3,5,9,10 and 11). Though the subdivision was coarse in z-direction the stratification is qualitatively correct calculated by CONTAIN.

5. NaOH Aerosol Concentrations

The experimental aerosol concentrations are given together with case 45 and 46 results in Fig. 6. The influence of radiative heat transfer is shown additionally. The aerosol depletion rate for case 45 is calculated very well for cell 11. Shape and absolute values agree better than could be expected. The accuracy of the measurements are in the order of 1.e-06 kg/m^3 as is illustrated by the scatter of the last 3 measured values. The CONTAIN calculation with radiation heat transfer stopped after about 25h with negative radii of the aerosol particles.

Both calculations show that during dry conditions (phase 3 and 4) results in cells 9 and 11 are nearly identical. The aerosol concentrations in cell 3 are smaller if radiation heat transfer is allowed by up to a factor of three but the shape is similar. The difference increases strongly for the time after the second aerosol injection during wet conditions. If radiation heat transfer is included the aerosol concentration decreases much faster than for case 45. This is in contradiction to the experiment.

Because cell 9 is located in the upper outer ring of the containment only 18% of the maximal aerosol concentration measured in the dome arrive there. The depletion is in qualitative agreement with the experiment. The calculated highest concentrations are of the same order. The decrease in phase 3 is underpredicted by CONTAIN by at least a factor of 20. This could be the result of the poor splitting of the condensate drain flow from cell 11. Cell 9 should get 56% of this condensate but in the calculations it is diverted directly to cell 10. Taking radiation heat transfer into account has nearly no influence on the calculated concentrations.

Only a small amount of the injected aerosol reaches the lower cell 3 of the model containment. The maximum experimental concentration is less than 2% compared to the initial dome concentration. CONTAIN calculates a much higher transport to cell 3 (14%). The measured decrease of the aerosol concentration in phase 3 is nearly two orders of magnitude while the code calculates only a factor of 10. Without radiation heat transfer CONTAIN overpredicts the aerosol concentration after the second injection by the same factor. But the shape of the depletion for this phase is comparable with the experimental one. Taking radiation heat transfer into account leads to a much steeper depletion rate in comparison to the above mentioned calculation and to the experiment.

6. Summary

This report presents results of a series of containment thermalhydraulic and aerosol studies made with the multicompartment code system CONTAIN 1.12 for the VANAM experiment M3 which was performed at the Battelle Model Containment in Frankfurt. This work was done as a participation to the open international standard problem OECD/CSNI/ISP-37.

The influence of simplifications was studied. Taking only oxygen instead of air as atmospheric gas resulted in higher pressure values during the heat up phase and the largest difference in temperatures compared to the measurements. Simulating the outer structures only by concrete of different thickness was not appropriate and could not describe the much higher surface temperatures which have a strong influence on the condensation effect. Using flow coefficients according to Idel'chick or improved values recommended by GRS and Battelle had much more effect than expected especially for lowly located rooms like cell 3. The calculated pressure is within the accuracy that can be obtained regarding the uncertainties of the boundary conditions. CONTAIN is able to calculate atmospheric stratifications as observed in the experiment.

VANAM M3 used water soluble NaOH aerosol to study a "dry" aerosol depletion phase and later after a second aerosol injection the behaviour in a "wet" environment. Although the depletion rate of the hygroscopic NaOH aerosol depends strongly on the relative humidity (rh) of the atmosphere and the volume condensation rate at rh = 100% the aerosol behaviour is predicted surprisingly well. The aerosol densities differ by more than an order of magnitude in the different compartments. Therefore one needs a multicell code like CONTAIN with its highly developped aerosol routines which include hygroscopic aerosol treatment. Additionally, the aerosol transport to different cells is calculated qualitatively correct.

A sensitivity calculation with respect to the effect of radiation heat transfer shows that a simple description of this effect has a strong influence on aerosol concentrations during bulk condensation in a wet environment. This is in contradiction to the experiment and has to be studied in future.

References

[1] M. Firnhaber, S. Schwarz, G. Weber, "Specification of the International Standard Problem ISP 37," GRS, Köln, April 1995

[2] K. K. Murata et. al., "Users Manual for CONTAIN 1.1," NUREG/CR-5026, Sandia National Laboratory (1989)

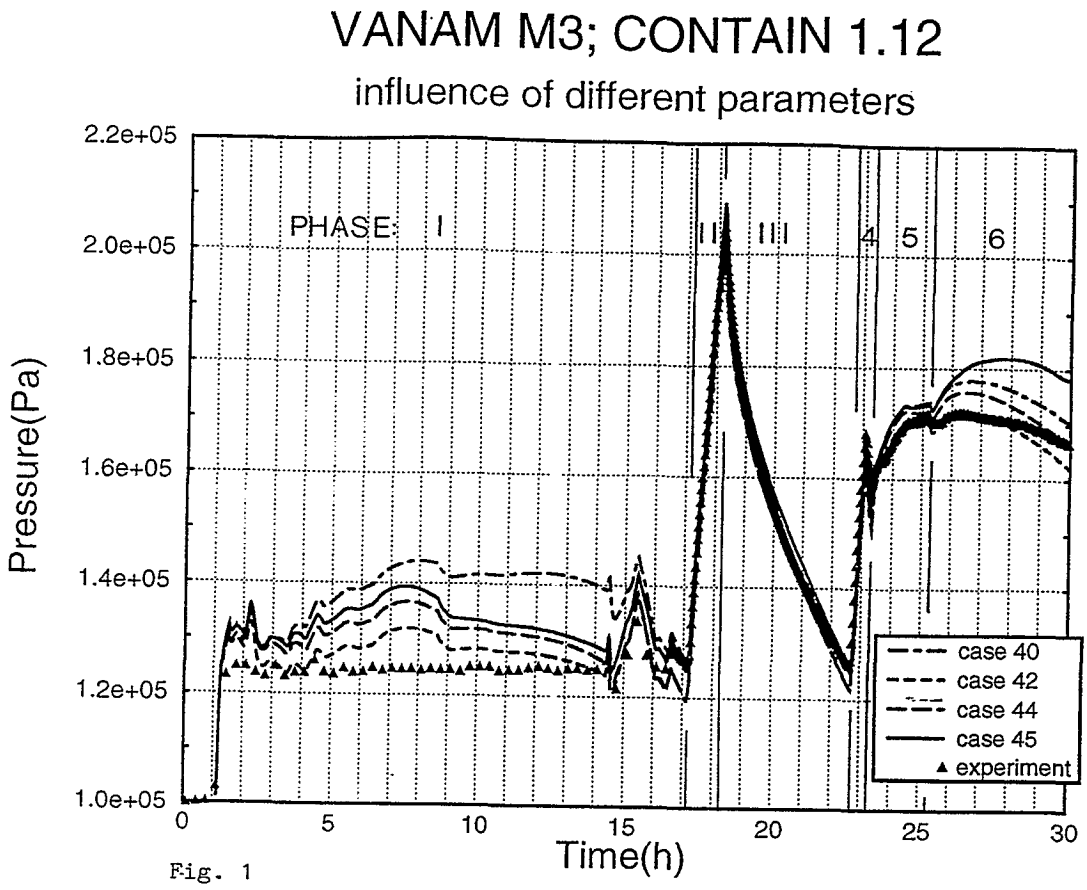
VANAM M3; CONTAIN 1.12
influence of different parameters
PHASE: I
II
III
4
5
6
Pressure(Pa)
2.2e+05
2.0e+05
1.8e+05
1.6e+05
1.4e+05
1.2e+05
1.0e+05
0
5
10
15
20
25
30
Time(h)
case 40
case 42
case 44
case 45
experiment

Fig. 1

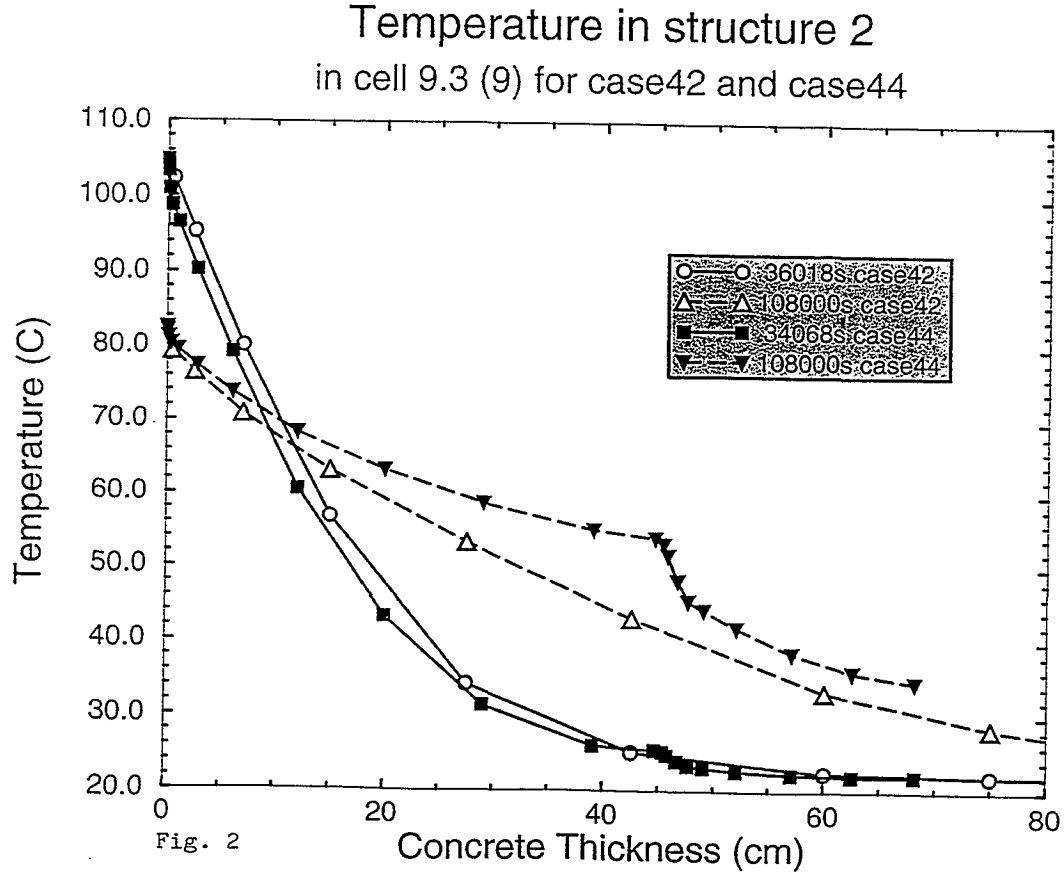
Temperature in structure 2
in cell 9.3 (9) for case42 and case44
Temperature (C)
110.0
100.0
90.0
80.0
70.0
60.0
50.0
40.0
30.0
20.0
0
20
40
60
80
Concrete Thickness (cm)
36018s case42
108000s case42
34068s case44
108000s case44

Fig. 2

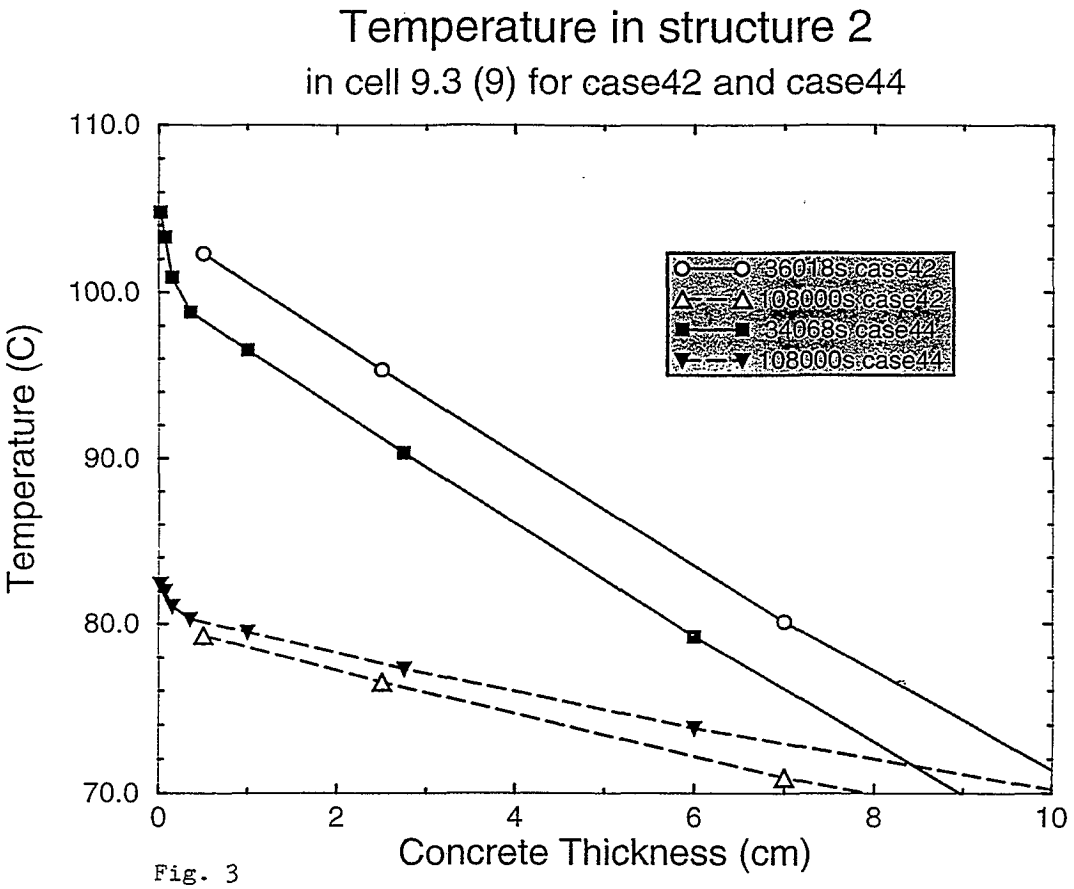
Temperature in structure 2
in cell 9.3 (9) for case42 and case44
110.0
100.0
90.0
80.0
70.0
Temperature (C)
0
2
4
6
8
10
Concrete Thickness (cm)
36018s case42
108000s case42
34068s case44
108000s case44

Fig. 3

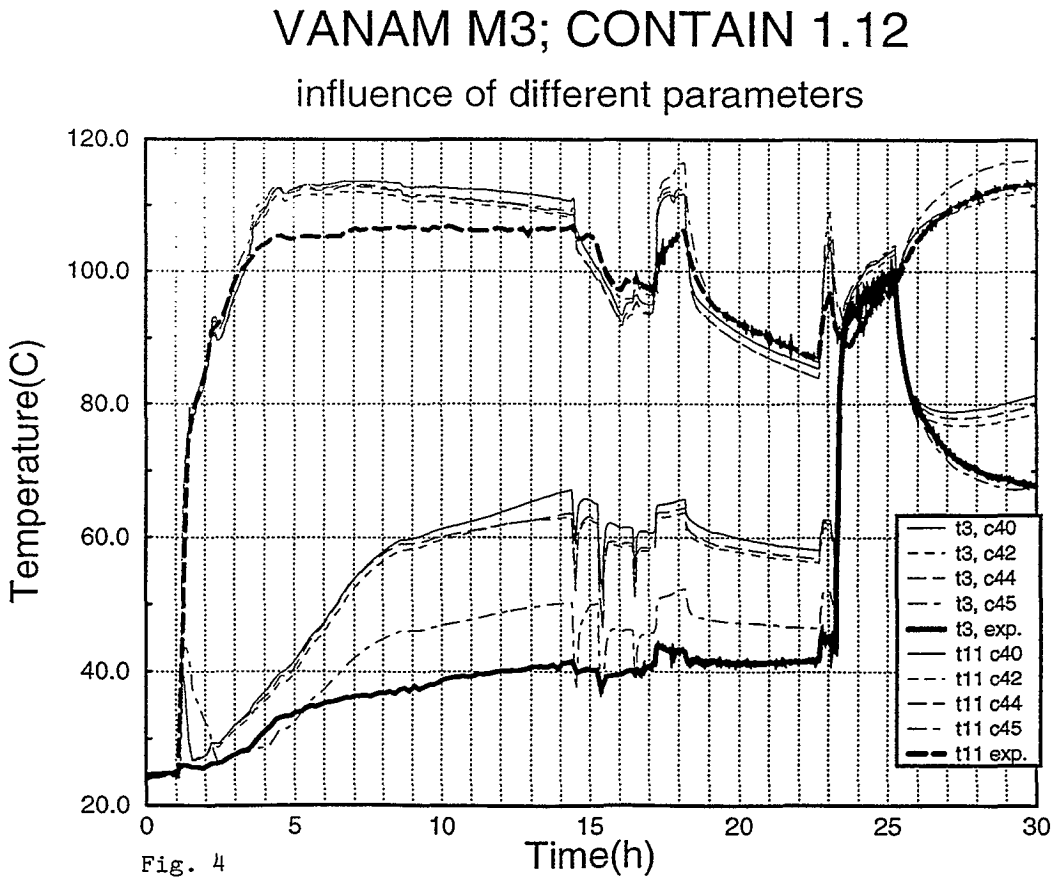
VANAM M3; CONTAIN 1.12
influence of different parameters
120.0
100.0
80.0
60.0
40.0
20.0
Temperature(C)
0
5
10
15
20
25
30
Time(h)
t3, c40
t3, c42
t3, c44
t3, c45
t3, exp.
t11 c40
t11 c42
t11 c44
t11 c45
t11 exp.

Fig. 4

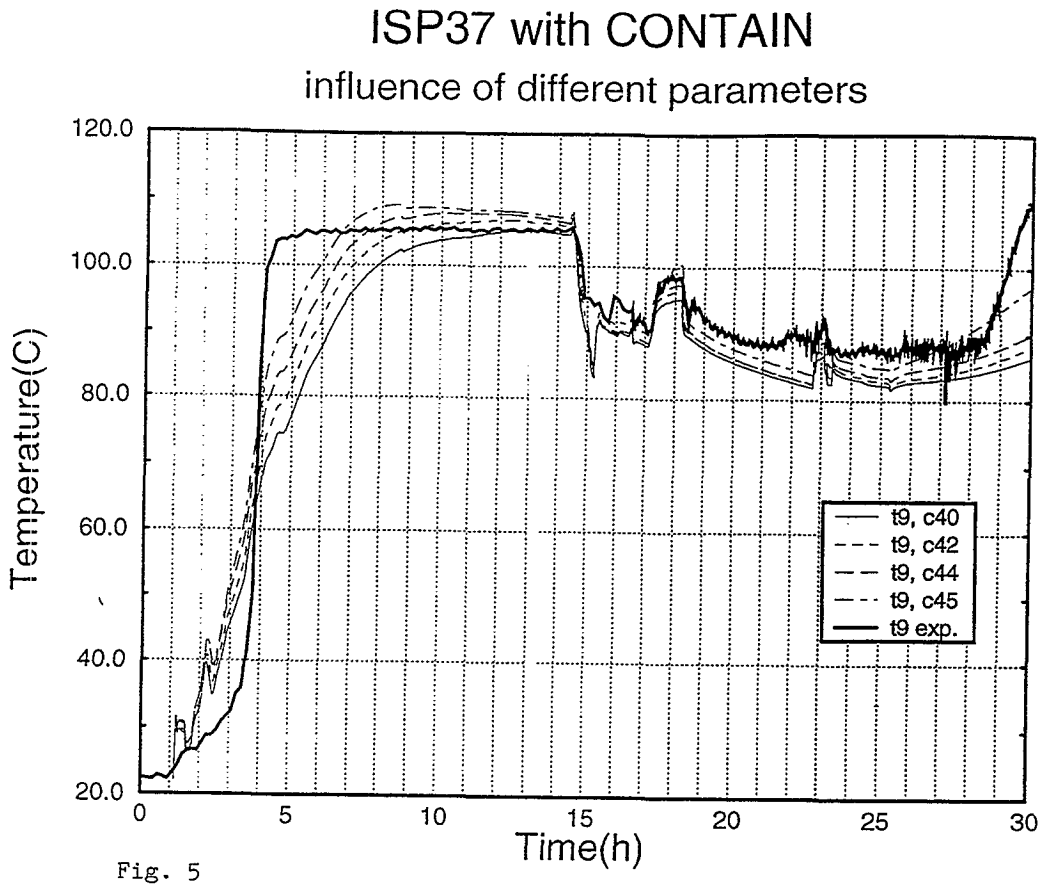
ISP37 with CONTAIN
influence of different parameters
Temperature(C)
120.0
100.0
80.0
60.0
40.0
20.0
0
5
10
15
20
25
30
Time(h)
t9, c40
t9, c42
t9, c44
t9, c45
t9 exp.

Fig. 5

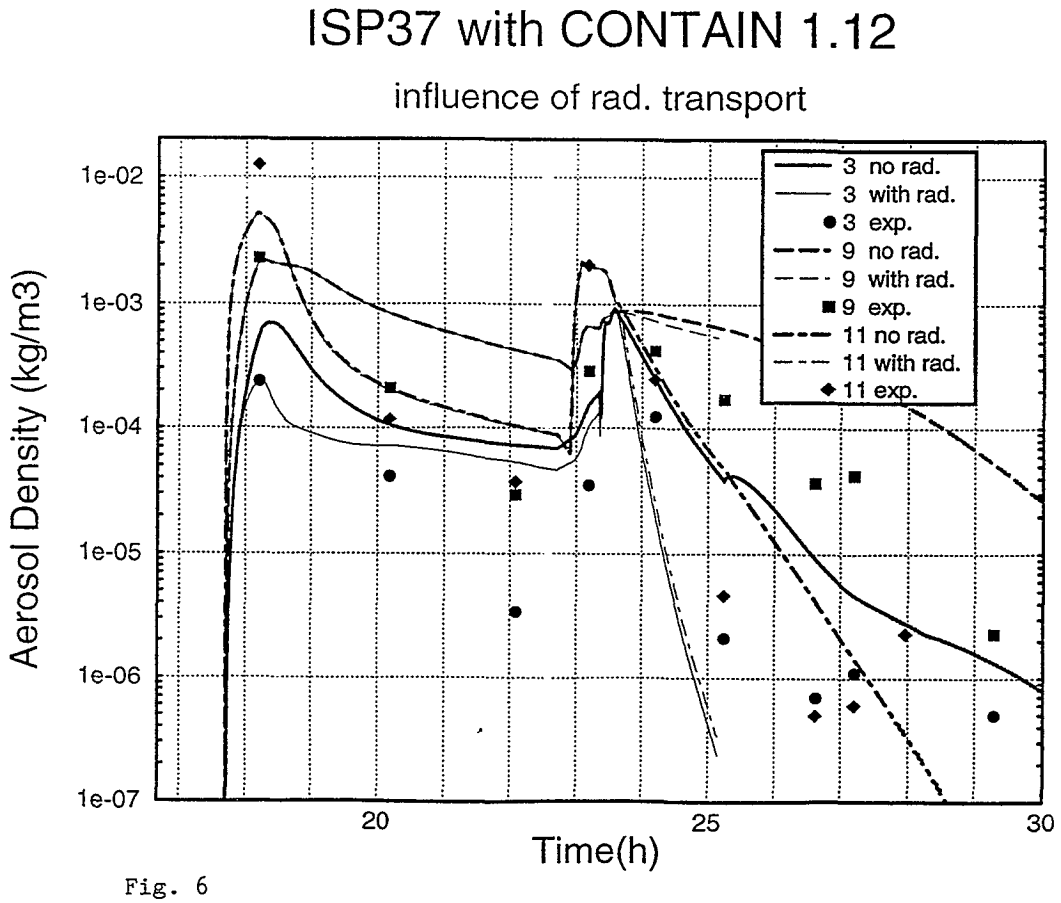
ISP37 with CONTAIN 1.12
influence of rad. transport
Aerosol Density (kg/m3)
1e-02
1e-03
1e-04
1e-05
1e-06
1e-07
20
25
30
Time(h)
3 no rad.
3 with rad.
3 exp.
9 no rad.
9 with rad.
9 exp.
11 no rad.
11 with rad.
11 exp.

Fig. 6

7.2 Additional Thermal-Hydraulic Investigations by GRS

Reasons for Different Pressures Obtained by the Reference Calculations Detailed Description

Summary

The differences between the pressures obtained by the reference calculations are very small. For FIPLOC, CONTAIN and MELCOR they can be almost fully explained:

The higher pressure of CONTAIN (CIEMAT) compared to FIPLOC (GRS/IPSN-Fs) is mainly the result of the higher air content used by CIEMAT. The lower pressure of MELCOR (NUP) is caused by a higher heat flux to the sumps and by the condensation heat transfer model.

The differences of the results of GOTHIC and FUMO in comparison to FIPLOC, CONTAIN and MELCOR can only partially explained, since GOTHIC (Battelle) had irregularities in the condensation heat transfer and FUMO (UPISA) did match the stratification in the inner rooms as the others.

Effect of air masses and heat flux to the sumps on the pressure

The effects of the differences in air masses and calculated heat fluxes to the sumps on the pressure can be quantified. They are listed in Tab. A1. For comparison reasons the FIPLOC values have been chosen as reference. A larger air mass results in a higher pressure, assuming the compared calculation had the reference air mass, its pressure has to be reduced. This was done by hand calculations. A higher heat flux to the sumps results in a lower pressure, assuming the compared calculation had the reference heat flux its pressure has to be increased. This was estimated by a FIPLOC parametric study (see below). The pressure differences caused by the above described effects are added to the pressures calculated by the codes. In Tab. A2 above the difference in the pressure calculated by the codes to the experiment are shown, below in parenthesis the differences between the corrected pressures and the experiment.

Table A1: Effect of the differences in sump simulation and air mass on the pressure in comparison to the reference values.

Participant Calculation		Phase 1 12.5 h	End of Phase 3	End exp. 30 h
Battelle GOTHIC	air mass sump effect sum	- 0.03 bar + 0.05 bar + 0.02 bar	- 0.08 bar - 0.05 bar - 0.13 bar	- 0.08 bar + 0.05 bar - 0.03 bar
NUP-MEL MELCOR	air mass sump effect sum	- 0.01 bar + 0.05 bar + 0.04 bar	+ 0.01 bar - 0.05 bar - 0.04 bar	- 0.02 bar + 0.05 bar + 0.03 bar
UPISA FUMO	air mass sump effect = ?	+ 0.01 bar	+ 0.02 bar	+ 0.04 bar
CIEMAT CONTAIN	air mass sump effect sum	- 0.03 bar 0.0 bar - 0.03 bar	- 0.09 bar - 0.05 bar - 0.14 bar	- 0.07 bar 0.0 bar - 0.07 bar

Table A2: Containment pressure, experiment and different codes used in ISP37, including "corrections of Tab. A1" to differences in sump simulation and air mass

Participant Calculation	$P_{calculated} - P_{experiment}$ (bar) Phase I 12.5 h	End of Phase III	End exp. 30 h	
GRS/IPSN-Fs FIPLOC	+ 0.15	- 0.02	+ 0.21	reference calculation for this comparison
Battelle GOTHIC	0. (0.02)	+ 0.05 (- 0.08)	+ 0.08 (+ 0.05)	$P_{calculated} - P_{experiment}$ $(P_{corrected} - P_{experiment})$
NUP-MEL MELCOR	+ 0.03 (0.07)	0. (- 0.04)	+ 0.14 (+ 0.17)	$P_{calculated} - P_{experiment}$ $(P_{corrected} - P_{experiment})$
UPISA FUMO	+ 0.09 (+ 0.1)	- 0.02 (0.)	+ 0.21 (+ 0.25)	$P_{calculated} - P_{experiment}$ $(P_{corrected} - P_{experiment})$
CIEMAT CONTAIN	+ 0.2 (+ 0.17)	+ 0.1 (- 0.04)	+ 0.34 (+ 0.27)	$P_{calculated} - P_{experiment}$ $(P_{corrected} - P_{experiment})$

Explanation for the remaining pressure differences between the reference calculations

Correcting the calculated pressures in respect to difference in sump modeling and air content shifts the results of FIPLOC, MELCOR and CONTAIN more close together. The remaining differences can be qualitatively explained by the condensation heat transfer models (see below):

- The "corrected" MELCOR pressure is at 12.5 h 0.08 bar and at 30 h 0.04 bar lower than the FIPLOC pressure. The remaining difference can be qualitatively explained by the heat transfer models. MELCOR generally needs for the steam condensation a smaller difference between the saturation and surface temperatures (T_{sat} - T_{surf}) than FIPLOC. This results in a lower T_{sat} and a lower partial steam pressure.
- The "corrected" CONTAIN and FIPLOC pressures are very close together: At 12.5 h CONTAIN is 0.02 bar and at 30 h 0.06 bar higher. The remaining difference can be qualitatively explained by the larger T_{sat} - T_{surf} for condensation generally needed by CONTAIN.

GOTHIC has the lowest pressure of the reference calculations. The correction due to the sump effect and air mass do not shift it towards the other results, since they almost counterbalance. One qualitative explanation is that the 2 mm thick coating on the outer shell is not simulated. Also irregularities in the condensation heat transfer might have an influence.

The comparison between FUMO and the other codes is not simple, since FUMO does not simulate the stratification in the inner rooms like the others. Therefore more steam condenses in the inner rooms, which may have an effect on the pressure. In addition the sump effect on the pressure cannot be easily evaluated. The effect of air mass a small T_{sat} - T_{surf} for condensation and the simulation of a small steam leakage decrease the pressure towards the experimental value.

FIPLOC Parametric Study Investigating the Effect of the Sump Temperatures on the Containment Pressure

The study was done with a modified[6] nodalization of the data set used for the FIPLOC calculation GRS/IPSN-Fs. This resulted in sump temperatures higher than GRS/IPSN-Fs but similar as calculated by NUP-MEL (MELCOR) (see Fig. A1). Only the sump temperature of R9.4 (not shown here) started deviating from 15 h on from the NUP-MEL result and was at 30 h about 10 ^{0}C higher. The containment pressure of the study was at 12.5 h 0.05 bar and at 30 h 0.1 bar lower than the GRS/IPSN-Fs pressure. Only at the end of phase 3 it was 0.05 bar higher, since the study simulates in contrast to GRS/IPSN-Fs evaporation of sump water (Fig. A1).

Based on these results it is estimated that the lower sump temperatures of GRS/IPSN-Fs increase its pressure from 12.5 h on by 0.05 bar compared to NUP-MEL (the deviation of the sump temperature in R9.4 to NUP-MEL result towards the end of the study is taken into account). The lack of evaporation in GRS/IPSN-Fs at the end of phase 3 counts for -0.05 bar. Since GOTHIC has similar sump temperatures as NUP-MEL approximately the same numbers were used for comparison to GRS/IPSN-Fs.

The higher sump temperatures calculated by CONTAIN are compensated by the lower heat transfer to the sump bottom. Therefore the sump modeling of CONTAIN is estimated to cause no pressure difference to FIPLOC, except for the end of phase 3 it counts for -0.05 bar (see above).

The difference in sump effect on the pressure between FIPLOC and FUMO cannot be evaluated, since the calculations have a different water distribution to the individual sumps.

Condensation heat transfer

Almost all injected steam condenses on the structures. The remaining part increases the partial steam pressure. Therefore the atmospheric pressure is determined mainly

[6] Modifications to the GRS/IPSN-Fs data set for the study: The nodalistion was modified in the way that the sumps of R3, R4, R6, R8 were in thermal equilibrium with the atmosphere above. The thickness of the heat conducter between the atmosphere and the sump of R9.4 was decreased. The drain simulation was modified in order to obtain the the same water distribution in the upper containment rooms as NUP-MEL.

by the geometry, heat capacity and conductivity of the structures and secondly by the condensation heat transfer model. The heat transfer model determines the temperature difference between the atmospheric saturation and the wall surface (T_{sat} - T_{surf}) and T_{sat} determines the partial steam pressure. The results of the FIPLOC group and parametric studies done by GRS and NUPEC show that the choice of different condensation heat transfer models can result in pressure differences of 0.05 to 0.1 bar.

Fig. 4.15a in the main report shows the atmospheric temperatures of the dome and the surface temperature on the containment side of structure 8. The difference between these temperatures are very small. Since almost during the entire experiment steam condenses on structure 8, this indicates that the dome is generally at or close to saturation and a small T_{sat} - T_{surf} is needed for condensation. This is the case for an almost pure steam atmosphere from 4 to 14.5h and a steam air mixture after 14.5 h.

The results of the reference calculations GRS/IPSN-Fs (FIPLOC), NUP-MEL (MELCOR) and UPISA (FUMO) (Fig. 4.15b, d, f) can be directly compared, since they calculate in agreement to the experiment also conditions at or close to saturation. Since CIEMAT (CONTAIN) calculates superheating its saturation temperatures are shown in Fig. A2. For almost pure steam atmosphere FIPLOC, MELCOR, CONTAIN and FUMO need only a small T_{sat} - T_{surf}. This is in good agreement with the experiment. For a steam - air mixture following tendency is found T_{sat} - T_{surf} is the smallest for MELCOR, slightly larger for FUMO and larger for FIPLOC and CONTAIN. The smaller value is in better agreement with the experiment. Further comparison show that CONTAIN has the tendency for a larger T_{sat} -T_{surf} than FIPLOC for example in R9.3 up to 15 h (Fig. 4-16b and Fig. A2).

The calculation of Battellle (GOTHIC) had oscillations in the heat flow to the dome structures from 3 to 10 h as can be seen in Fig. 4.15e on the atmosphere and the surface temperature. An evaluation as for the other reference calculations was not possible, since in addition the atmospheric flows oscillated during this time span.

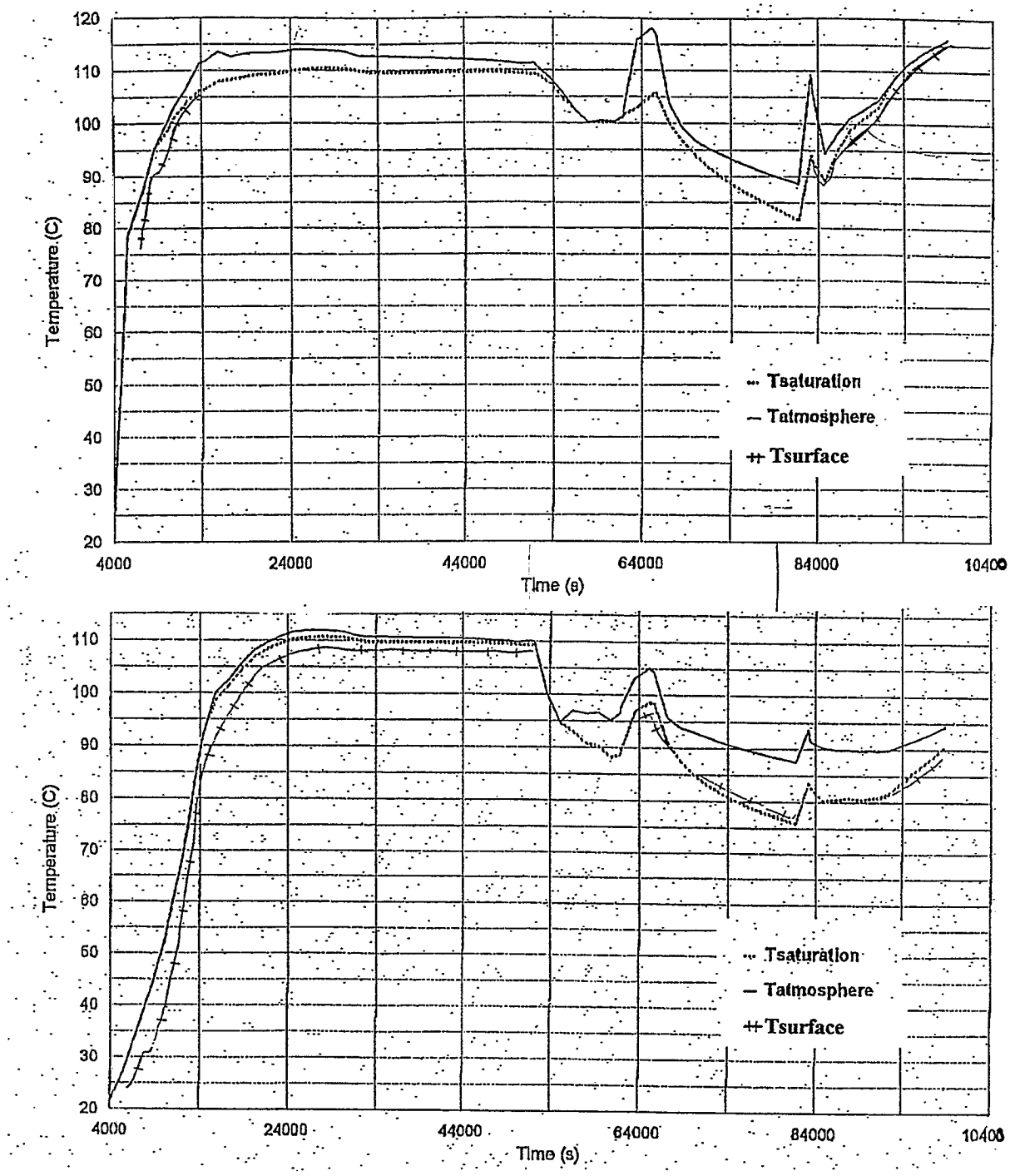

Fig. A2: CIEMAT (CONTAIN) temperatures of atmosphere, atmospheric saturation structure surface (above: dome an structure 8, below: R9.3 and structure 3)

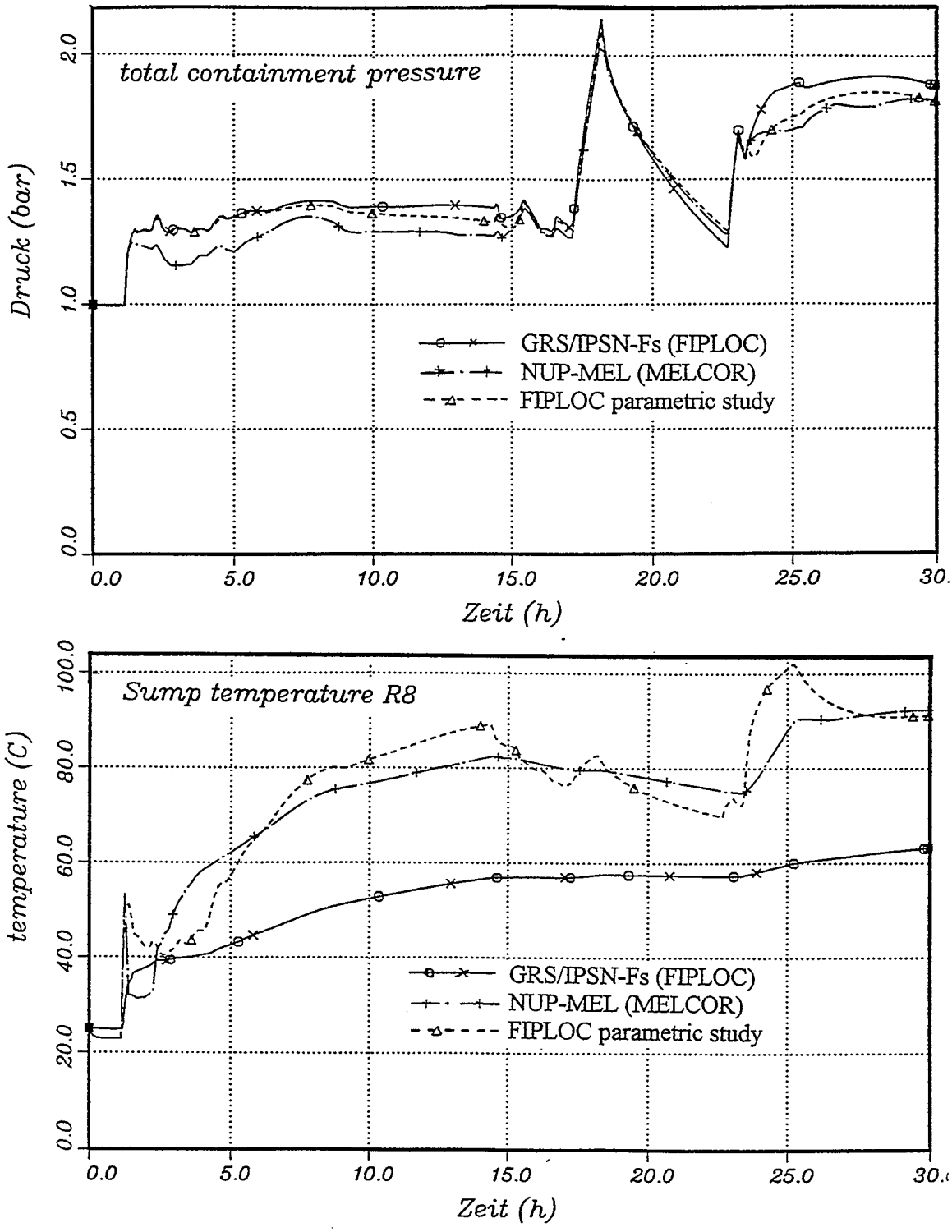

Fig. A1: FIPLOC parametric study investigating the effect of the sump temperatures on the pressure: comparison to the results of GRS/IPSN-Fs and NUP-MEL

8 Figures

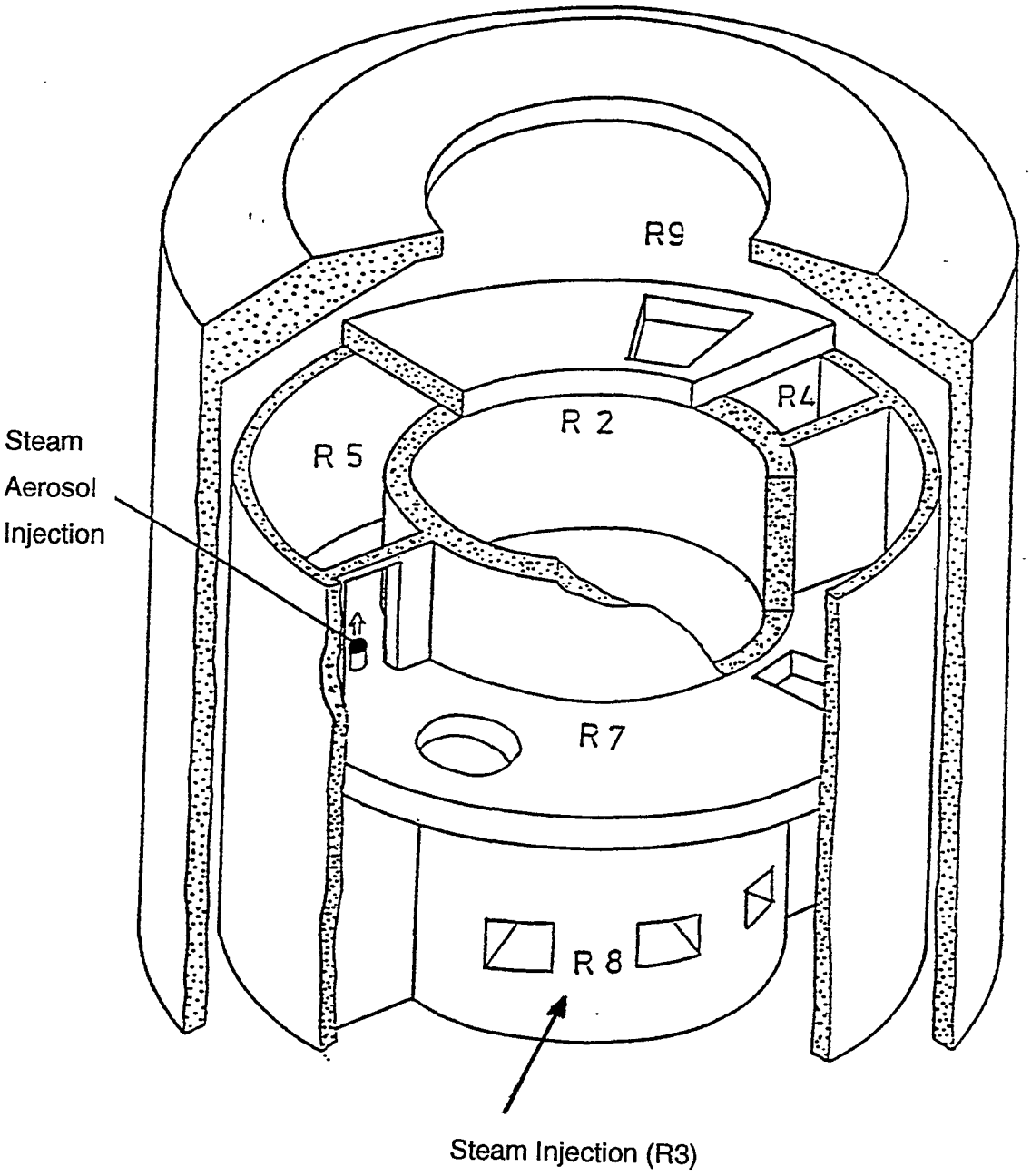

Fig. 3.1 Battelle Model Containment in VANAM Test Configuration

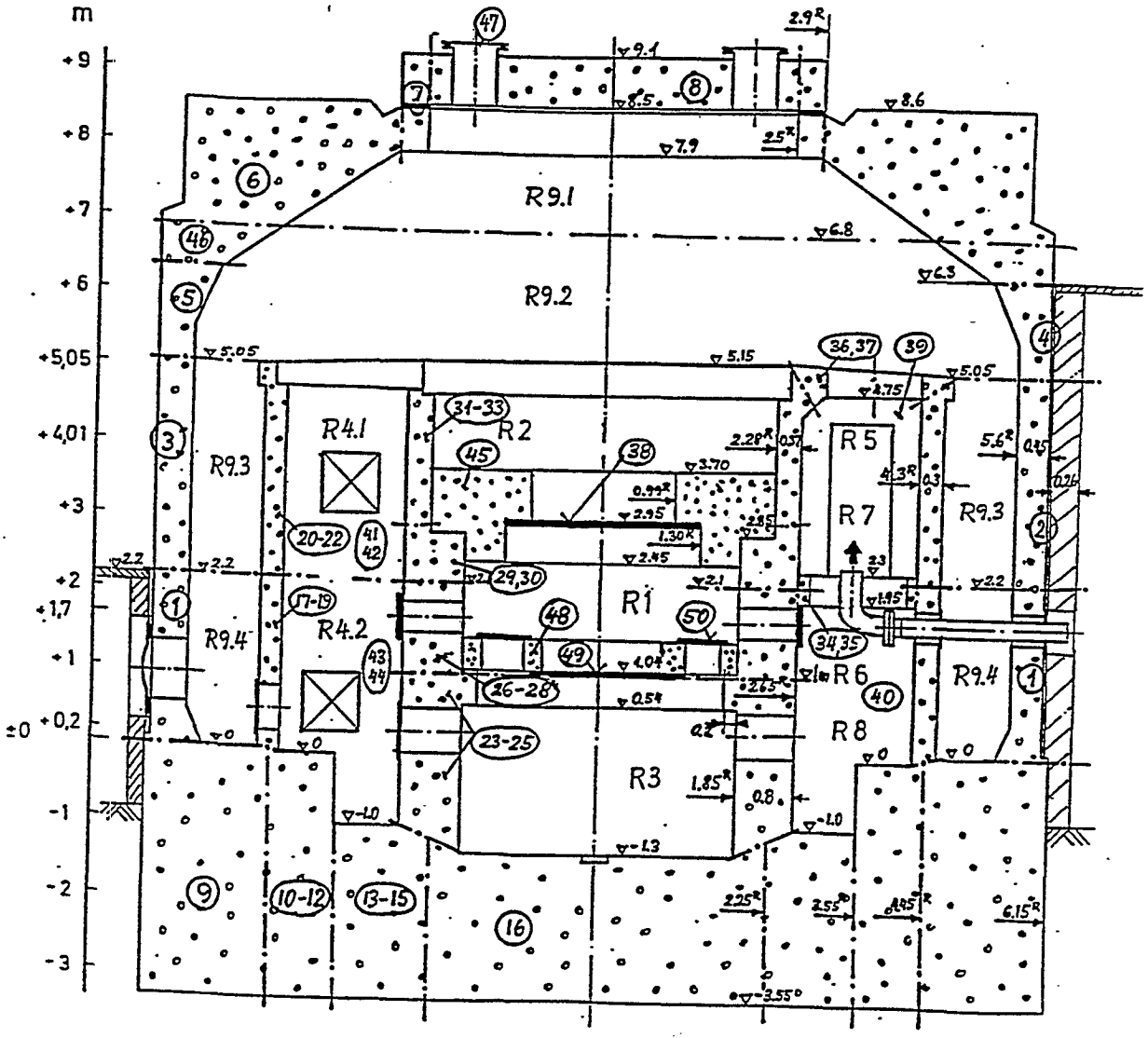

Fig. 3.2 Cross Section of Battelle Model Containment

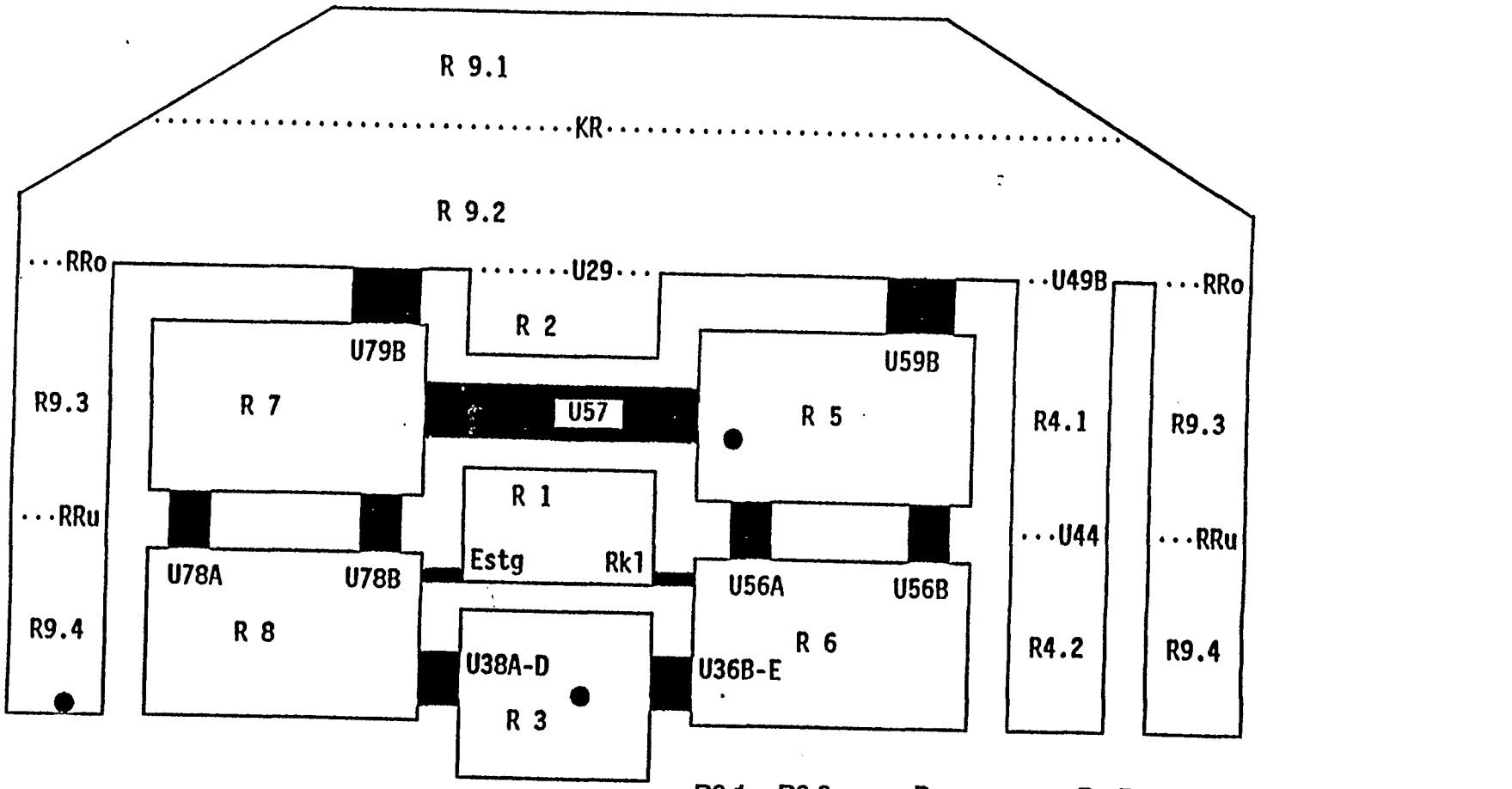

Fig. 3.3 Nodalization Scheme of Battelle Model Containment

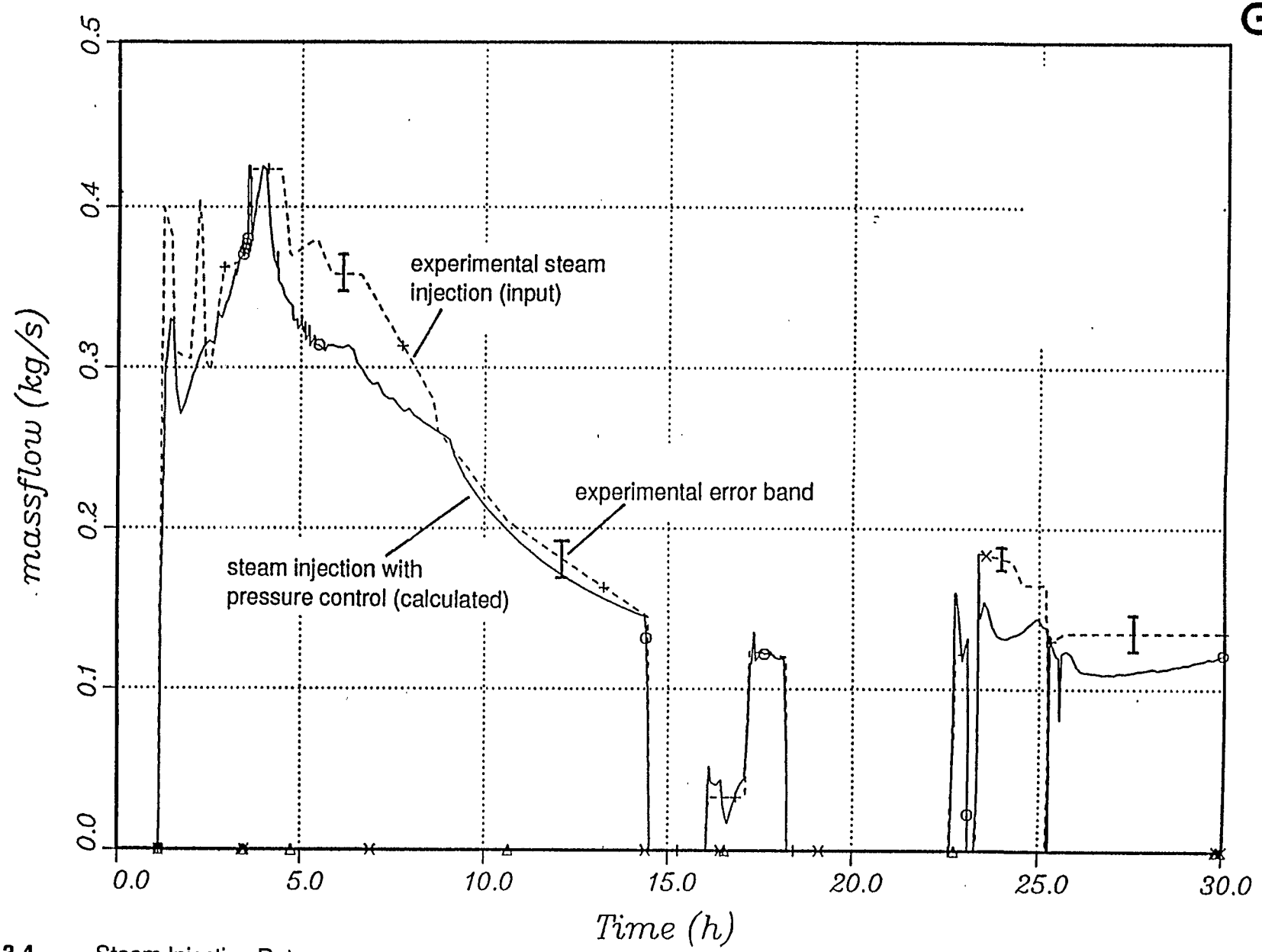

Fig. 3.4 Steam Injection Rate

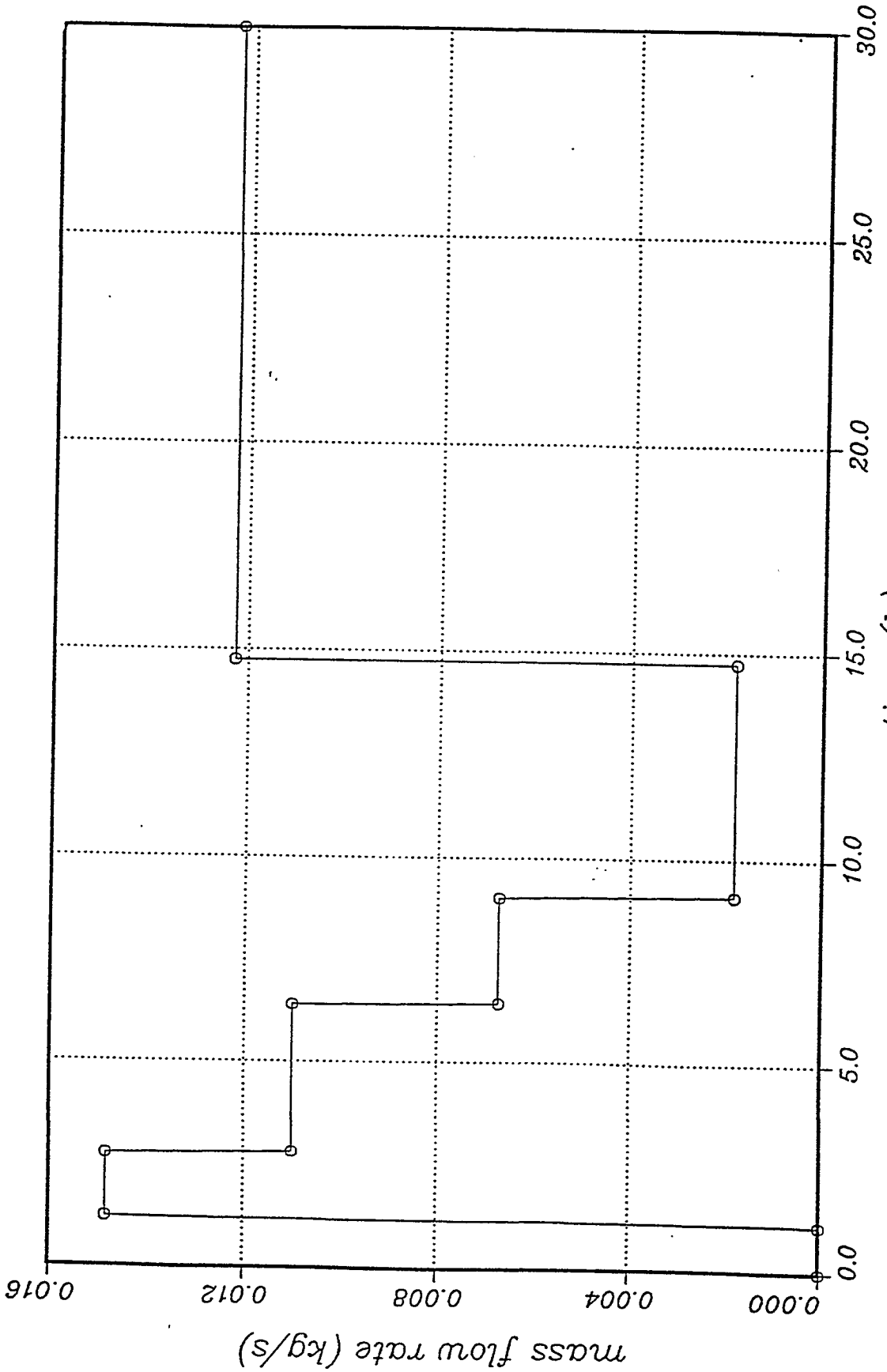

Fig. 3.5 Air Leak Rate

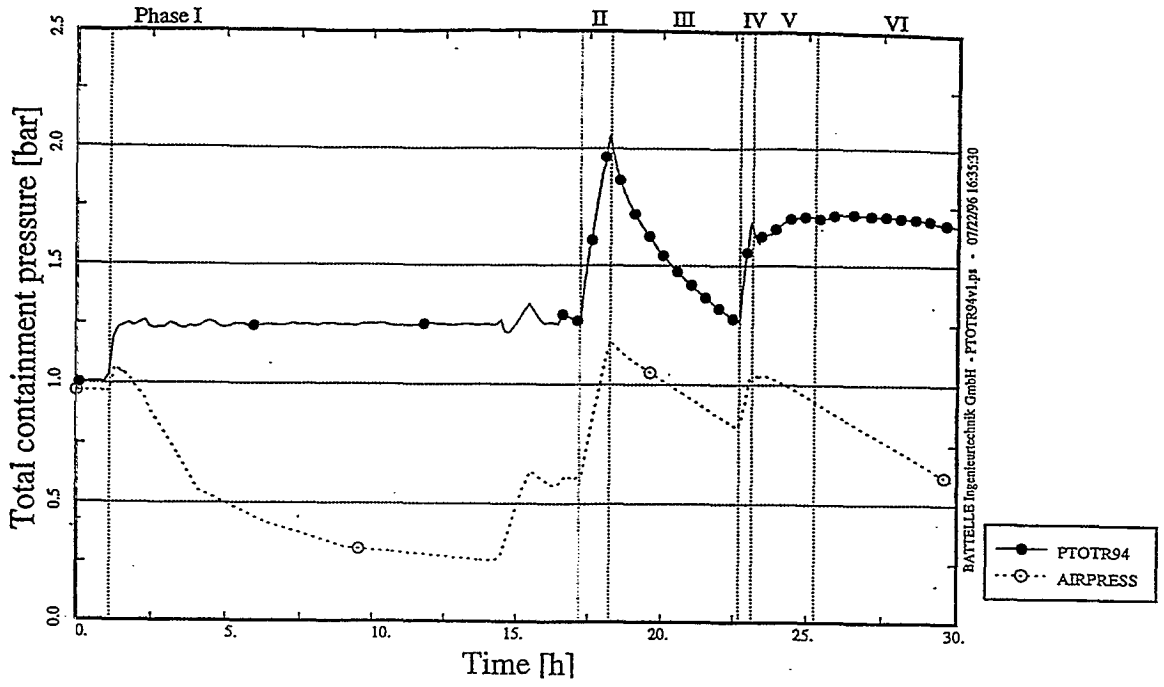

Fig. 3.7a Containment Pressure and Total Calculated Partial Air Pressure

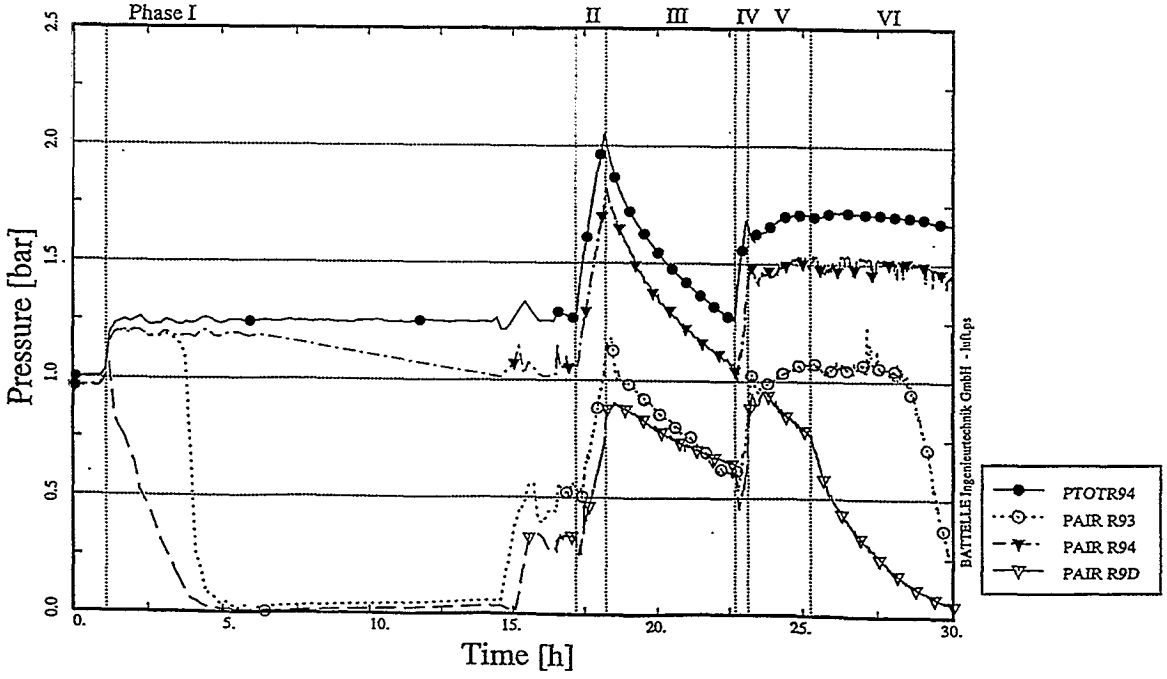

Fig. 3.7b Containment Pressure and Calculated Air Pressure for Different Compartments

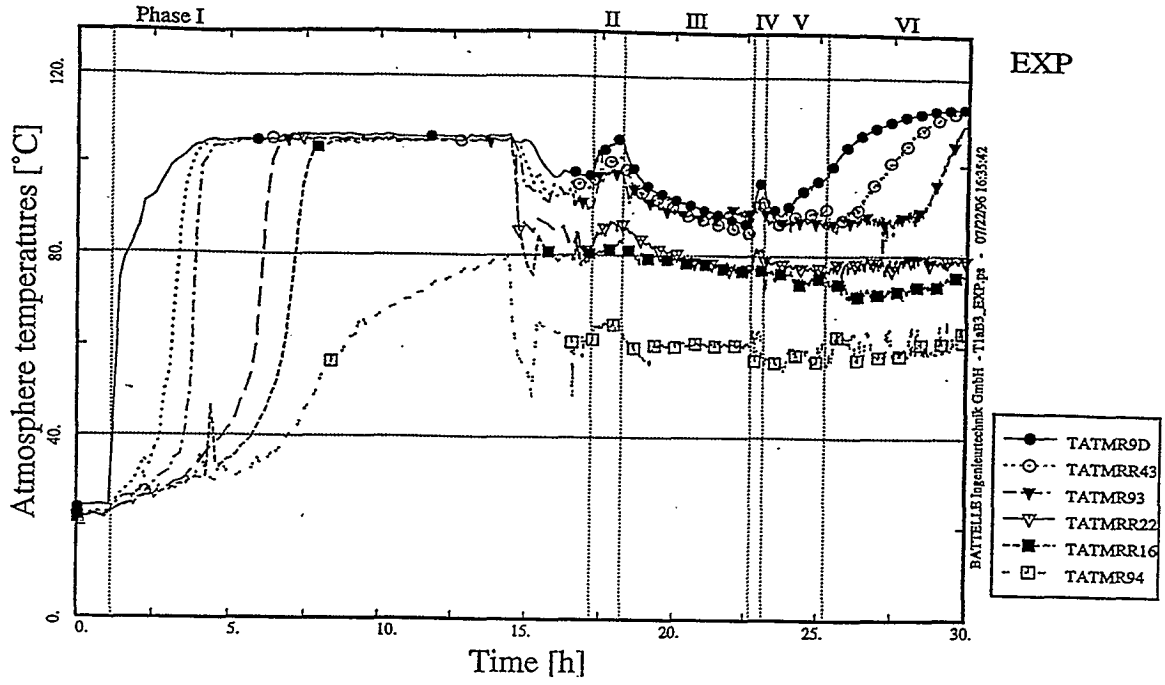

Fig. 3.8a Experimental Atmospheric Temperature (Dome, Annulus)

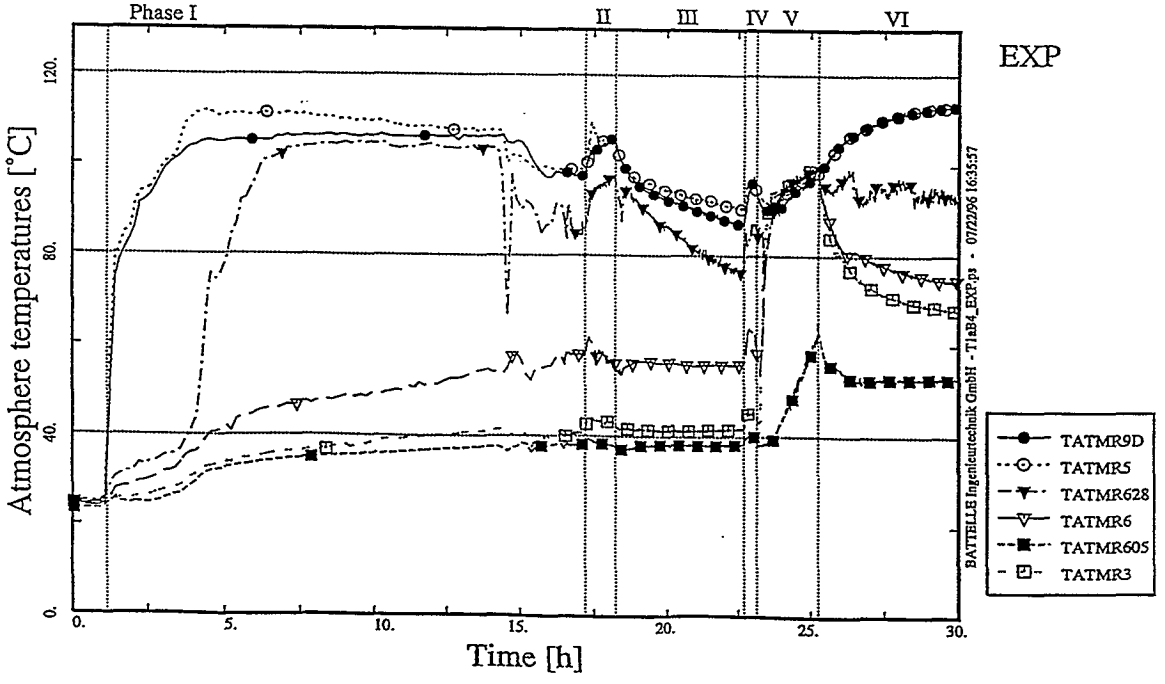

Fig. 3.8b Experimental Atmospheric Temperature (Dome, R5, R6, R3)

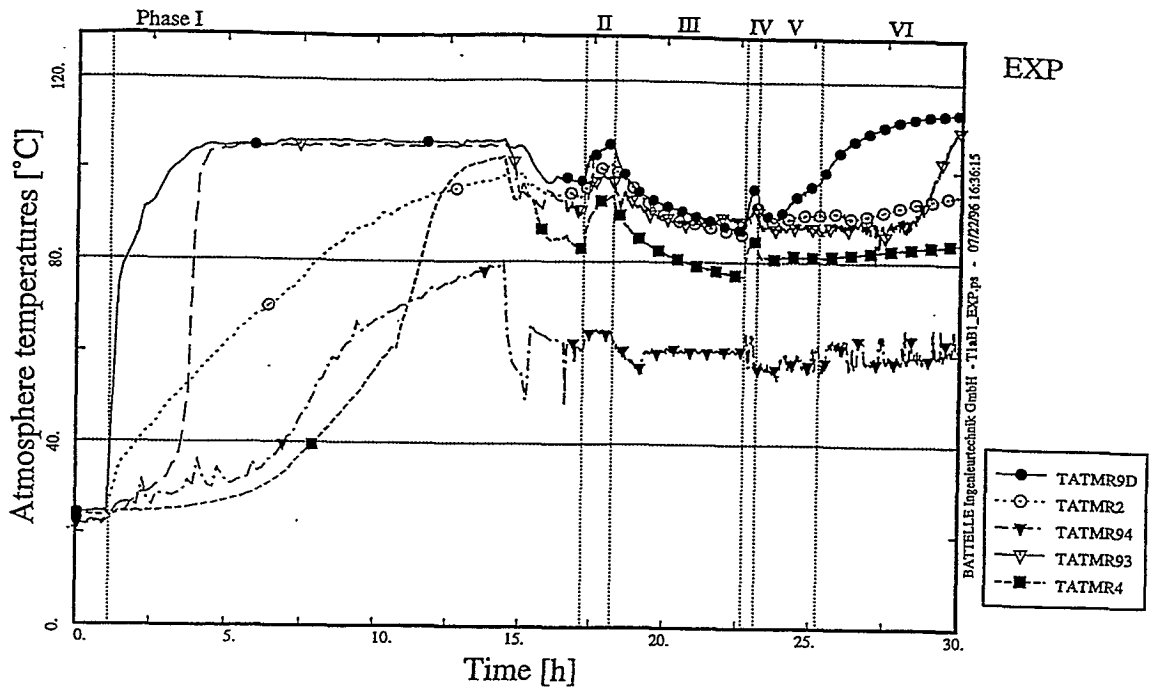

Fig. 3.9a Experimental Atmospheric Temperature (Dome, Annulus, R2, R4)

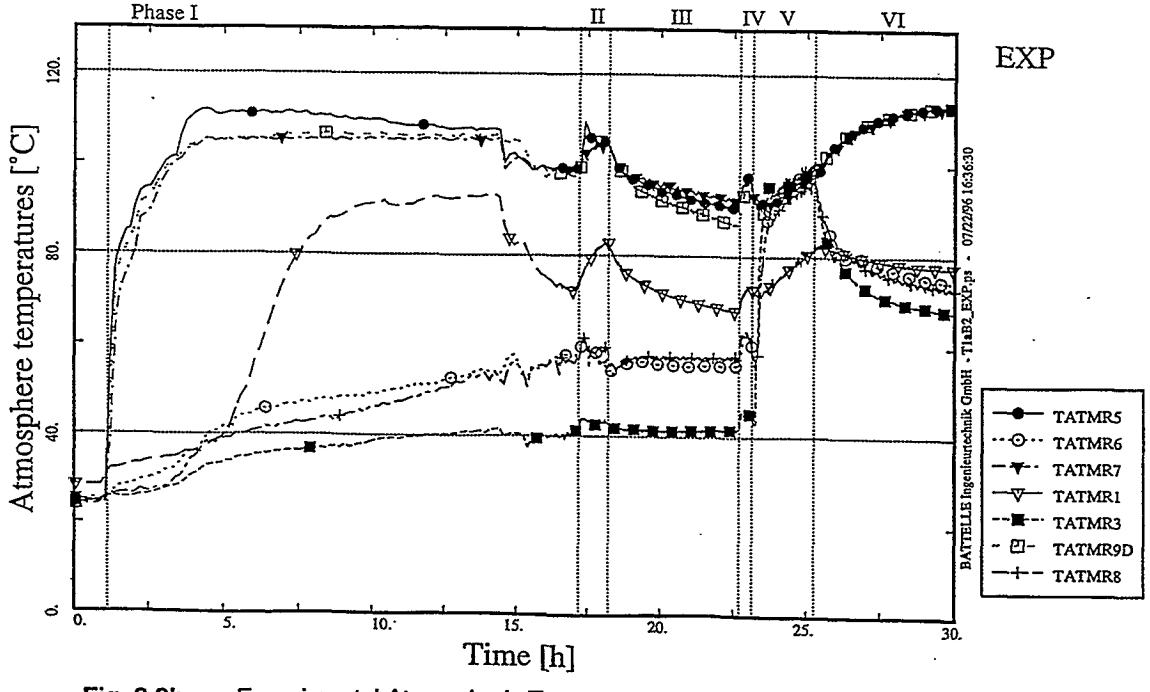

Fig. 3.9b Experimental Atmospheric Temperature
(Dome, R1, R3, R5, R6, R7, R8)

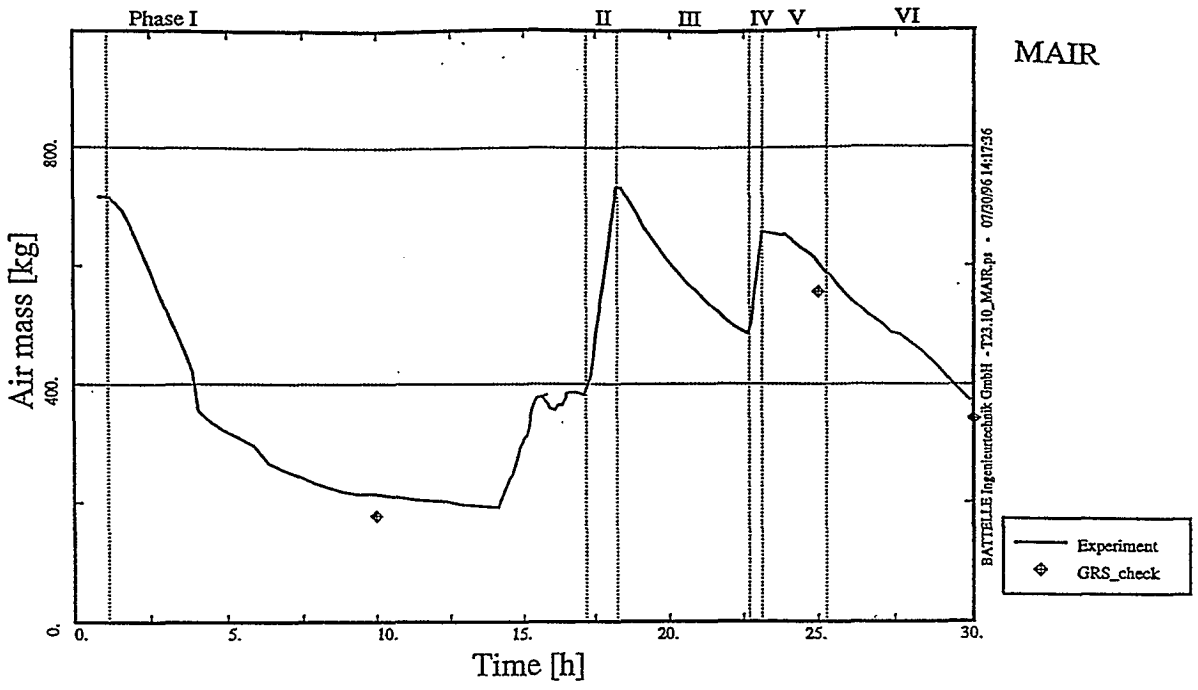

Fig. 3.10 Air Mass Inventory Determined from Measurements (including GRS check calculation)

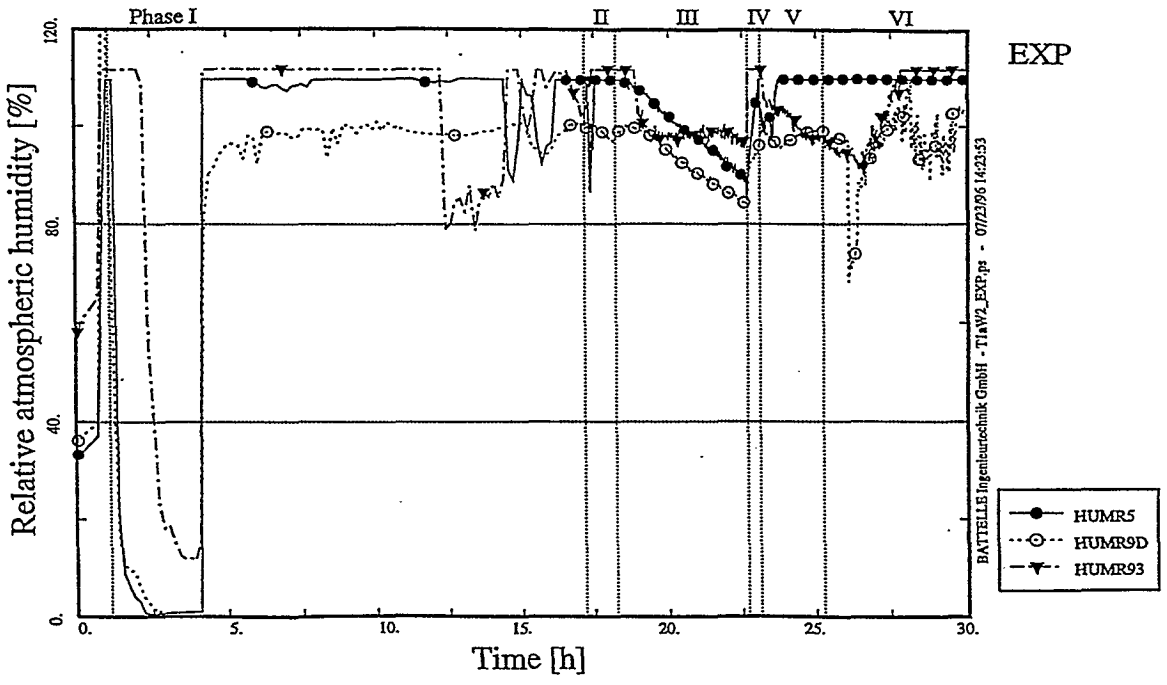

Fig. 3.11 Measured Humidities in Dome, Annulus and Compartment R5

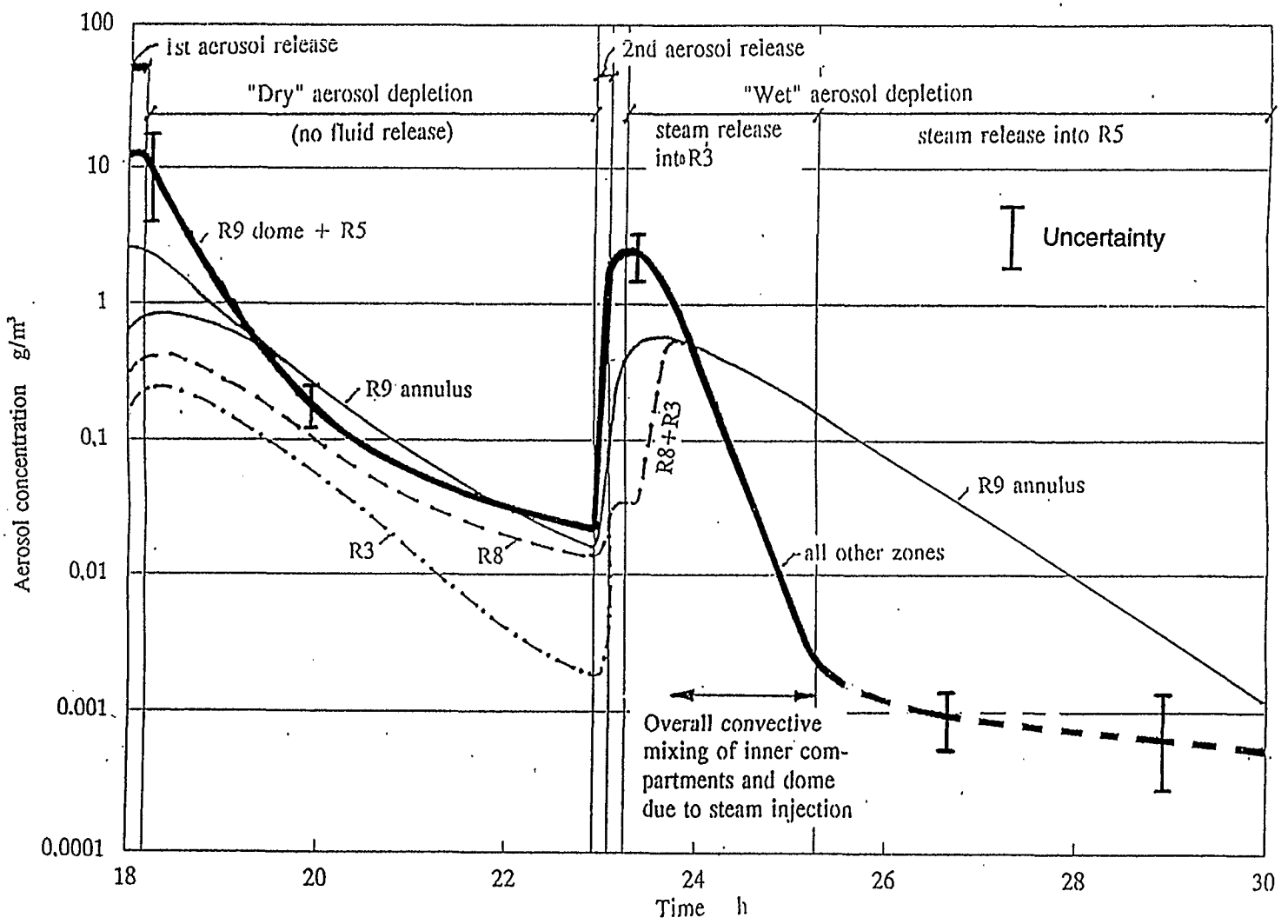

Fig. 3.12 NaOH Aerosol Concentration

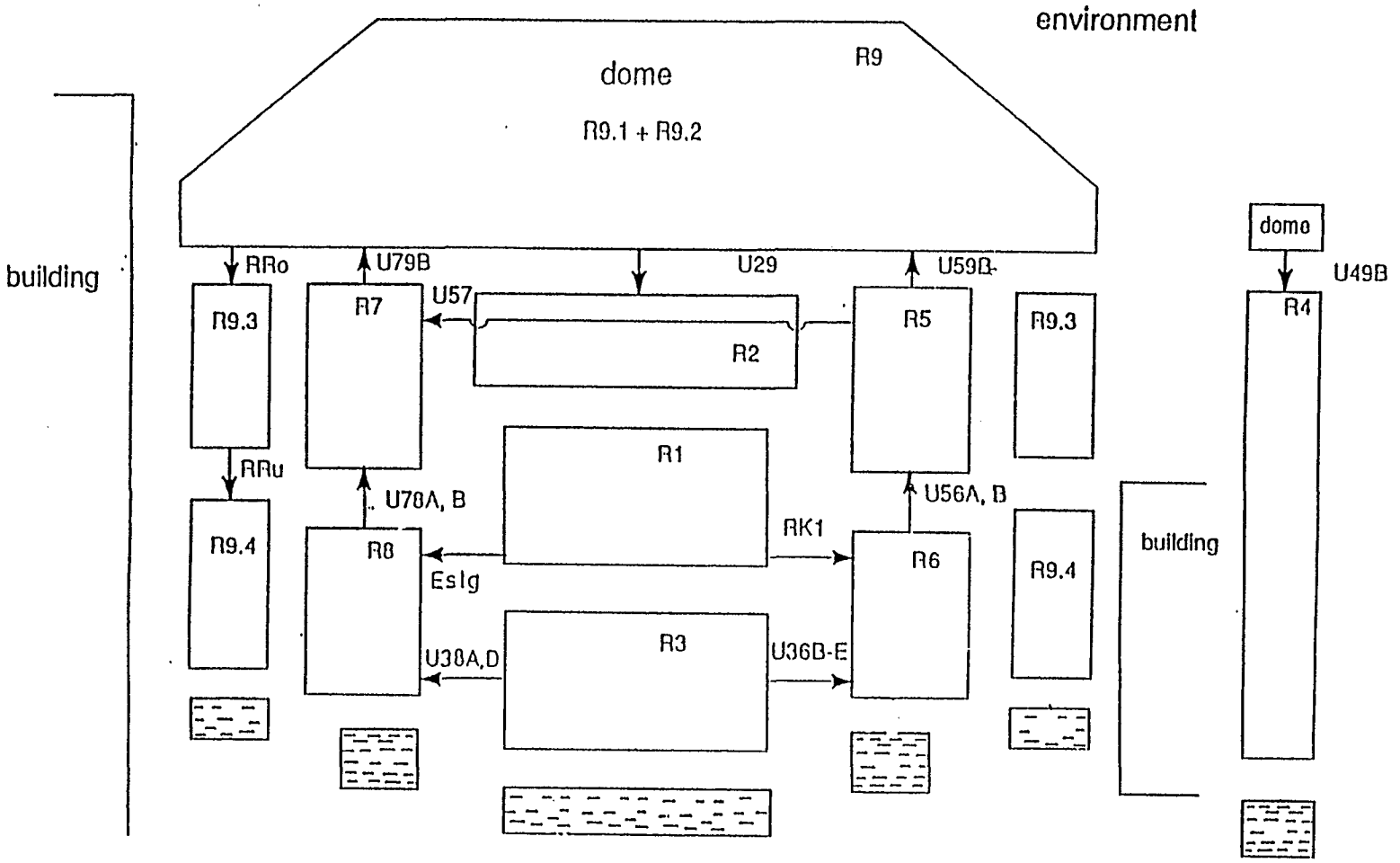

Fig. 4.1 Proposed Nosalization

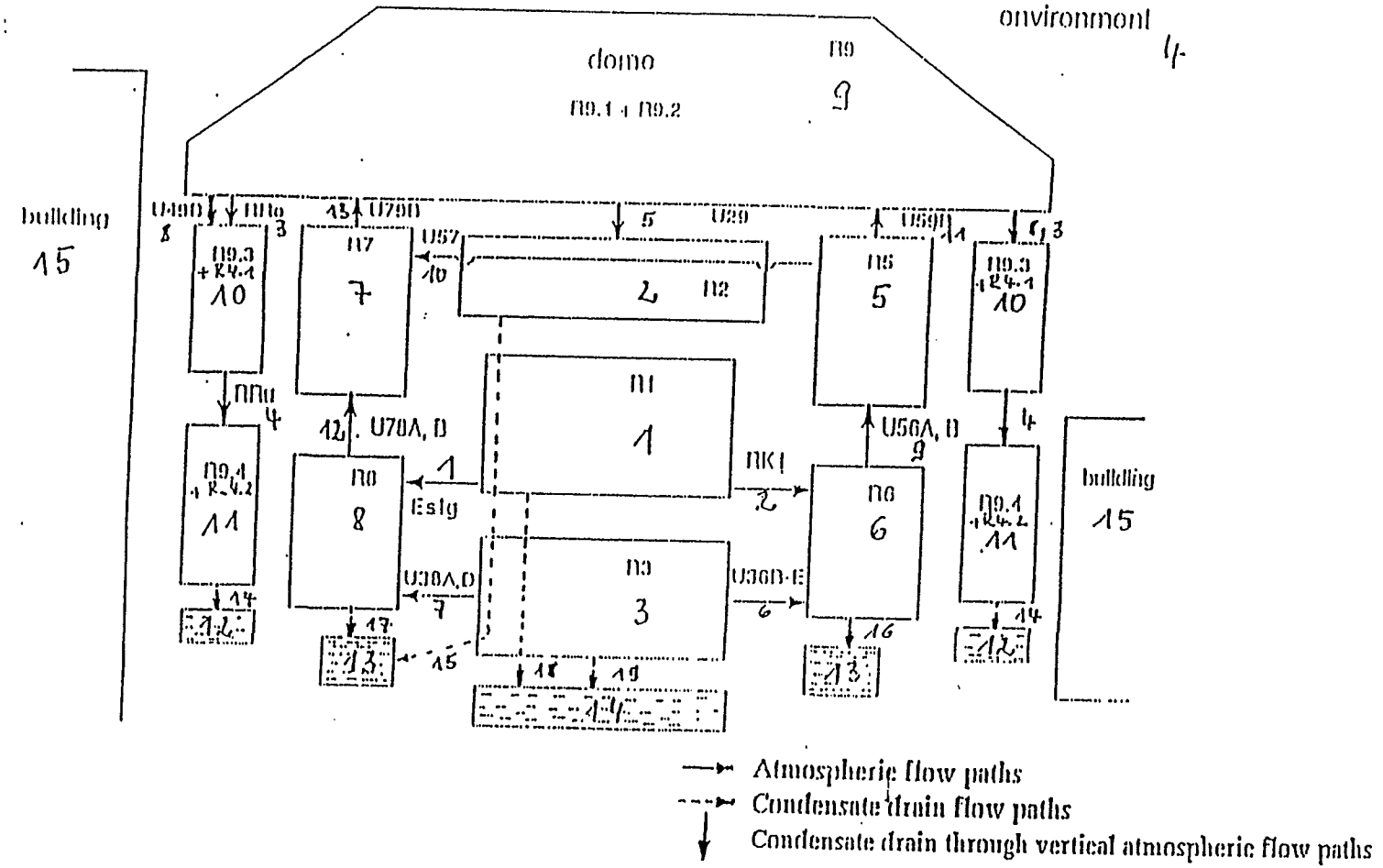

Fig. 4.2a Nosalization Used by IFE

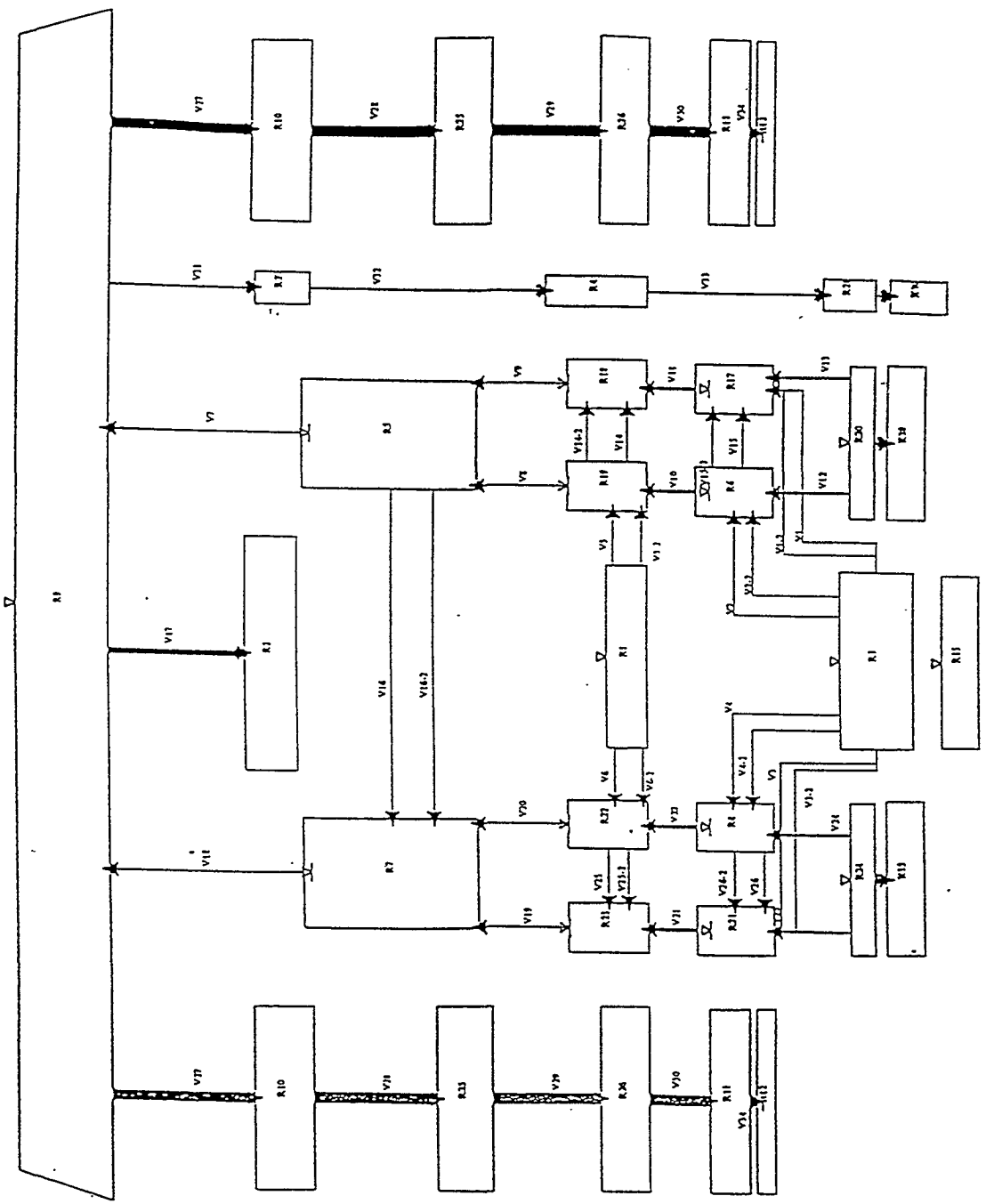

Fig. 4.2b Nosalization Used by GRS/IPSN-FE and -Re

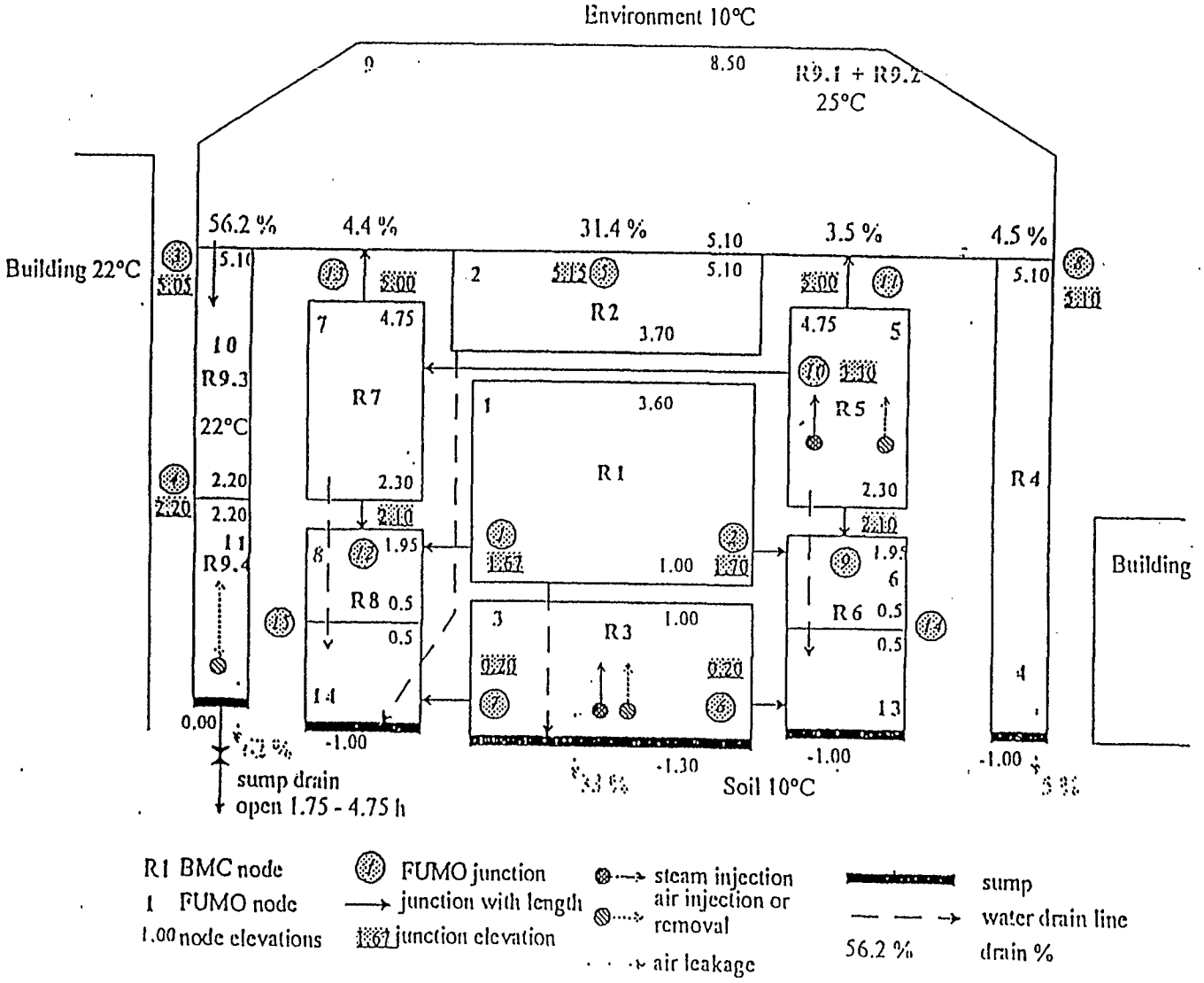

Fig. 4.2c Nosalization Used by UPISA

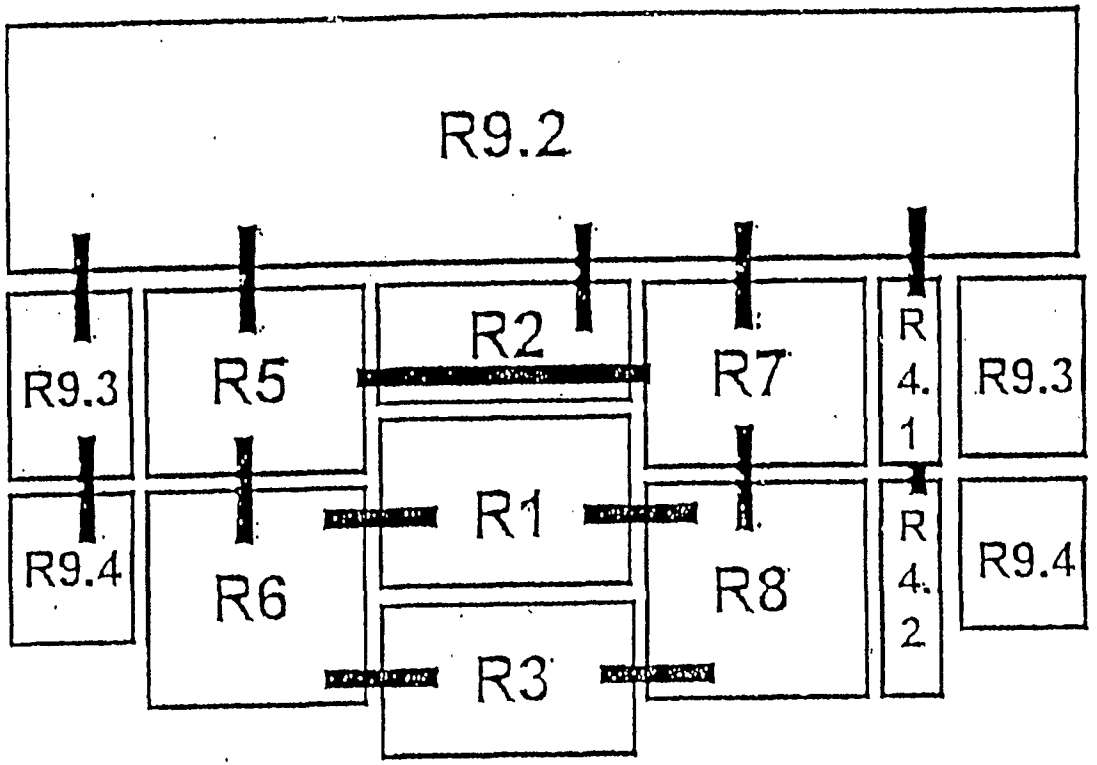

Fig. 4.2d Nosalization Used by CIEMAT

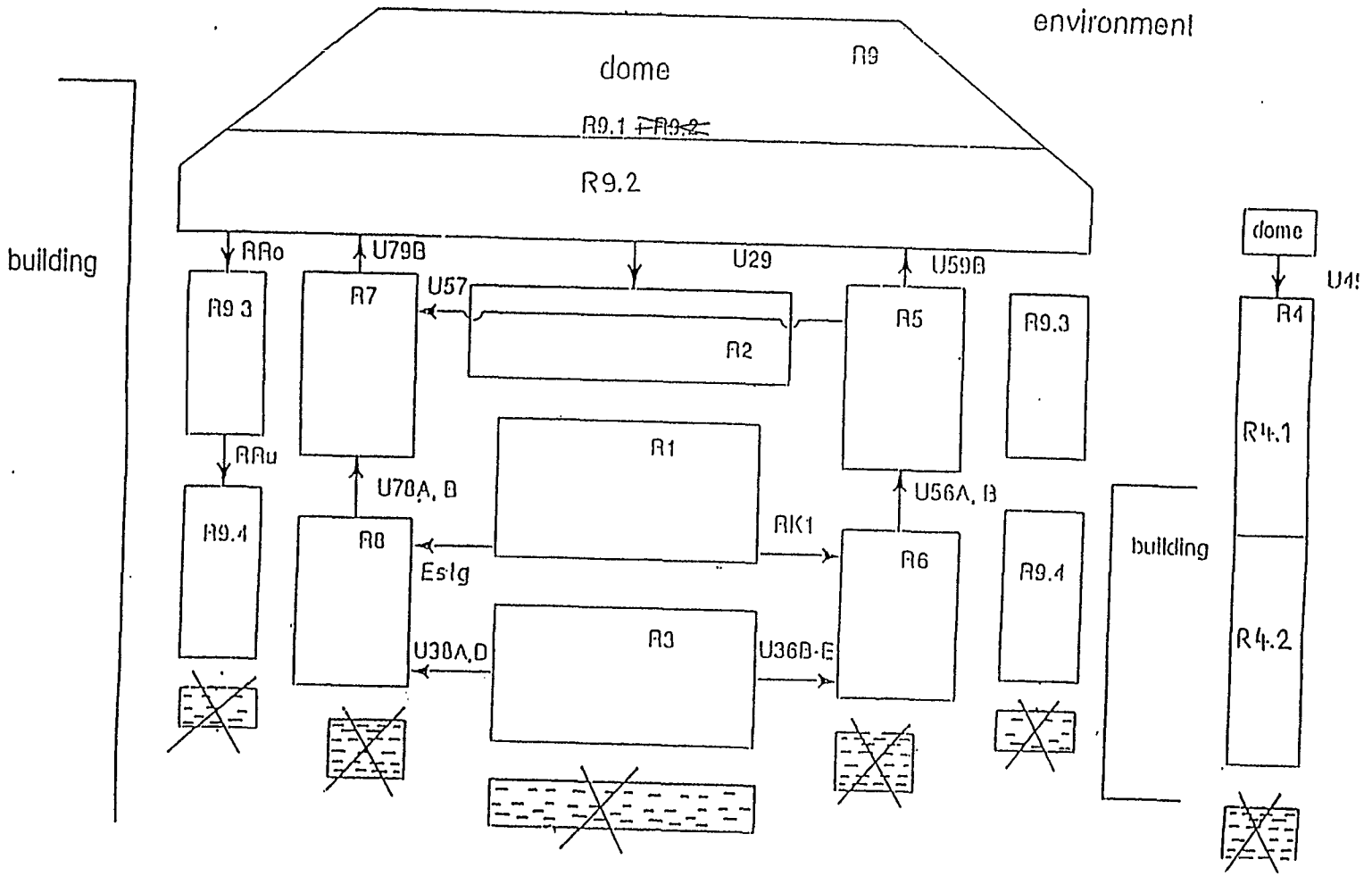

Fig. 4.2e Nosalization Used by VUJE-MEL

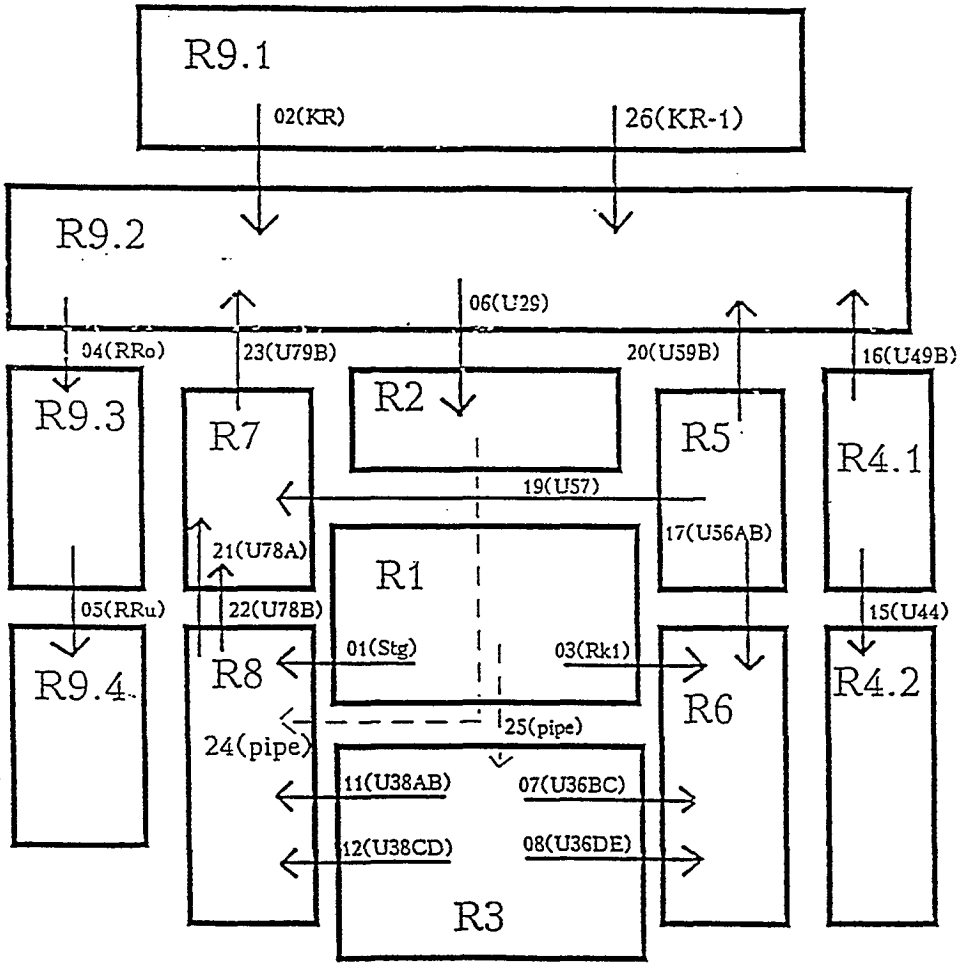

Fig. 4.2f Nosalization Used by KI-MEL

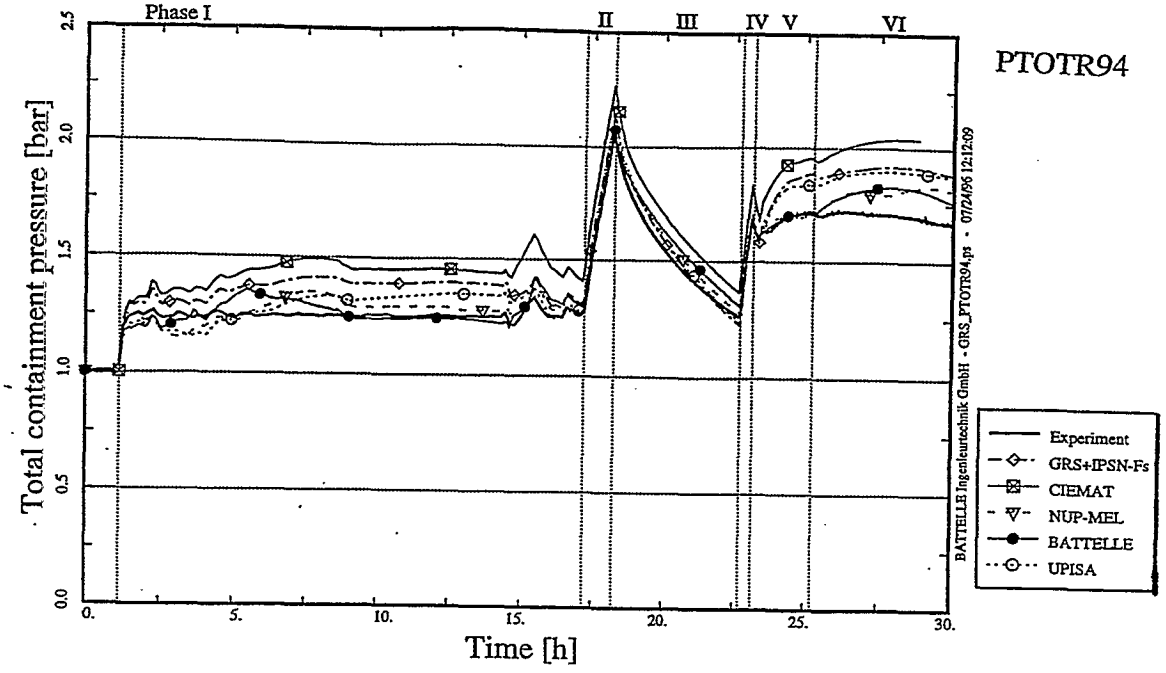

Fig. 4.3 Containment Pressure (Reference Calculation)

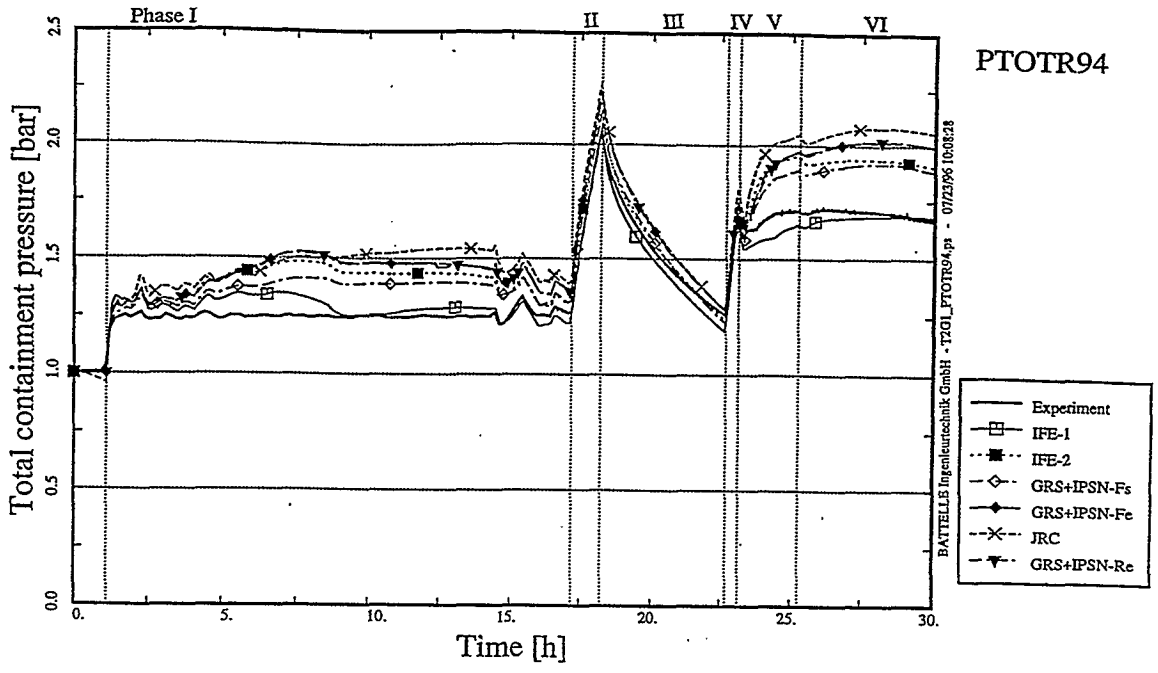

Fig. 4.4a Containment Pressure (FIPLOC / RALOC)

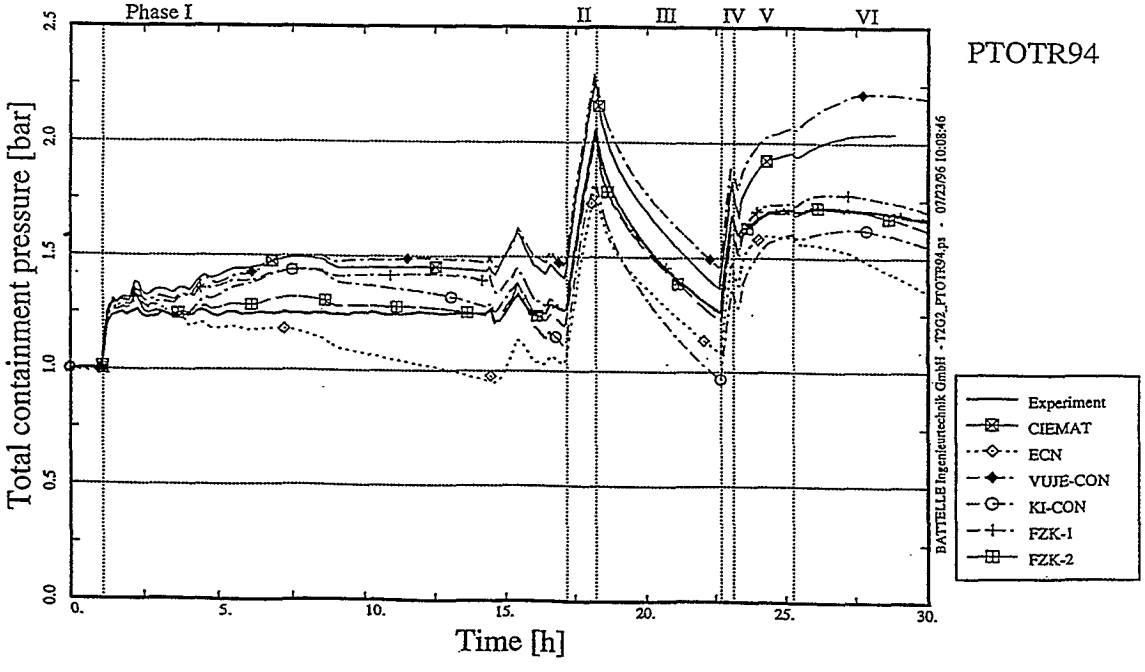

Fig. 4.4b Containment Pressure (CONTAIN)

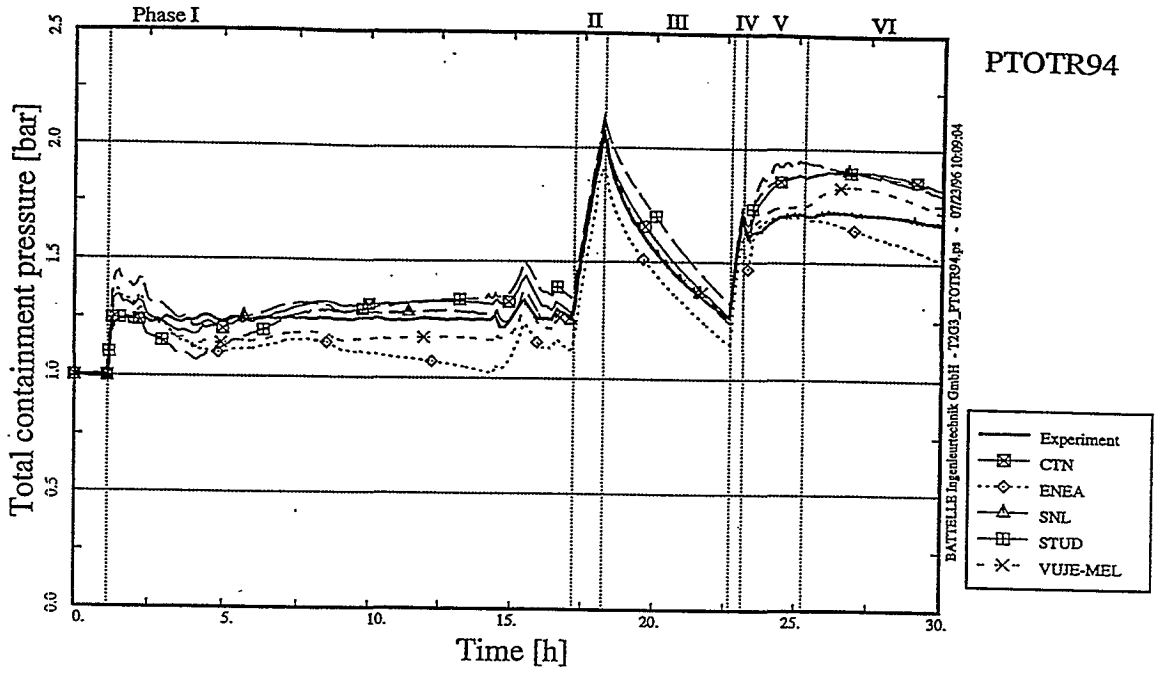

Fig. 4.4c Containment Pressure (MELCOR, part I)

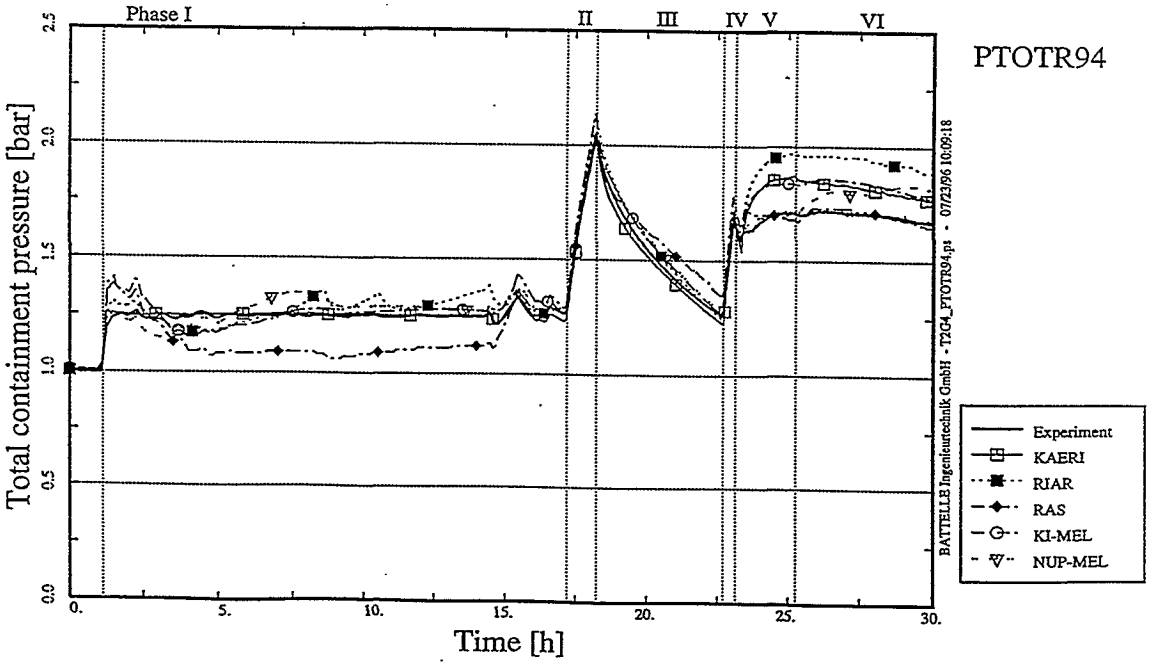

Fig. 4.4d Containment Pressure (MELCOR, part II)

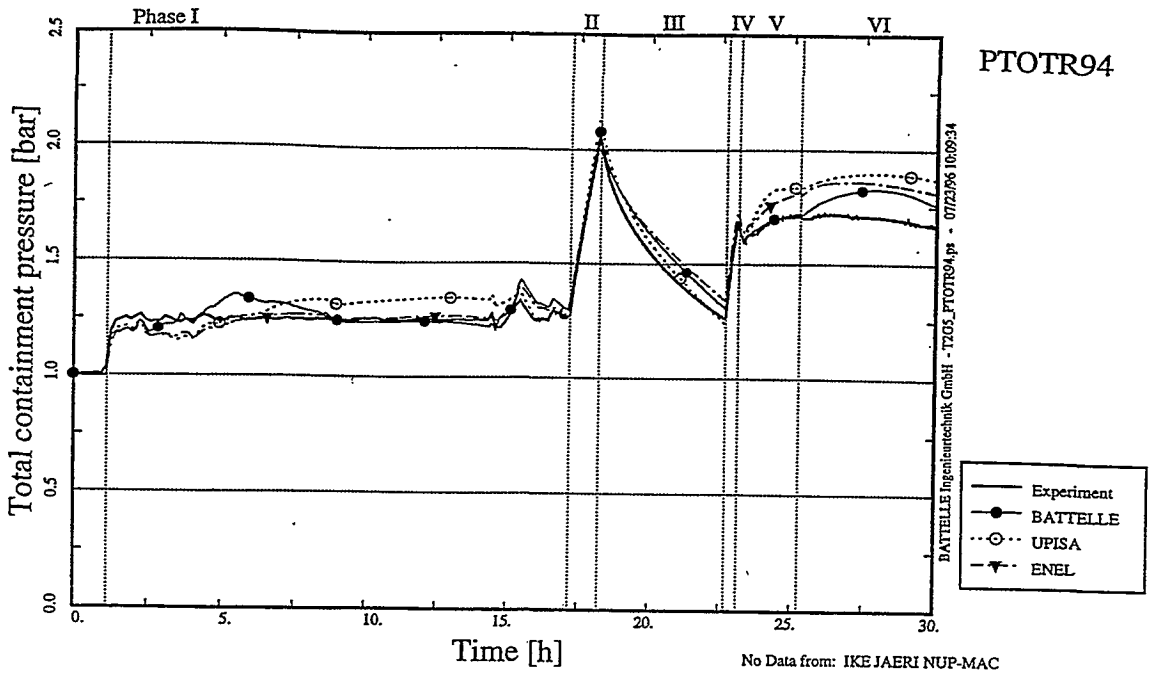

Fig. 4.4e Containment Pressure (ECART, FUMO, GOTHIC)

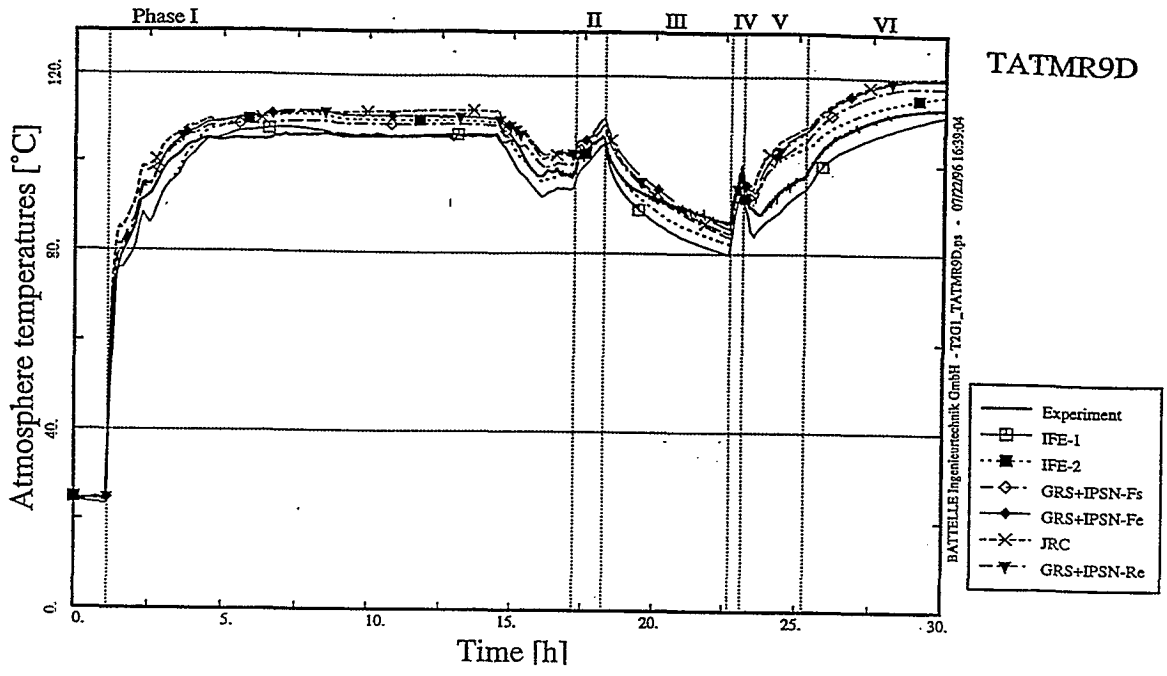

Fig. 4.5a Dome Temperature (FIPLOC / RALOC)

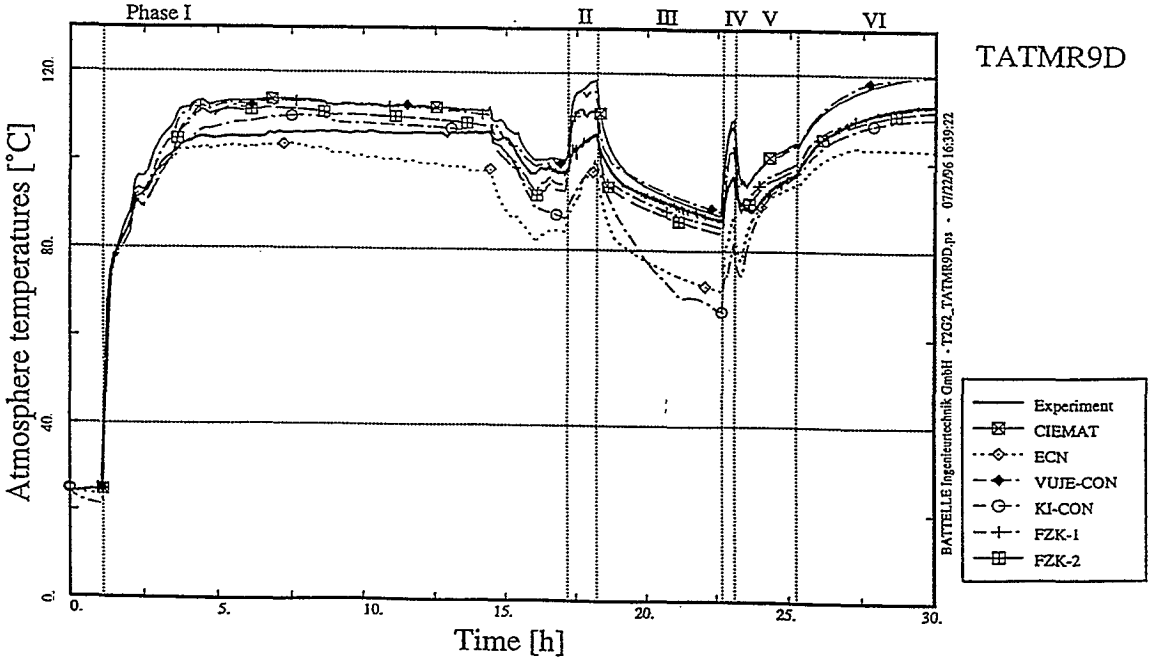

Fig. 4.5b Dome Temperature (CONTAIN)

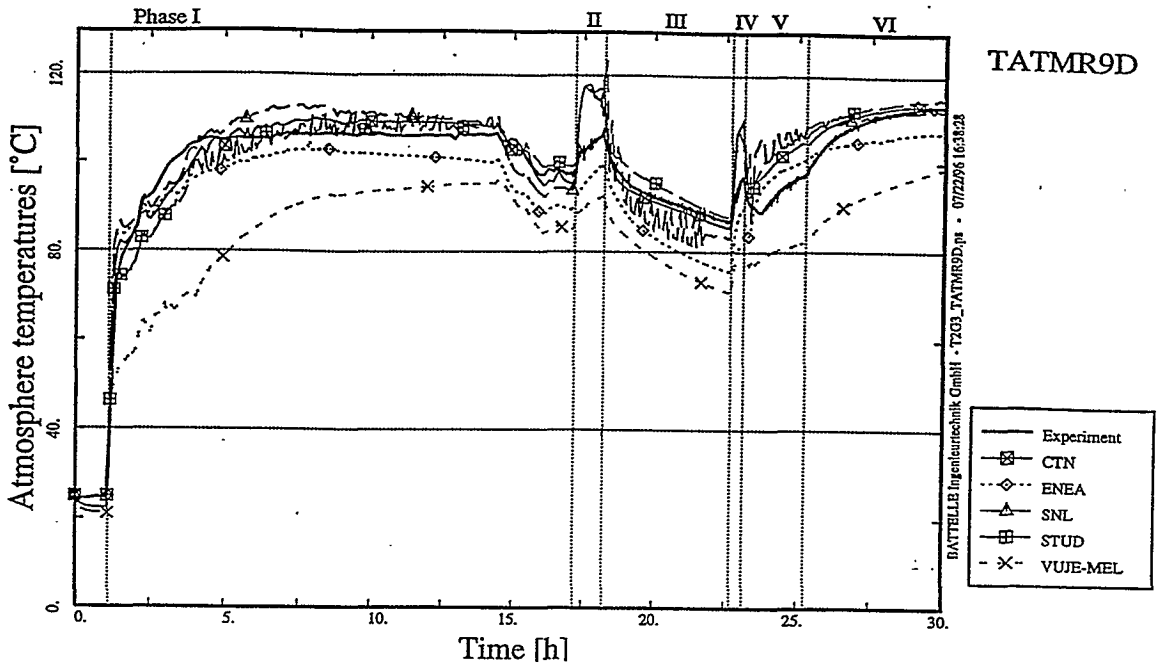

Fig. 4.5c Dome Temperature (MELCOR, part I)

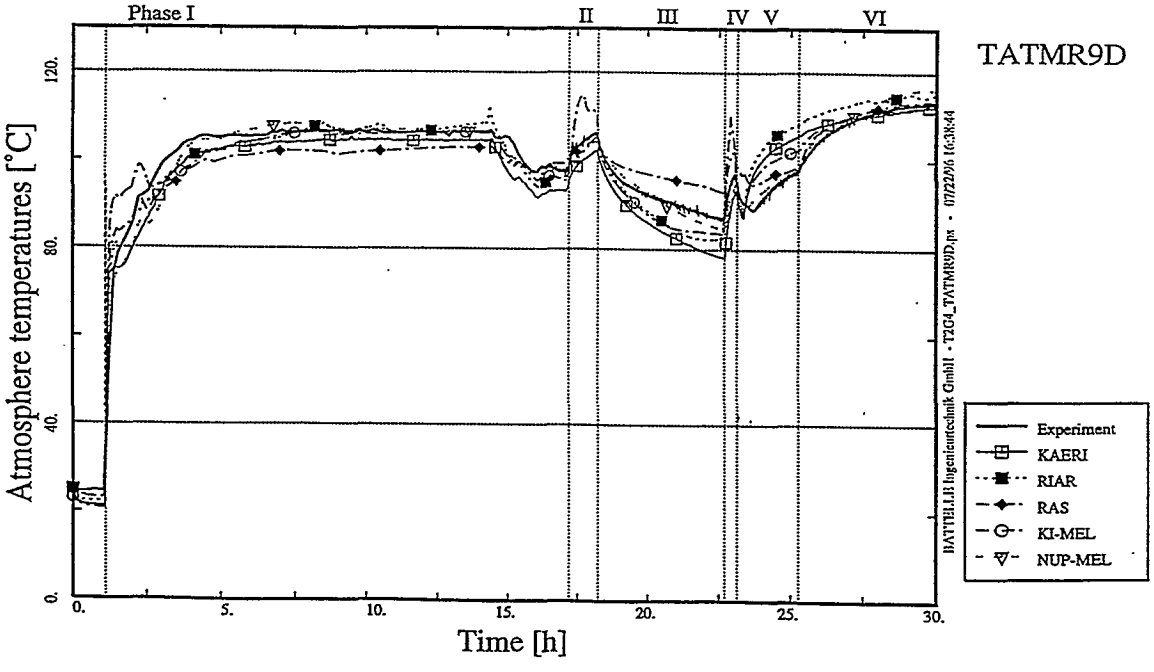

Fig. 4.5d Dome Temperature (MELCOR, part II)

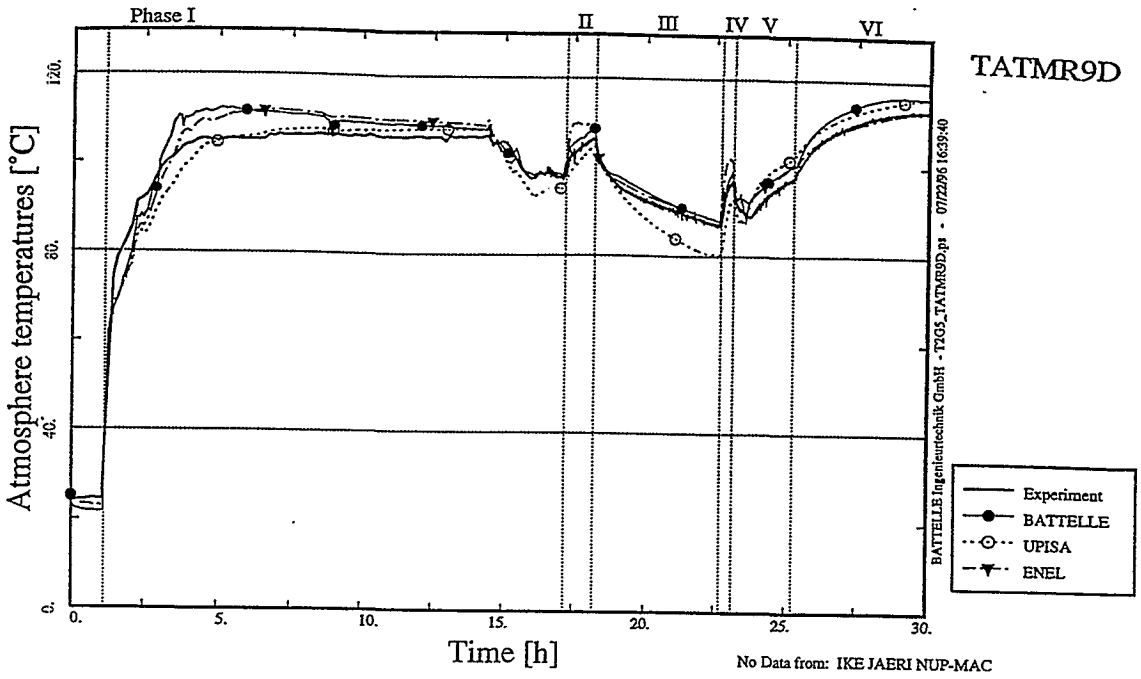

Fig. 4.5e Dome Temperature (ECART, FUMO, GOTHIC)

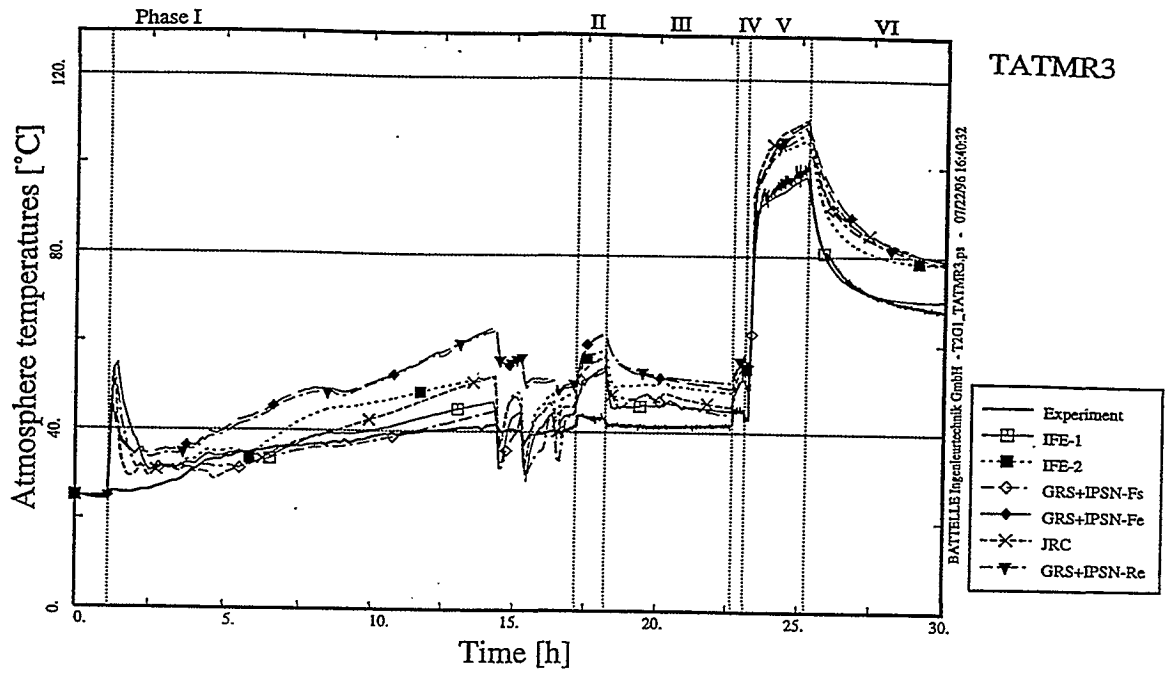

Fig. 4.6a Temperature in Compartment R3 (FIPLOC / RALOC)

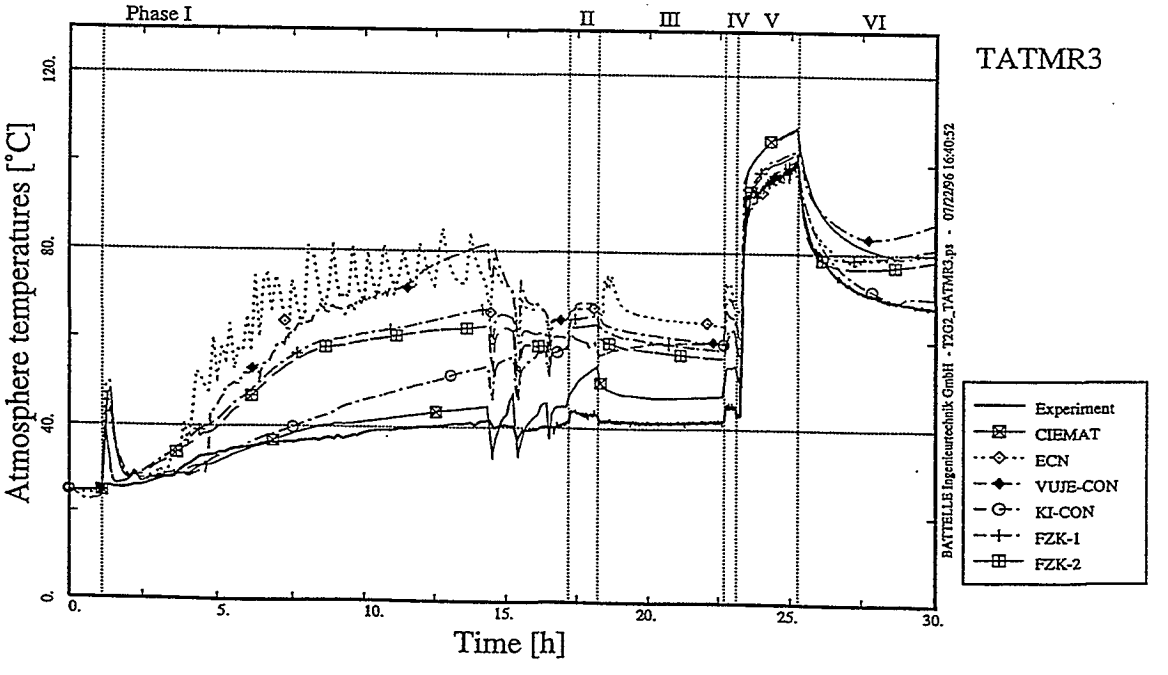

Fig. 4.6b Temperature in Compartment R3 (CONTAIN)

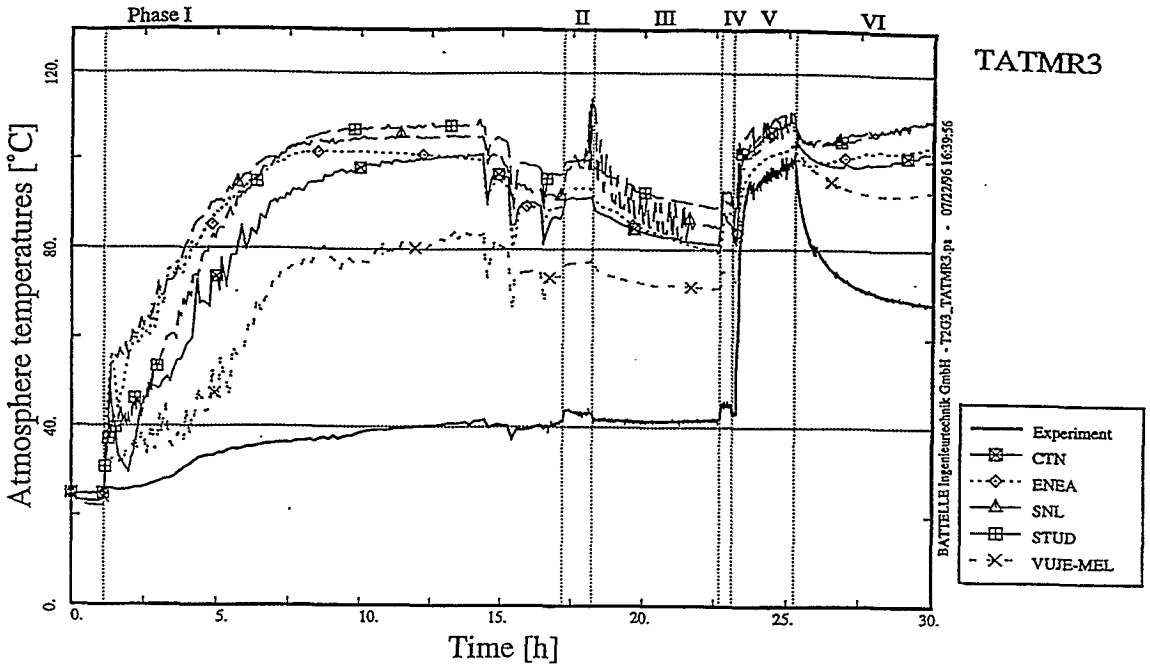

Fig. 4.6c Temperature in Compartment R3 (MELCOR, part I)

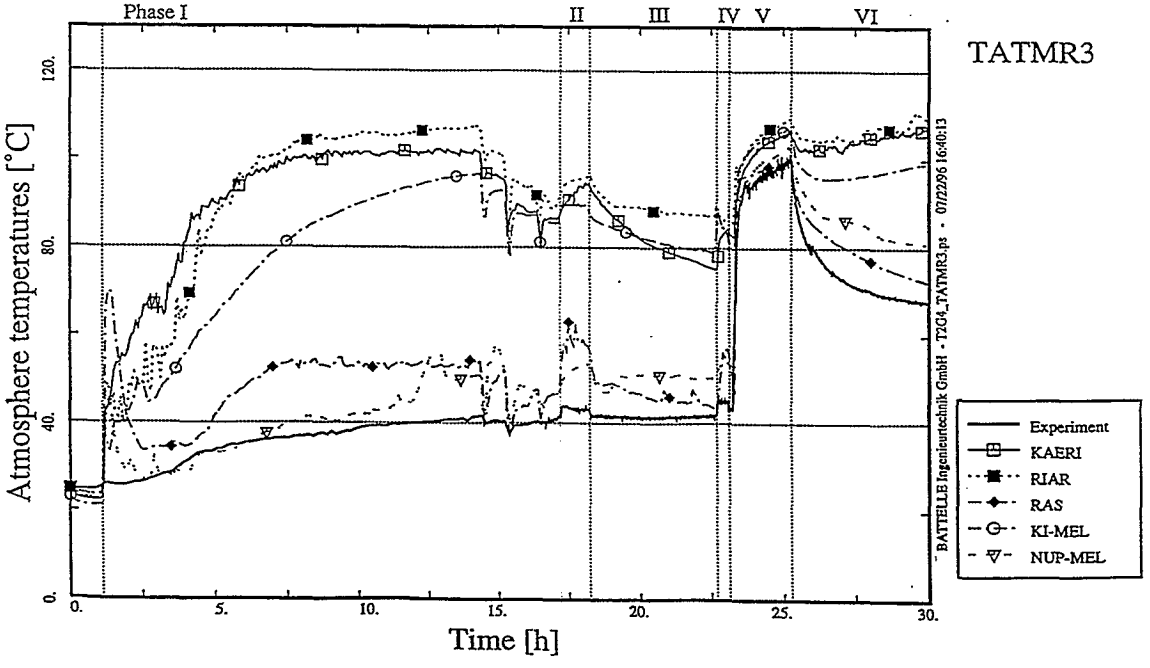

Fig. 4.6d Temperature in Compartment R3 (MELCOR, part II)

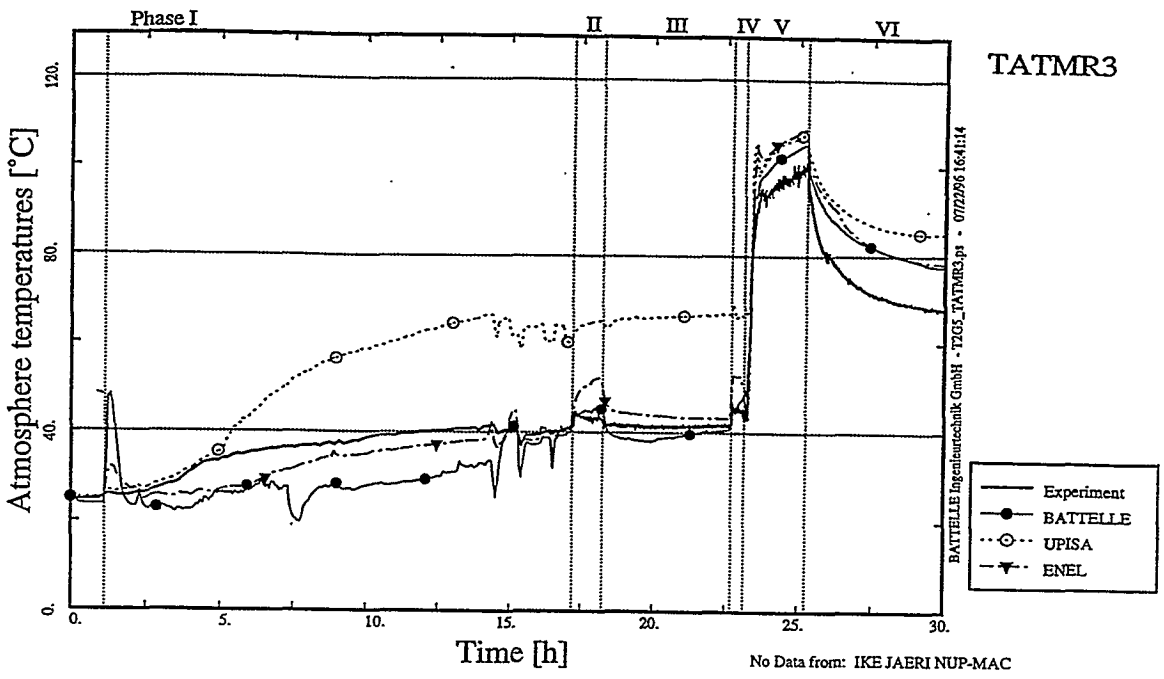

Fig. 4.6e Temperature in Compartment R3 (ECART, FUMO, GOTHIC)

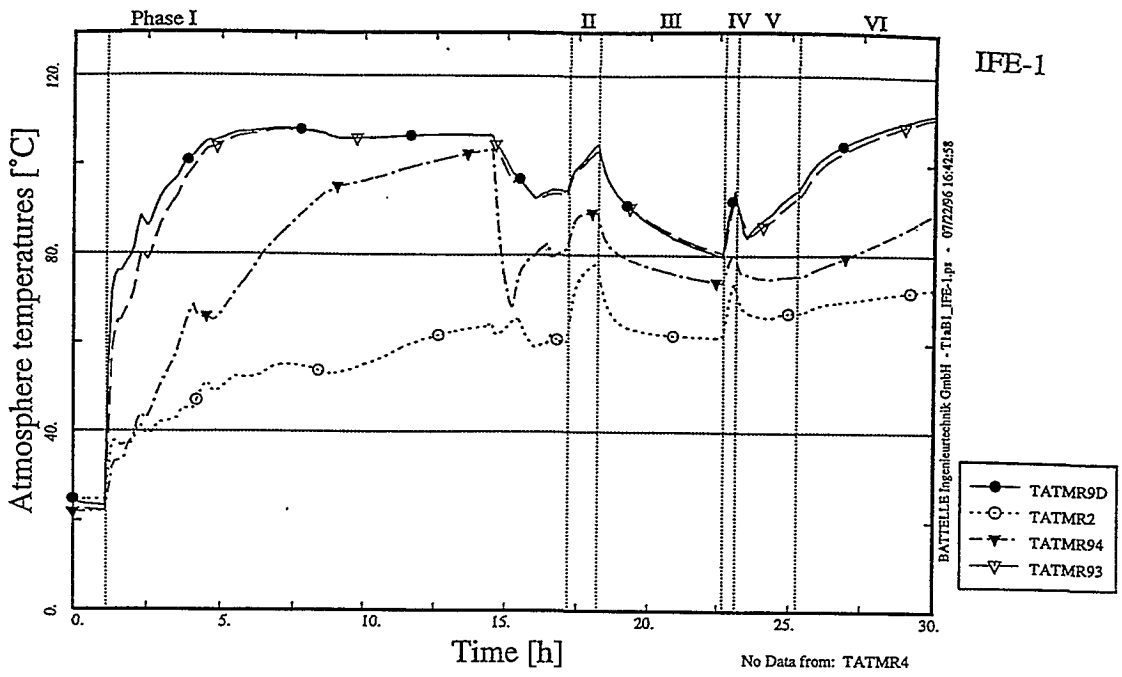

Fig. 4.8a Temperature in Dome, Annulus, R2, R4 (IFE-1)

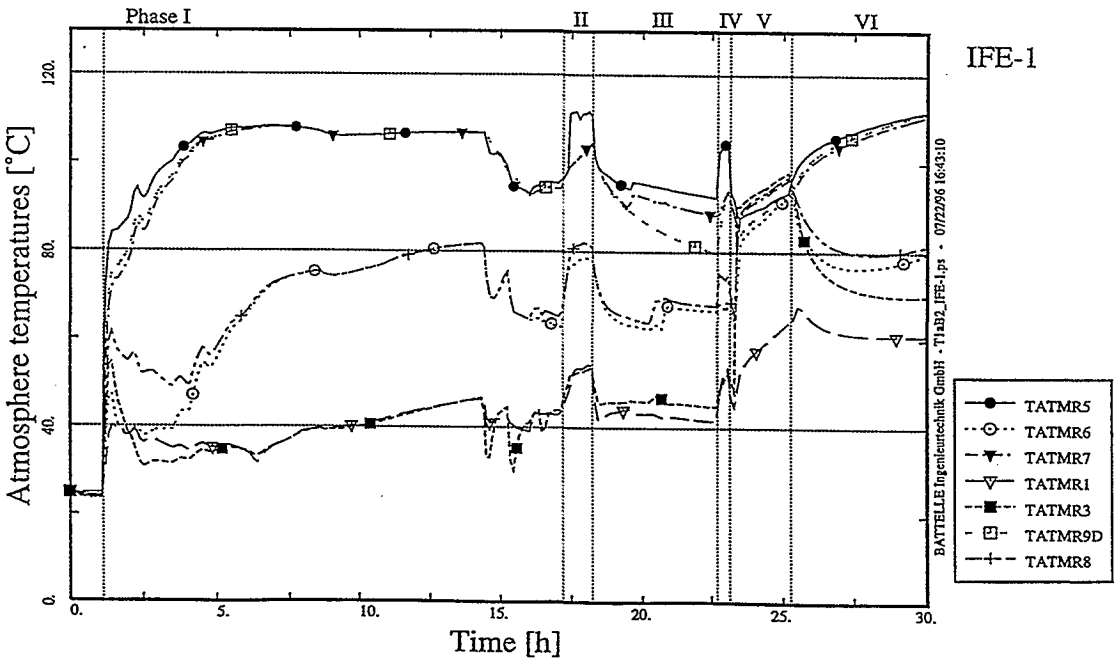

Fig. 4.9a Temperature in Dome, R1, R3, R5, R6, R7, R8 (IFE-1)

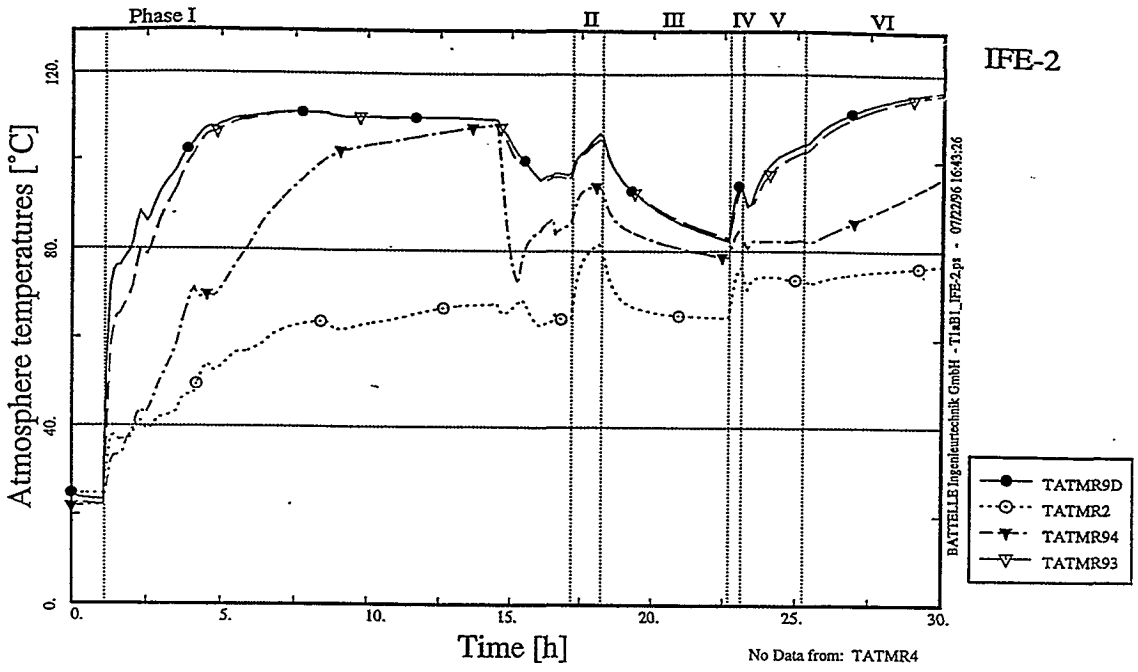

Fig. 4.8b Temperature in Dome, Annulus, R2, R4 (IFE-2)

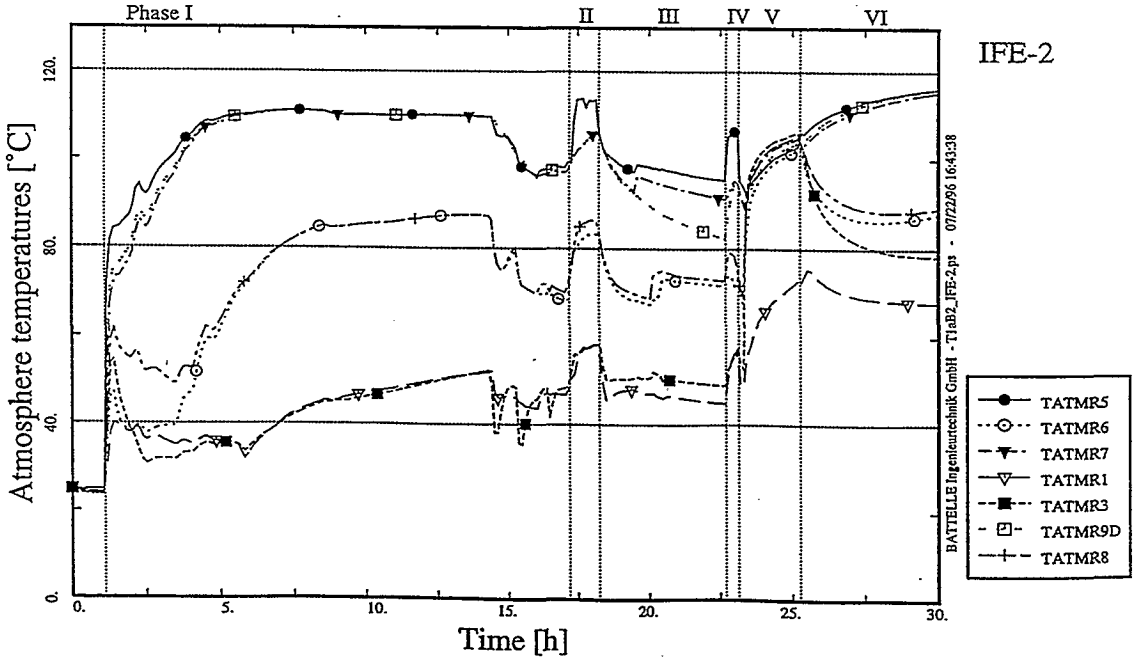

Fig. 4.9b Temperature in Dome, R1, R3, R5, R6, R7, R8 (IFE-2)

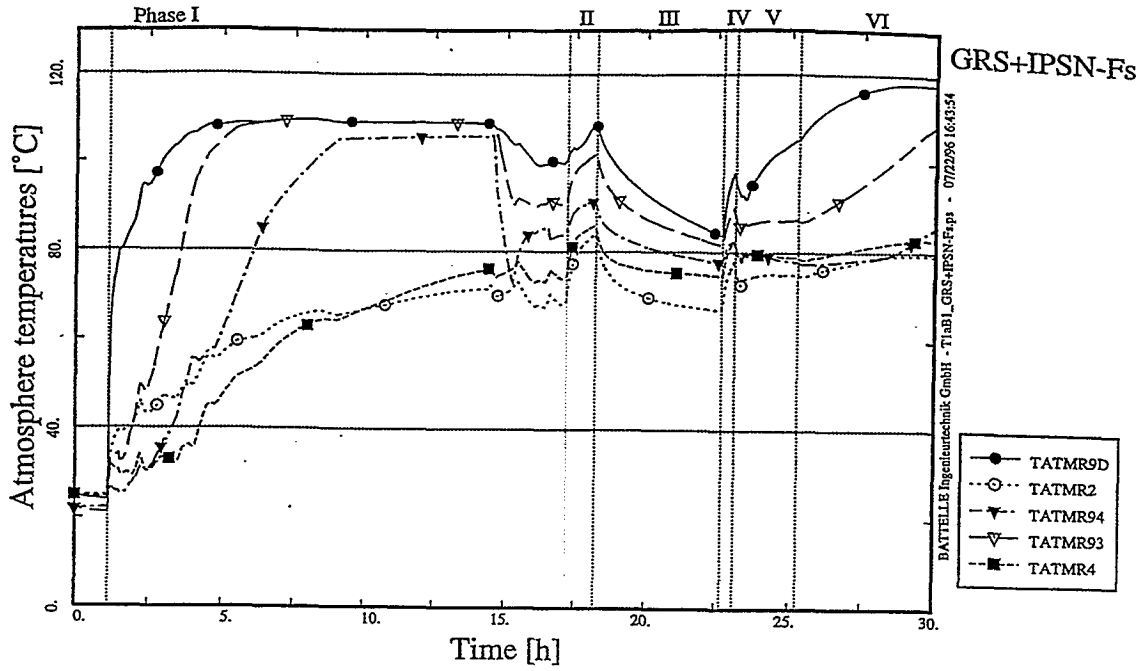

Fig. 4.8c Temperature in Dome, Annulus, R2, R4 (GRS / IPSN - Fs)

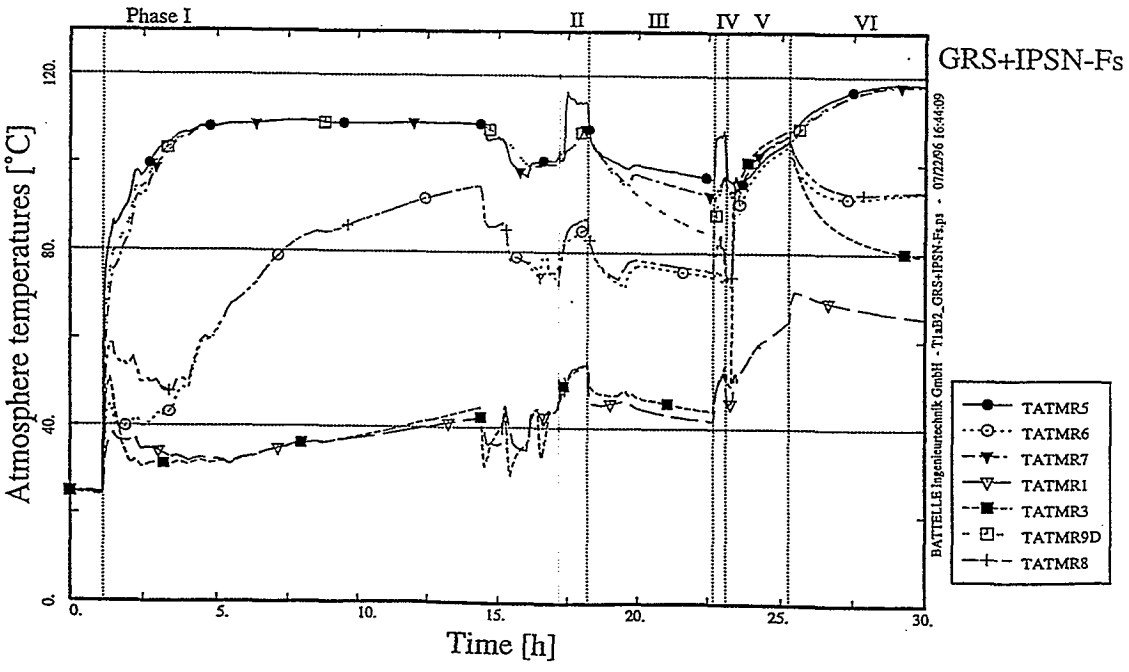

Fig. 4.9c Temperature in Dome, R1, R3, R5, R6, R7, R8 (GRS / IPSN - Fs)

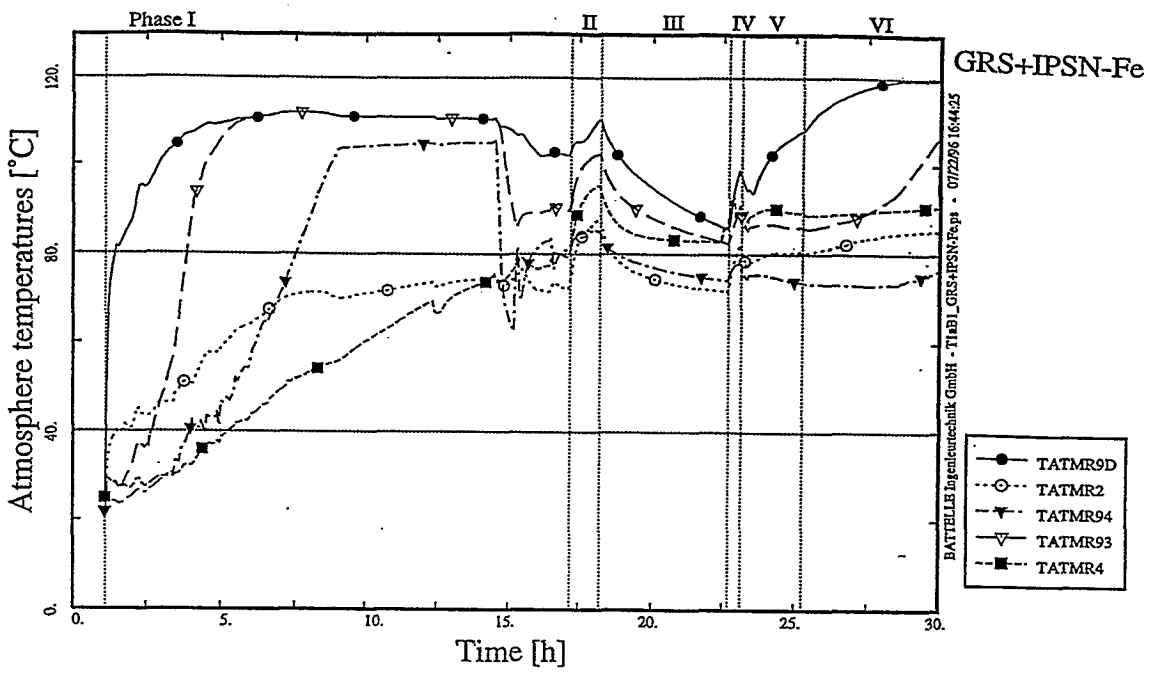

Fig. 4.8d Temperature in Dome, Annulus, R2, R4 (GRS / IPSN - Fe)

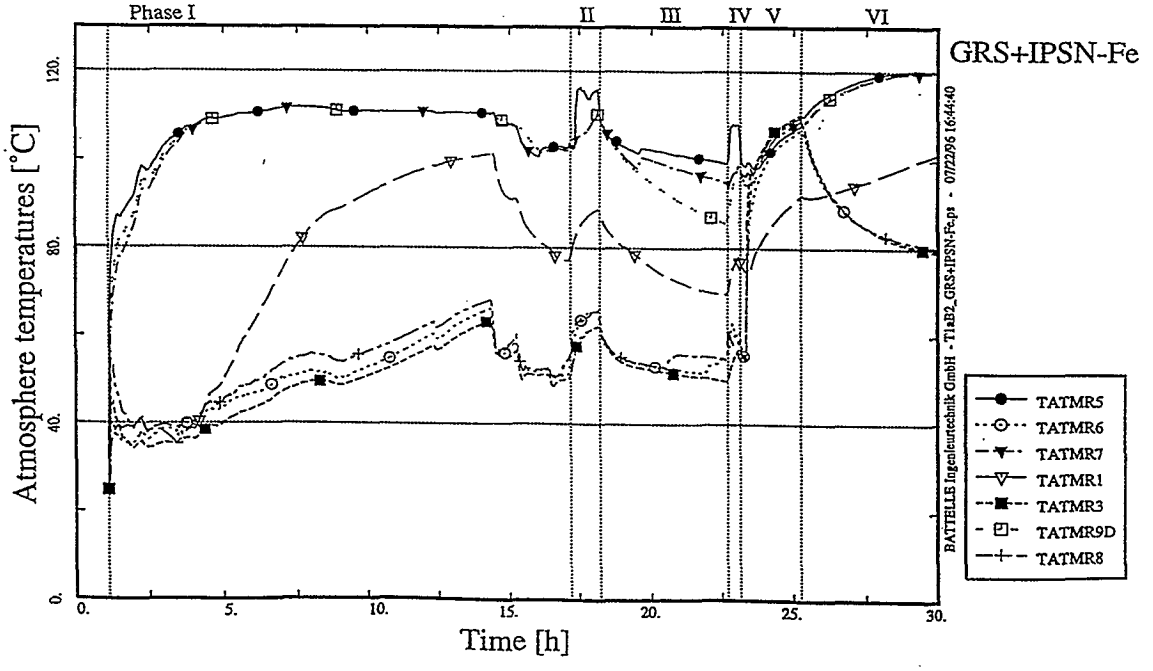

Fig. 4.9d Temperature in Dome, R1, R3, R5, R6, R7, R8 (GRS / IPSN - Fe)

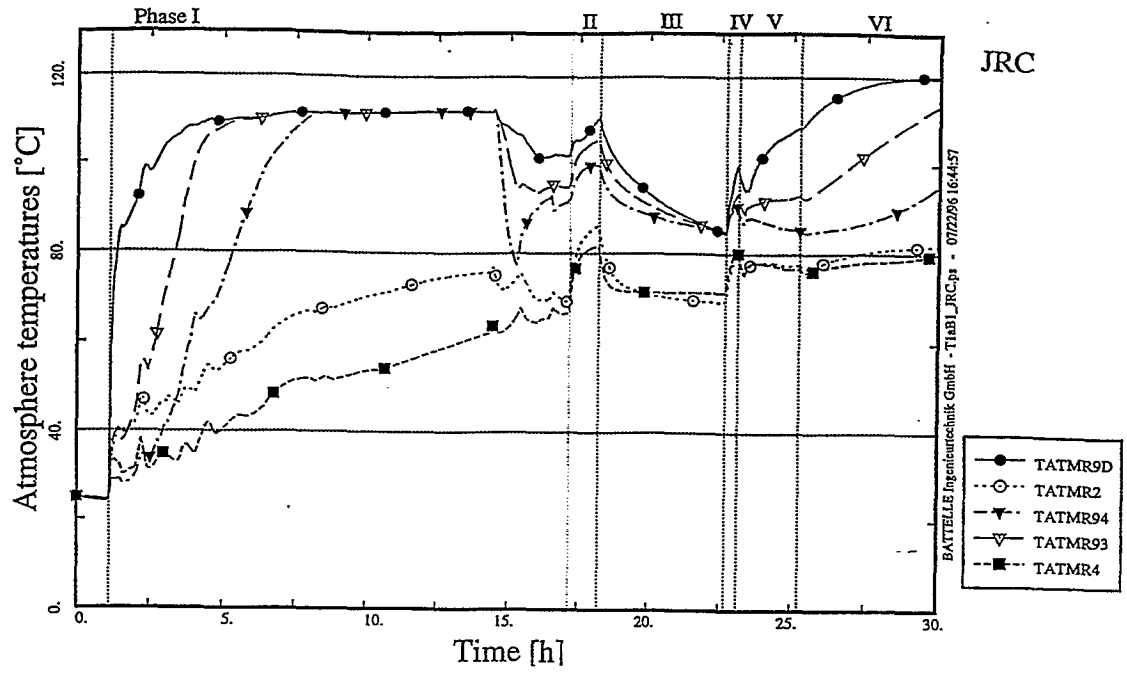

Fig. 4.8e Temperature in Dome, Annulus, R2, R4 (JRC)

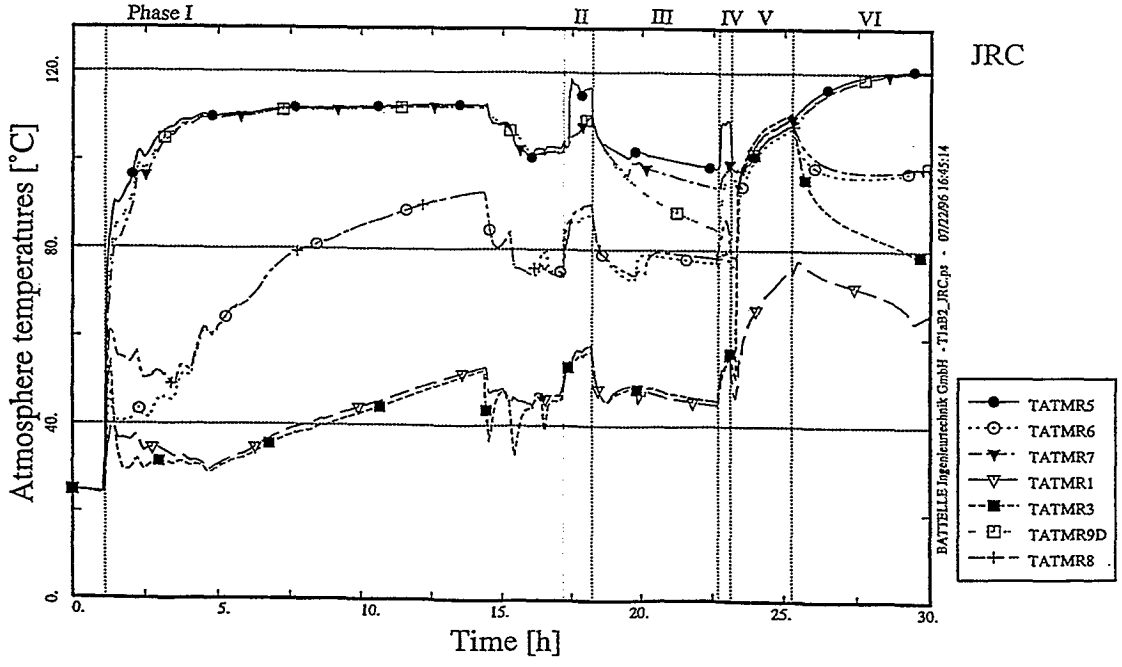

Fig. 4.9e Temperature in Dome, R1, R3, R5, R6, R7, R8 (JRC)

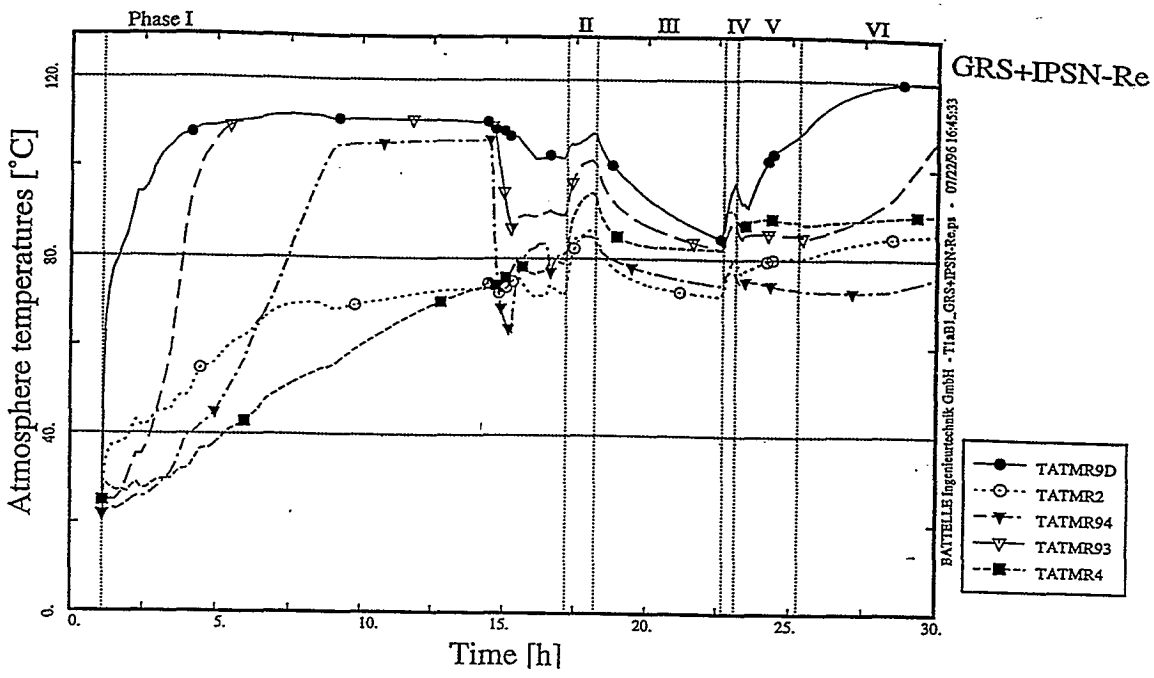

Fig. 4.8f Temperature in Dome, Annulus, R2, R4 (GRS / IPSN - Re)

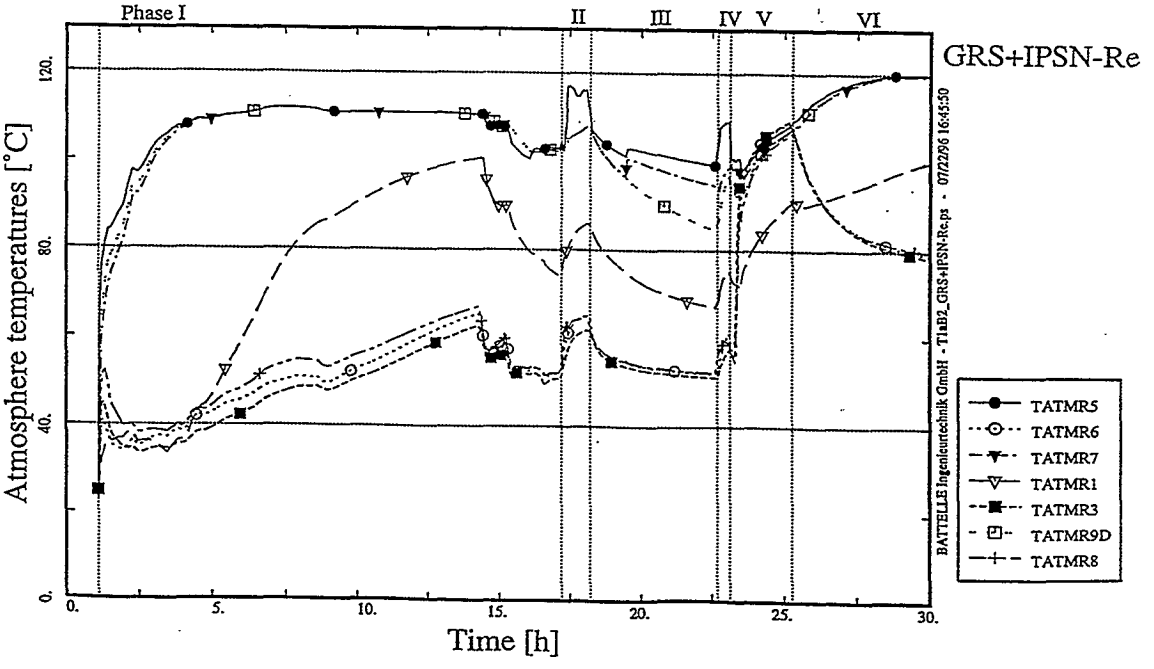

Fig. 4.9f Temperature in Dome, R1, R3, R5, R6, R7, R8 (GRS / IPSN - Re)

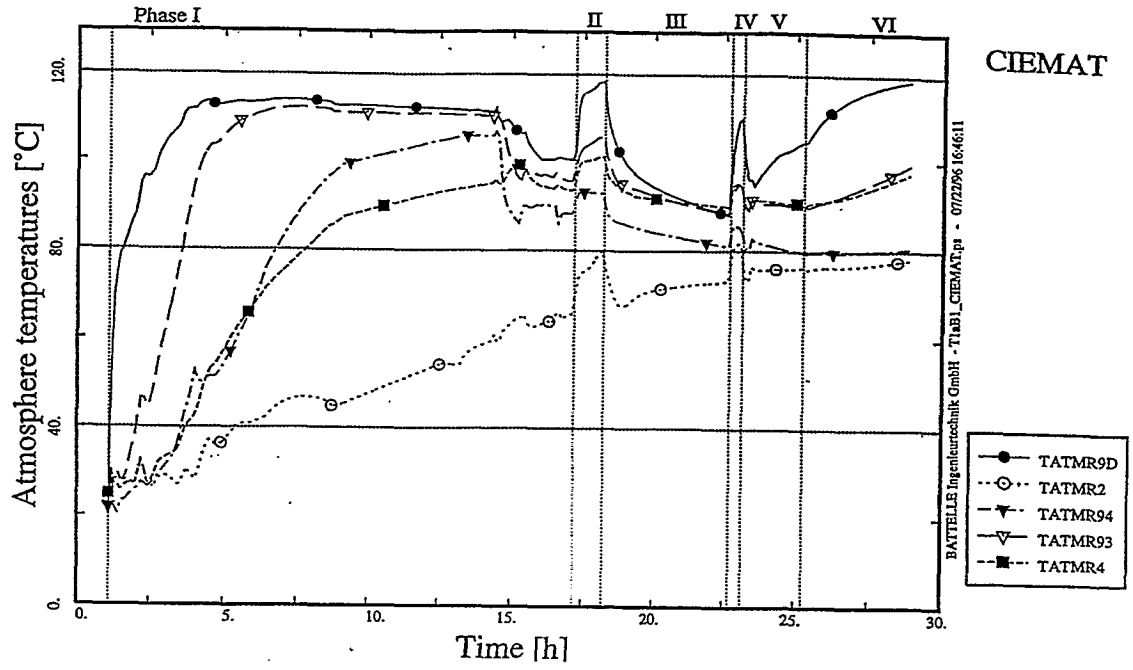

Fig. 4.8g Temperature in Dome, Annulus, R2, R4 (CIEMAT)

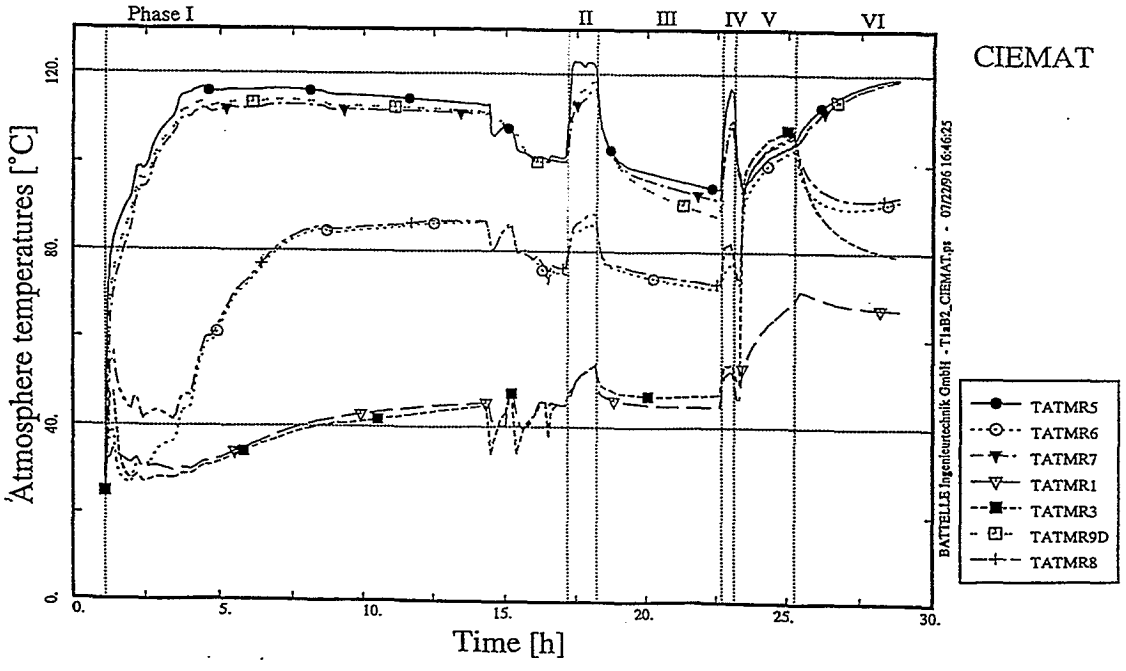

Fig. 4.9g Temperature in Dome, R1, R3, R5, R6, R7, R8 (CIEMAT)

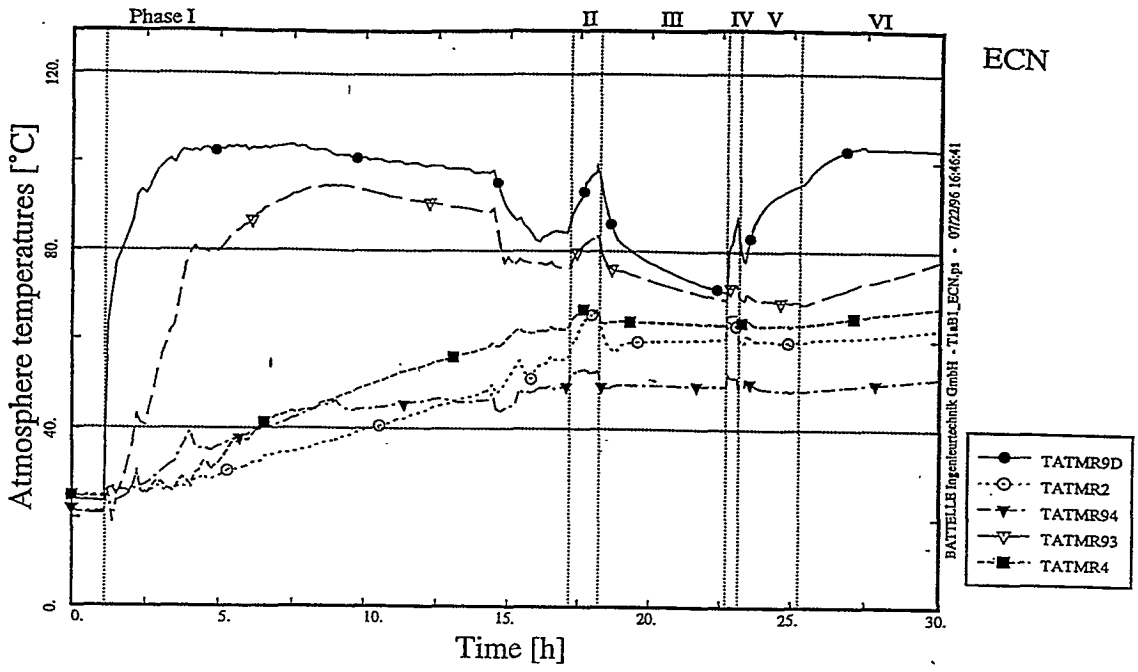

Fig. 4.8h Temperature in Dome, Annulus, R2, R4 (ECN)

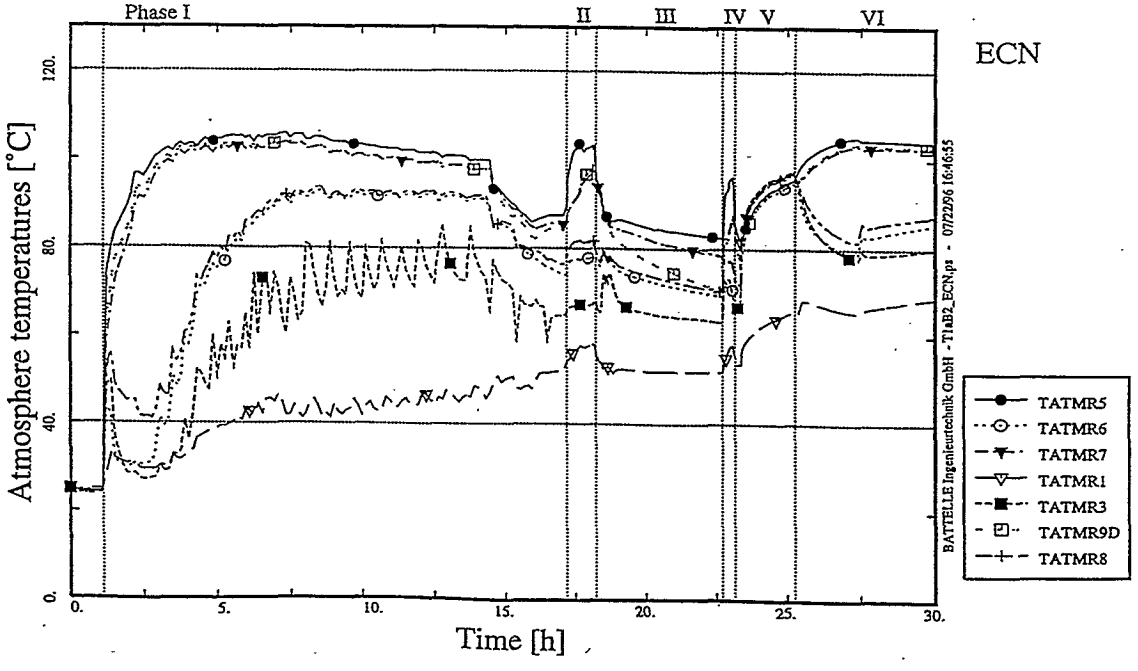

Fig. 4.9h Temperature in Dome, R1, R3, R5, R6, R7, R8 (ECN)

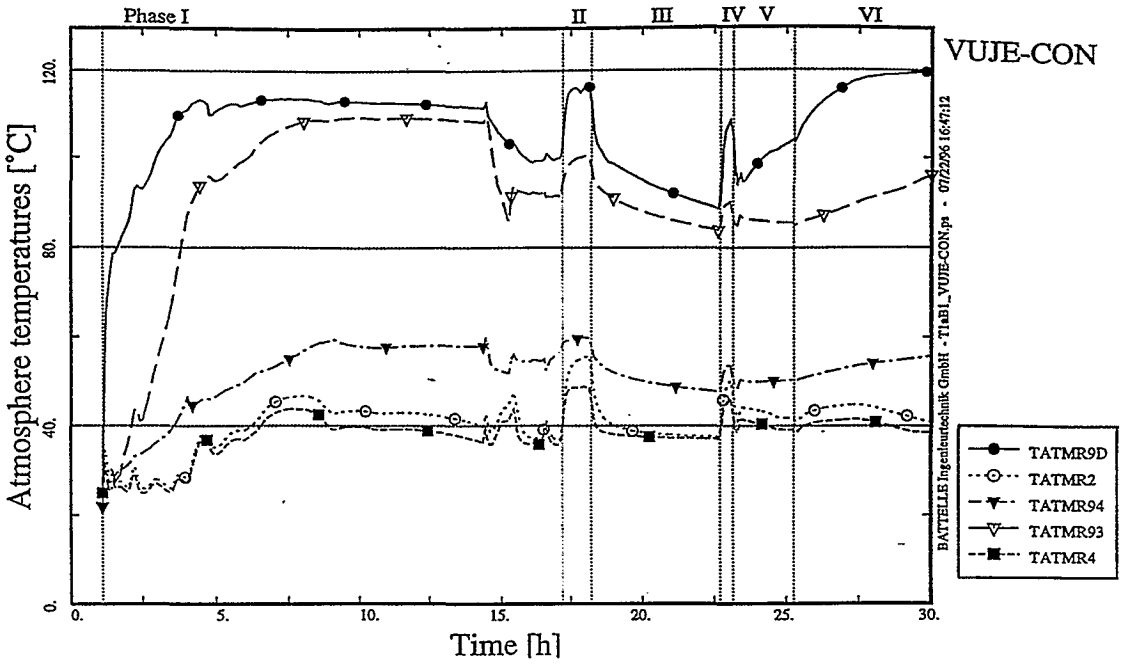

Fig. 4.8i Temperature in Dome, Annulus, R2, R4 (VUJE-CON)

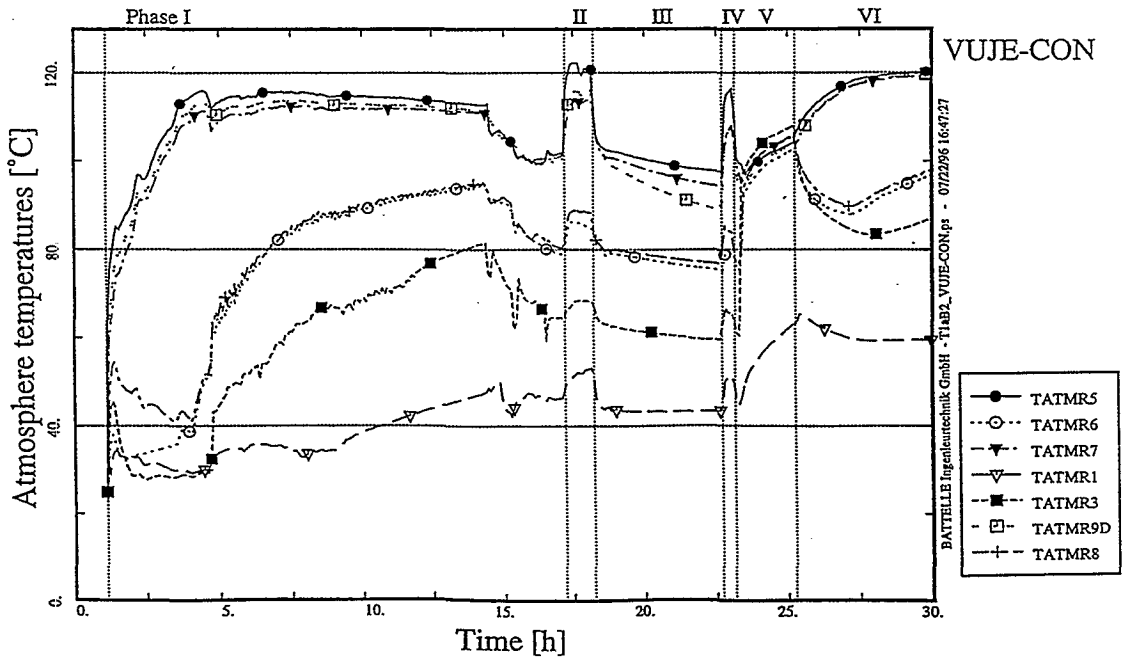

Fig. 4.9i Temperature in Dome, R1, R3, R5, R6, R7, R8 (VUJE-CON)

159

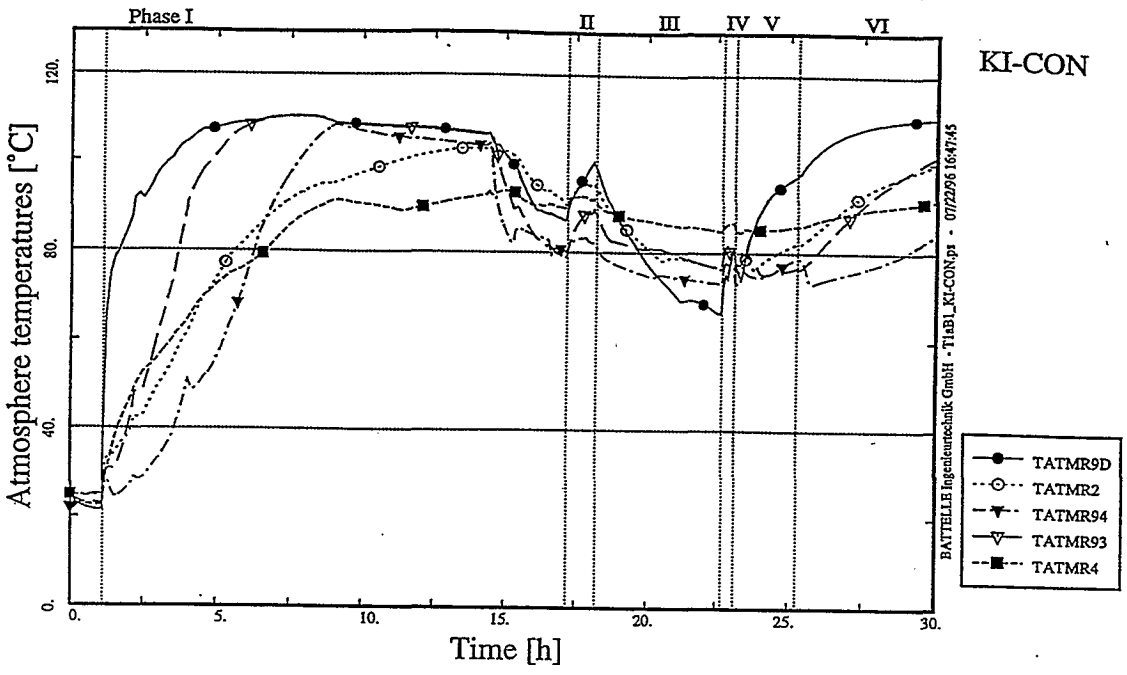

Fig. 4.8j Temperature in Dome, Annulus, R2, R4 (KI-CON)

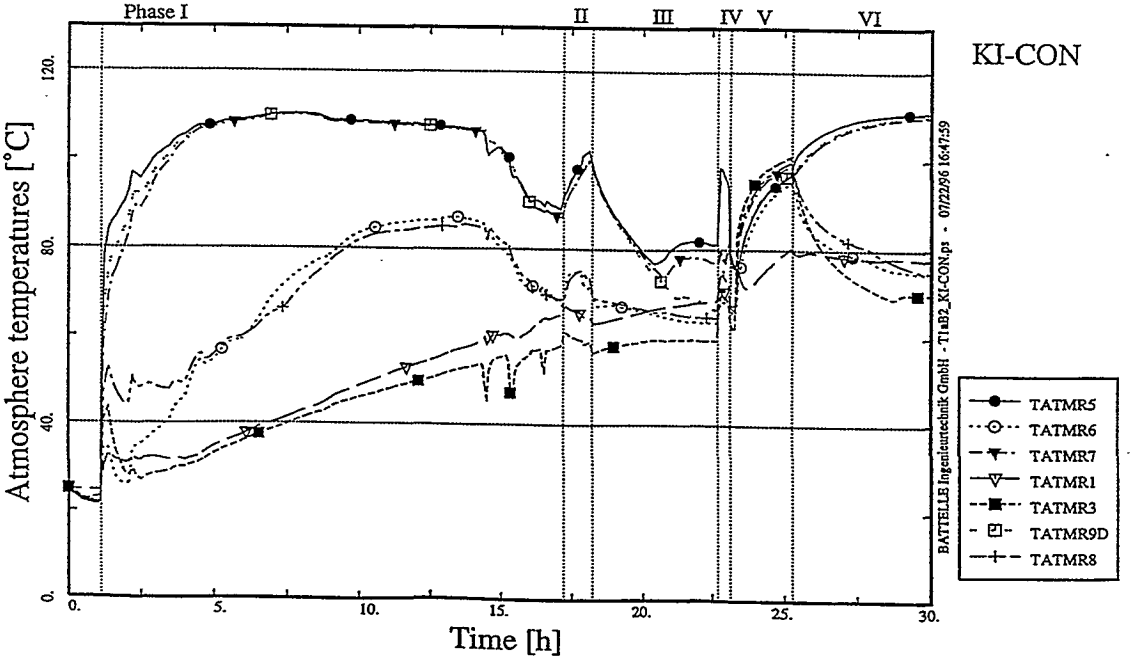

Fig. 4.9j Temperature in Dome, R1, R3, R5, R6, R7, R8 (KI-CON)

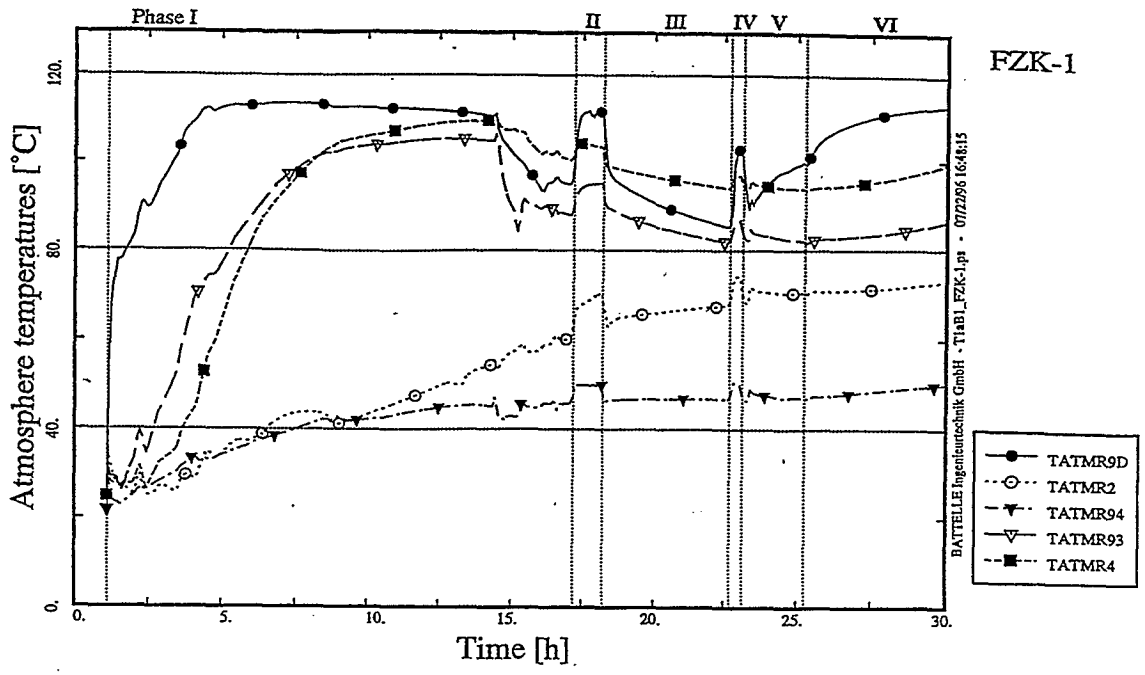

Fig. 4.8k Temperature in Dome, Annulus, R2, R4 (FZK-1)

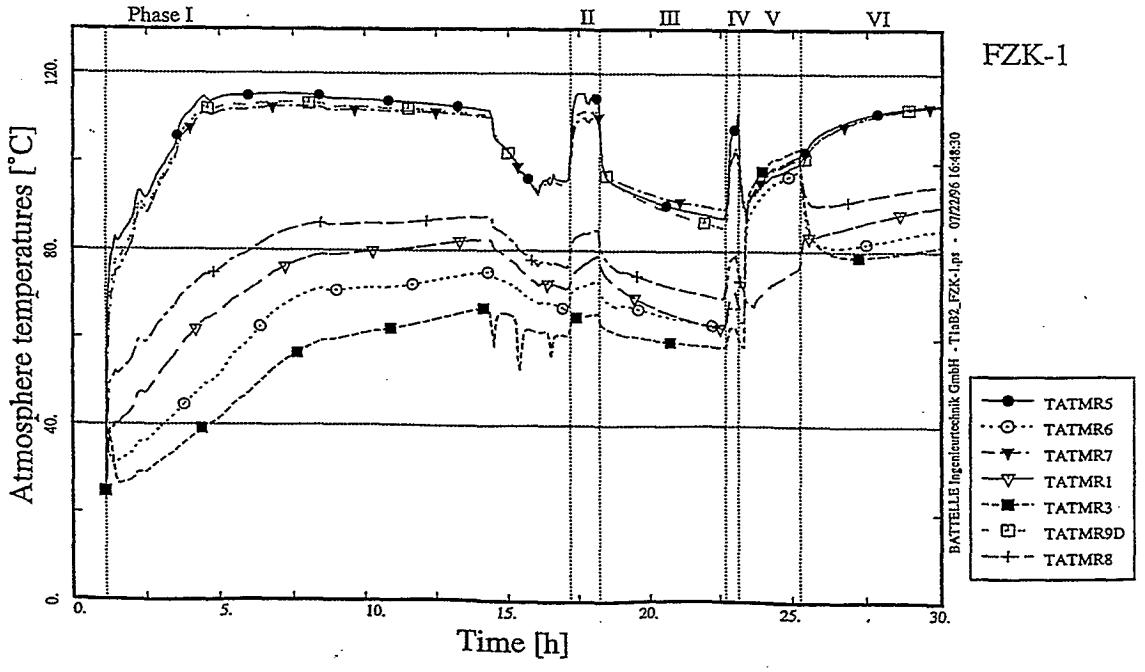

Fig. 4.9k Temperature in Dome, R1, R3, R5, R6, R7, R8 (FZK-1)

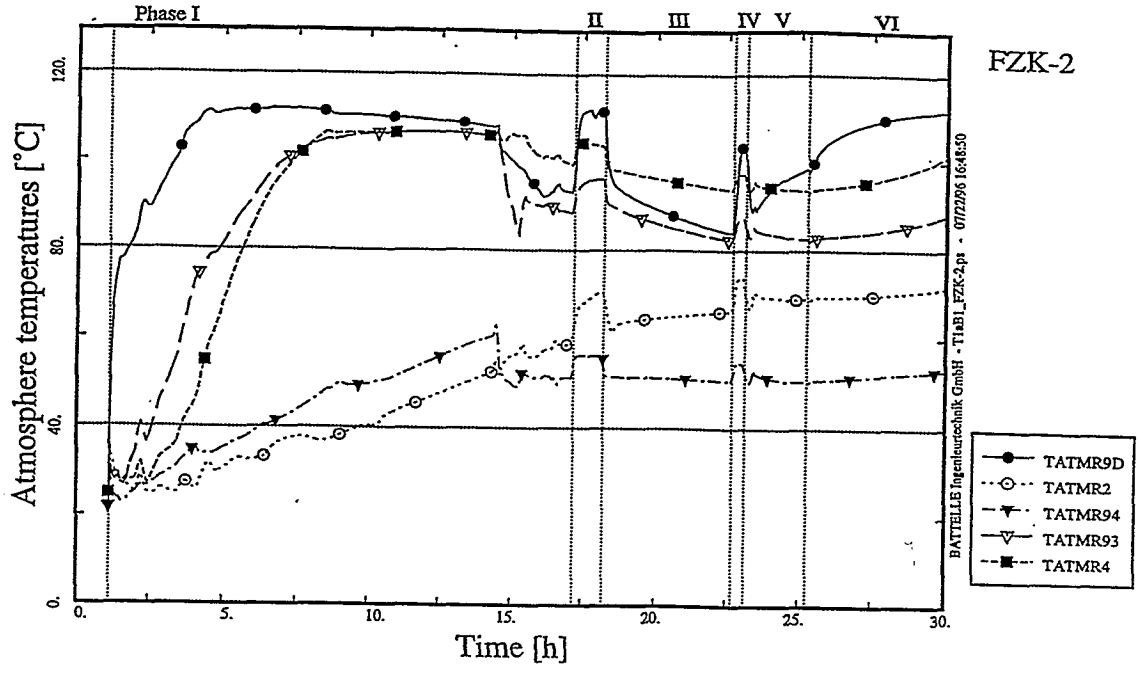

Fig. 4.8l Temperature in Dome, Annulus, R2, R4 (FZK-2)

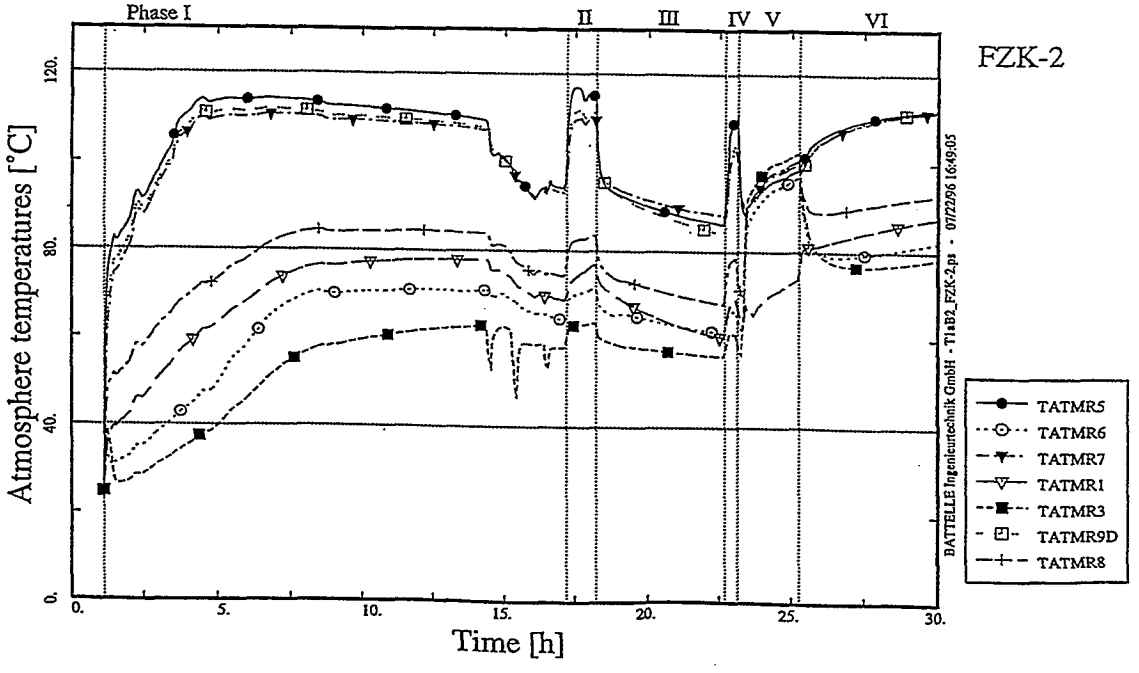

Fig. 4.9l Temperature in Dome, R1, R3, R5, R6, R7, R8 (FZK-2)

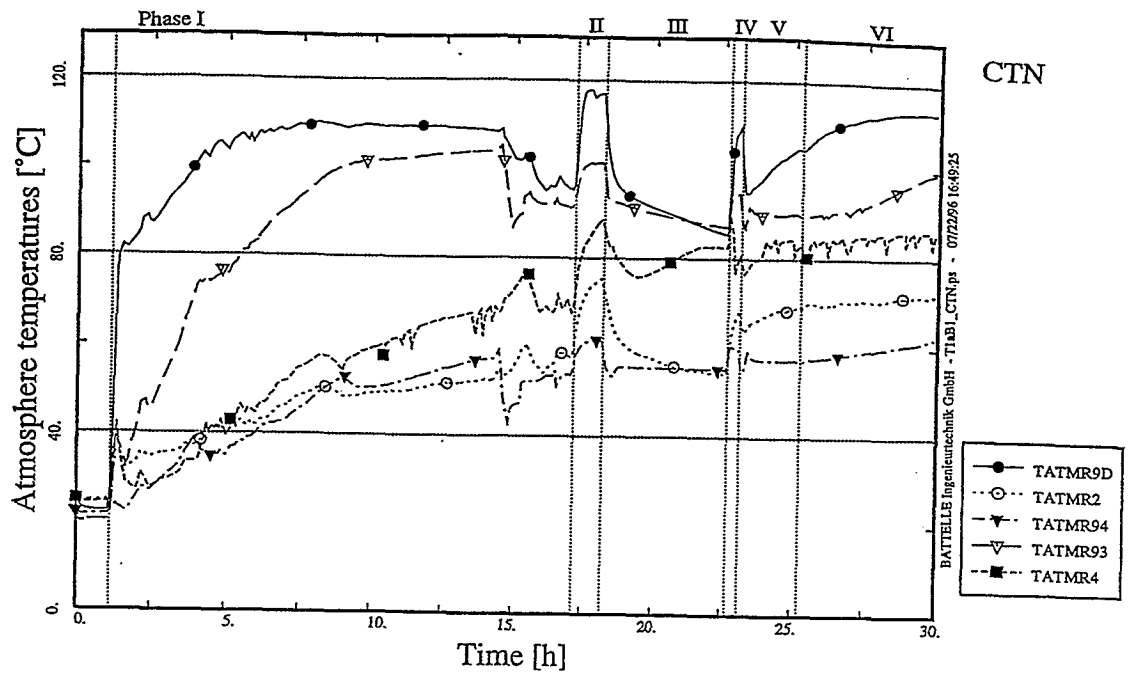

Fig. 4.8m Temperature in Dome, Annulus, R2, R4 (CTN)

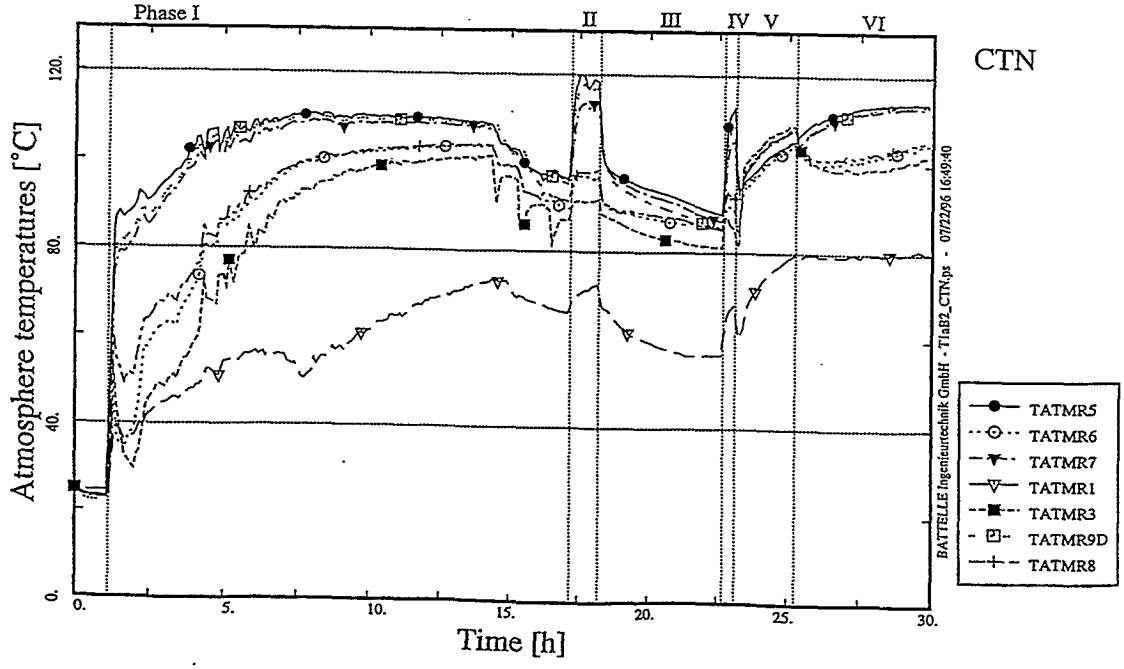

Fig. 4.9m Temperature in Dome, R1, R3, R5, R6, R7, R8 (CTN)

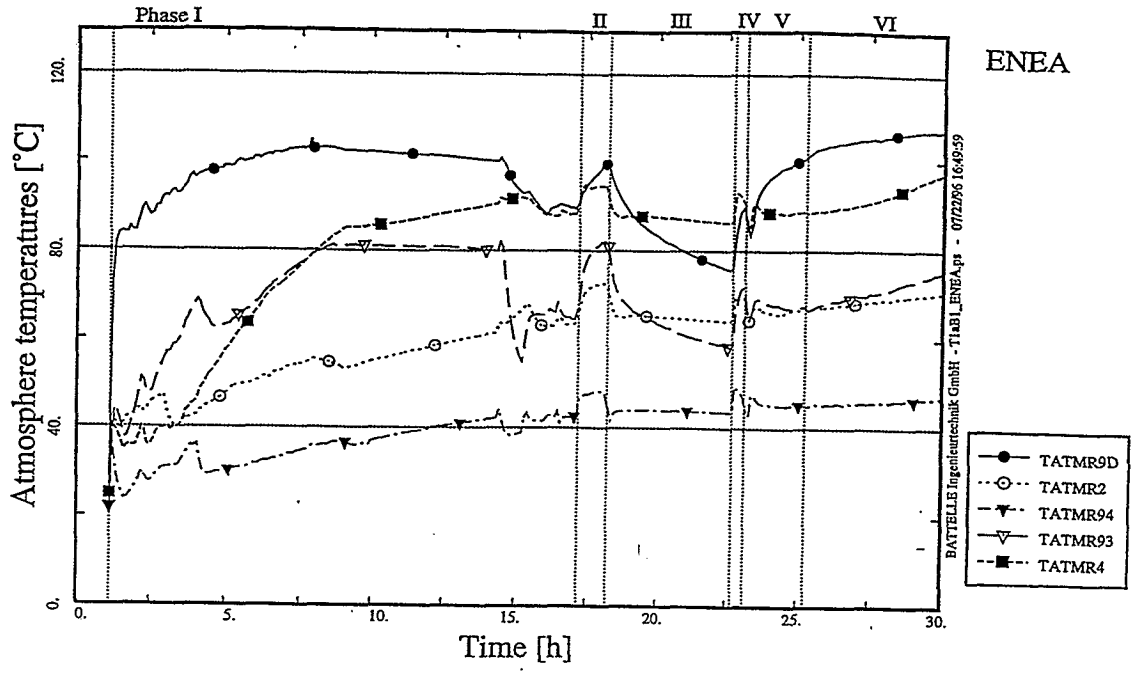

Fig. 4.8n Temperature in Dome, Annulus, R2, R4 (ENEA)

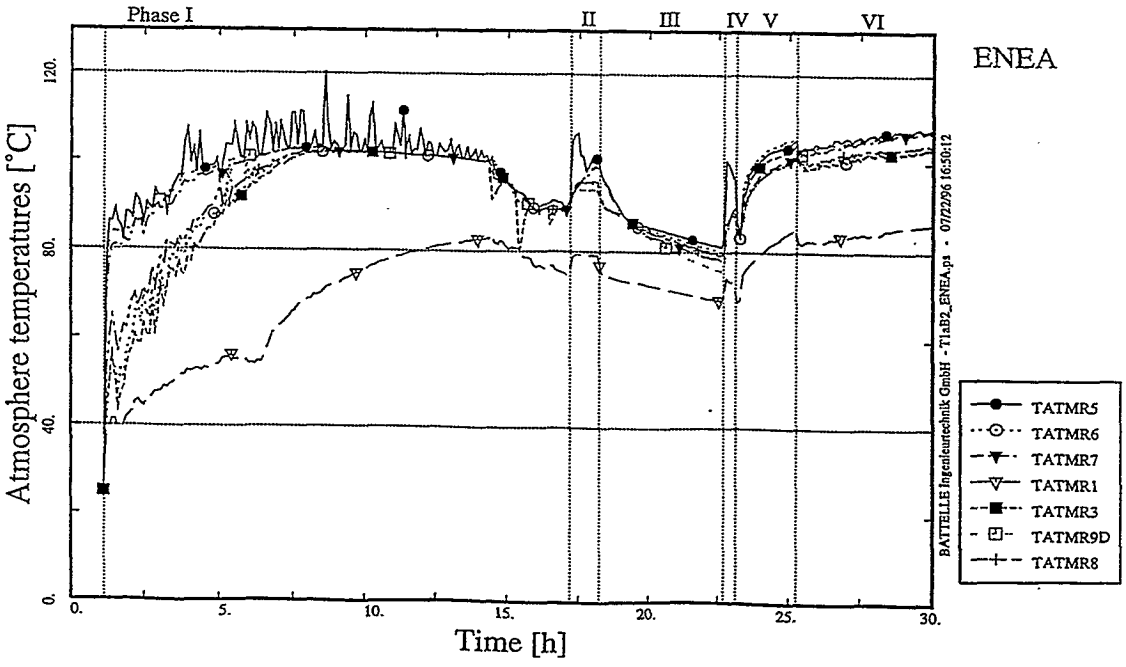

Fig. 4.9n Temperature in Dome, R1, R3, R5, R6, R7, R8 (ENEA)

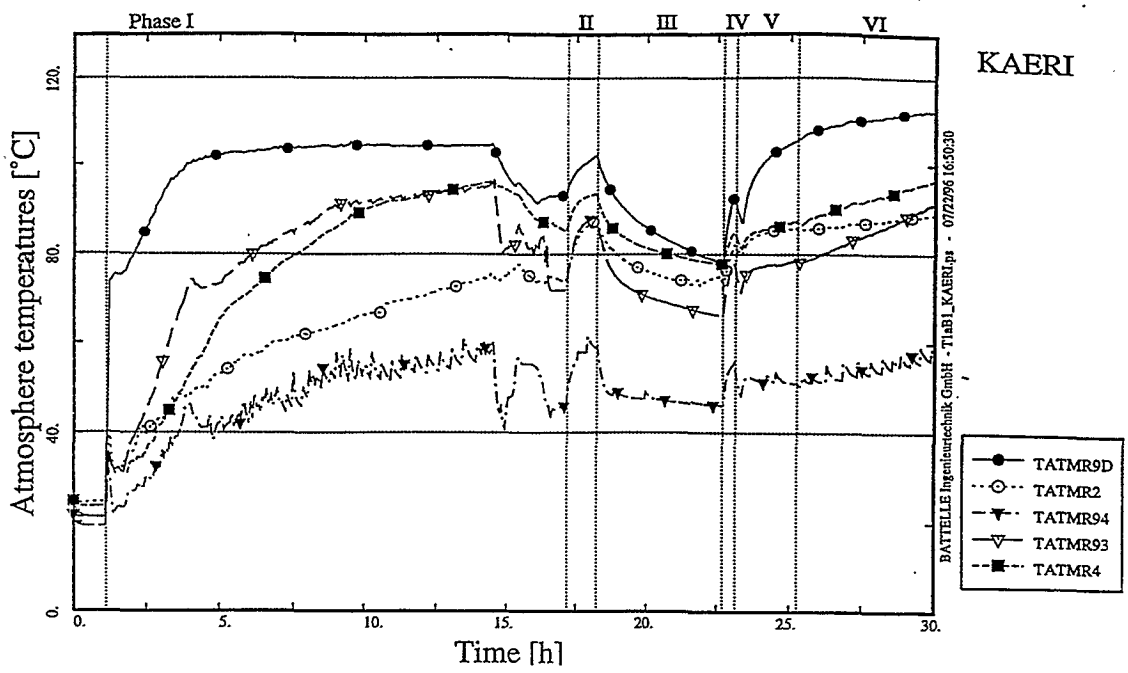

Fig. 4.8o Temperature in Dome, Annulus, R2, R4 (KAERI)

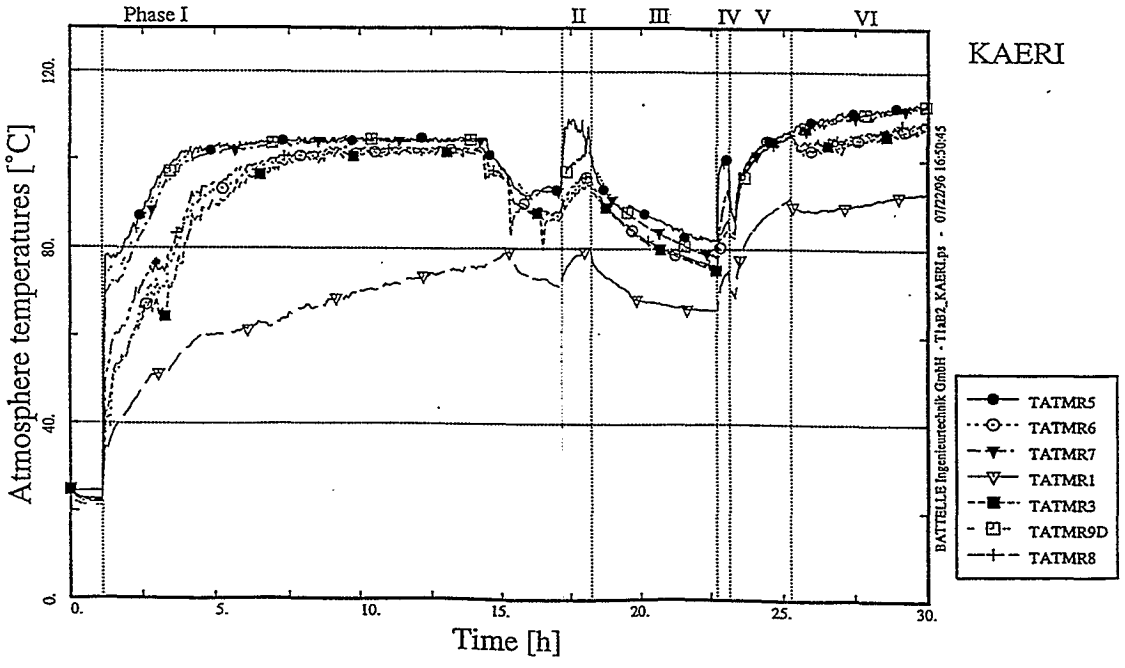

Fig. 4.9o Temperature in Dome, R1, R3, R5, R6, R7, R8 (KAERI)

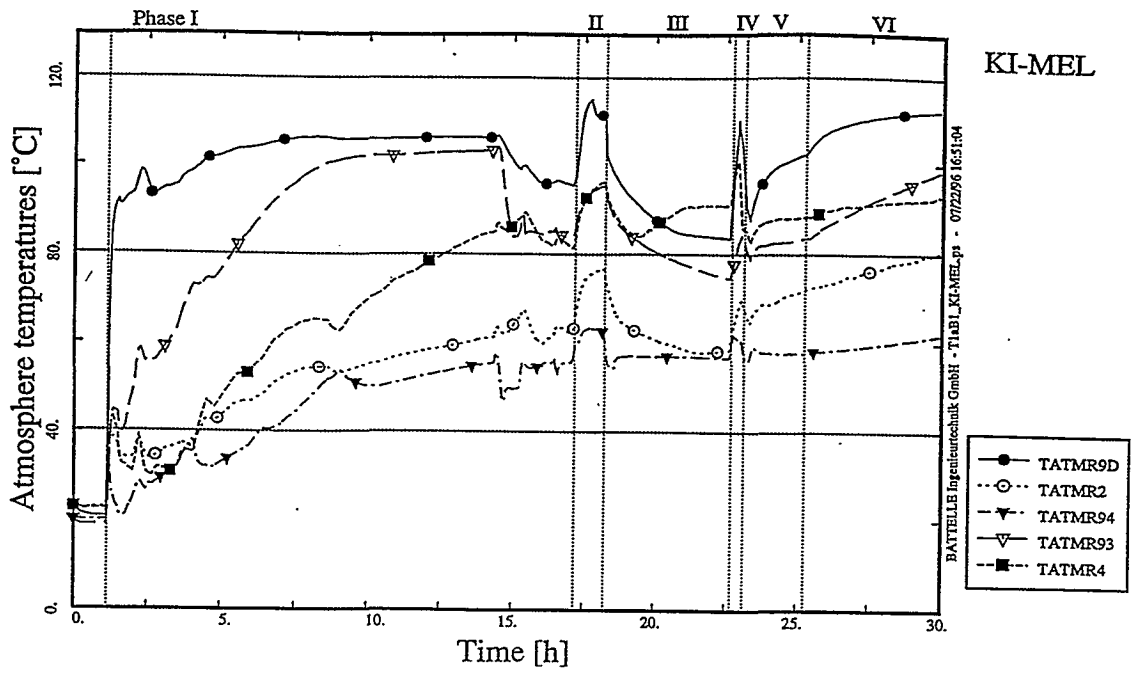

Fig. 4.8p Temperature in Dome, Annulus, R2, R4 (KI-MEL)

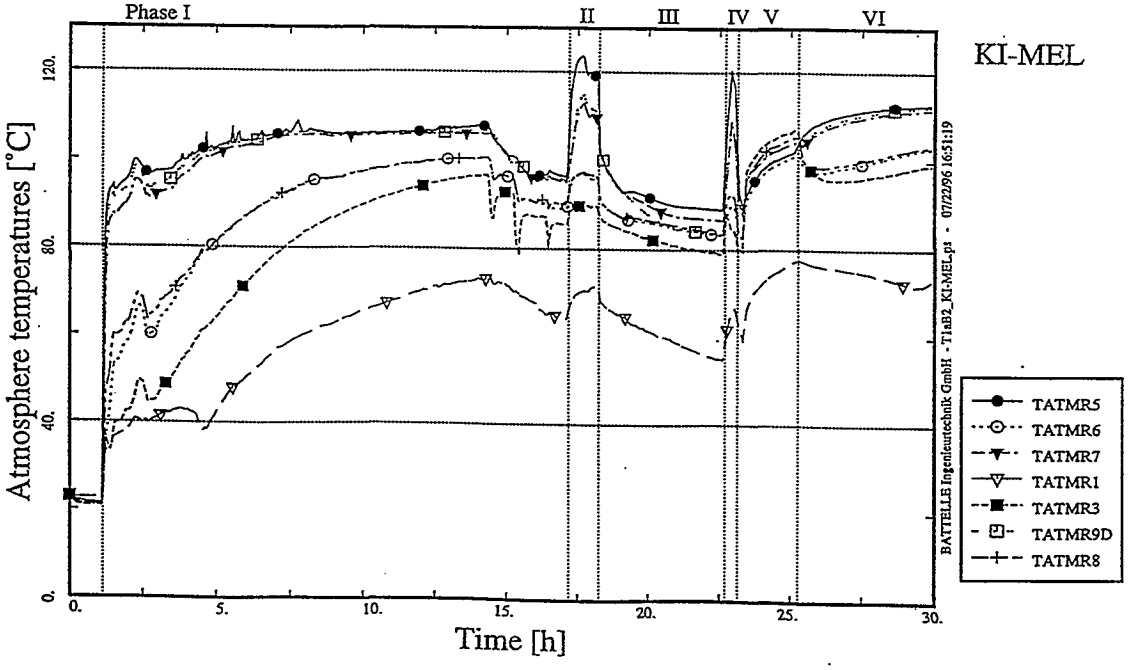

Fig. 4.9p Temperature in Dome, R1, R3, R5, R6, R7, R8 (KI-MEL)

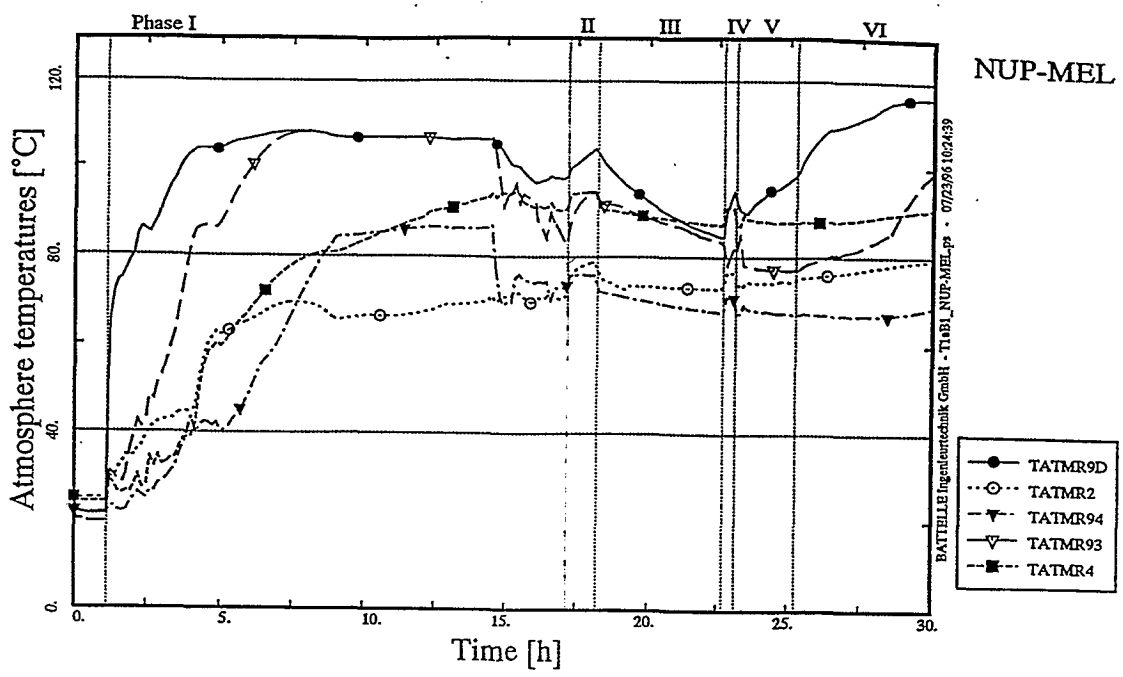

Fig. 4.8q Temperature in Dome, Annulus, R2, R4 (NUP-MEL)

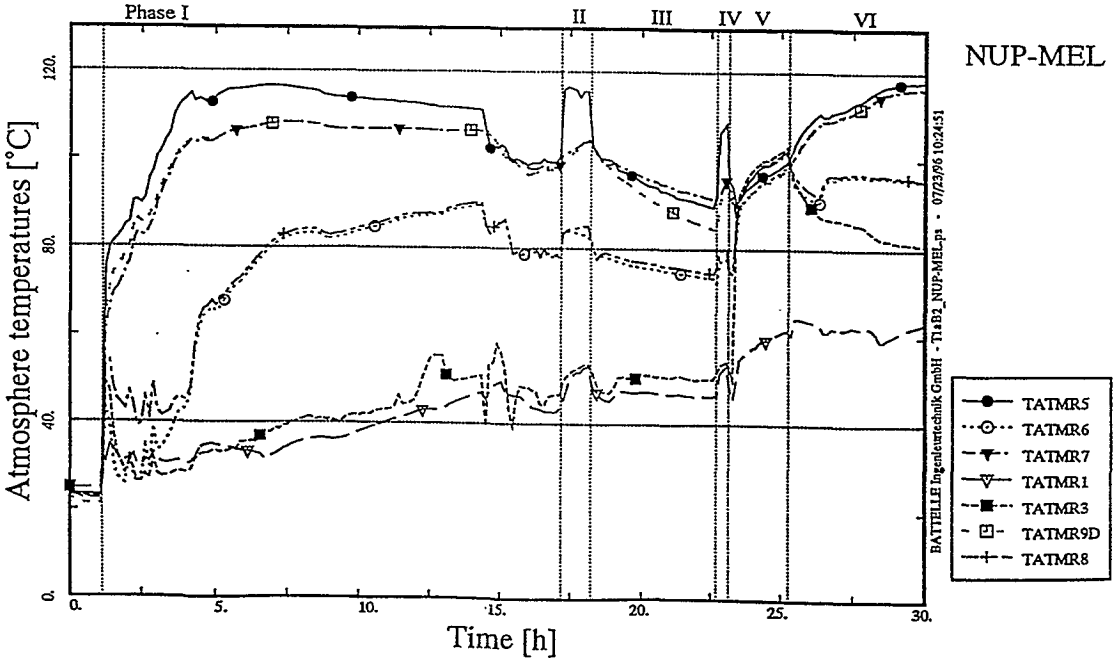

Fig. 4.9q Temperature in Dome, R1, R3, R5, R6, R7, R8 (NUP-MEL)

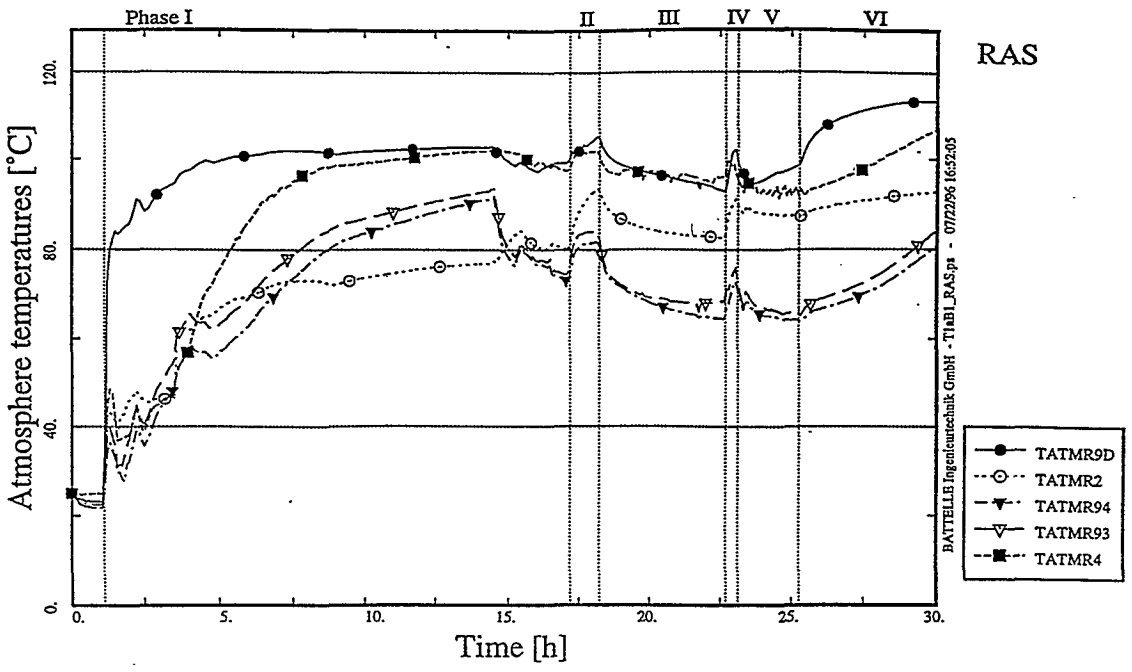

Fig. 4.8r Temperature in Dome, Annulus, R2, R4 (RAS)

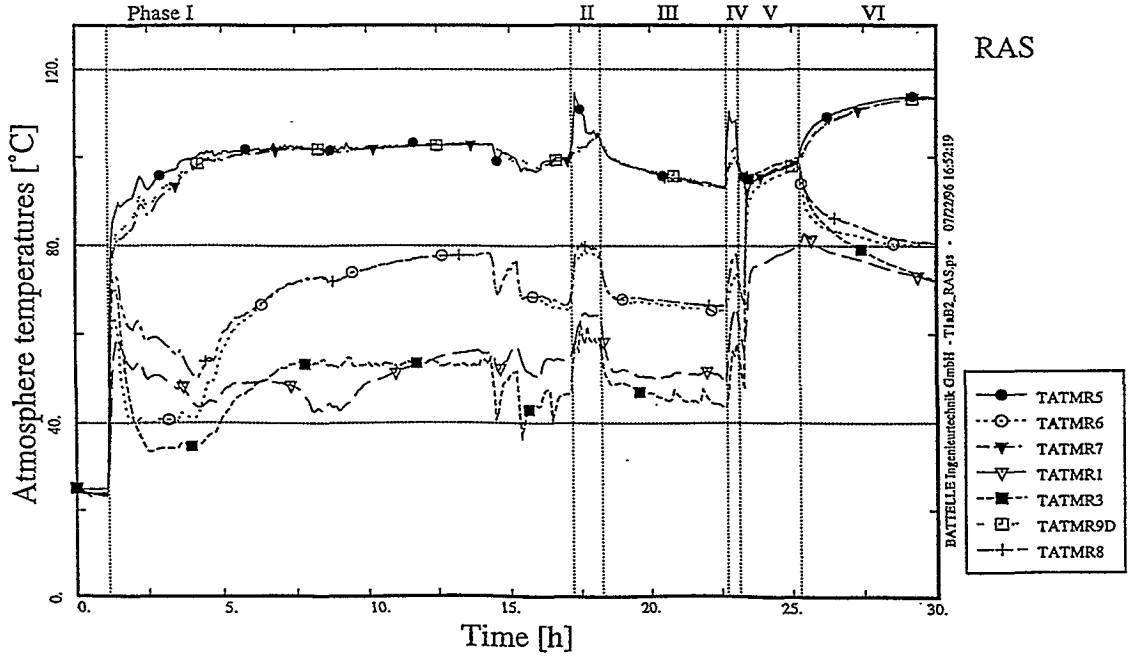

Fig. 4.9r Temperature in Dome, R1, R3, R5, R6, R7, R8 (RAS)

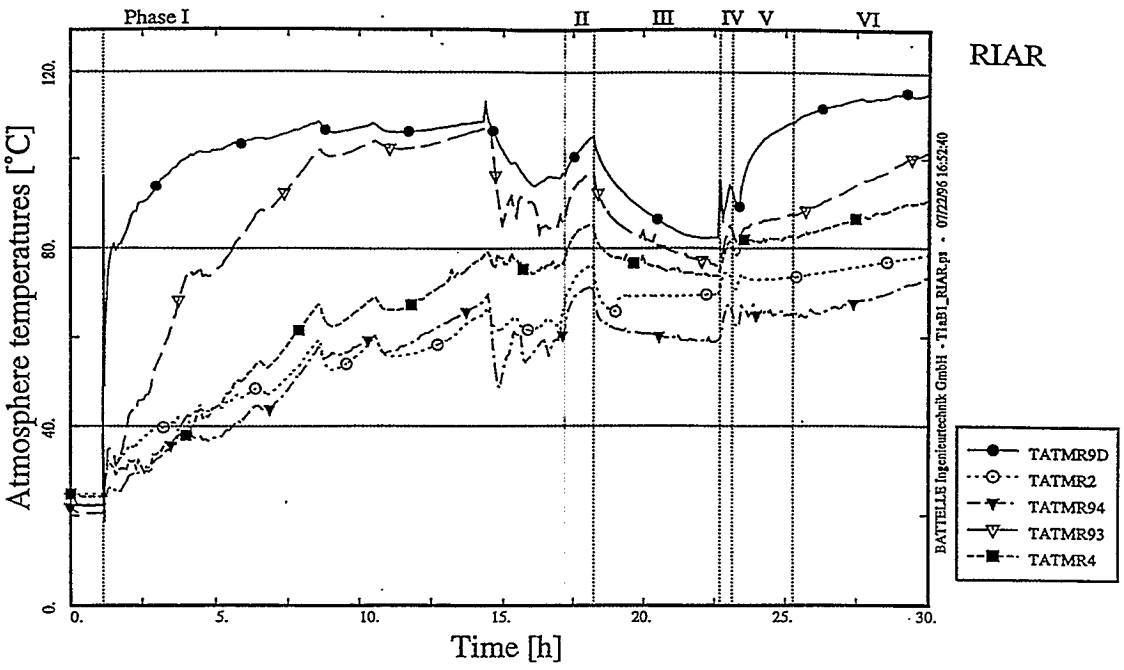

Fig. 4.8s Temperature in Dome, Annulus, R2, R4 (RIAR)

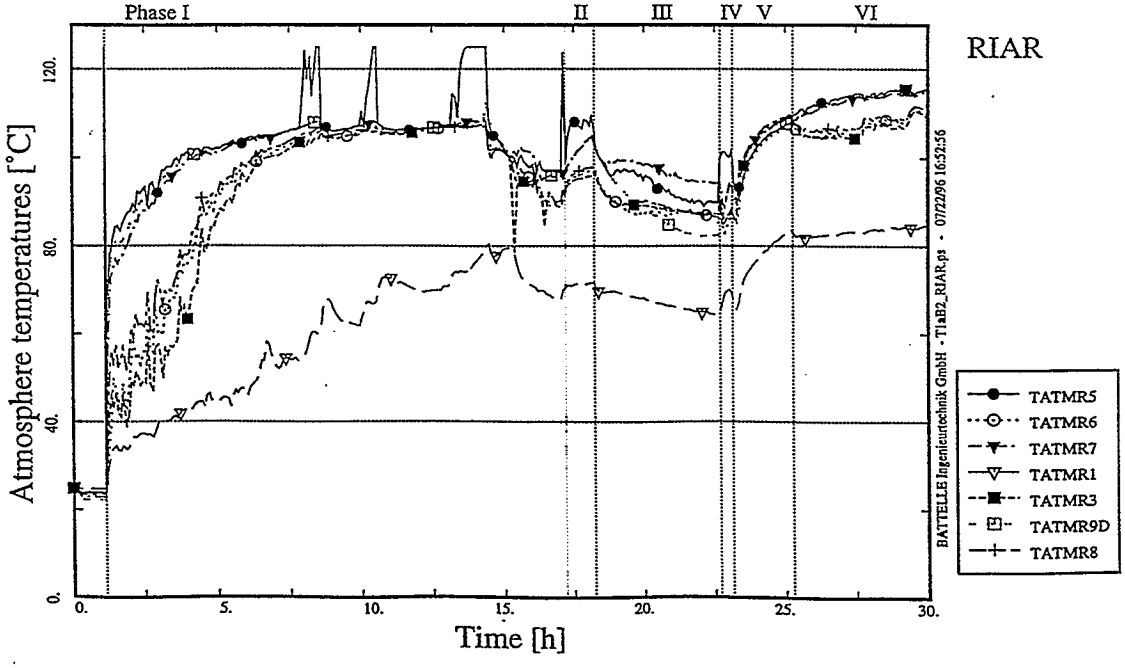

Fig. 4.9s Temperature in Dome, R1, R3, R5, R6, R7, R8 (RIAR)

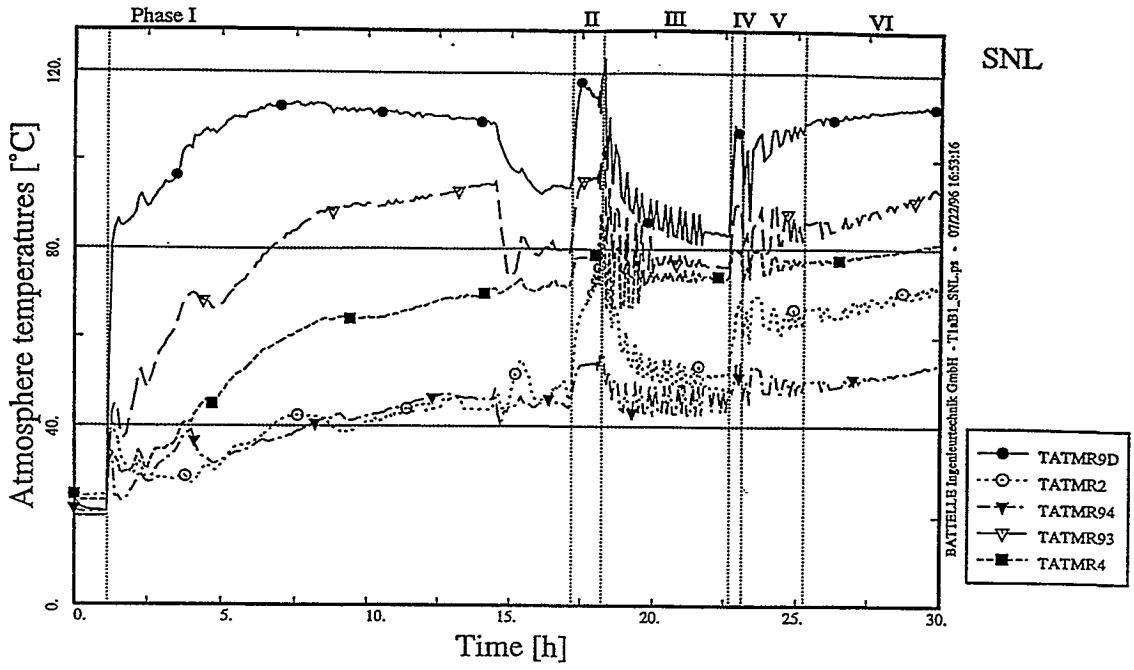

Fig. 4.8t Temperature in Dome, Annulus, R2, R4 (SNL)

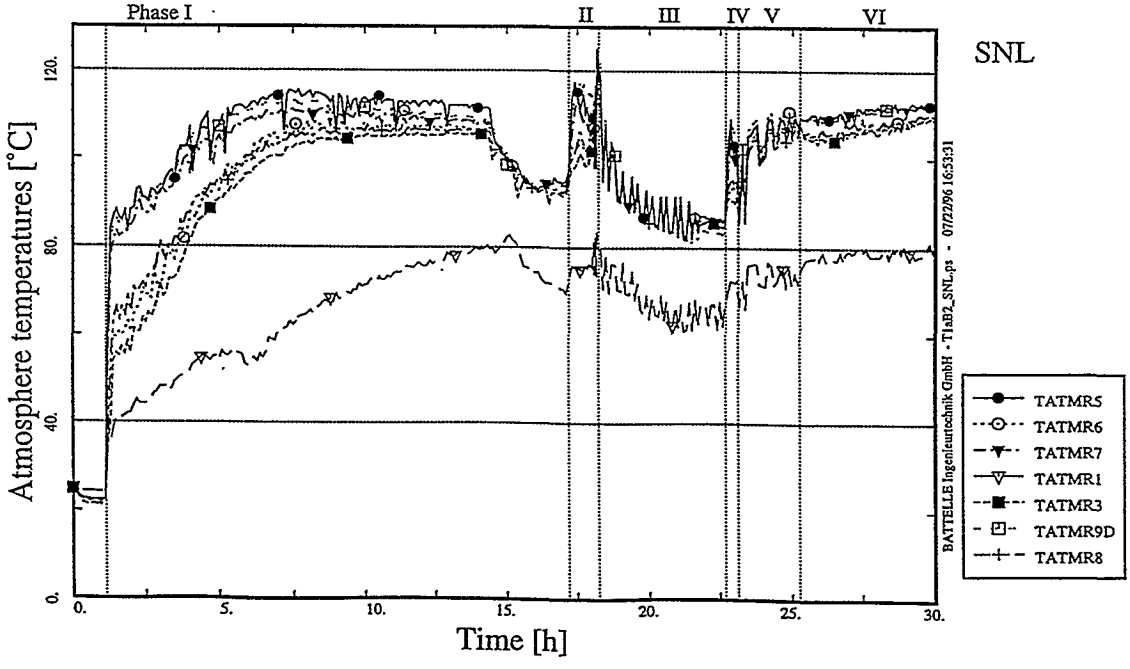

Fig. 4.9t Temperature in Dome, R1, R3, R5, R6, R7, R8 (SNL)

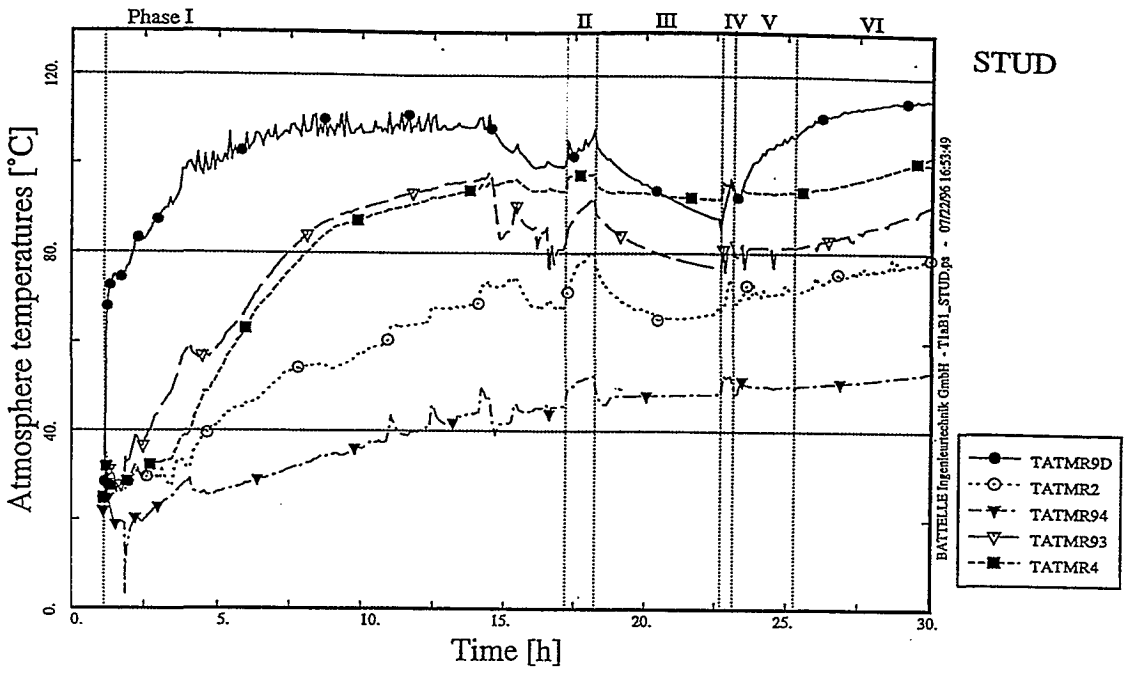

Fig. 4.8u Temperature in Dome, Annulus, R2, R4 (STUD)

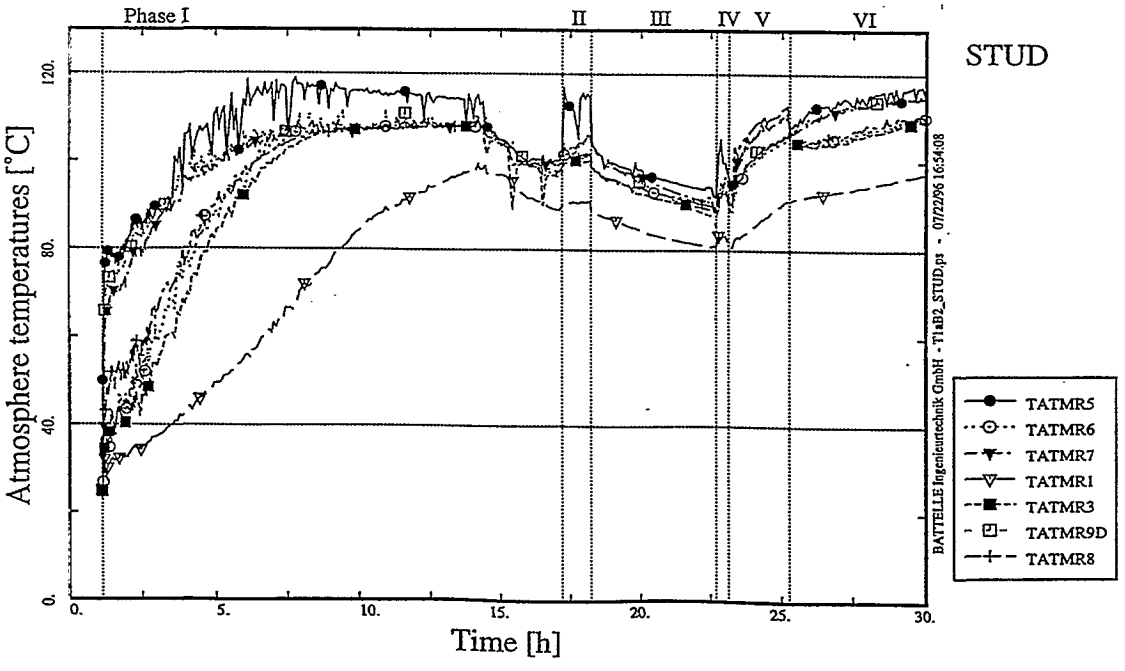

Fig. 4.9u Temperature in Dome, R1, R3, R5, R6, R7, R8 (STUD)

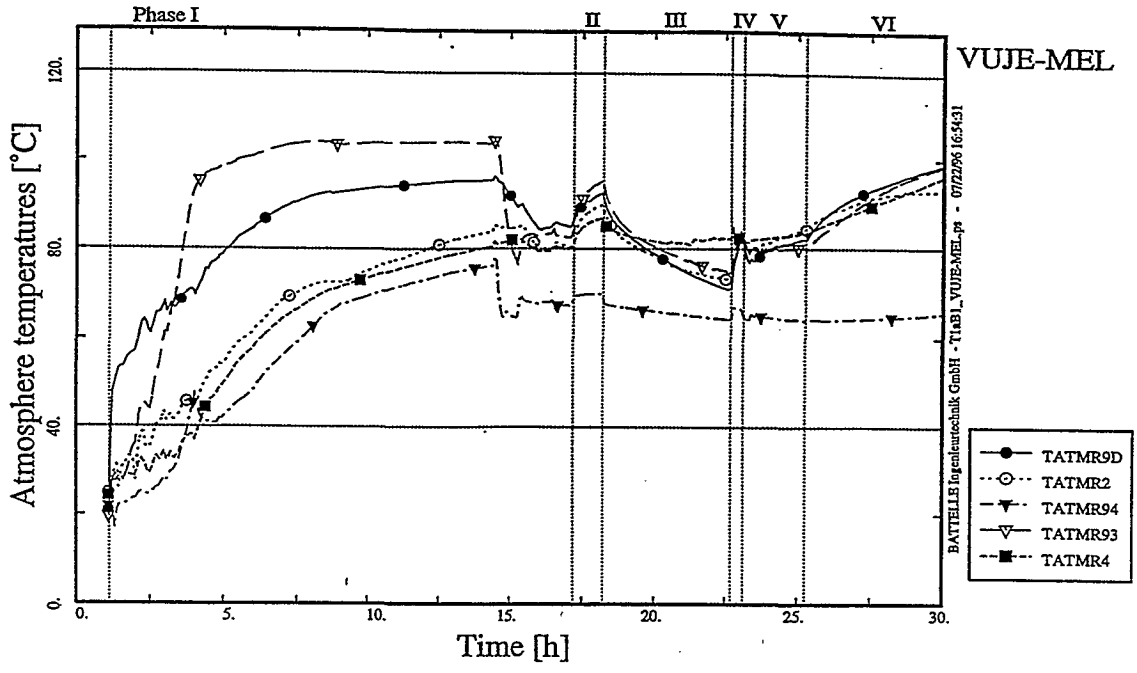

Fig. 4.8v Temperature in Dome, Annulus, R2, R4 (VUJE-MEL)

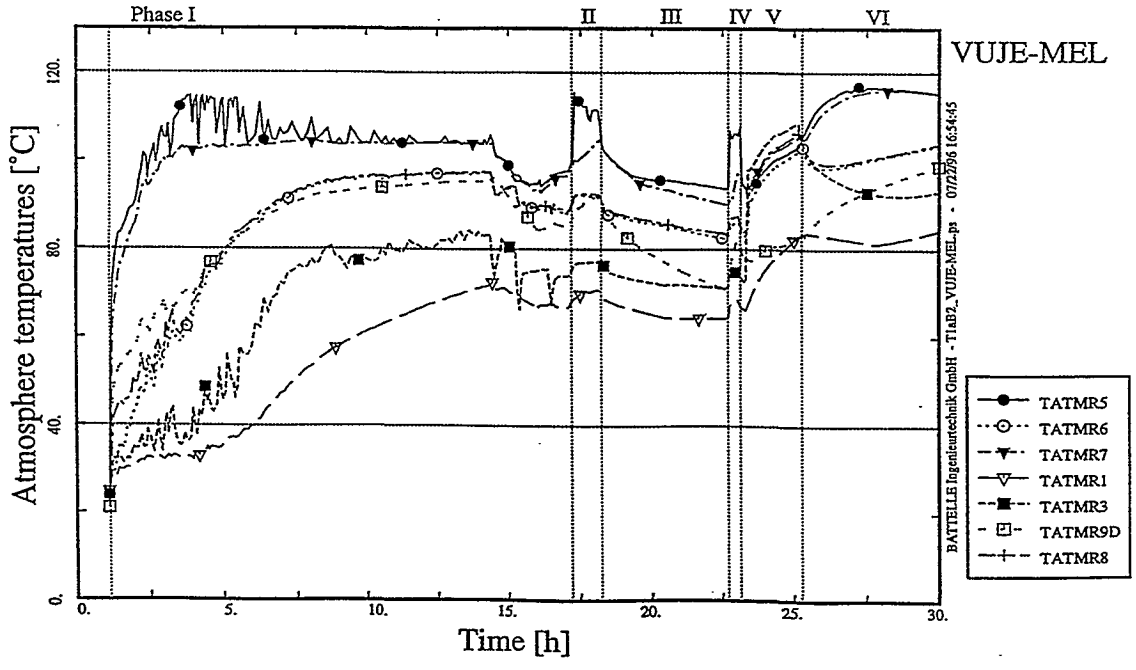

Fig. 4.9v Temperature in Dome, R1, R3, R5, R6, R7, R8 (VUJE-MEL)

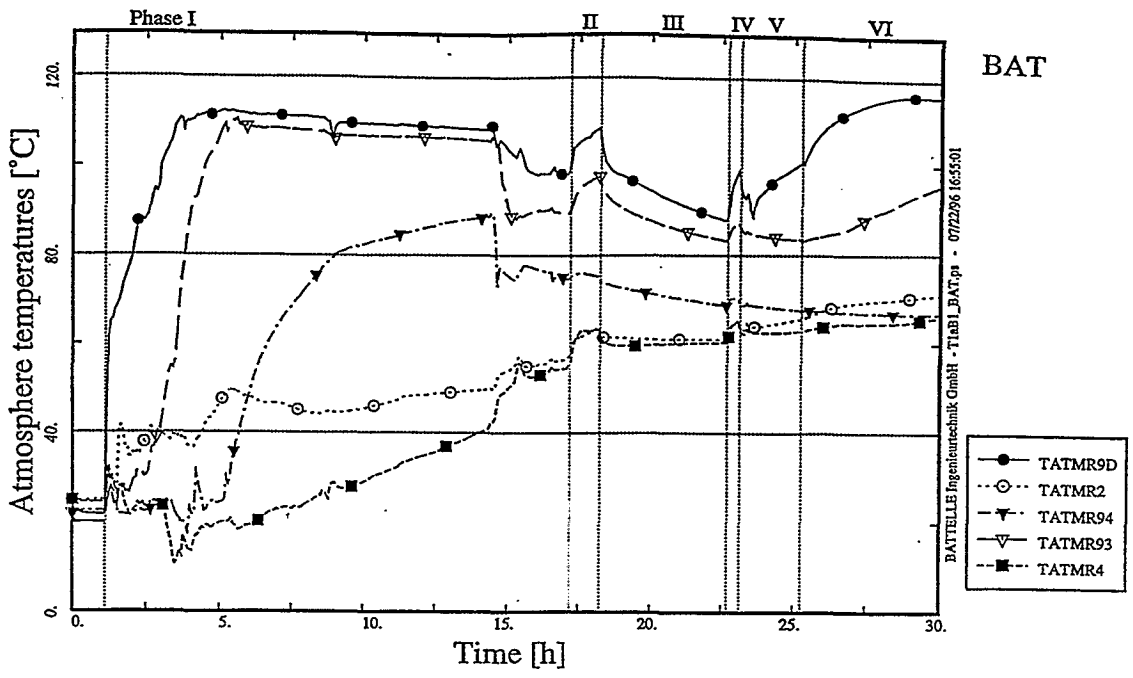

Fig. 4.8w Temperature in Dome, Annulus, R2, R4 (BAT)

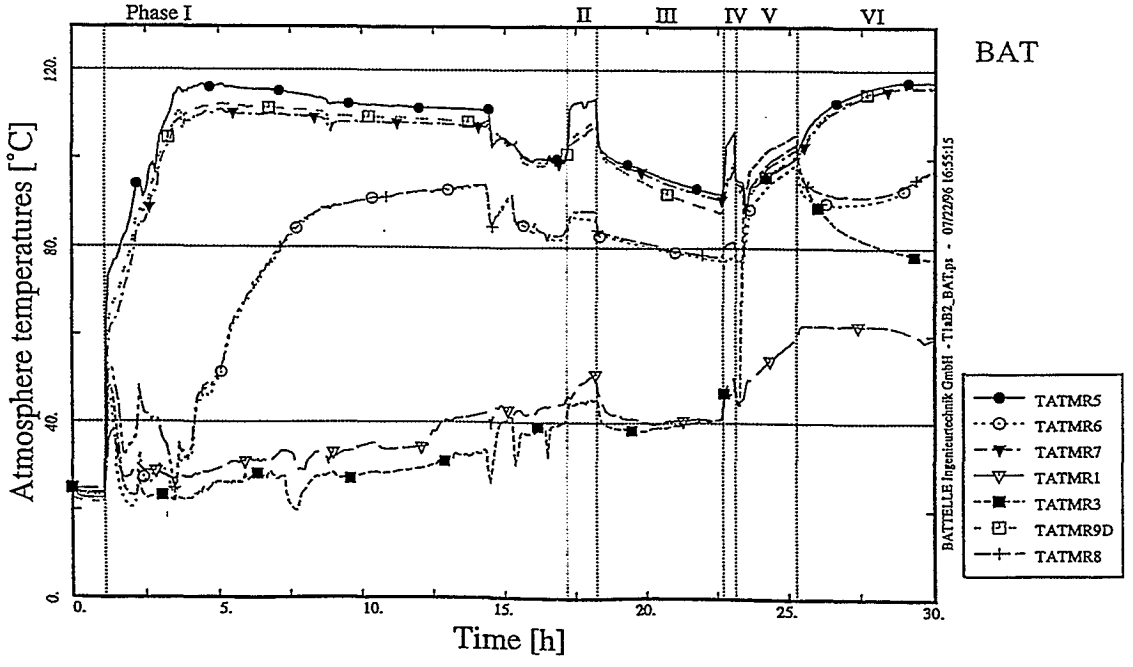

Fig. 4.9w Temperature in Dome, R1, R3, R5, R6, R7, R8 (BAT)

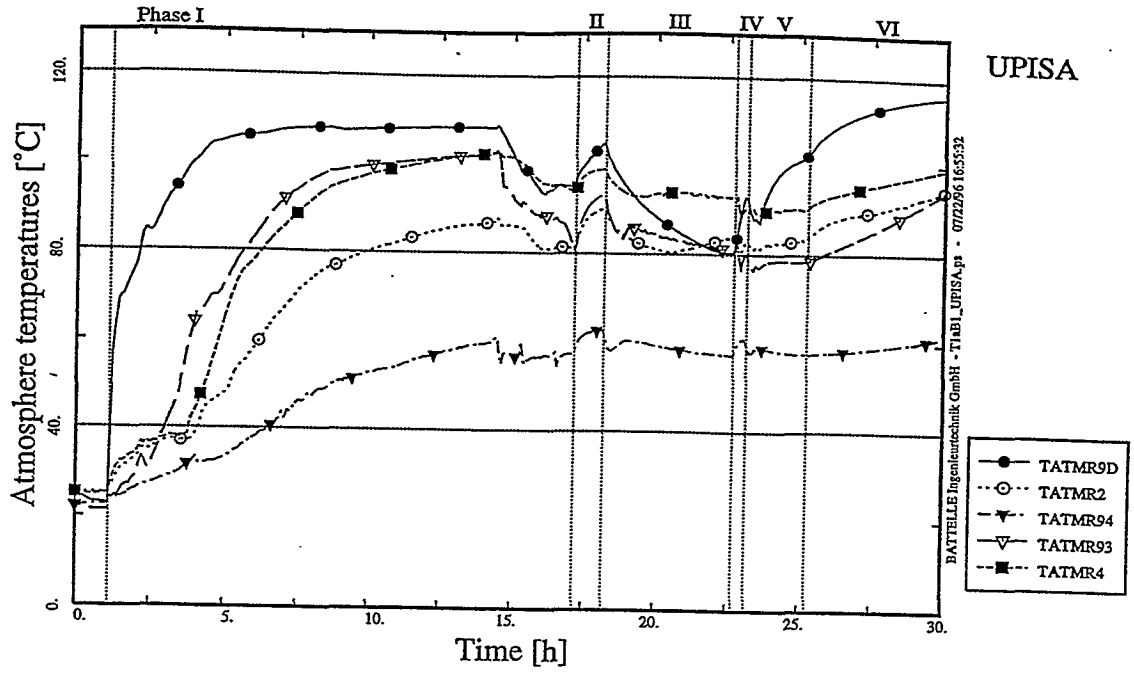

Fig. 4.8x Temperature in Dome, Annulus, R2, R4 (UPISA)

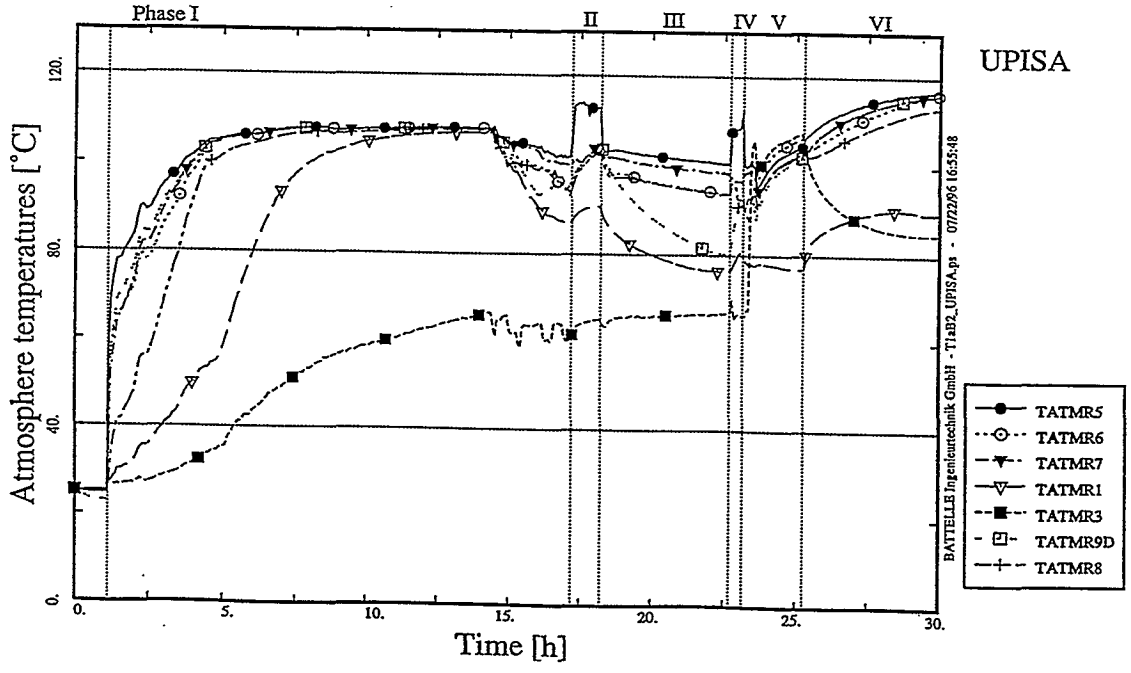

Fig. 4.9x Temperature in Dome, R1, R3, R5, R6, R7, R8 (UPISA)

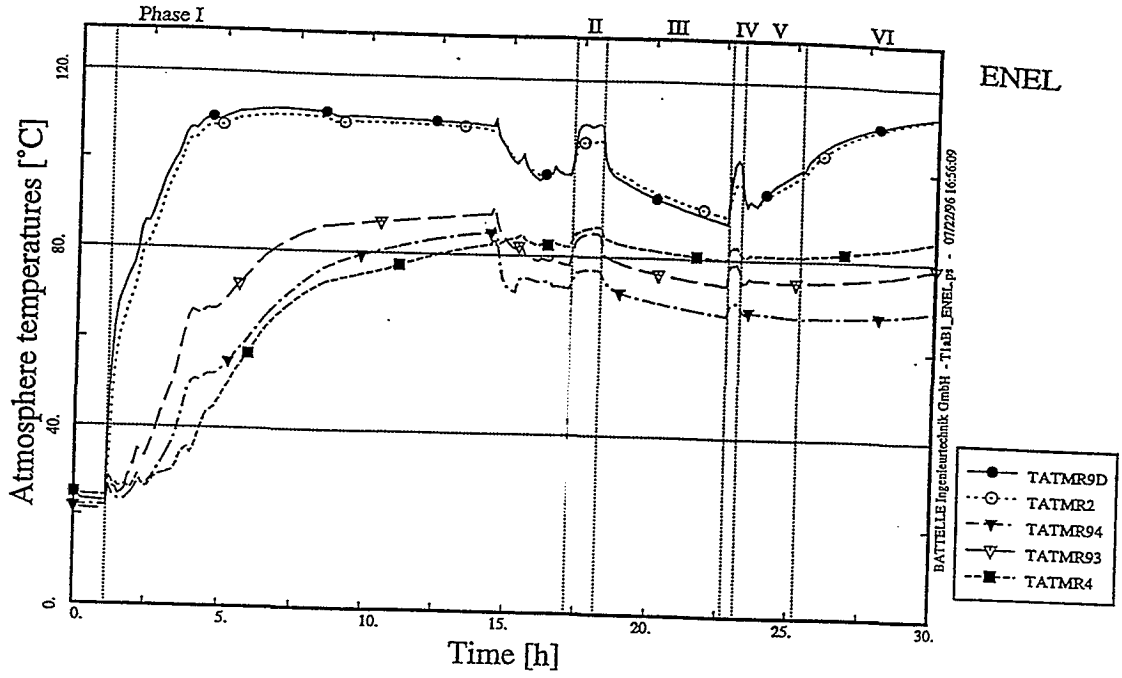

Fig. 4.8y Temperature in Dome, Annulus, R2, R4 (ENEL)

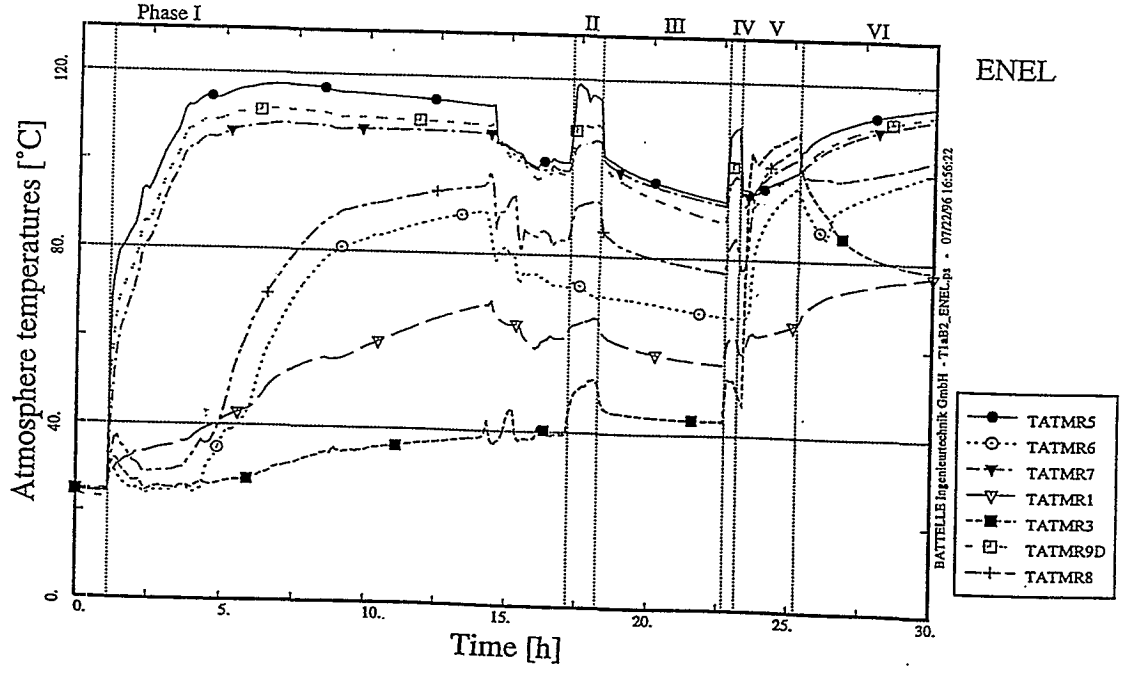

Fig. 4.9y Temperature in Dome, R1, R3, R5, R6, R7, R8 (ENEL)

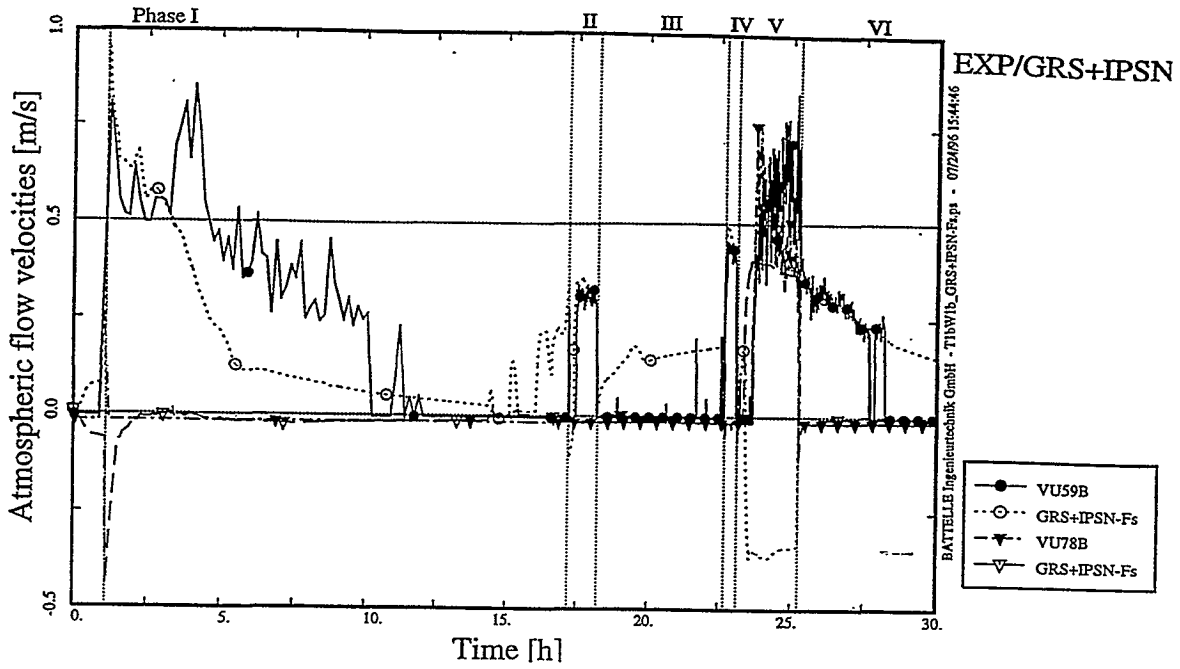

Fig. 4.10a Atmospheric Flow Velocity, Inner Compartments (GRS / IPSN - Fs)

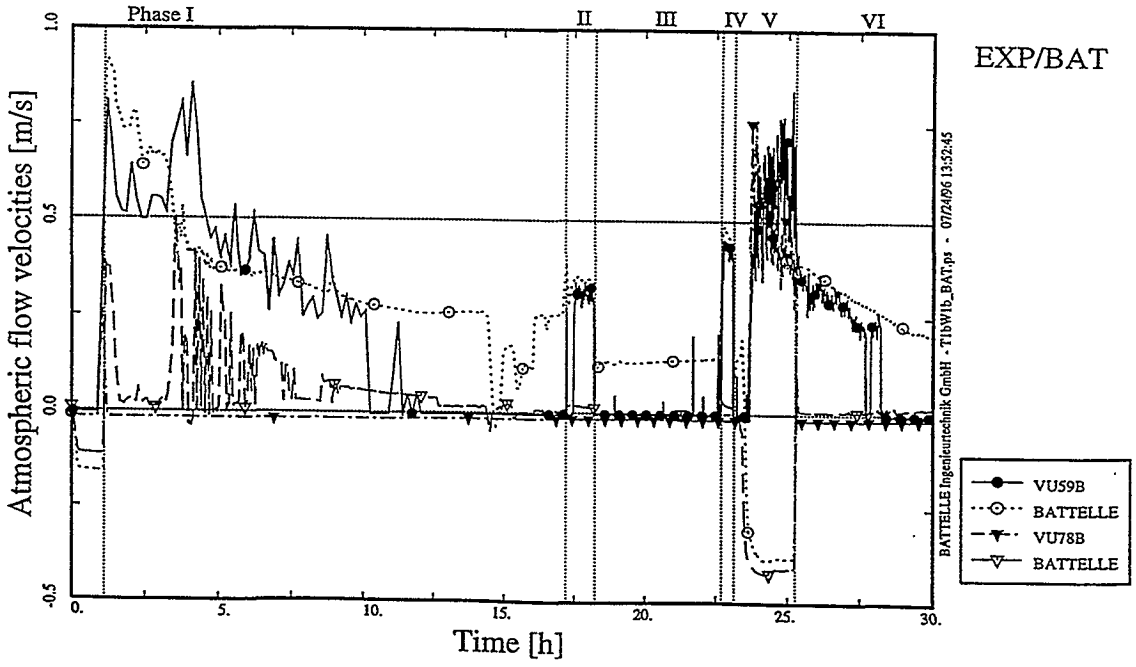

Fig. 4.10b Atmospheric Flow Velocity, Inner Compartments (BAT)

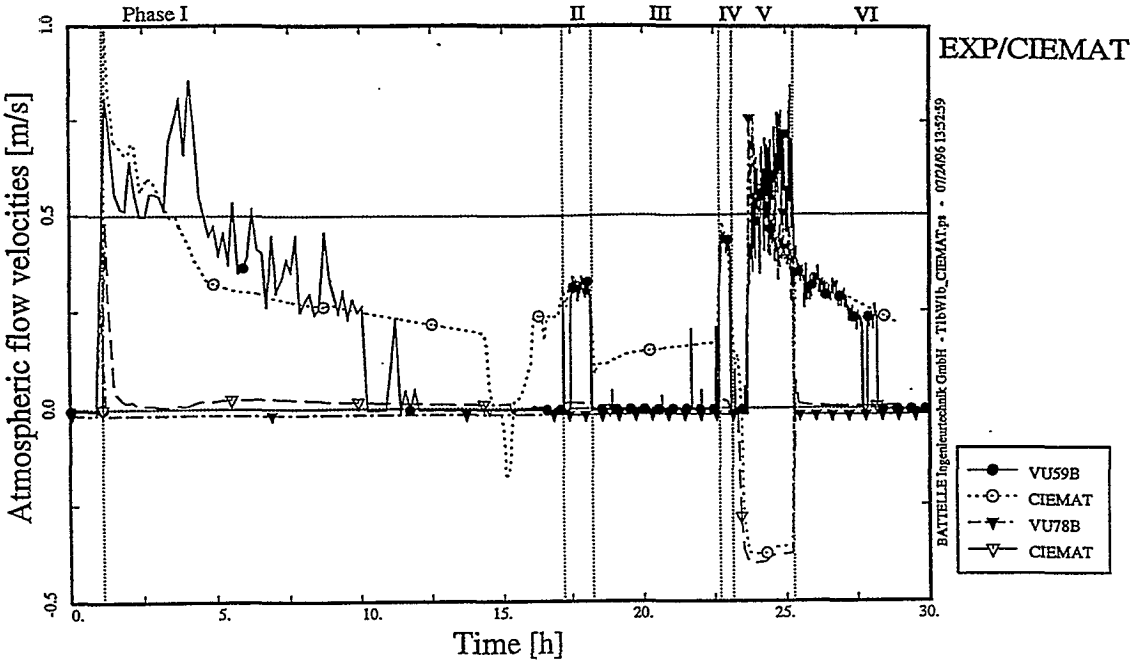

Fig. 4.10c Atmospheric Flow Velocity, Inner Compartments (CIEMAT)

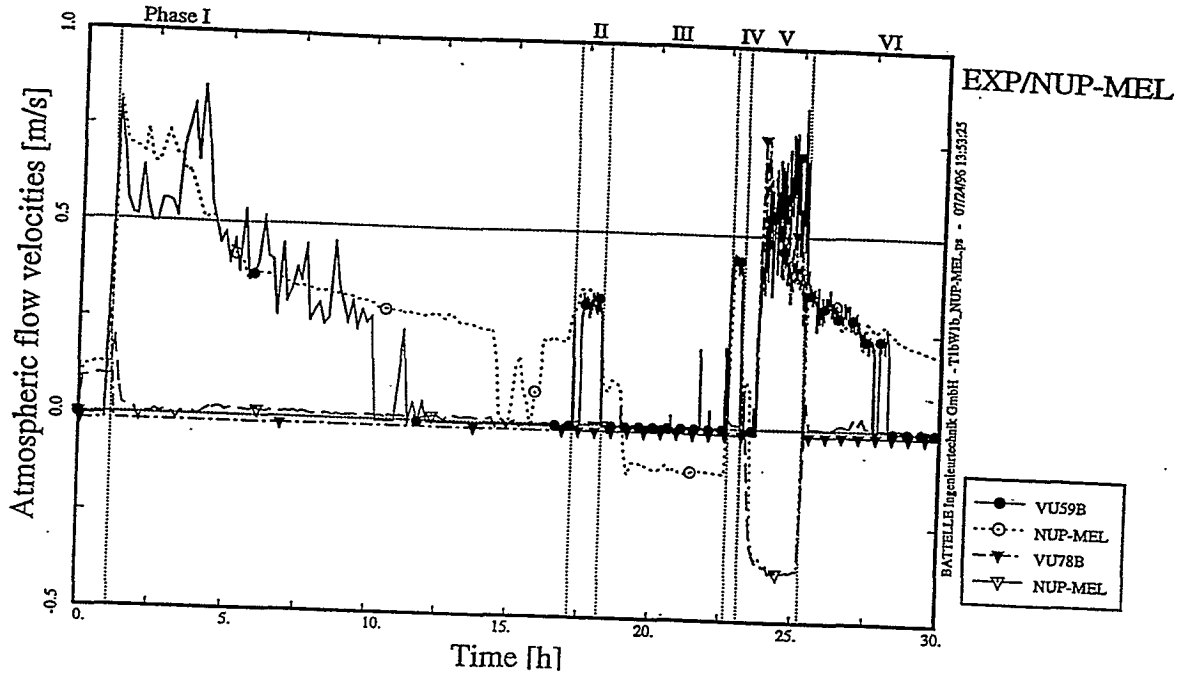

Fig. 4.10d Atmospheric Flow Velocity, Inner Compartments (NUP-MEL)

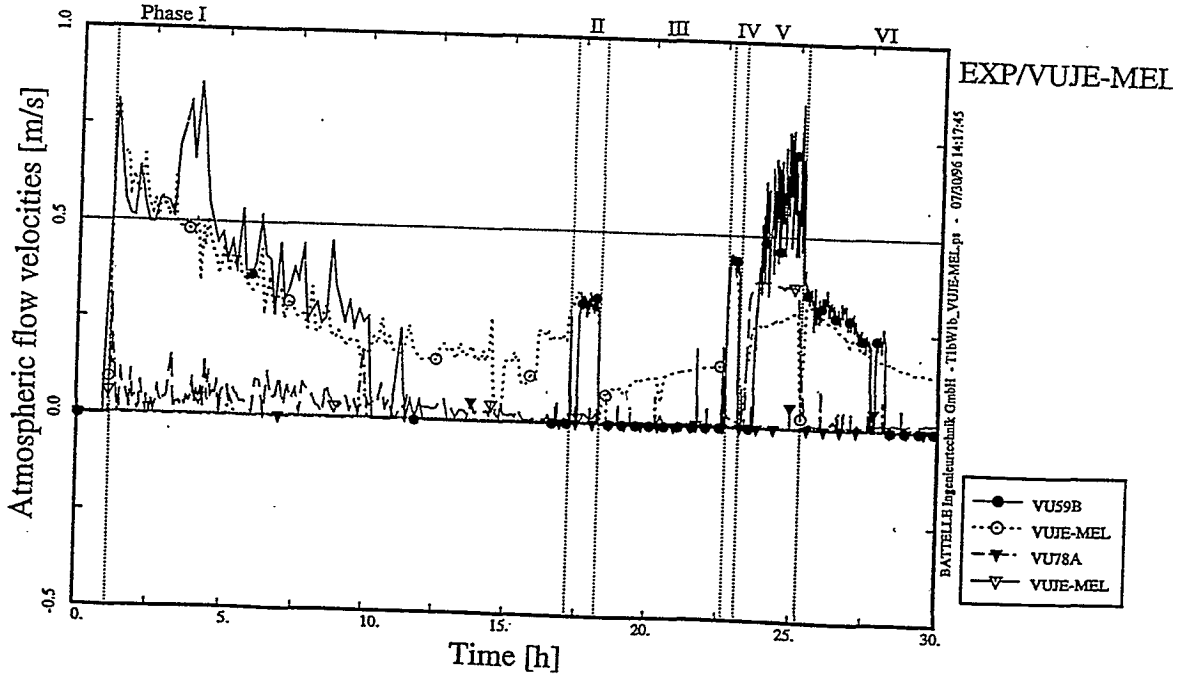

Fig. 4.10e Atmospheric Flow Velocity, Inner Compartments (VUJE-MEL)

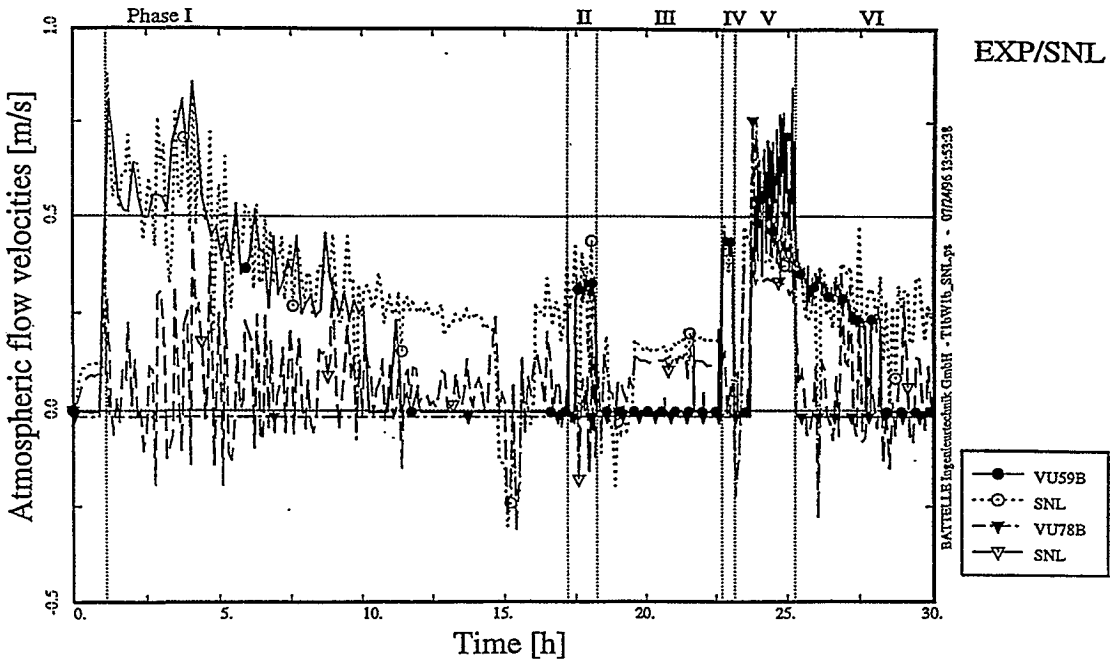

Fig. 4.10f Atmospheric Flow Velocity, Inner Compartments (SNL)

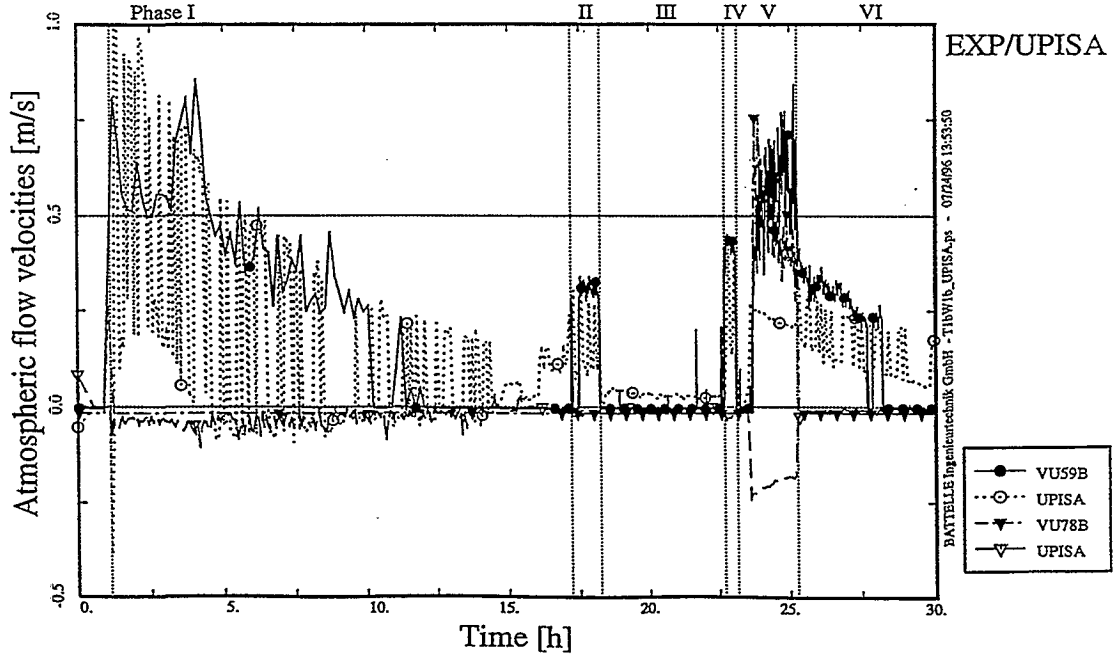

Fig. 4.10g Atmospheric Flow Velocity, Inner Compartments (UPISA)

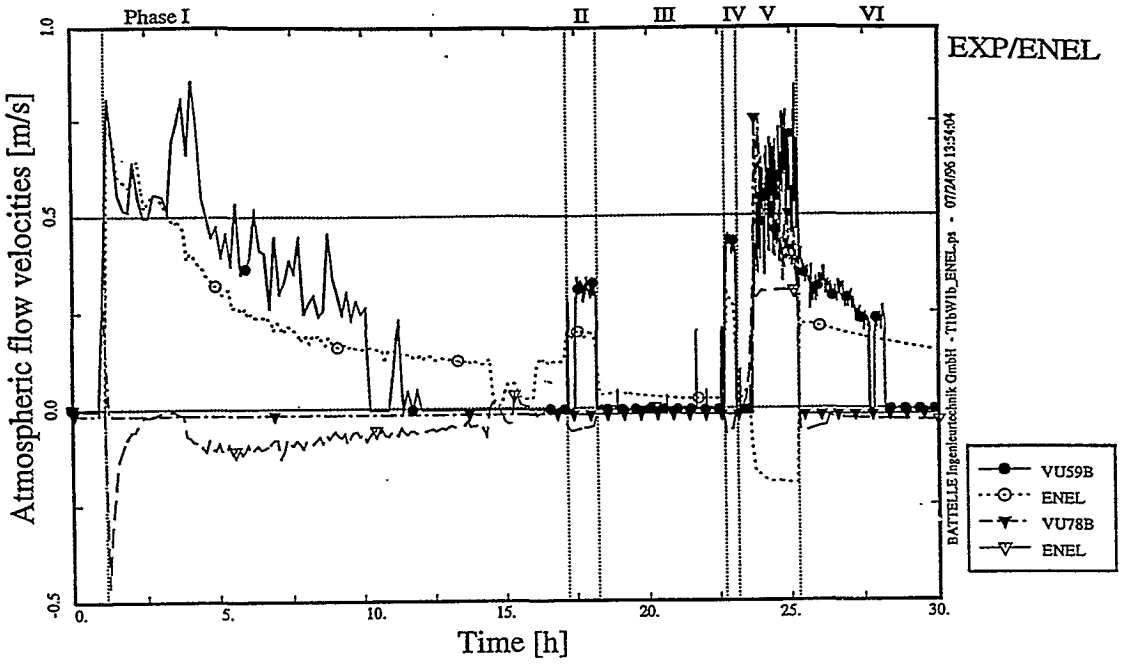

Fig. 4.10h Atmospheric Flow Velocity, Inner Compartments (ENEL)

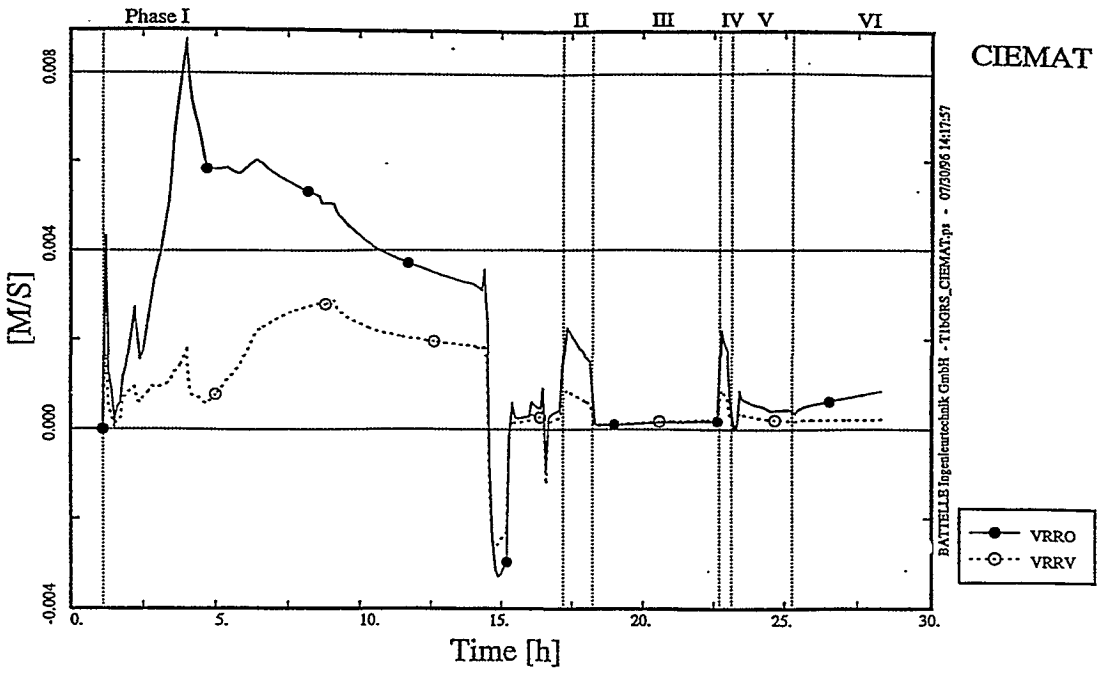

Fig. 4.11 Atmospheric Flow Velocity, Annuls (CIEMAT)

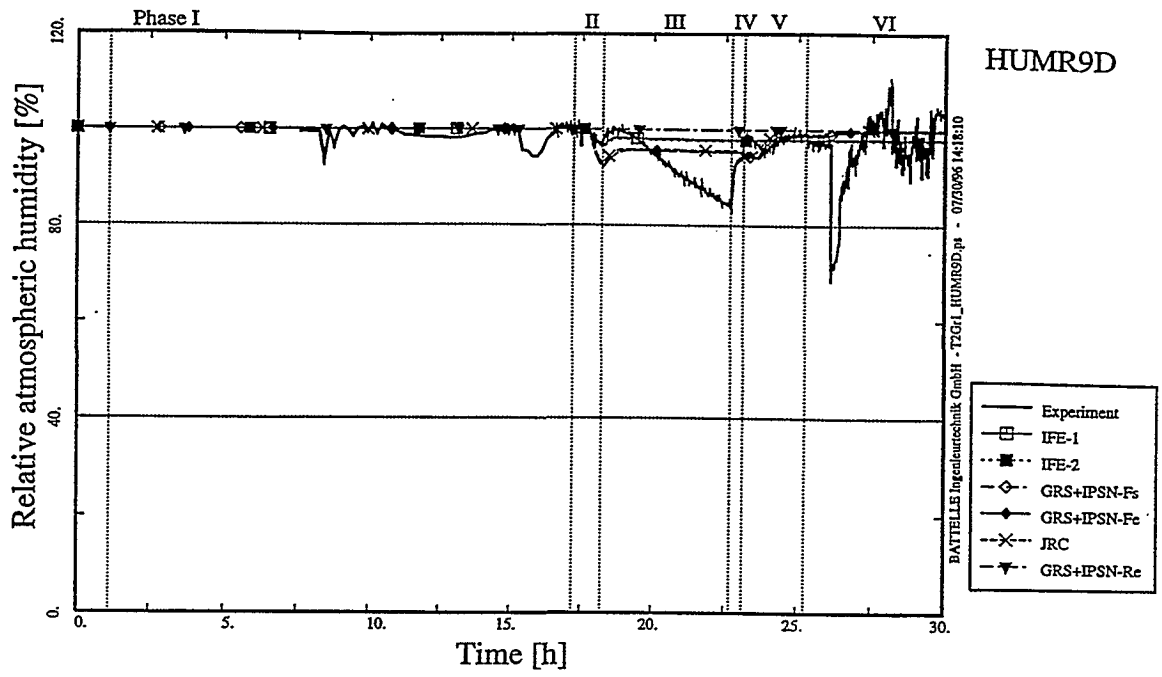

Fig. 4.12a Relative Atmospheric Humidity, Dome (FIPLOC / RALOC)

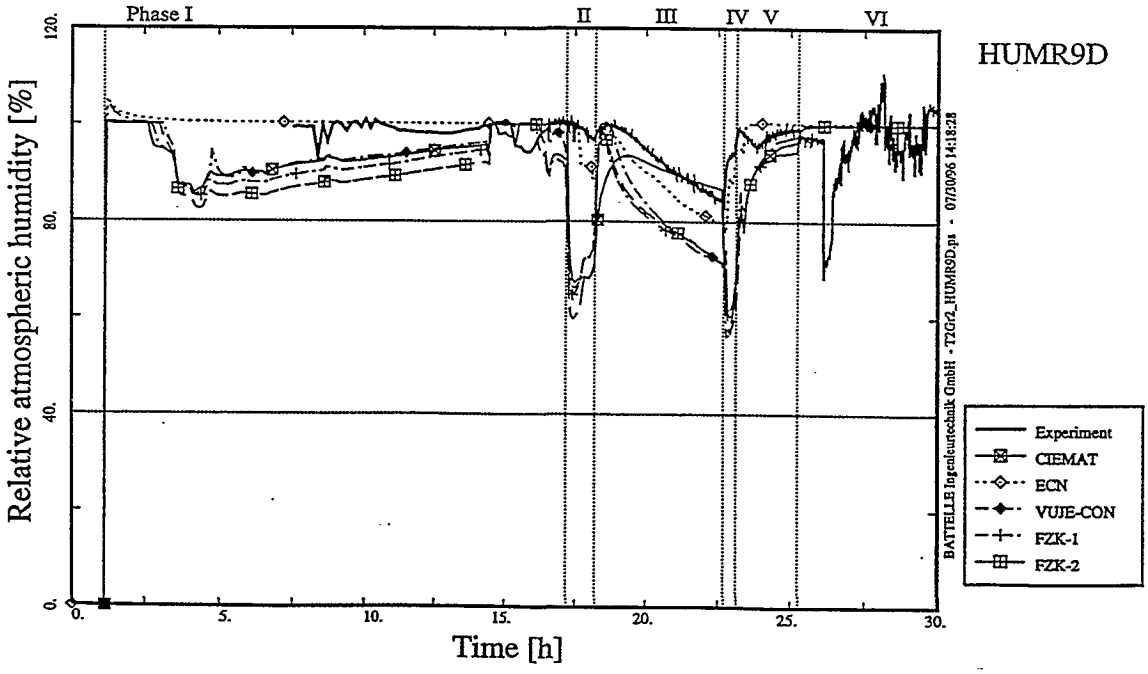

Fig. 4.12b Relative Atmospheric Humidity, Dome (CONTAIN)

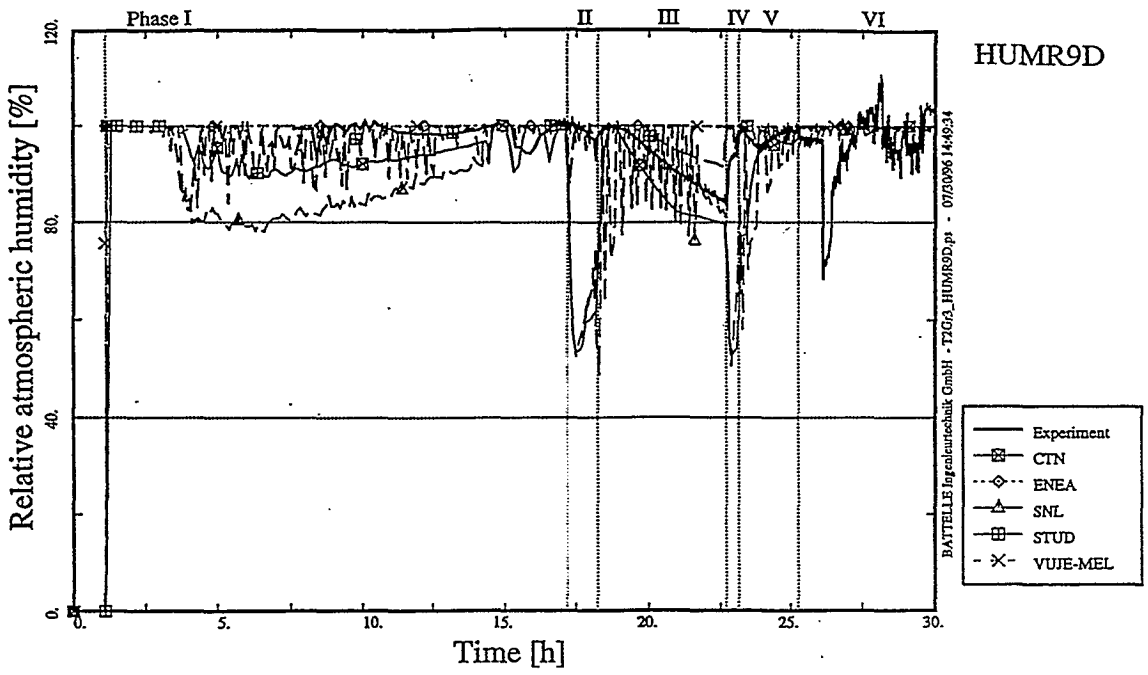

Fig. 4.12c Relative Atmospheric Humidity, Dome (MELCOR, part I)

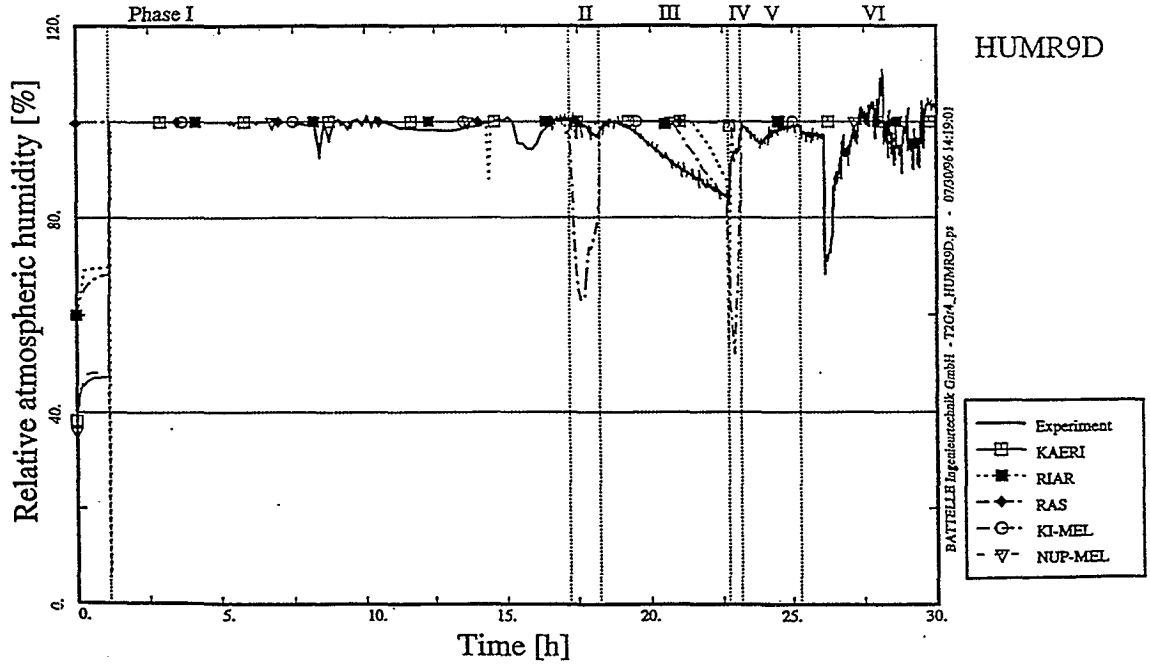

Fig. 4.12d Relative Atmospheric Humidity, Dome (MELCOR, part II

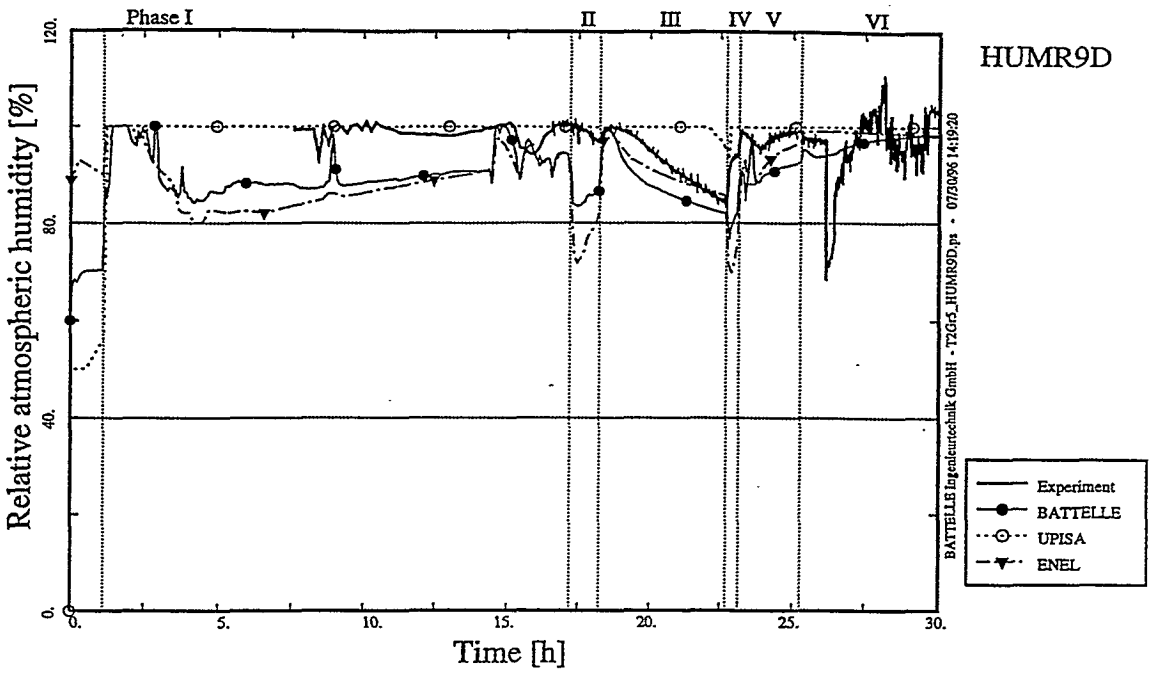

Fig. 4.12e Relative Atmospheric Humidity, Dome (ECART, FUMO, GOTHIC)

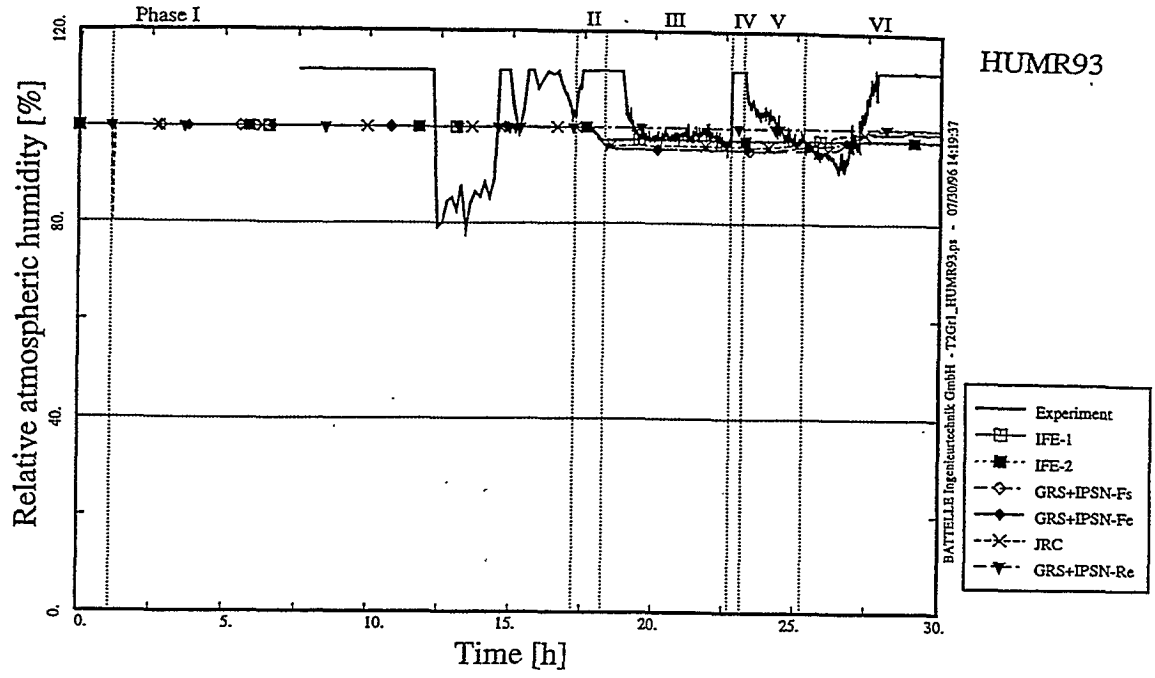

Fig. 4.12f Relative Atmospheric Humidity, Annuls (FIPLOC / RALOC)

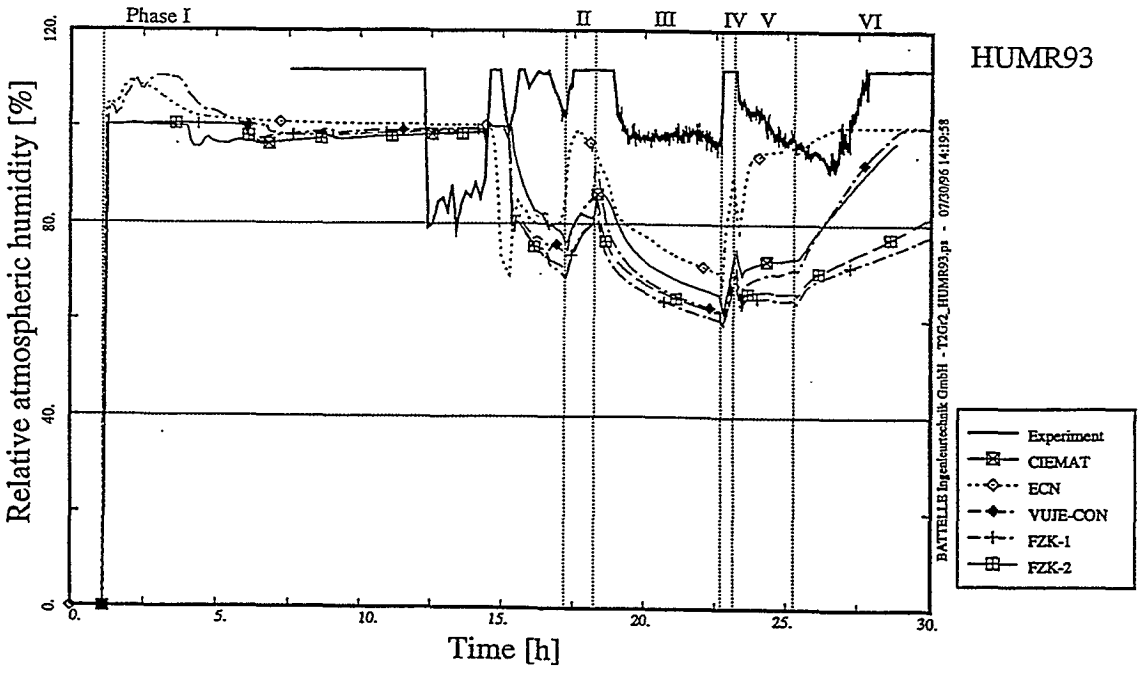

Fig. 4.12g Relative Atmospheric Humidity, Annulus (CONTAIN)

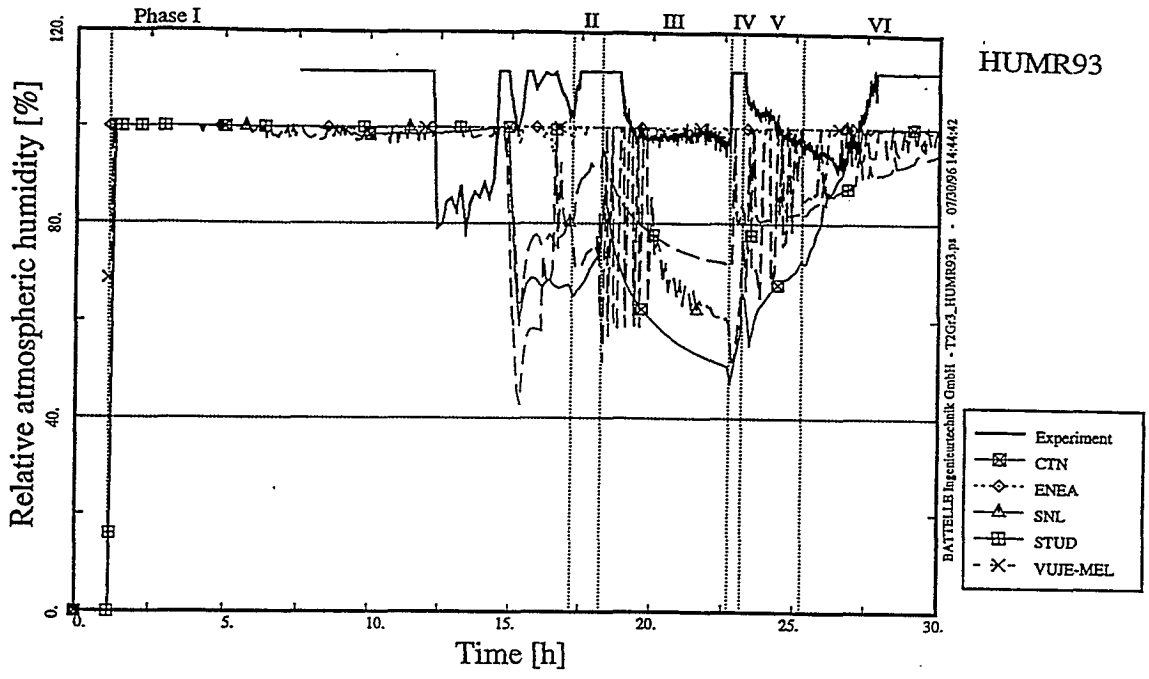

Fig. 4.12h Relative Atmospheric Humidity, Annulus (MELCOR, part I)

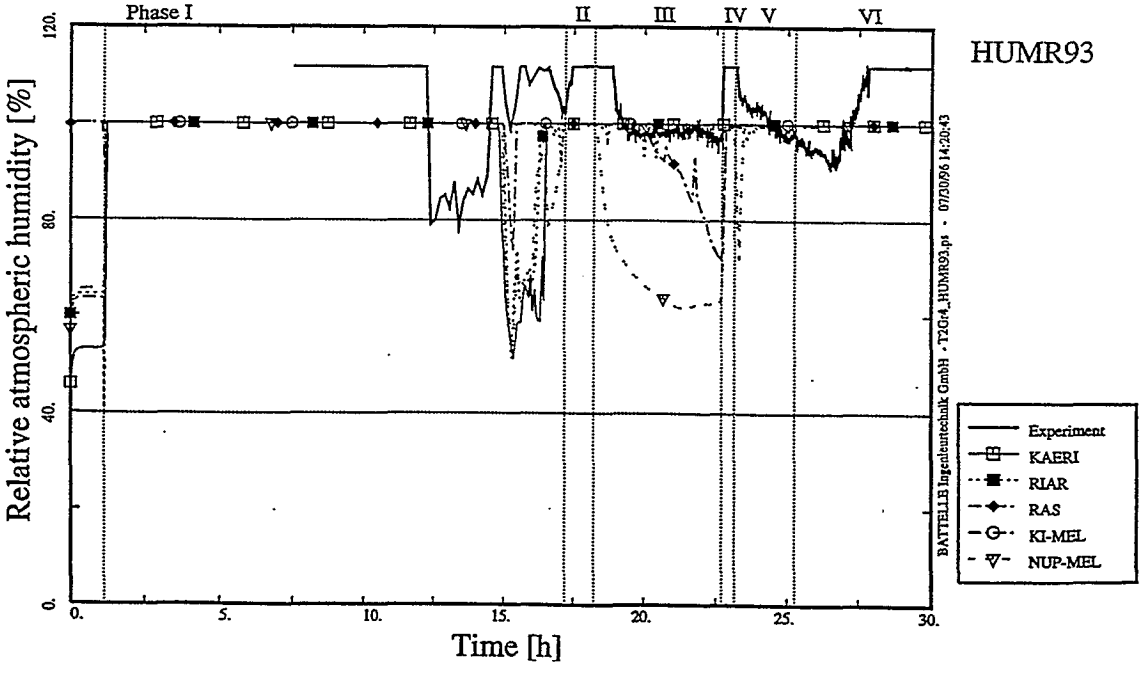

Fig. 4.12i Relative Atmospheric Humidity, Annulus (MELCOR, part II)

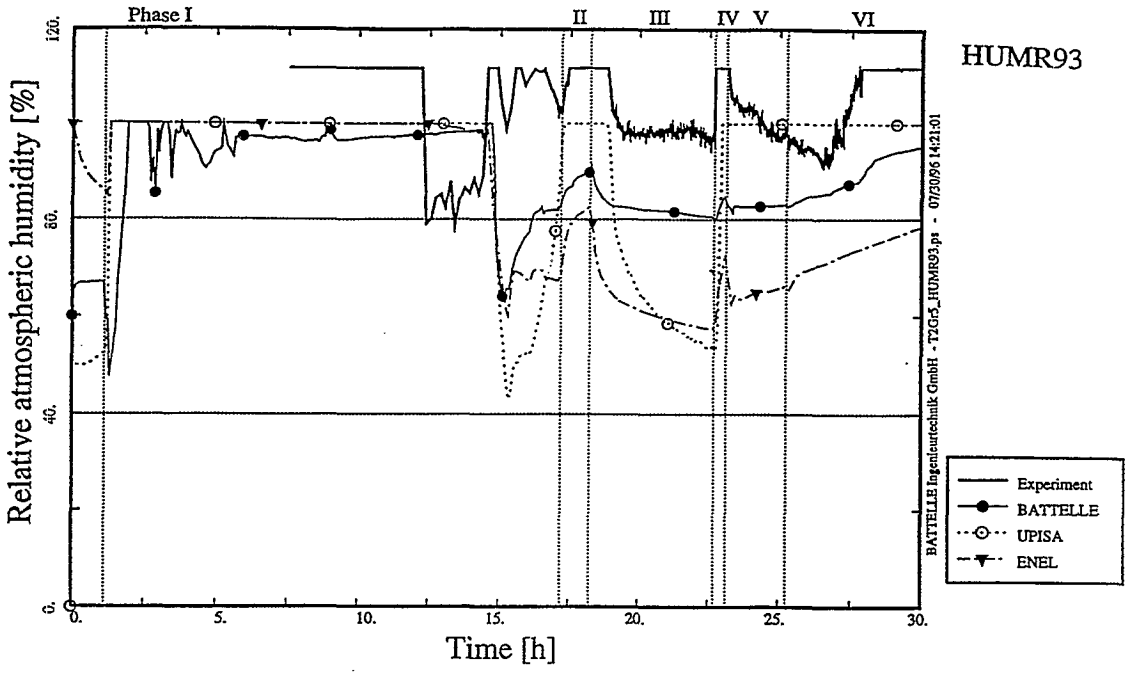

Fig. 4.12j Relative Atmospheric Humidity. Annulus (ECART, FUMO, GOTHIC)

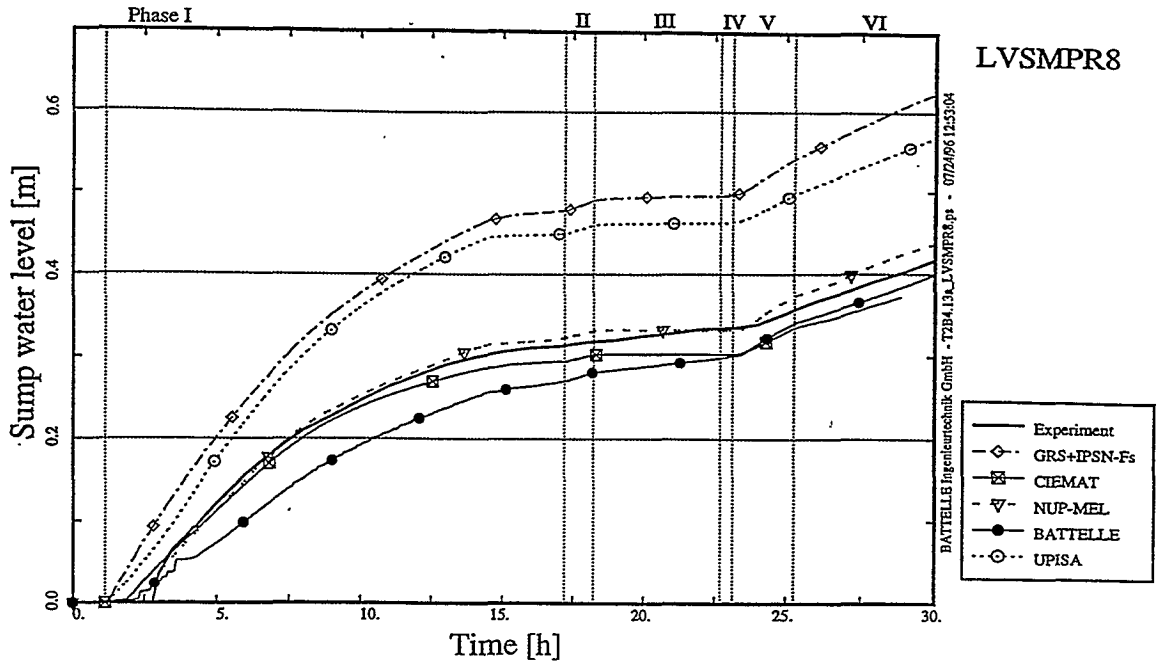

Fig. 4.13a Sump Water Level, Lower Inner Room (Reference Calculations)

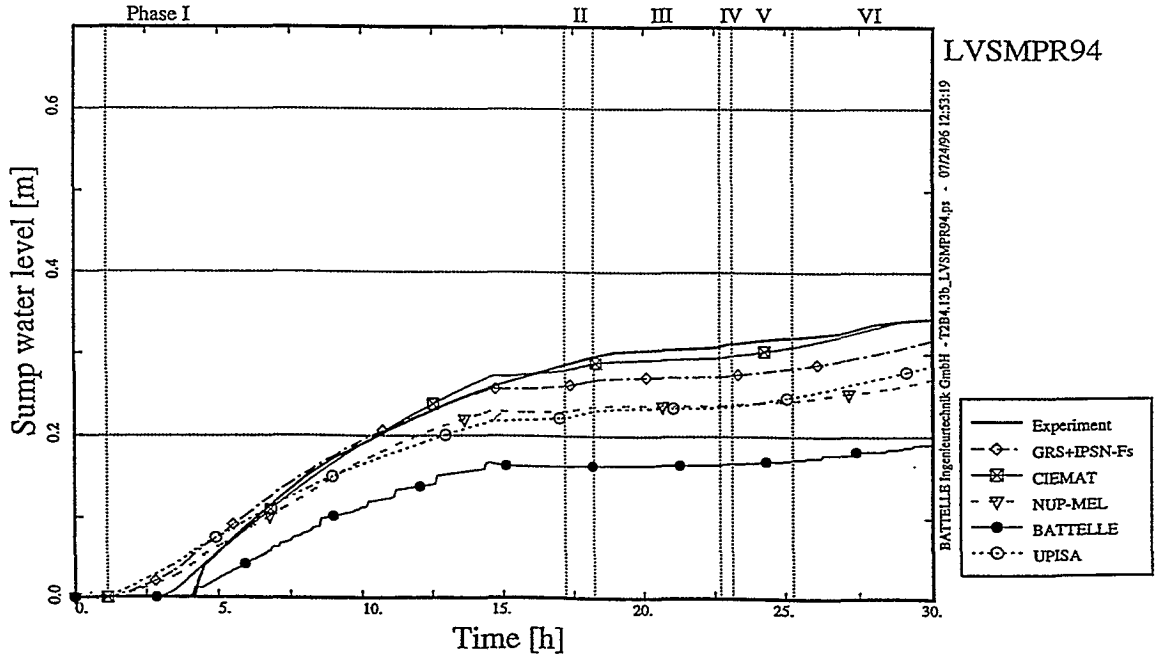

Fig. 4.13b Sump Water Level, Annulus (Reference Calculations)

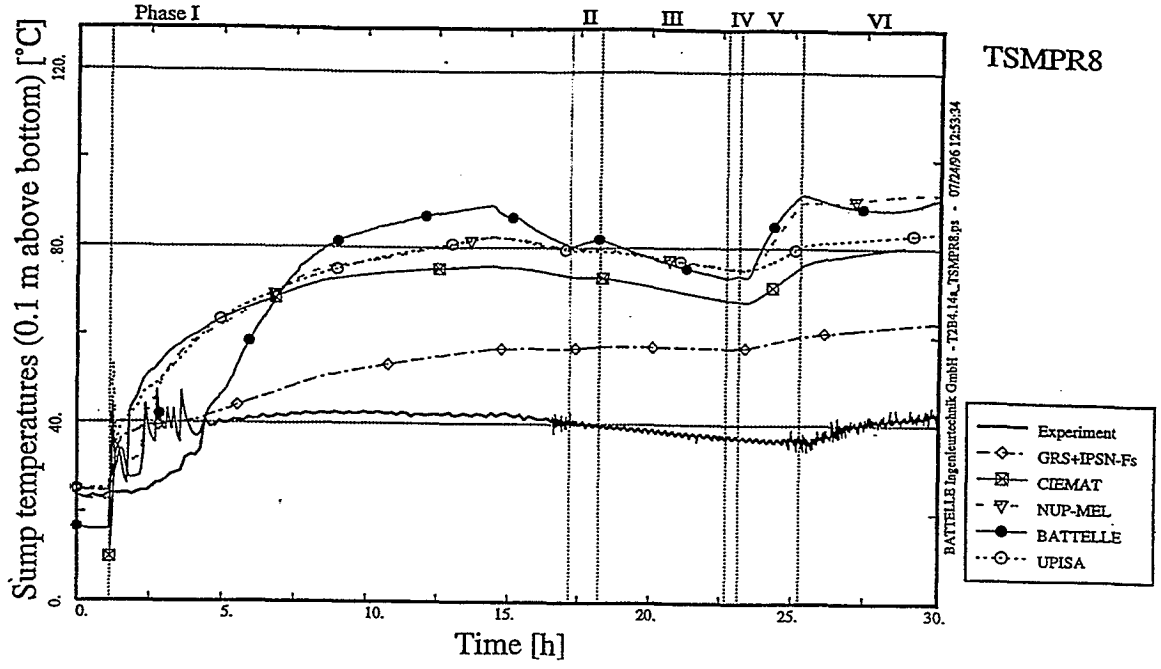

Fig. 4.14a Sump Water Temperature, Lower Inner Room (Reference Calculations)

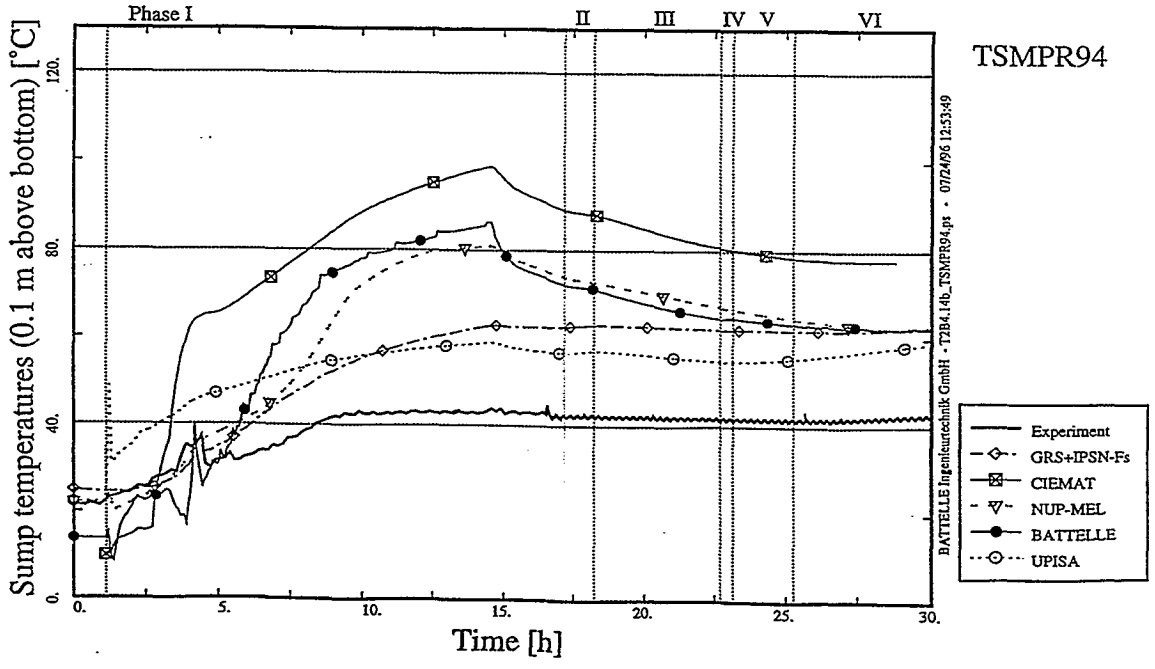

Fig. 4.14b Sump Water Temperature, Annulus (Reference Calculations)

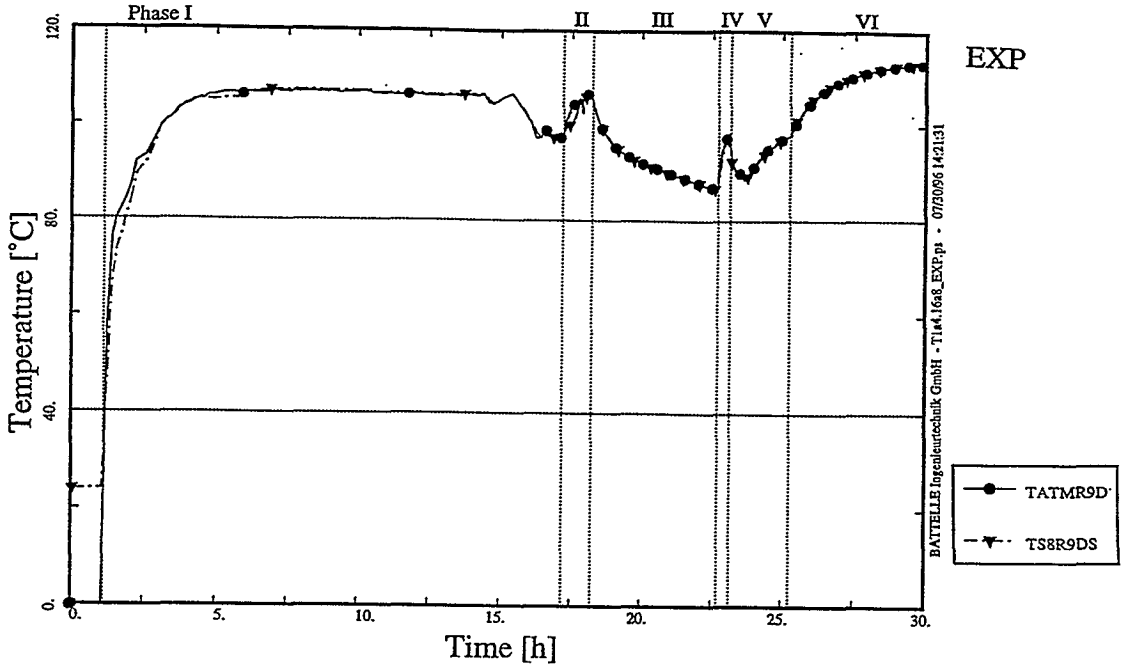

Fig. 4.15a Temperature Dome and Structure 8 Surface (EXP)

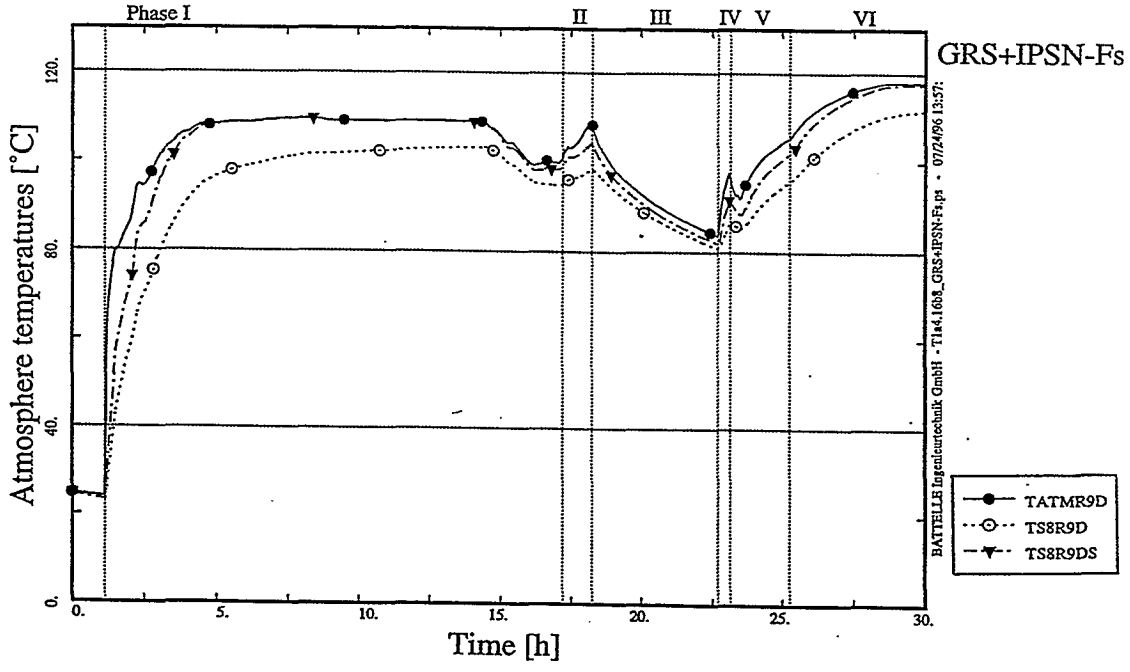

Fig. 4.15b Temperature Dome, Structure 8 Surface and Below Surface (GRS / IPSN - Fs)

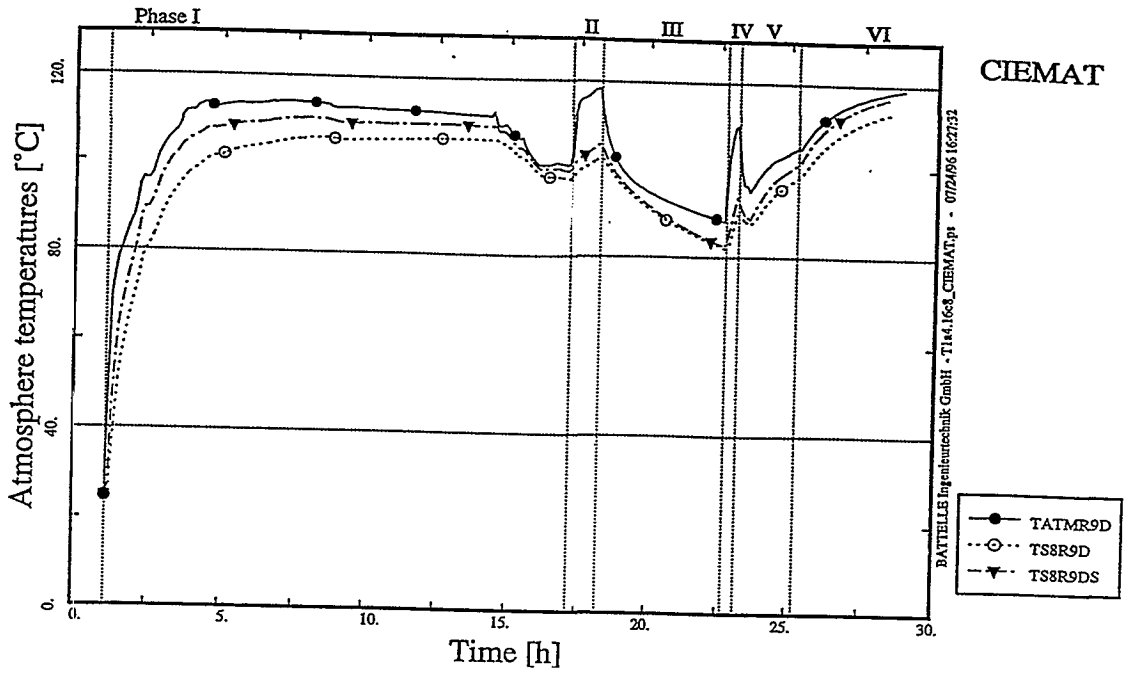

Fig. 4.15c Temperature Dome, Structure 8 Surface and Below Surface (CIEMAT)

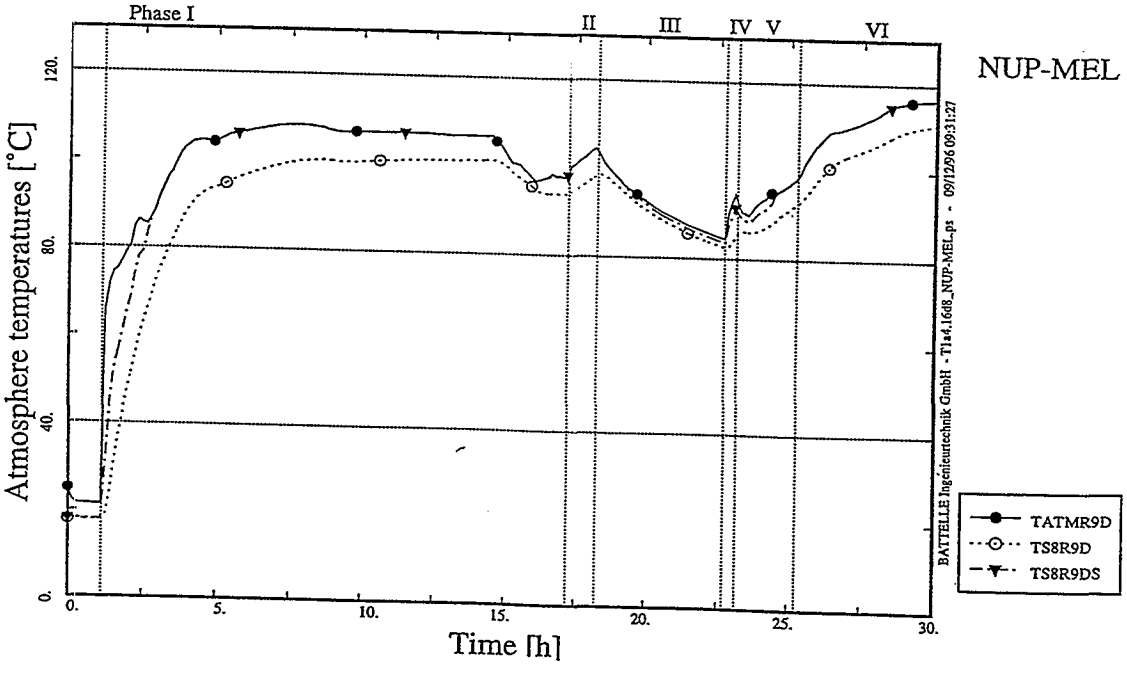

Fig. 4.15d Temperature Dome, Structure 8 Surface and Below Surface (NUP-MEL)

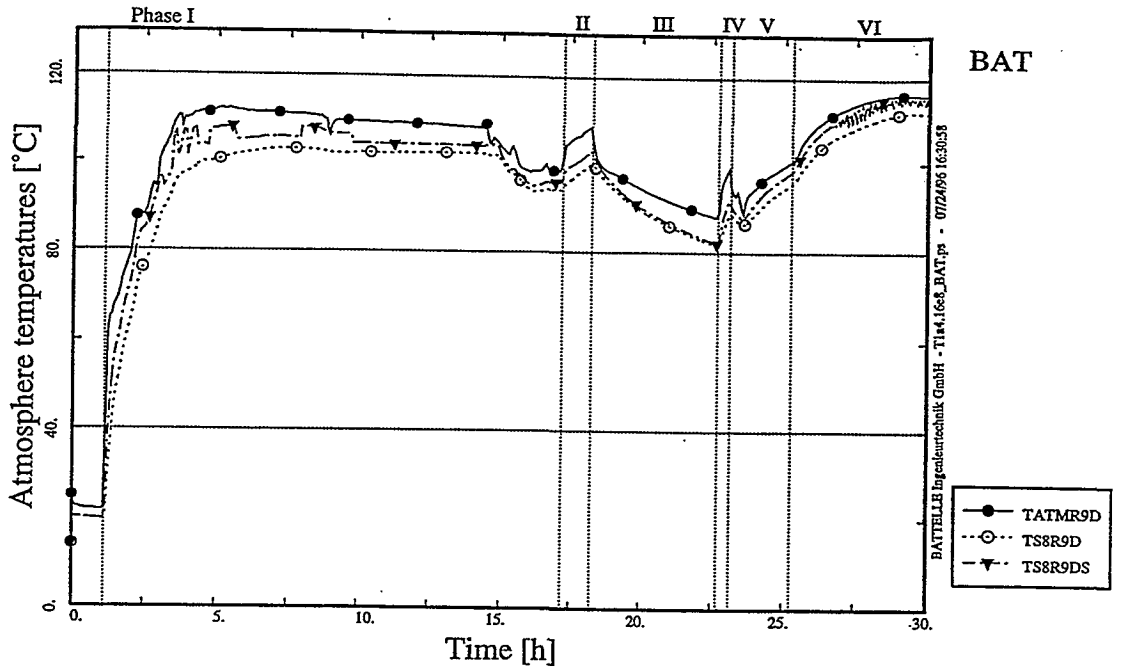

Fig. 4.15e Temperature Dome, Structure 8 Surface and Below Surface (BAT)

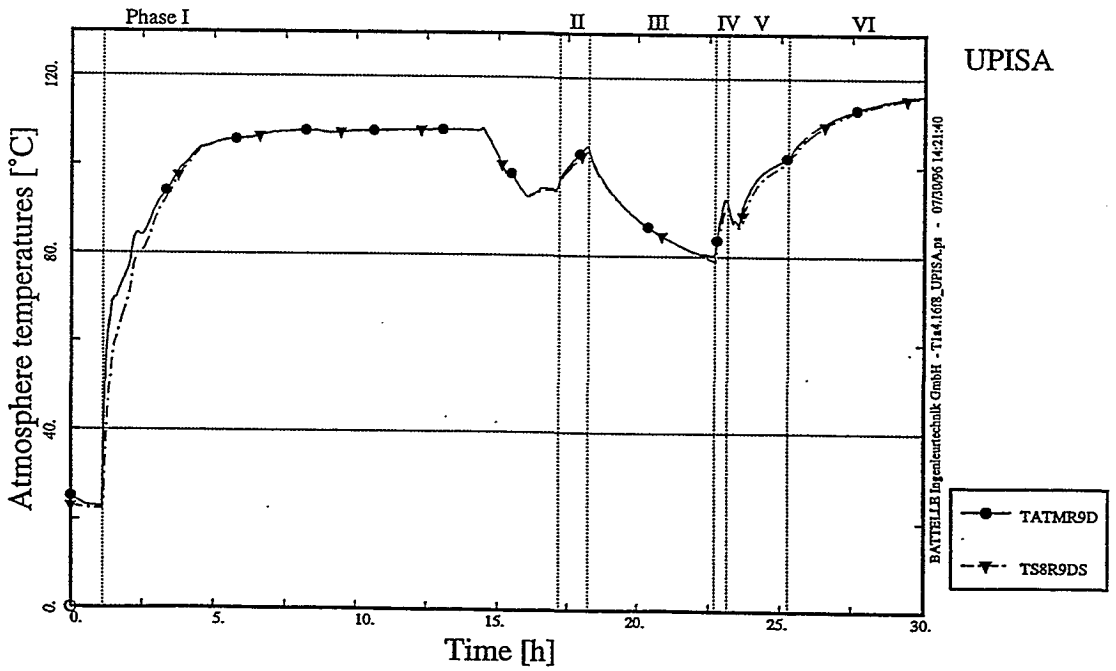

Fig. 4.15f Temperature Dome, Structure 8 Surface and Below Surface (UPISA)

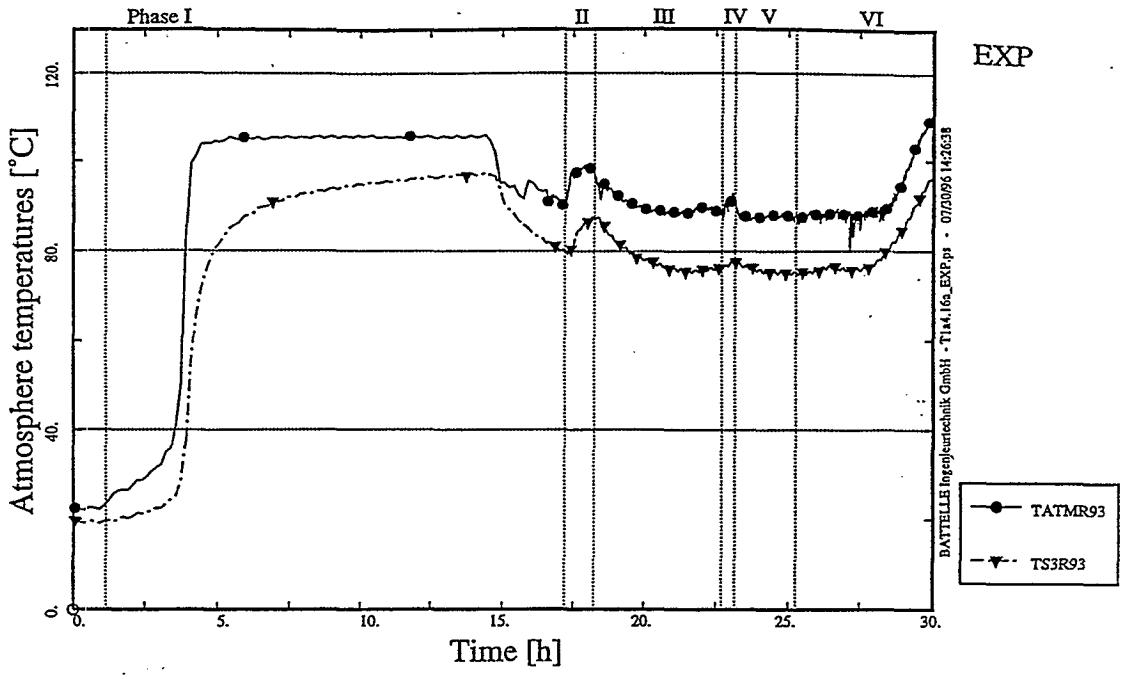

Fig. 4.16a Temperature Annulus and Structure 3 Surface (EXP)

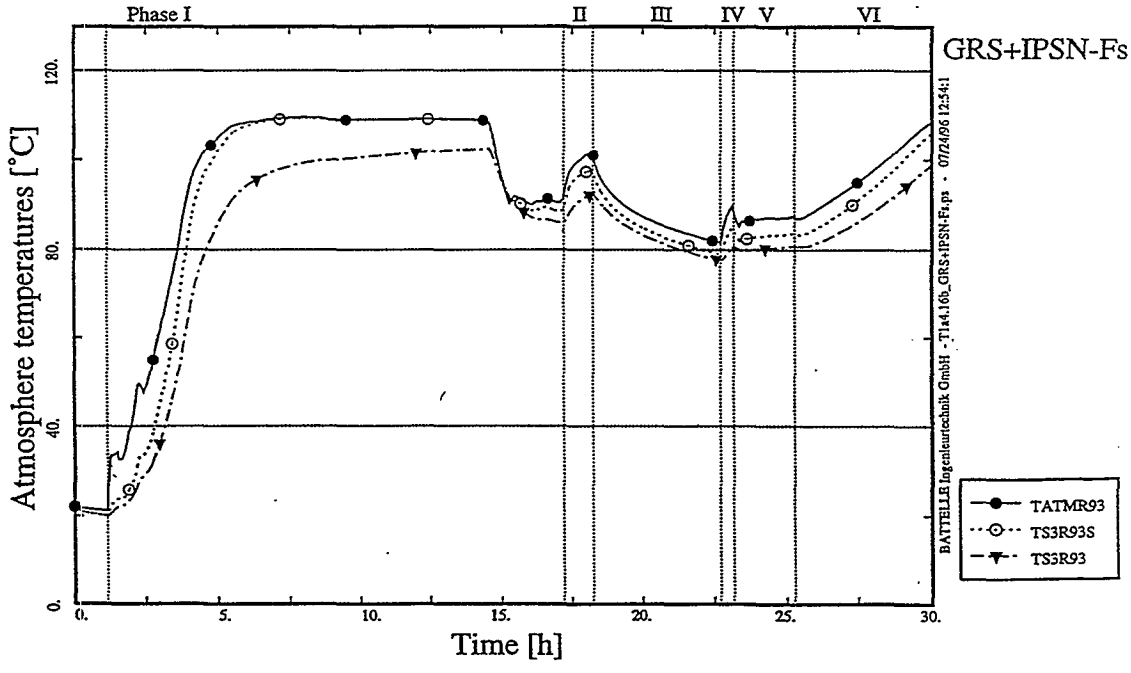

Fig. 4.16b Temperature Annulus, Structure 3 Surface and Below Surface (GRS / IPSN - Fs)

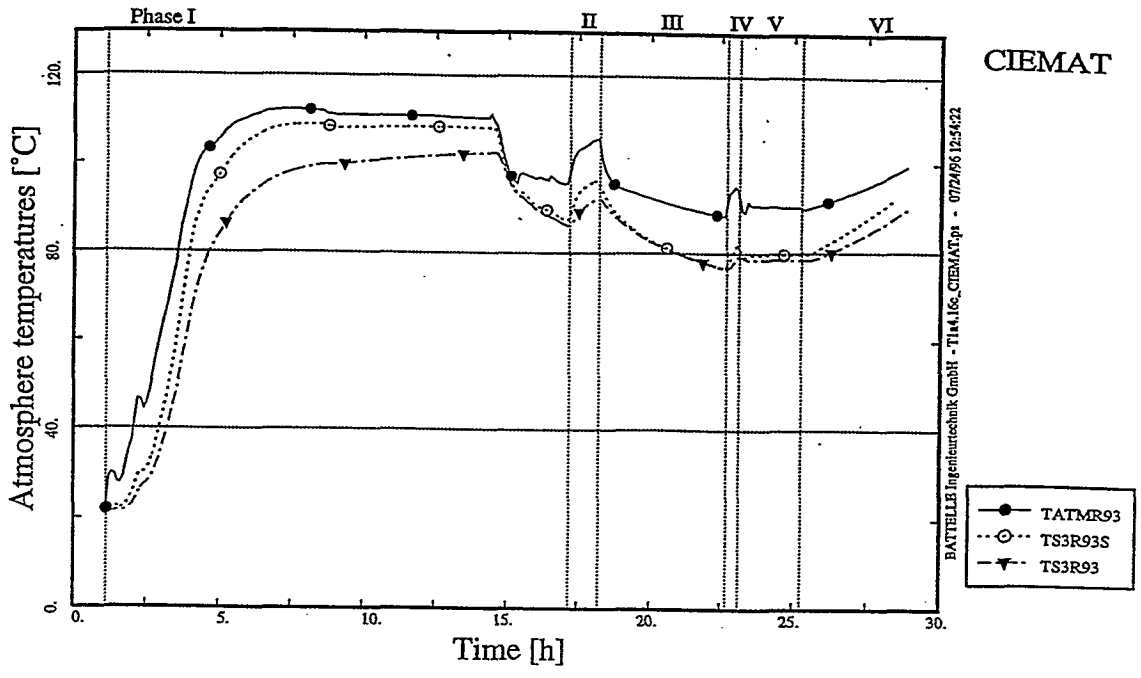

Fig. 4.16c Temperature Annulus, Structure 3 Surface and Below Surface (CIEMAT)

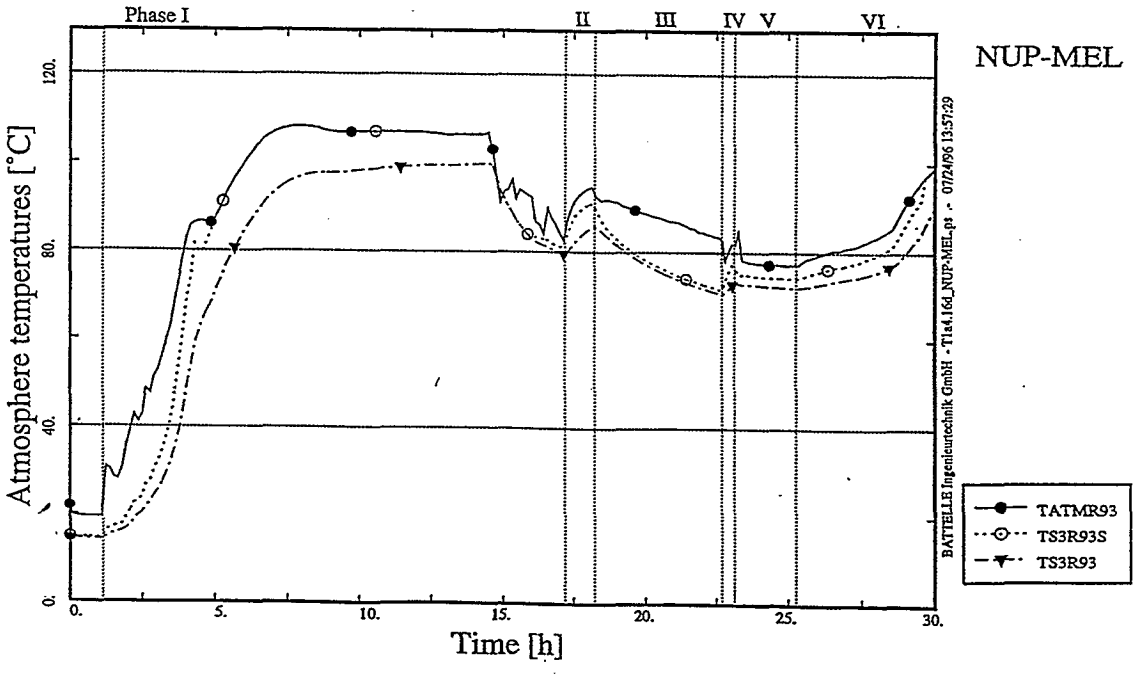

Fig. 4.16d Temperature Annulus, Structure 3 Surface and Below Surface (NUP-MEL)

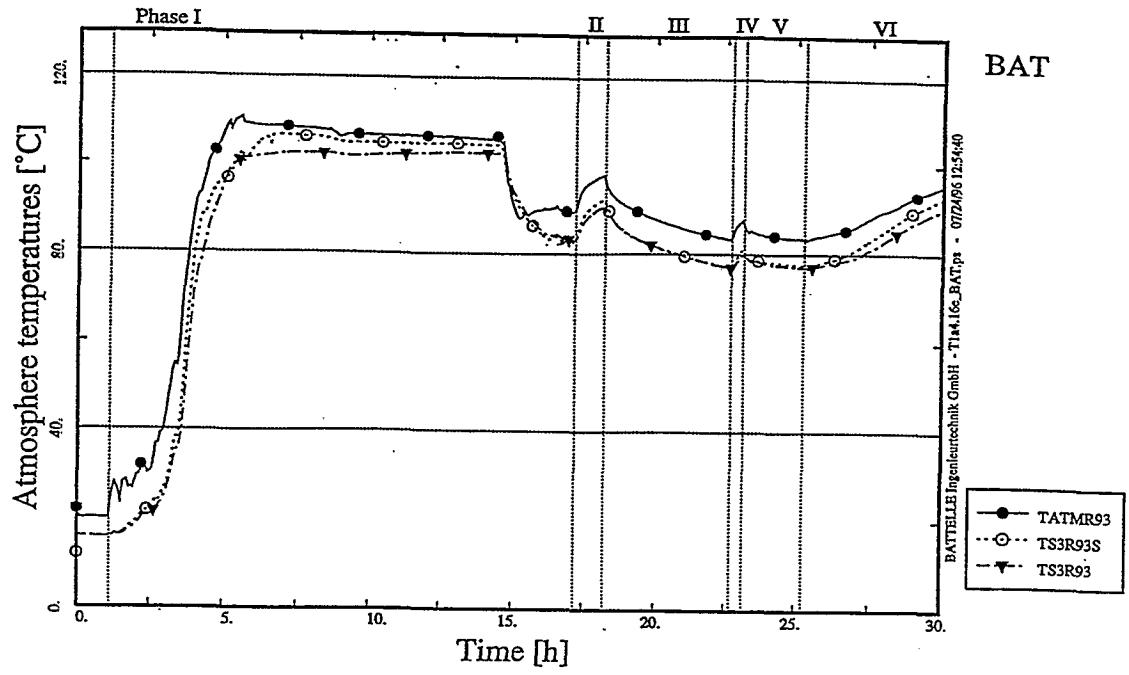

Fig. 4.16e Temperature Annulus, Structure 3 Surface and Below Surface (BAT)

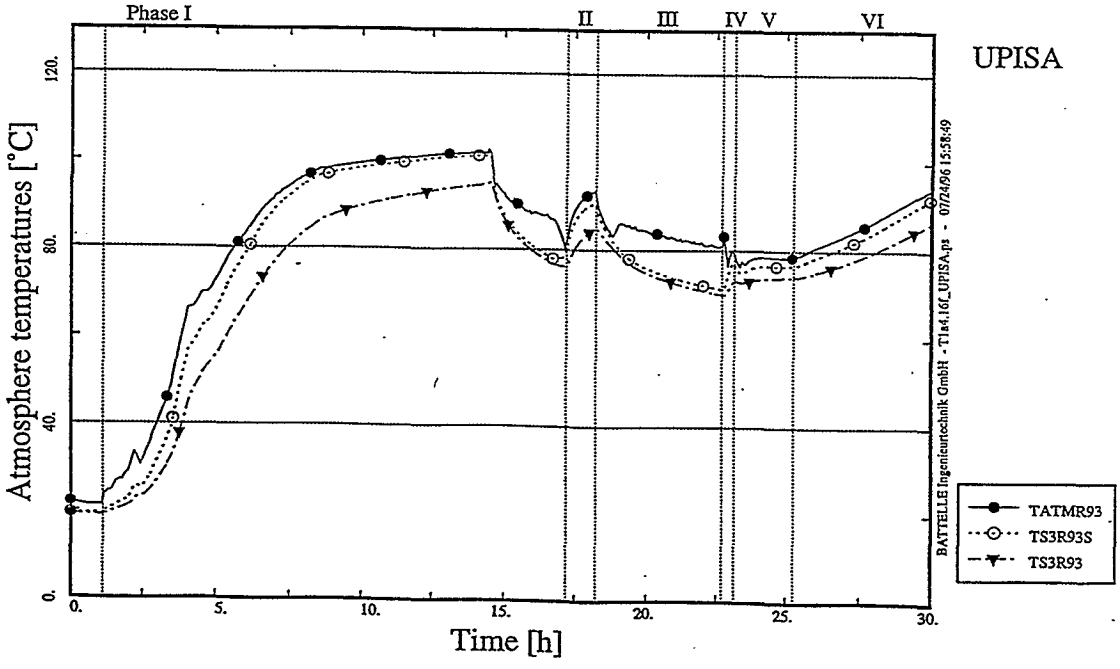

Fig. 4.16f Temperature Annulus, Structure 3 Surface and Below Surface (UPISA)

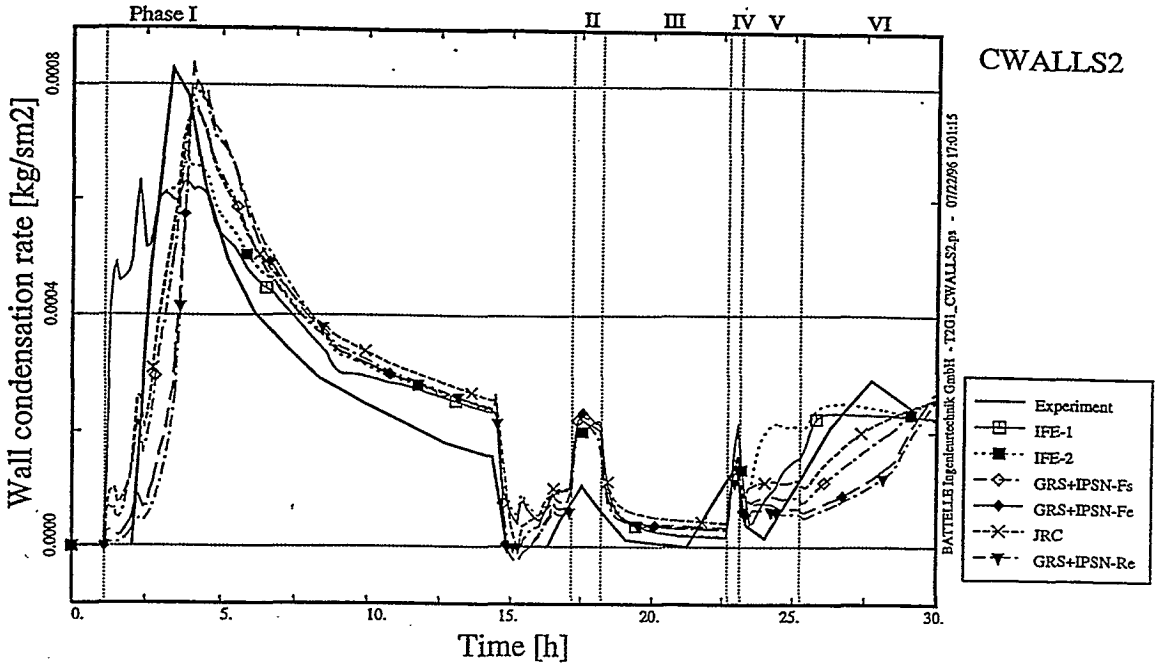

Fig. 4.17a Wall Condensation Rate (FIPLOC)

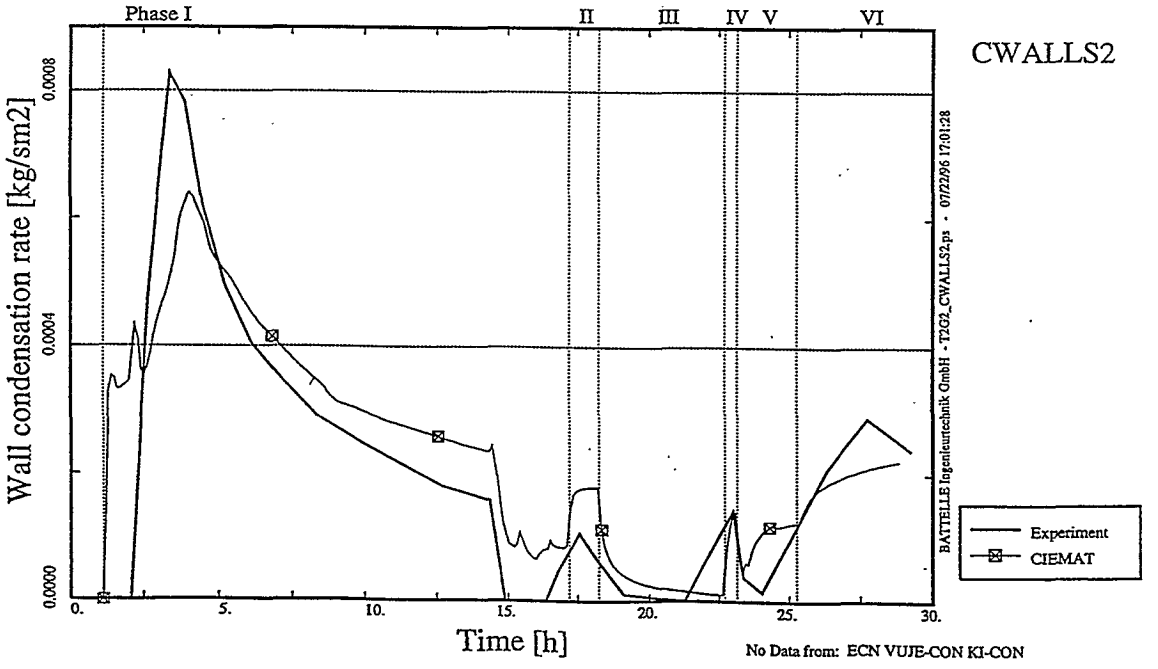

Fig. 4.17b . Wall Condensation Rate (CONTAIN)

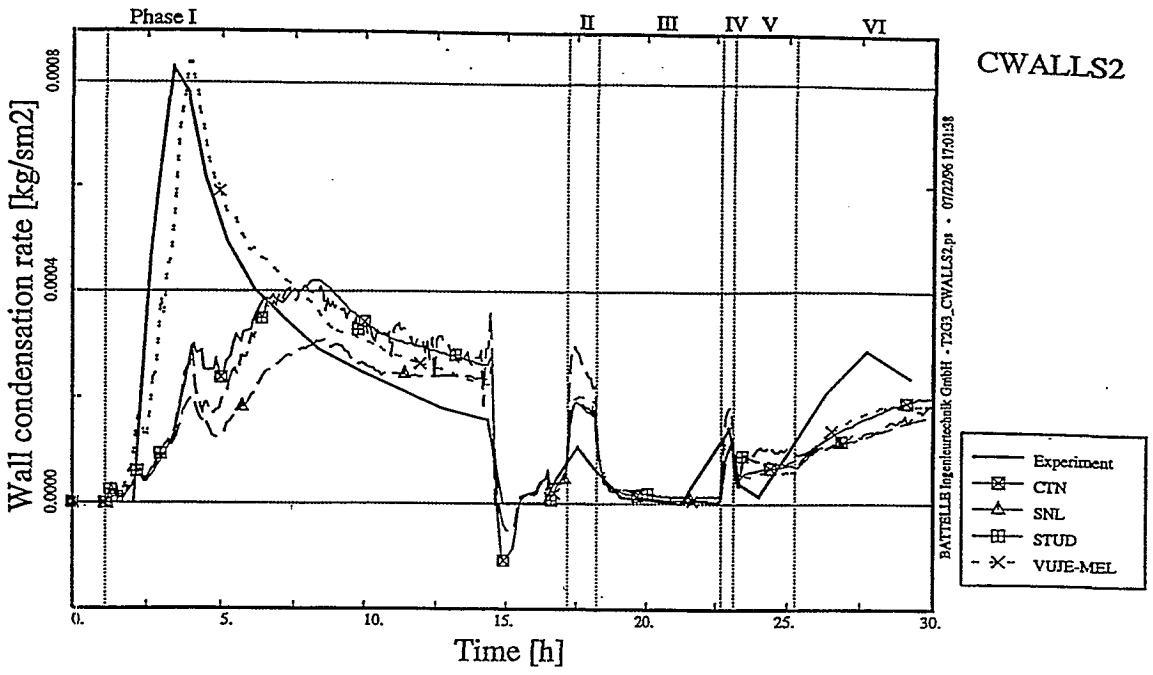

Fig. 4.17c Wall Condensation Rate (MELCOR, part I)

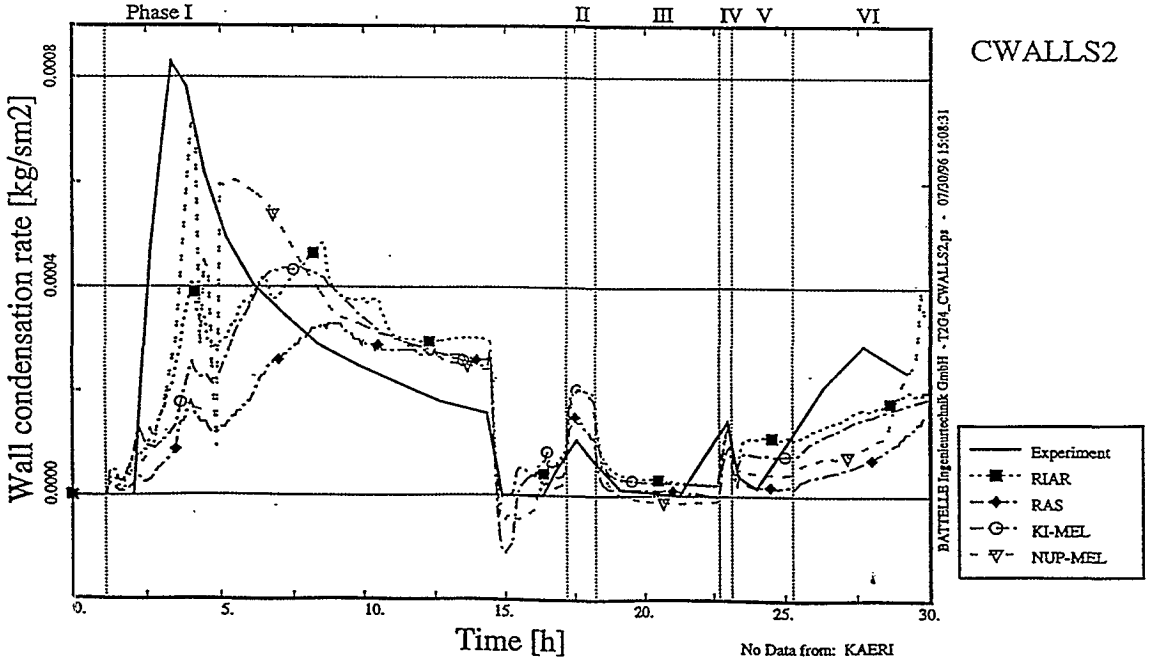

Fig. 4.17d Wall Condensation Rate (MELCOR, part II)

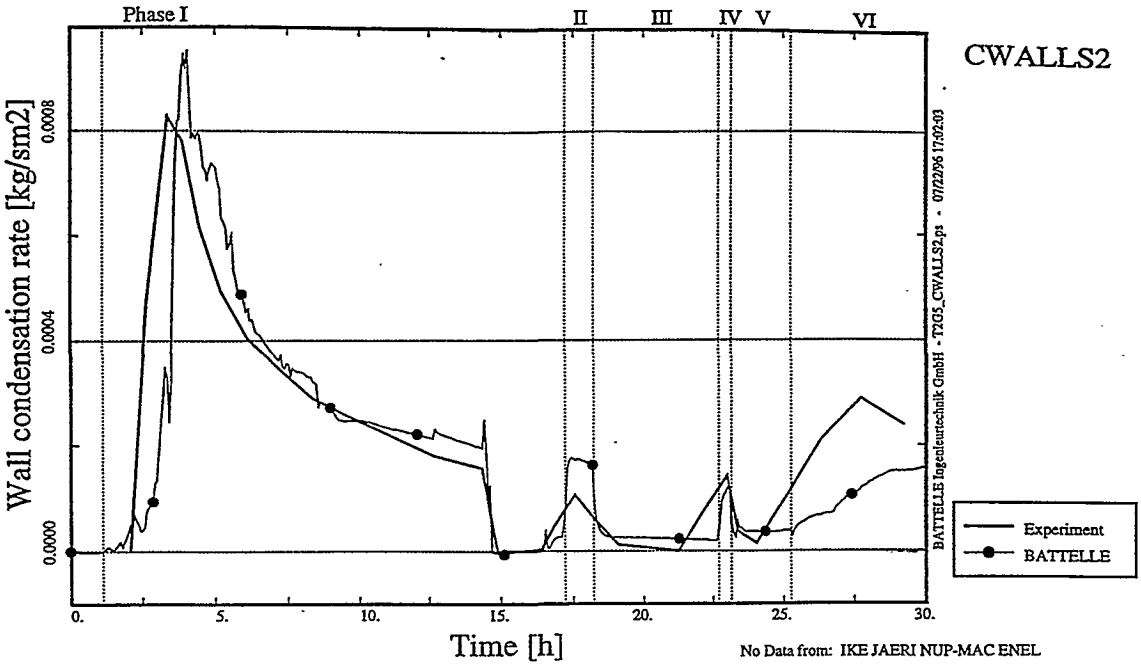

Fig. 4.17e Wall Condensation Rate (BAT)

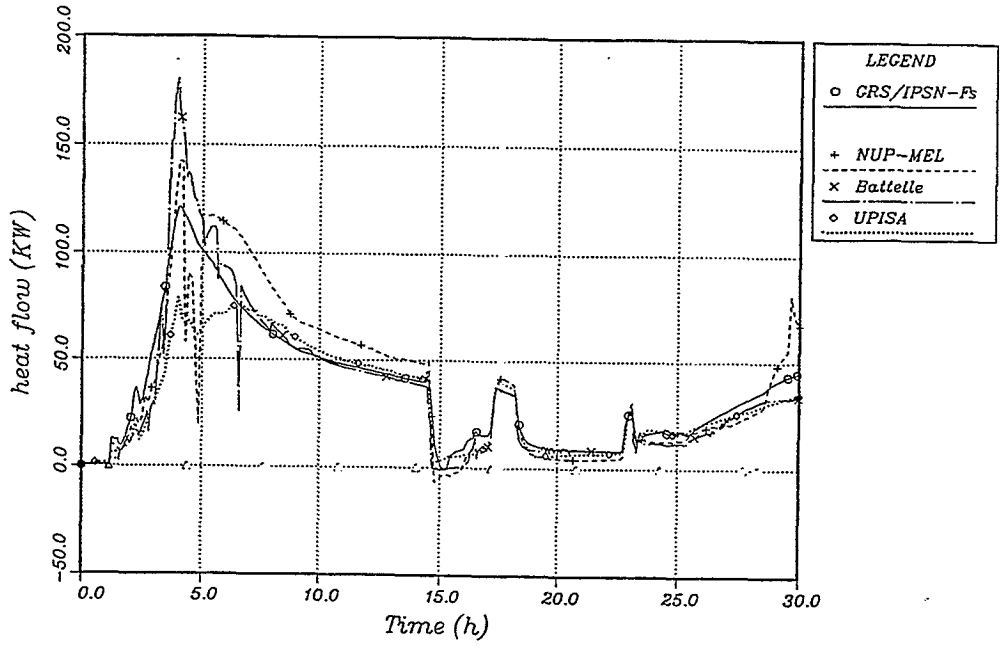

Fig. 4.18a Heat Flow (Reference Calculations)

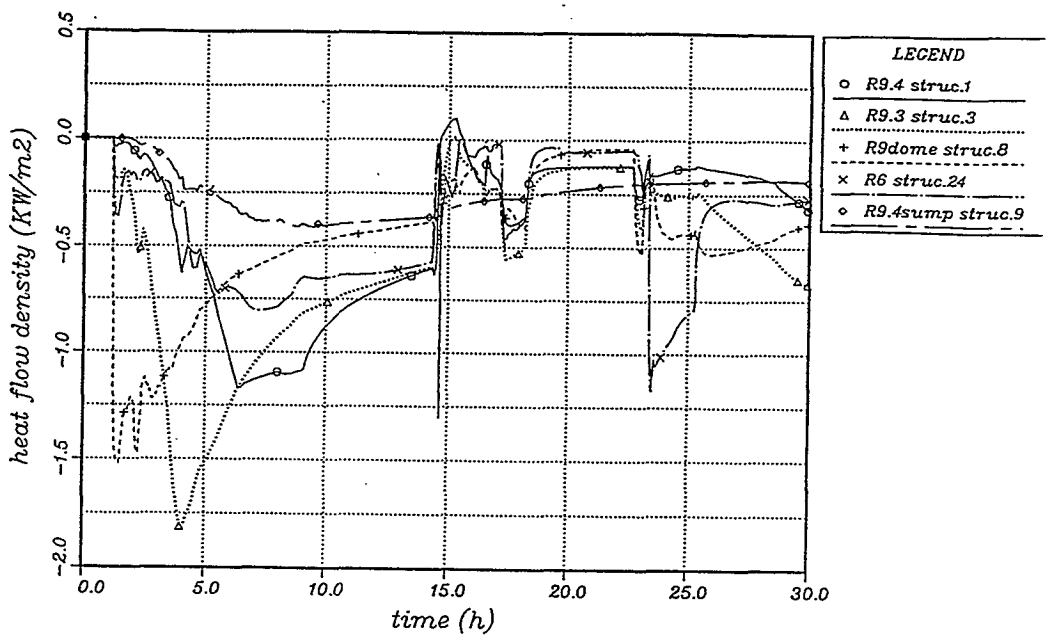

Fig. 4.18b Heat Flow Density (GRS / IPSN - Fs)

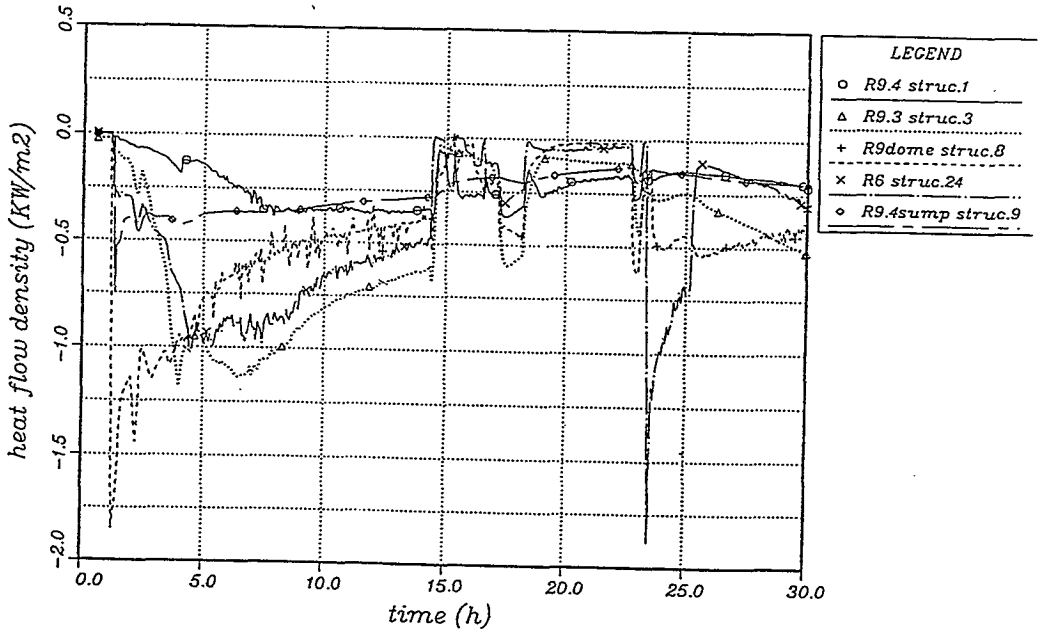

Fig. 4.18c Heat Flow Density (UPISA)

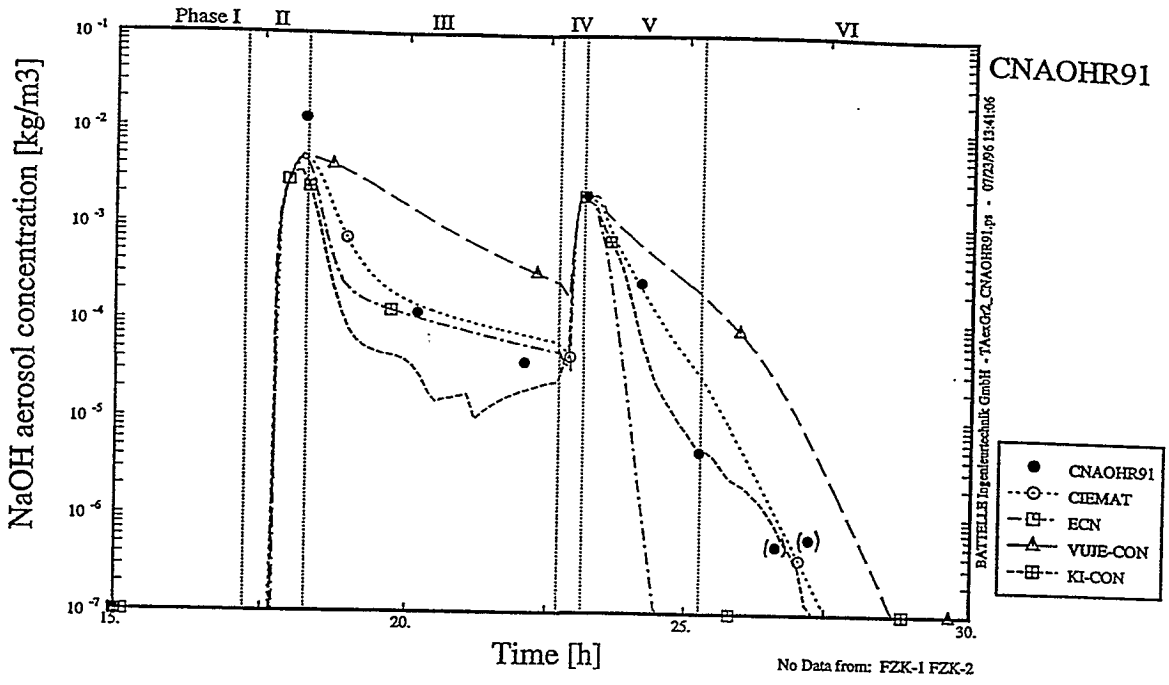

Fig. 4.19a NaOH Aerosol Concentration in the Dome (CONTAIN)

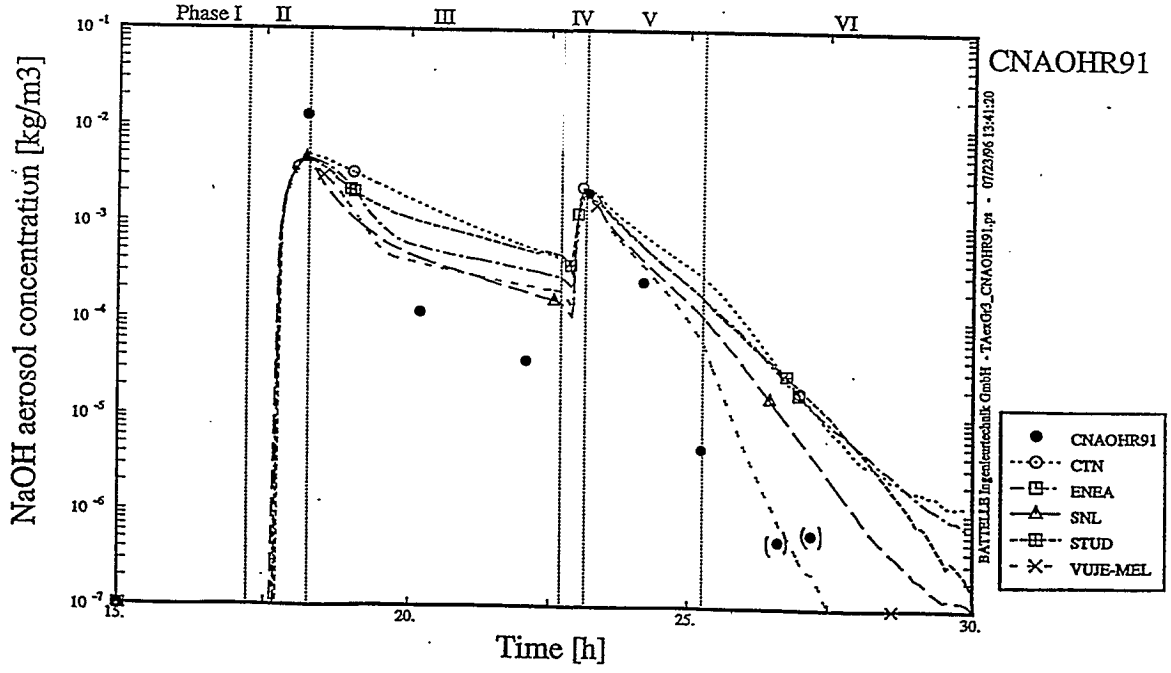

Fig. 4.19b NaOH Aerosol Concentration in the Dome (MELCOR, part I)

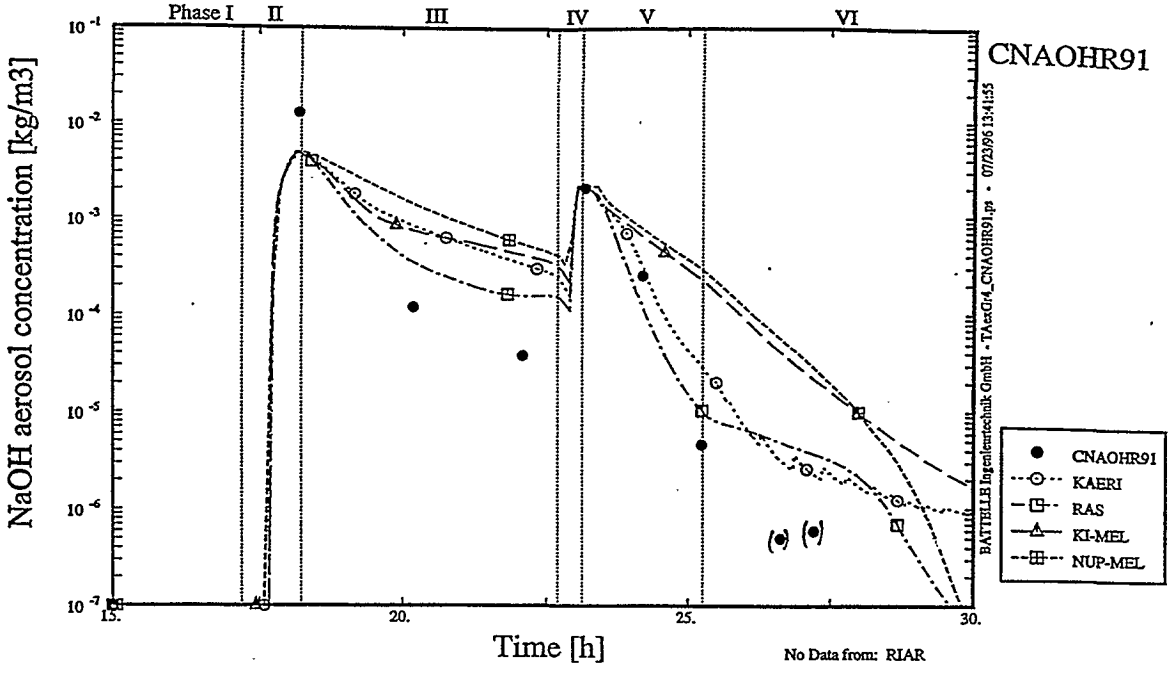

Fig. 4.19c NaOH Aerosol Concentration in the Dome (MELCOR, part II)

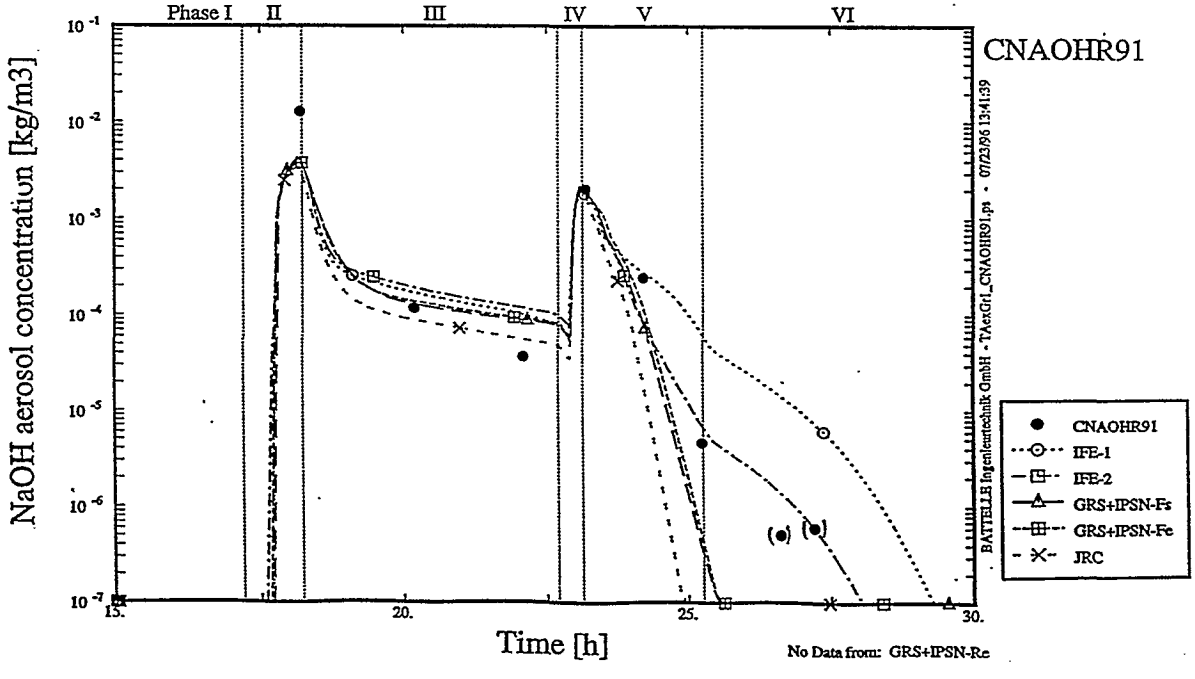

Fig. 4.19d NaOH Aerosol Concentration in the Dome (FIPLOC)

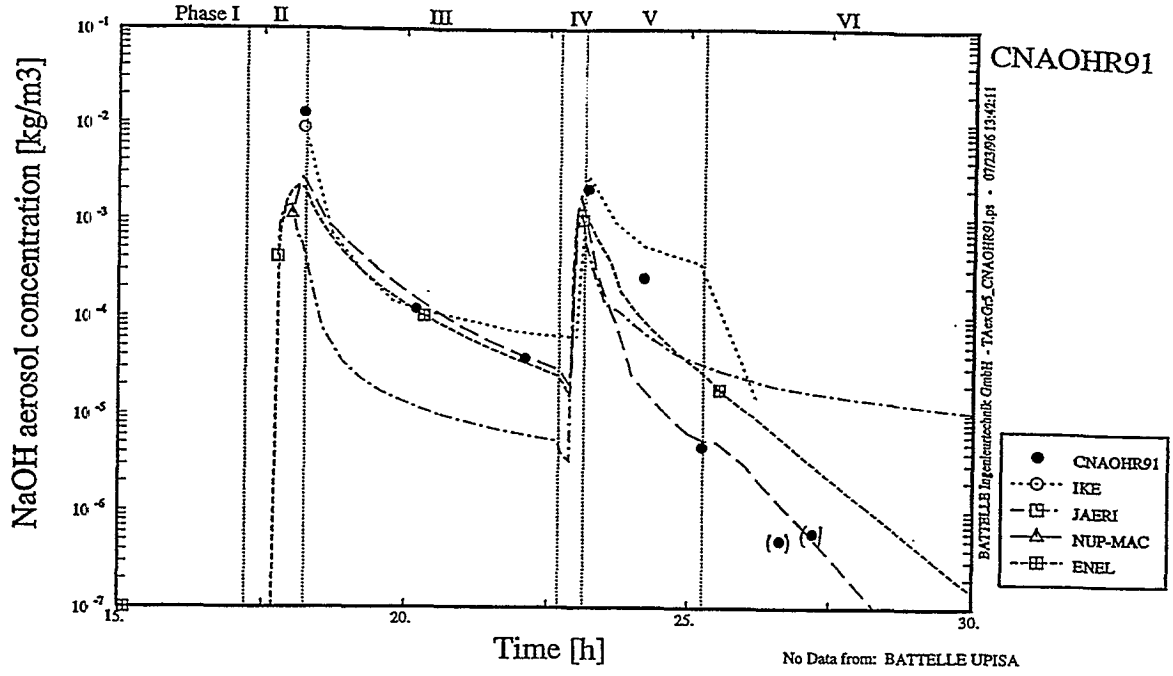

Fig. 4.19e NaOH Aerosol Concentration in the Dome (Stand Alone Codes and ECART)

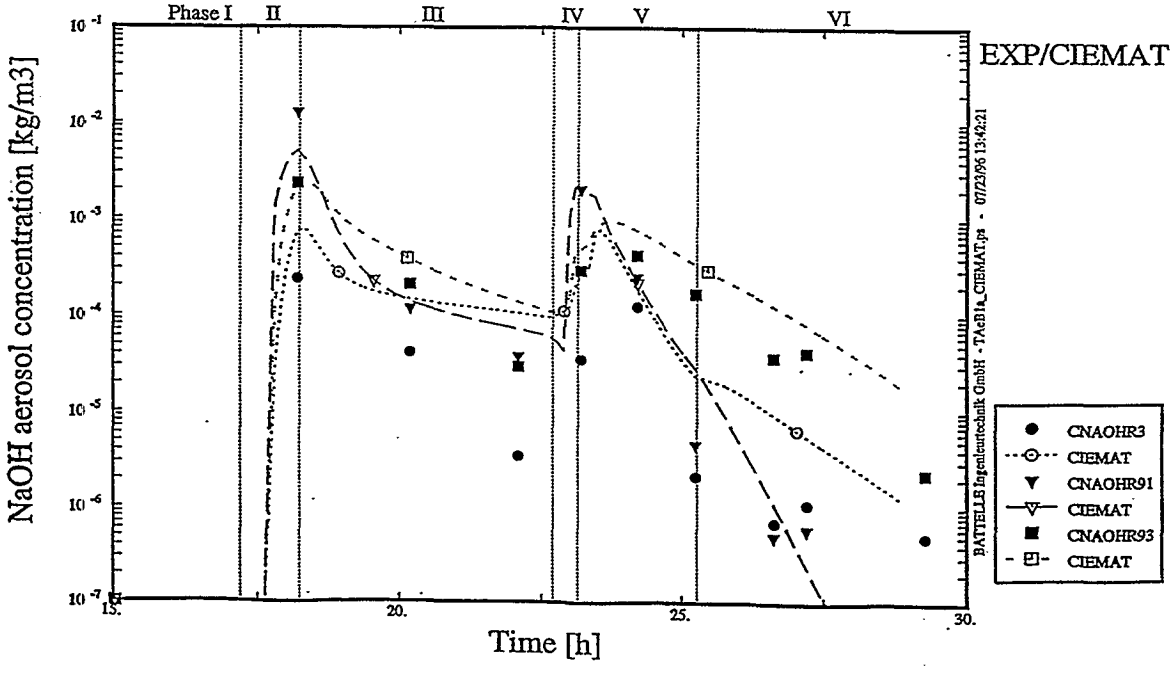

Fig. 4.20a NaOH Aerosol Concentration in Dome, Annulus, R3 (CIEMAT)

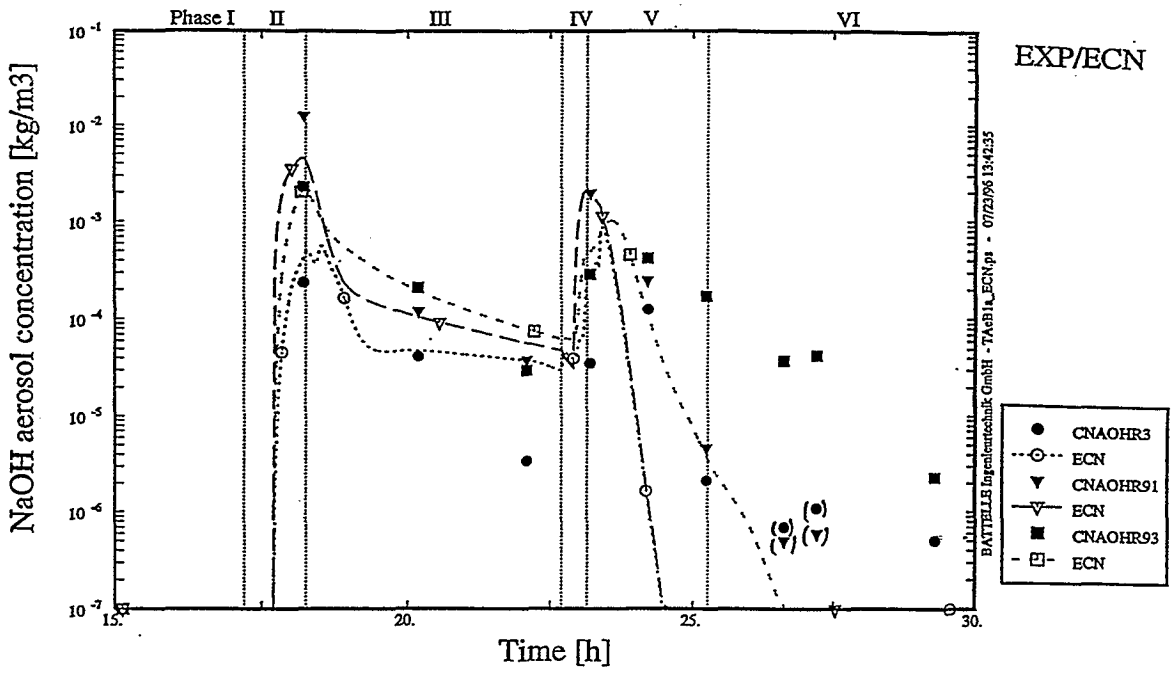

Fig. 4.20b NaOH Aerosol Concentration in Dome, Annulus, R3 (ECN)

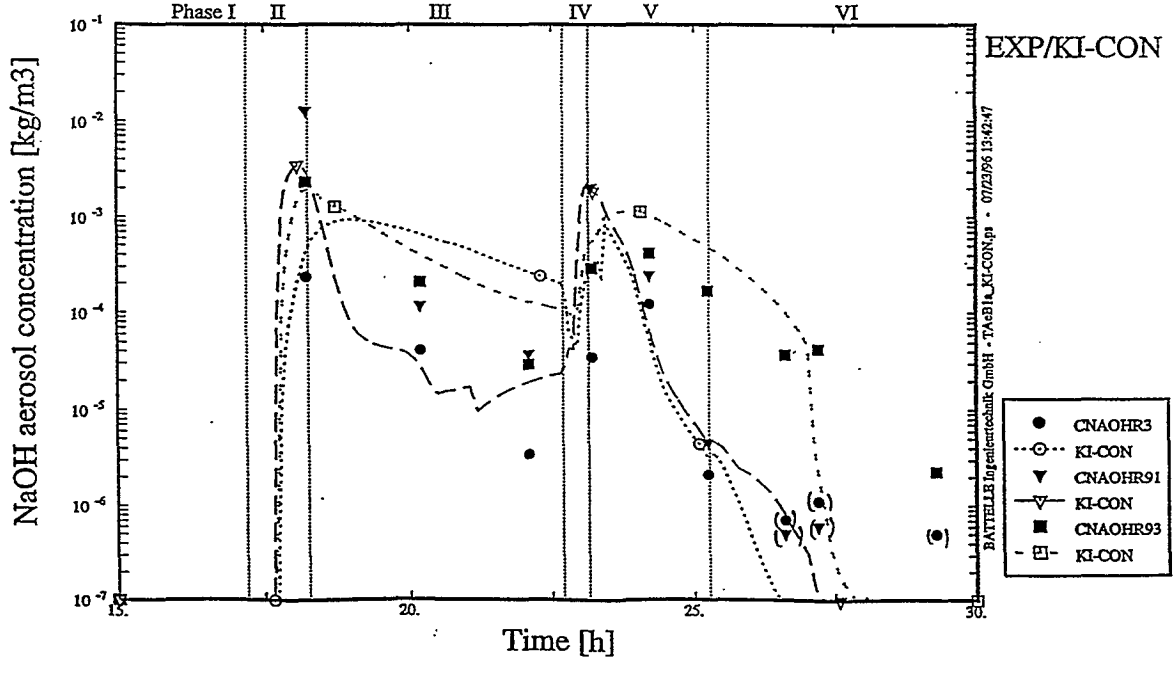

Fig. 4.20c NaOH Aerosol Concentration in Dome, Annulus, R3 (KI-CON)

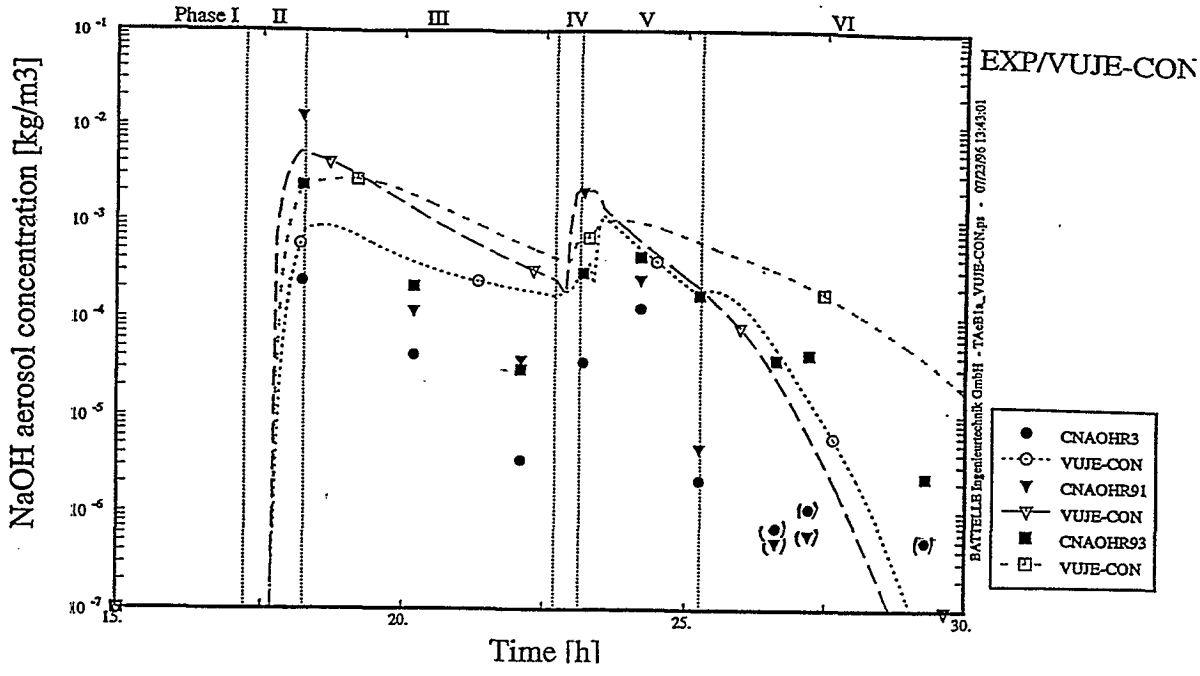

Fig. 4.20d NaOH Aerosol Concentration in Dome, Annulus, R3 (VUJE - CON)

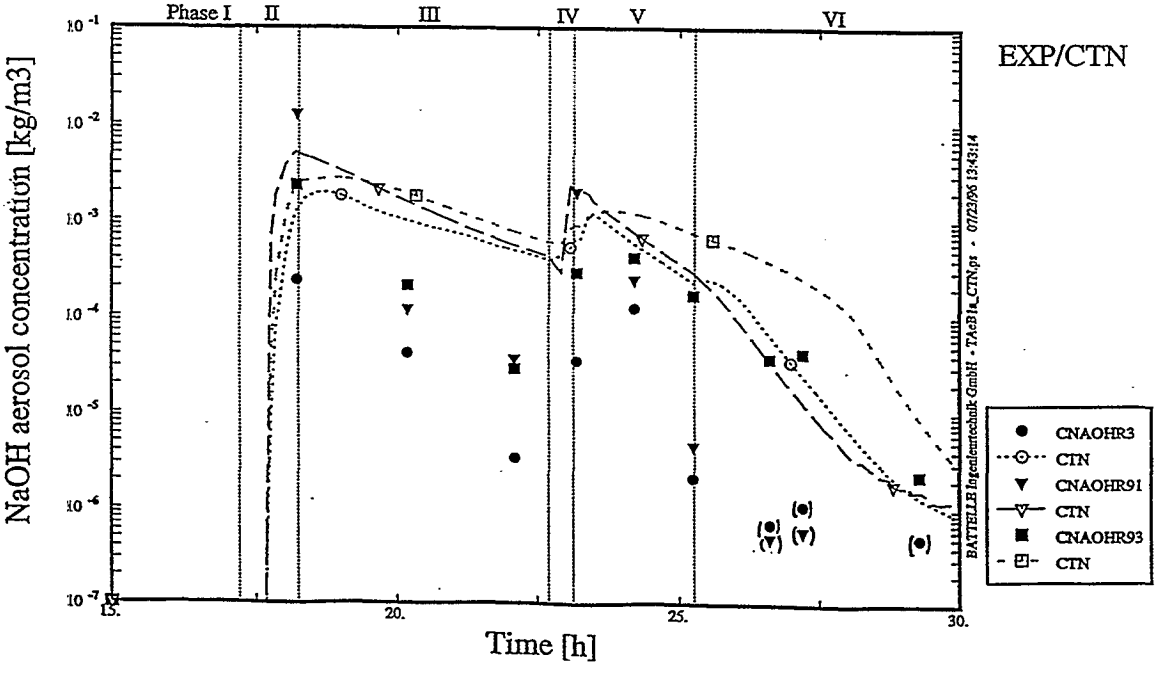

Fig. 4.20e NaOH Aerosol Concentration in Dome, Annulus, R3 (CTN)

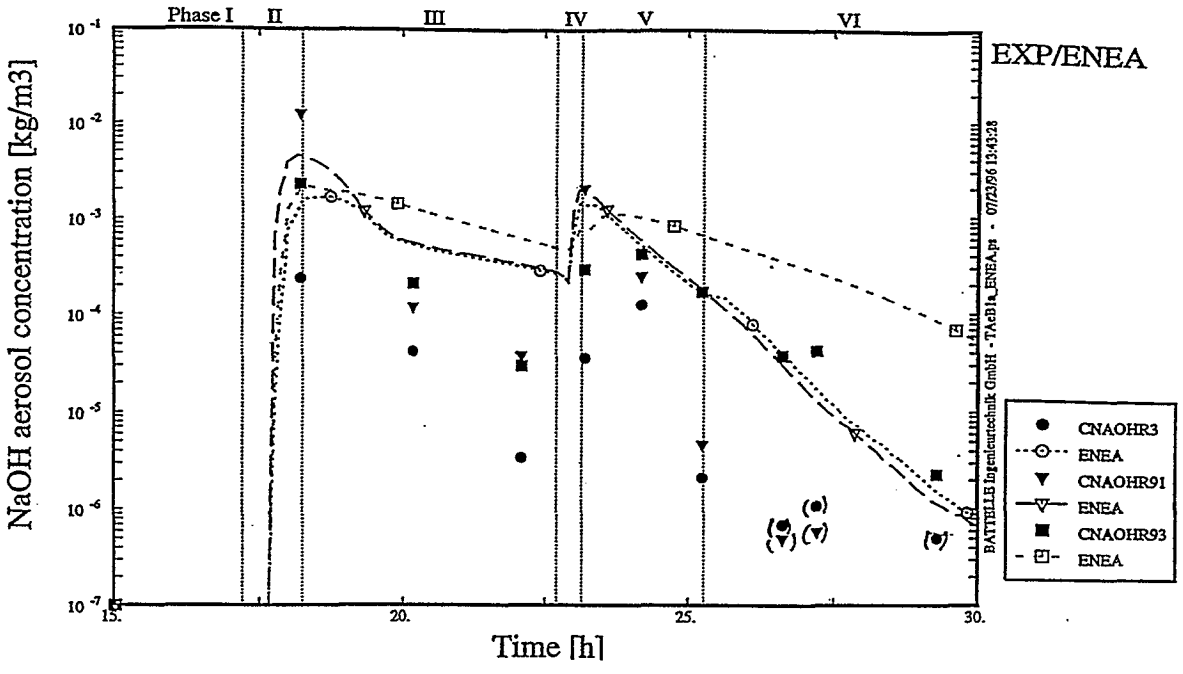

Fig. 4.20f NaOH Aerosol Concentration in Dome, Annulus, R3 (ENEA)

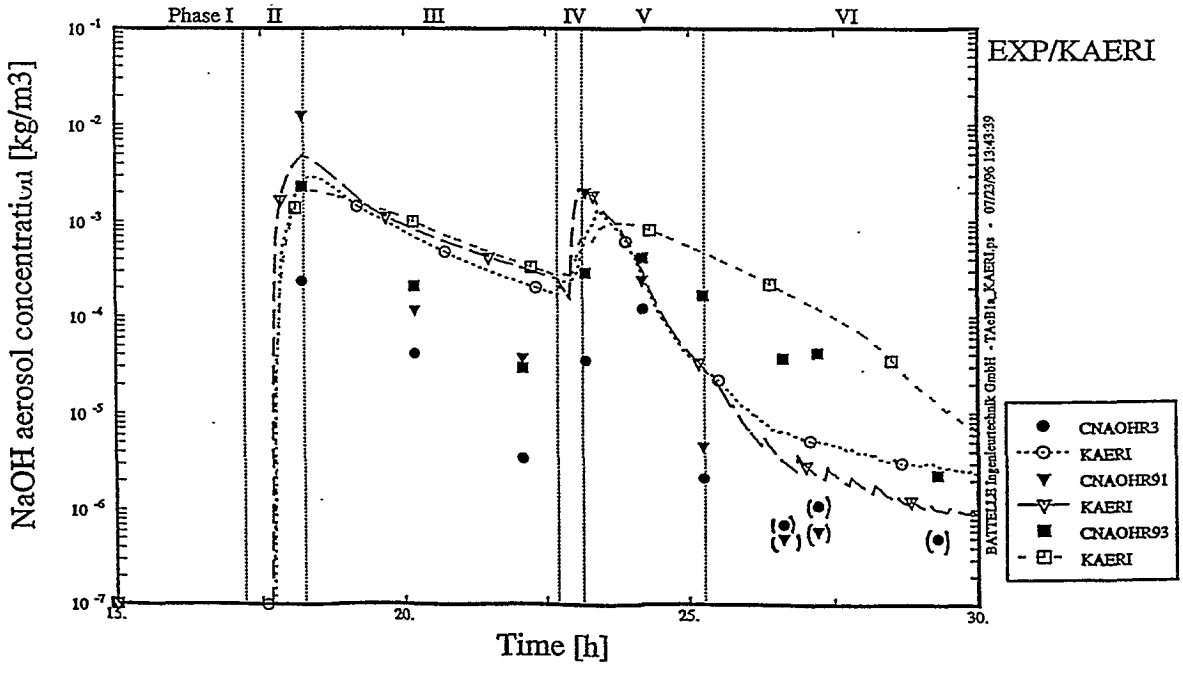

Fig. 4.20g NaOH Aerosol Concentration in Dome, Annulus, R3 (KAERI)

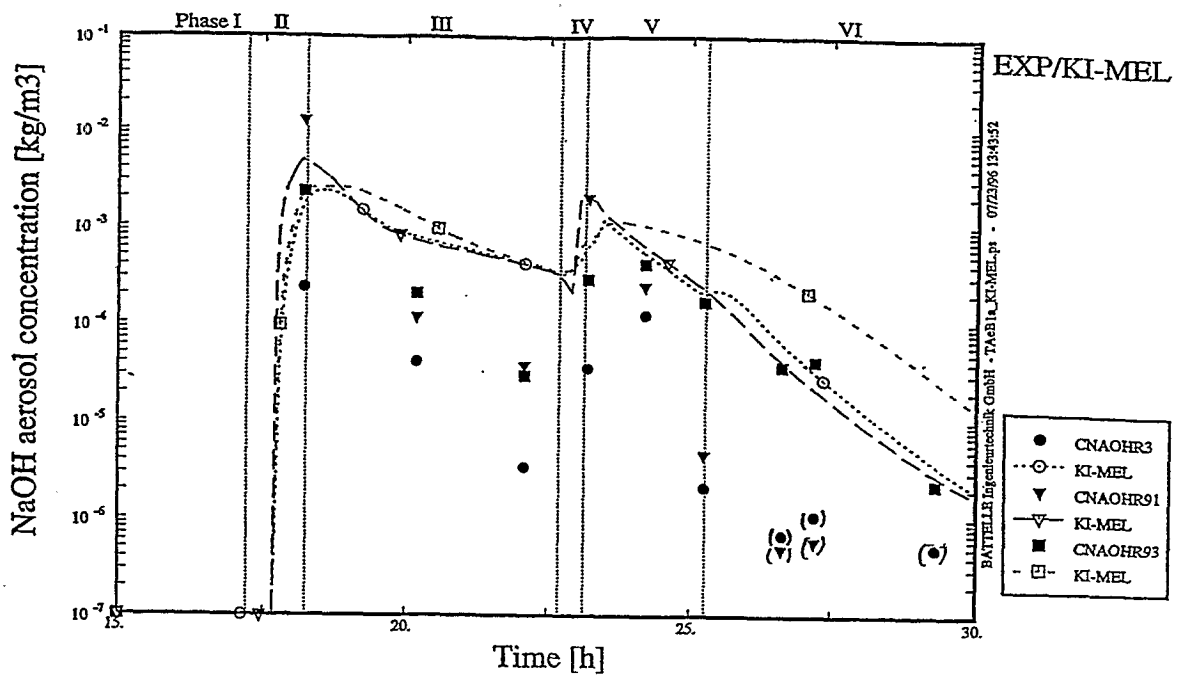

Fig. 4.20h NaOH Aerosol Concentration in Dome, Annulus, R3 (KI-MEL)

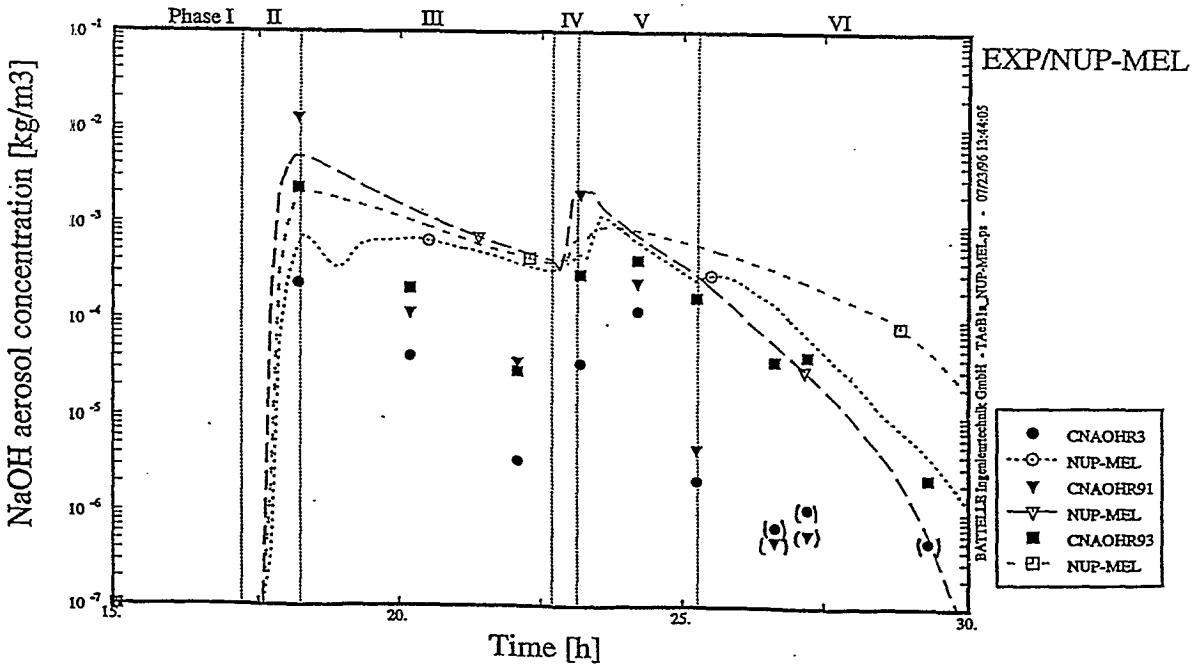

Fig. 4.20i NaOH Aerosol Concentration in Dome, Annulus, R3 (NUP-MEL)

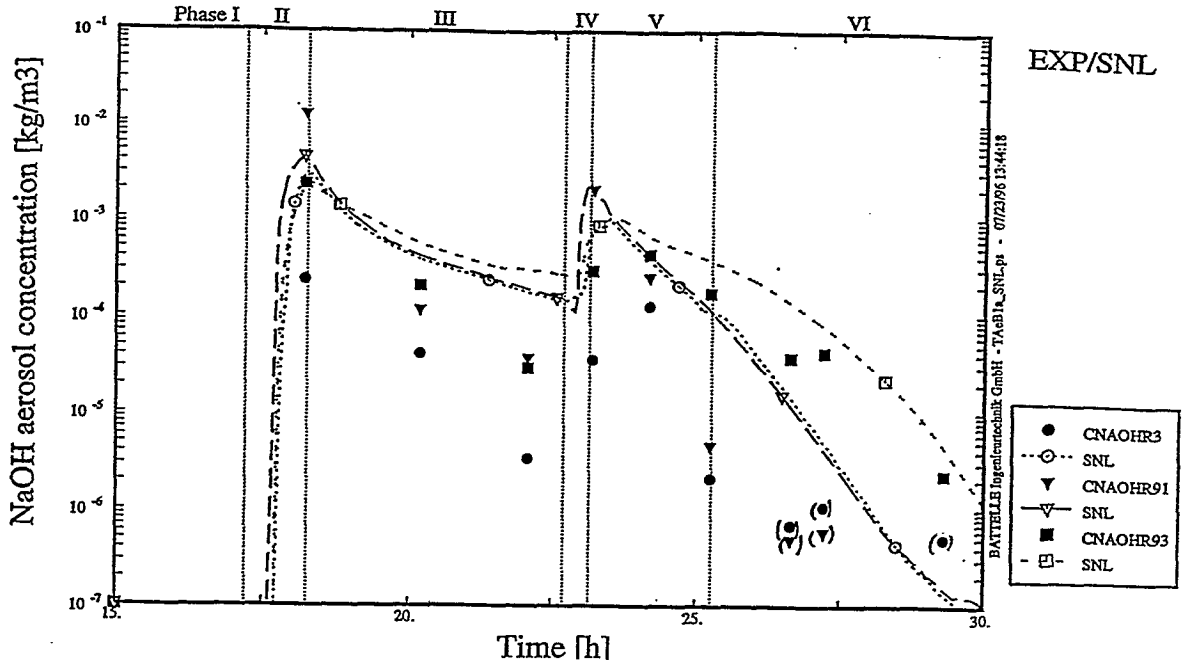

Fig. 4.20k NaOH Aerosol Concentration in Dome, Annulus, R3 (SNL)

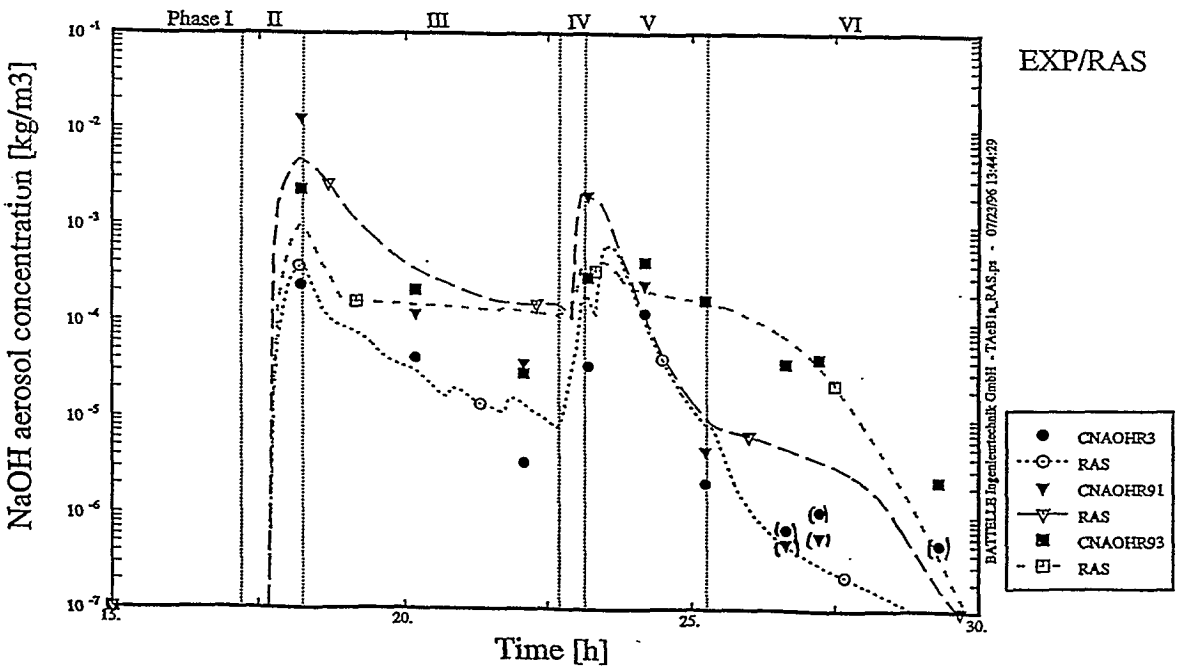

Fig. 4.20j NaOH Aerosol Concentration in Dome, Annulus, R3 (RAS)

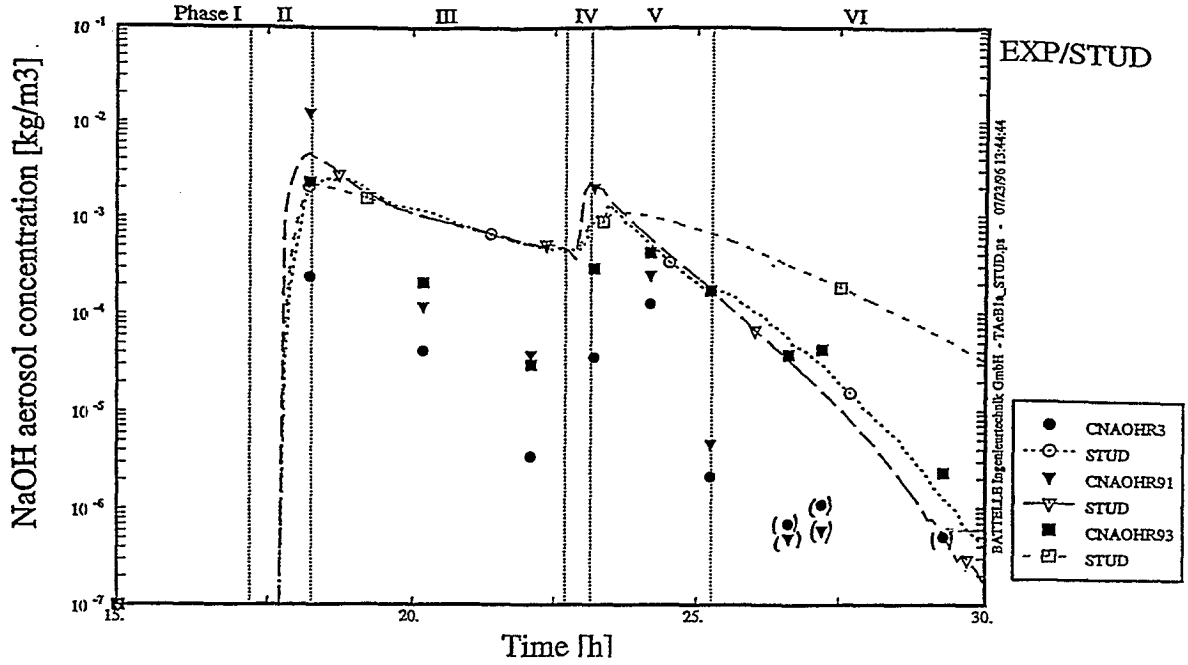

Fig. 4.20l NaOH Aerosol Concentration in Dome, Annulus, R3 (STUD)

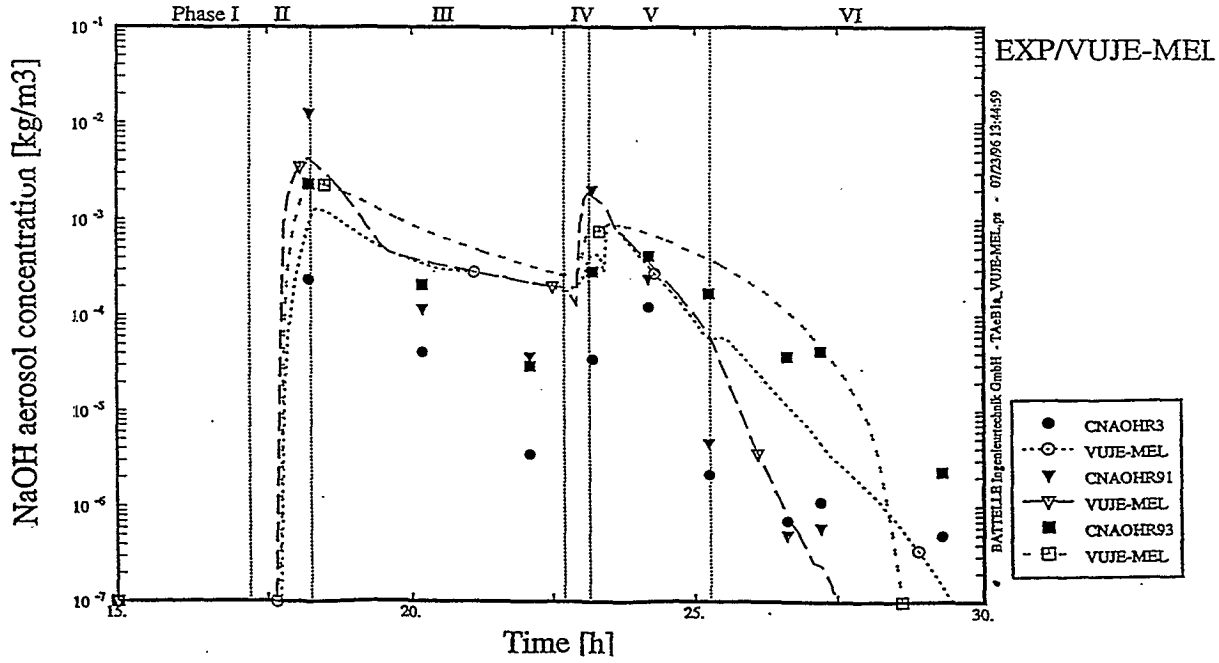

Fig. 4.20m NaOH Aerosol Concentration in Dome, Annulus, R3 (VUJE-MEL)

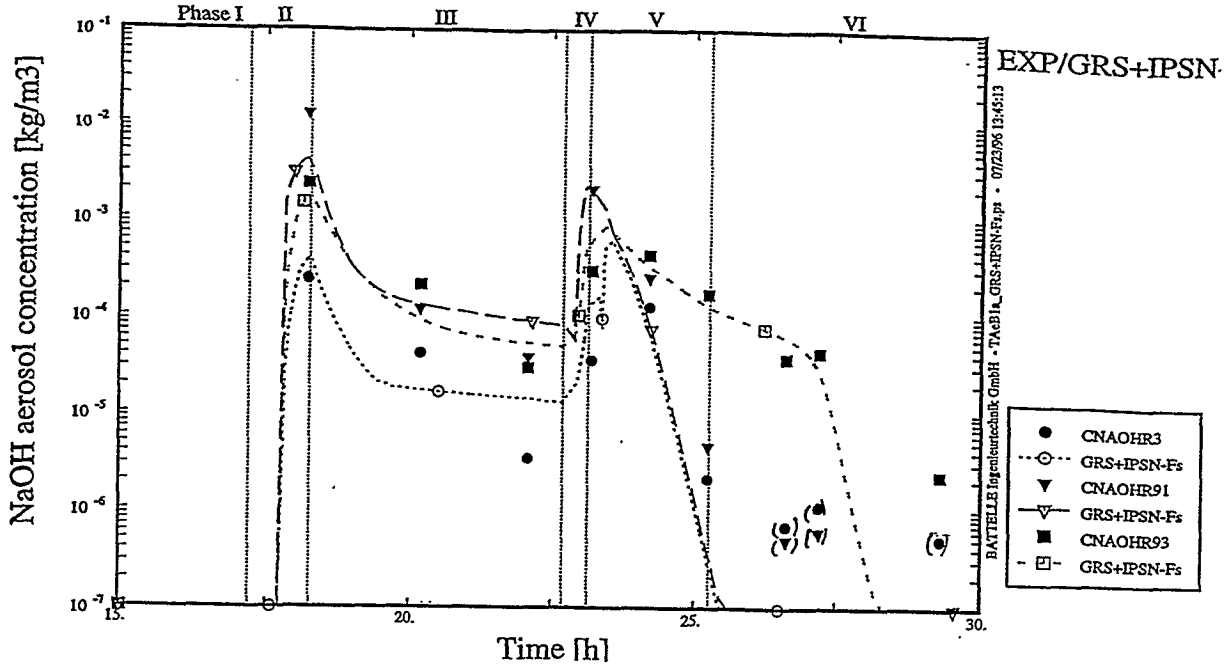

Fig. 4.20n NaOH Aerosol Concentration in Dome, Annulus, R3 (GRS / IPSN - Fs)

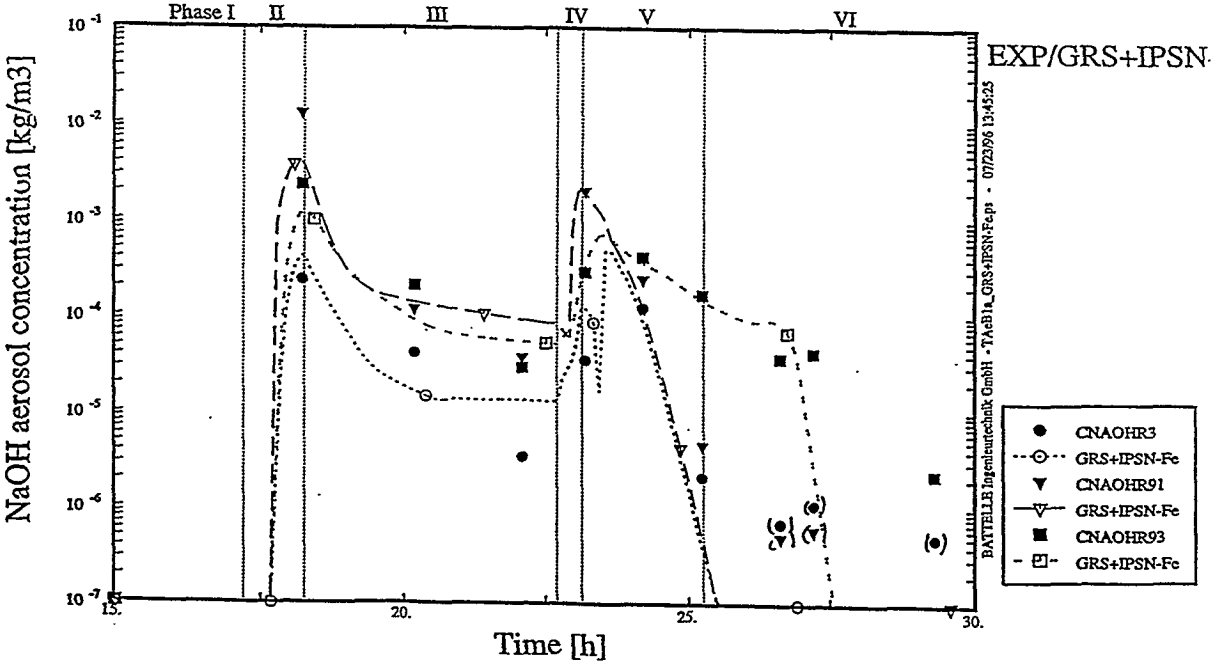

Fig. 4.20o NaOH Aerosol Concentration in Dome, Annulus, R3 (GRS / IPSN - Fe)

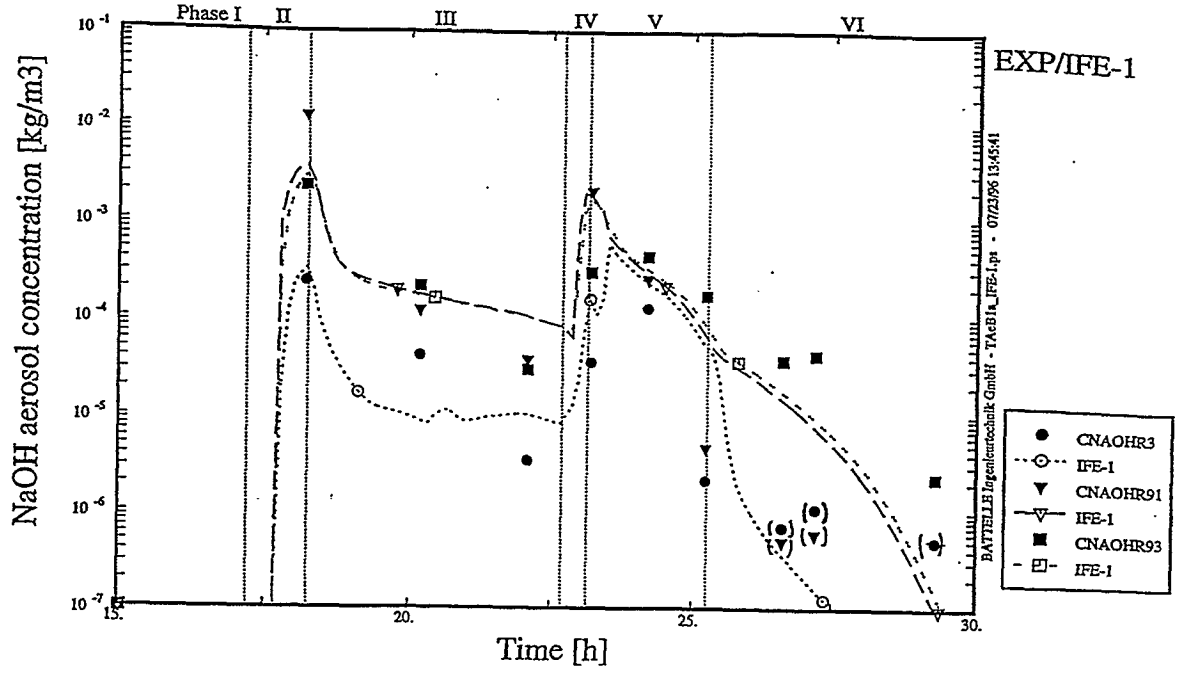

Fig. 4.20p NaOH Aerosol Concentration in Dome, Annulus, R3 (IFE-1)

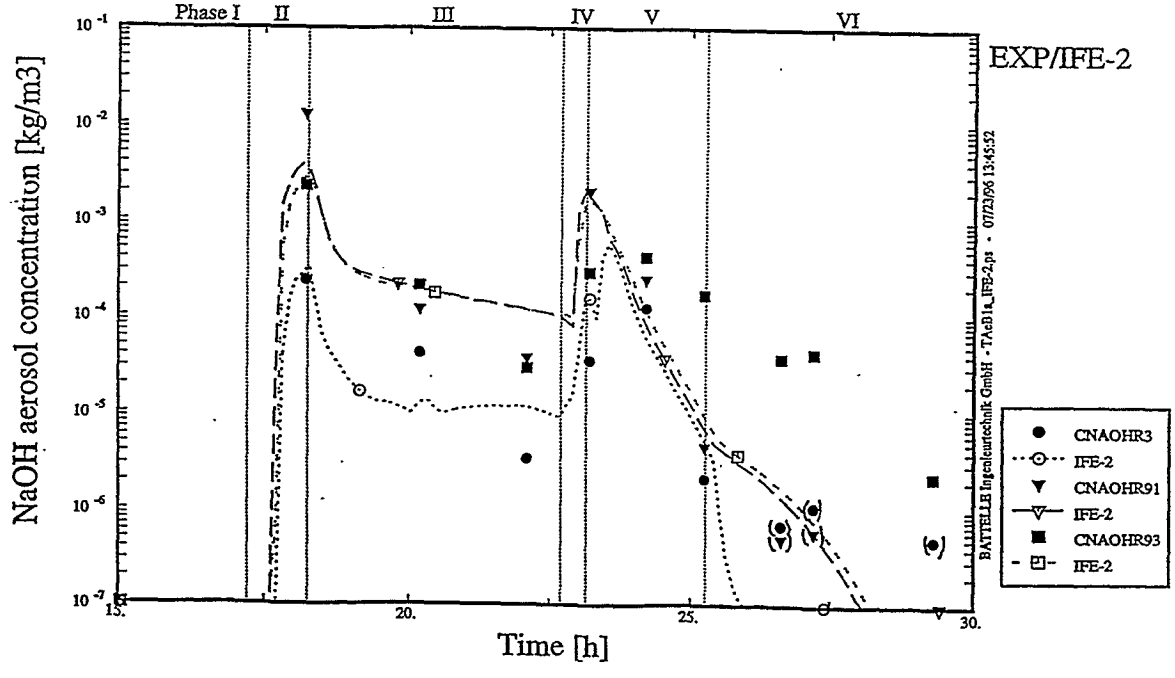

Fig. 4.20q NaOH Aerosol Concentration in Dome, Annulus, R3 (IFE-2)

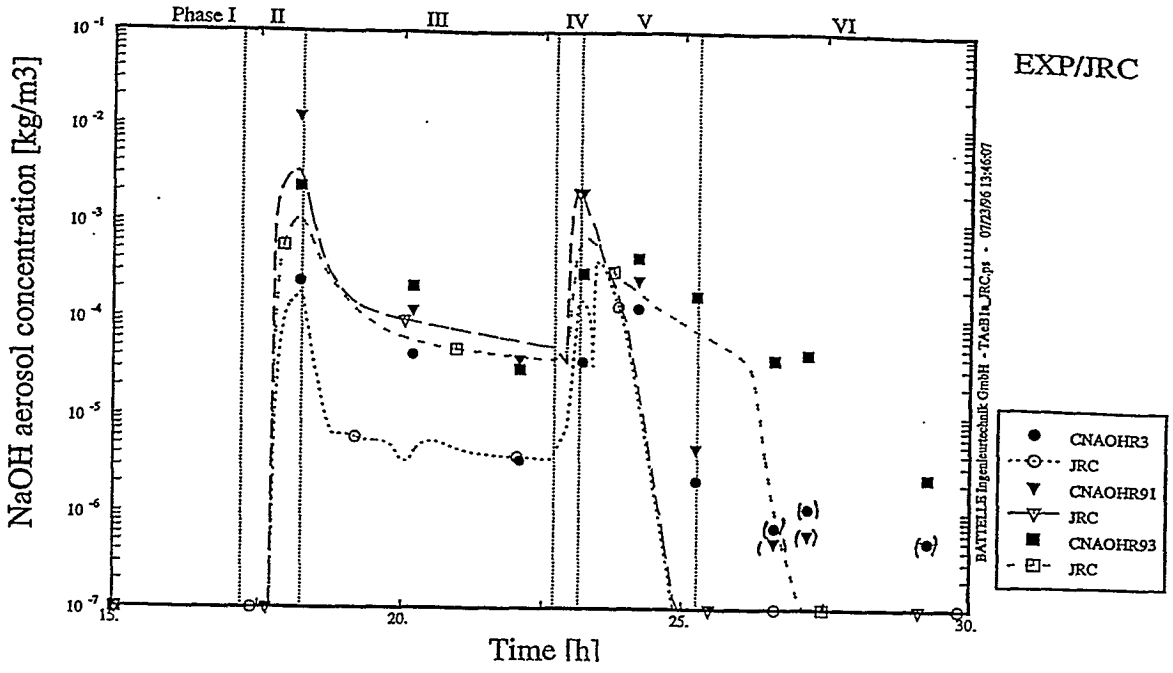

Fig. 4.20r NaOH Aerosol Concentration in Dome, Annulus, R3 (JRC)

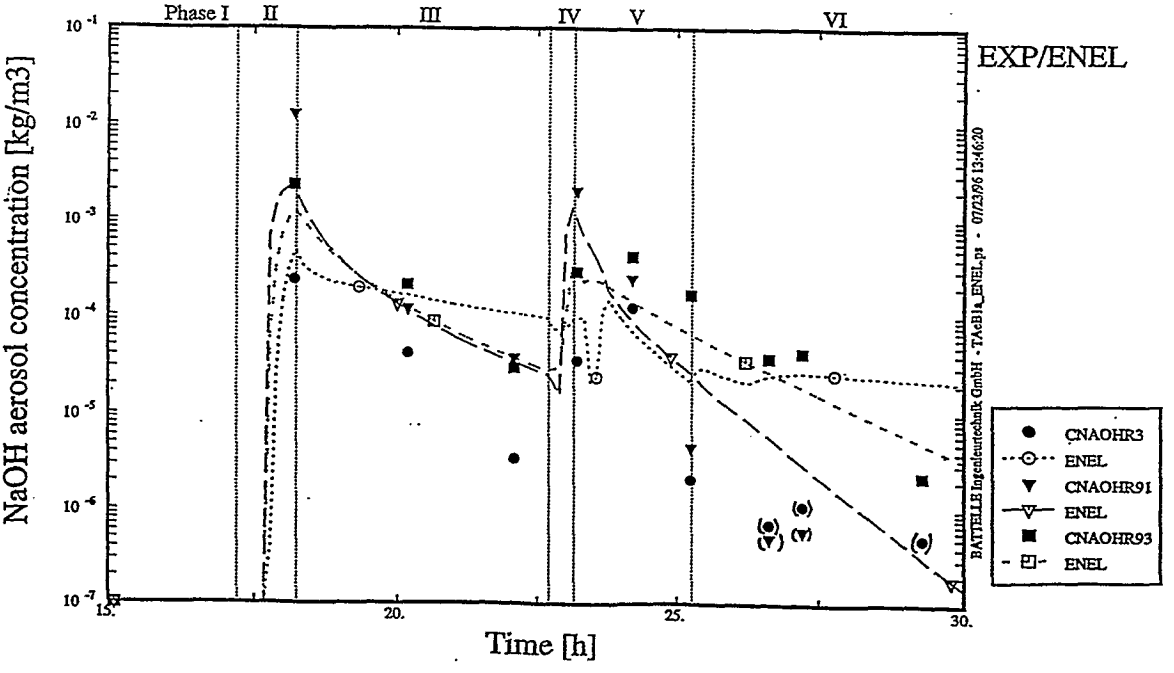

Fig. 4.20s NaOH Aerosol Concentration in Dome, Annulus, R3 (ENEL)

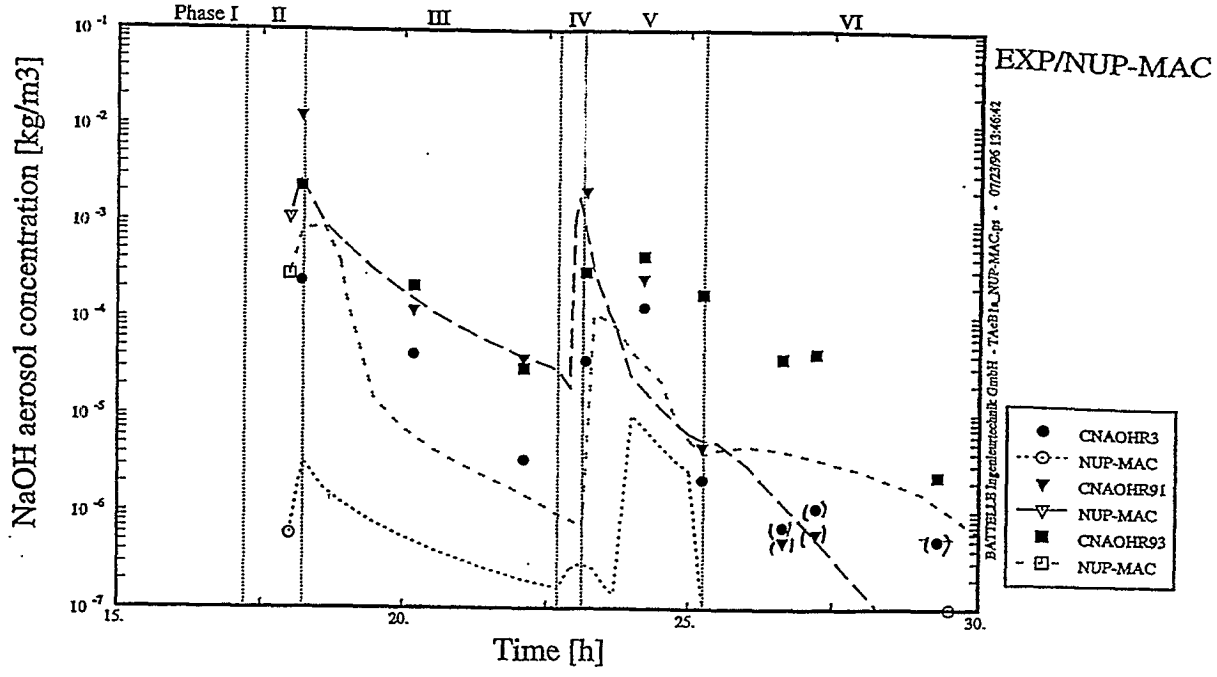

Fig. 4.20t NaOH Aerosol Concentration in Dome, Annulus, R3 (NUP-MAC)

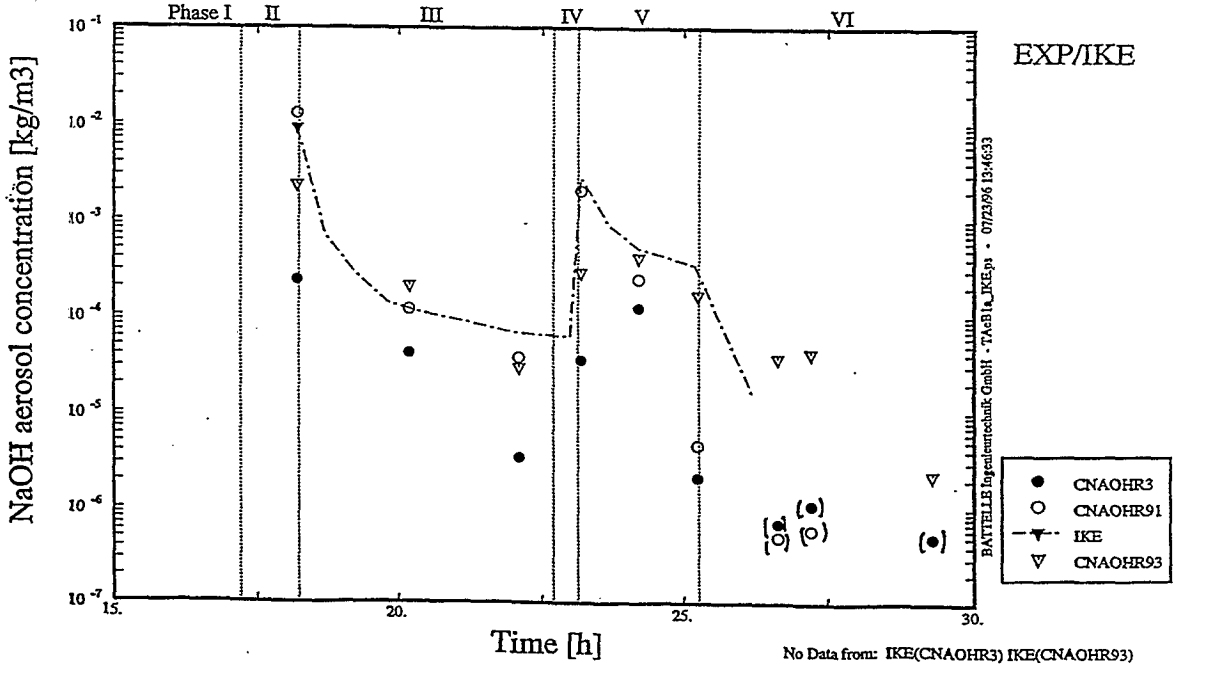

Fig. 4.20u NaOH Aerosol Concentration in Dome, Annulus, R3 (IKE)

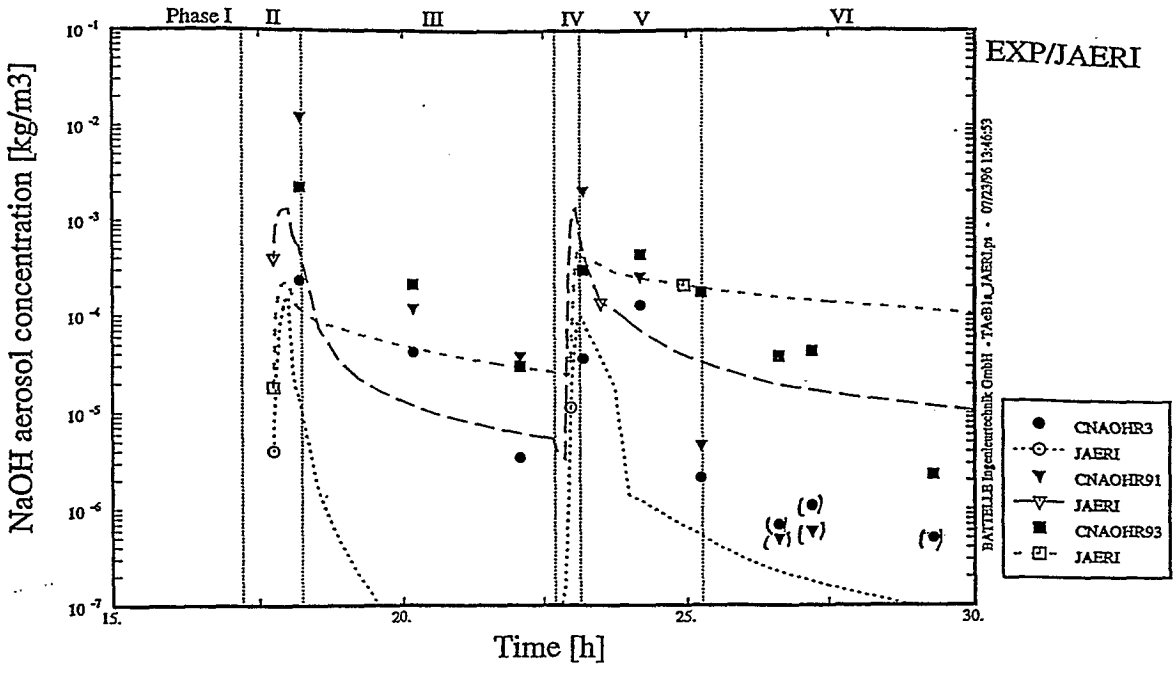

Fig. 4.20v NaOH Aerosol Concentration in Dome, Annulus, R3 (JAERI)

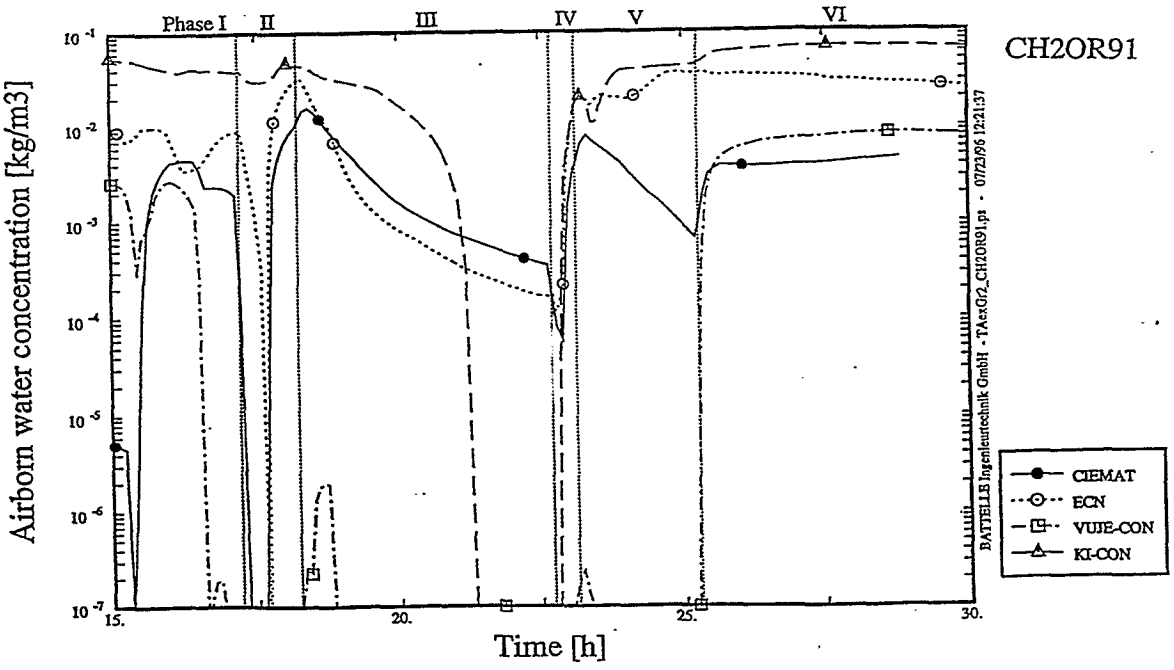

Fig. 4.21a Airborne Water (CONTAIN)

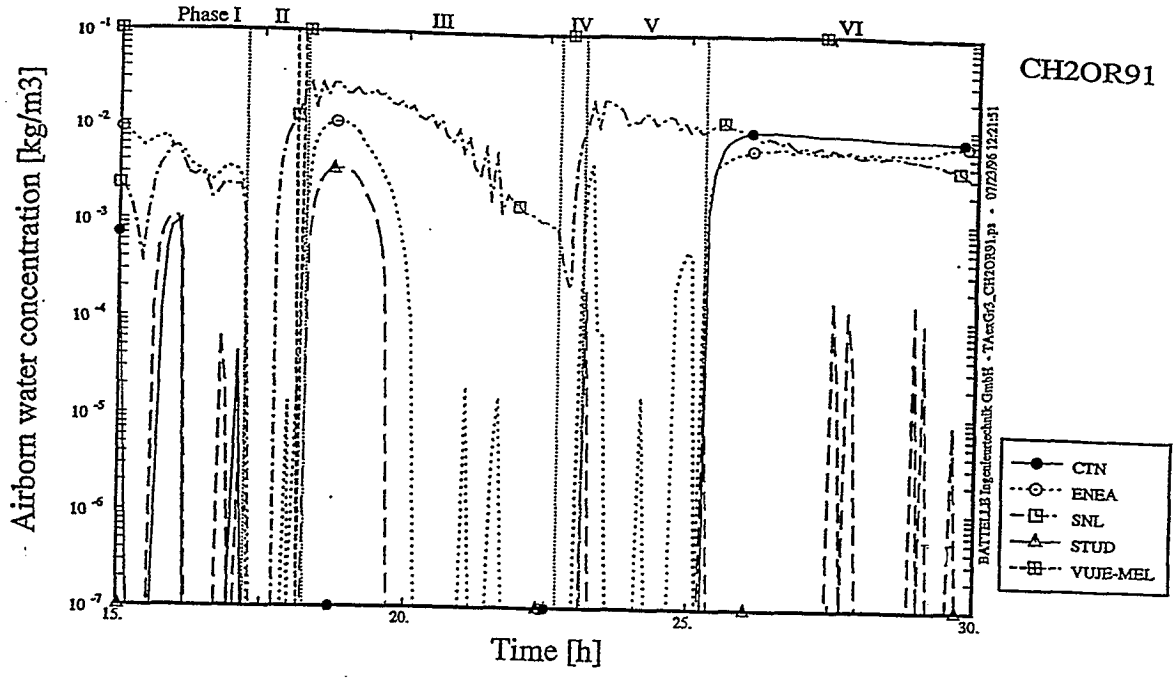

Fig. 4.21b Airborne Water (MELCOR part 1)

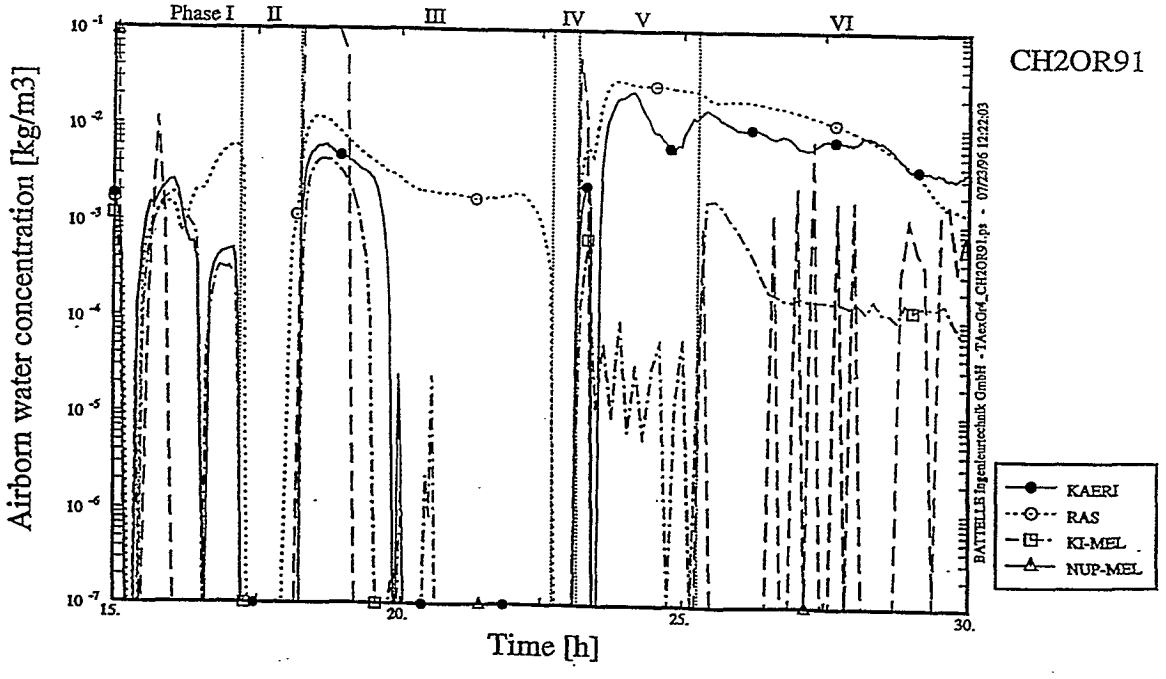

Fig. 4.21c Airborne Water (MELCOR part 2)

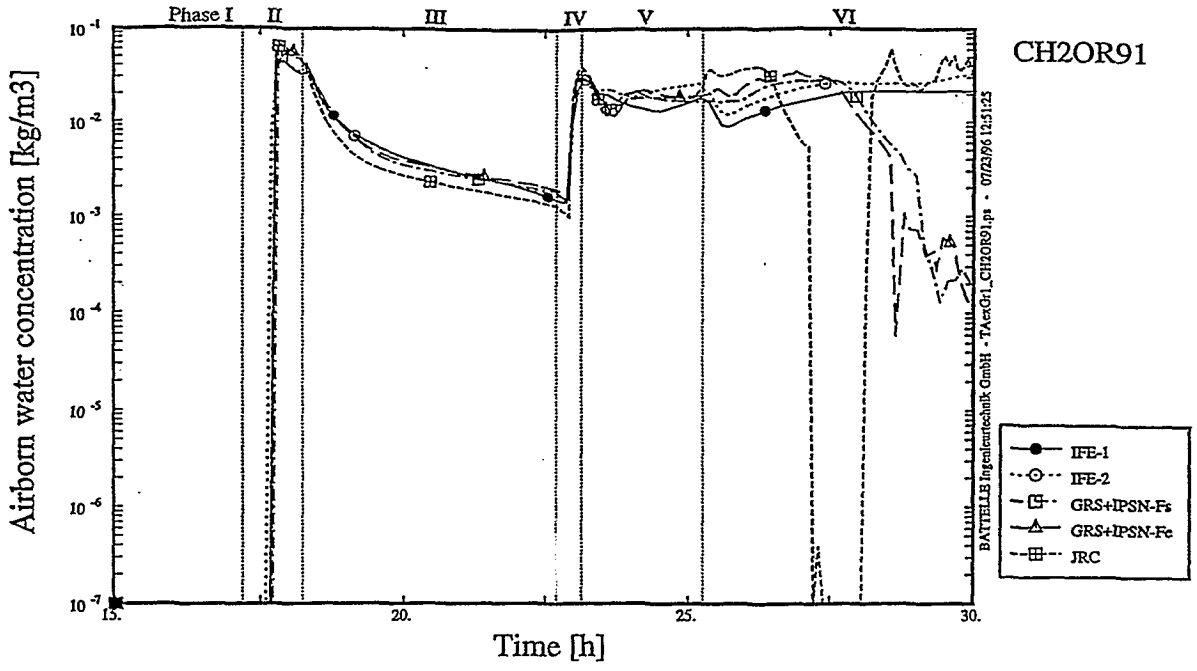

Fig. 4.21d Airborne Water (FIPLOC)

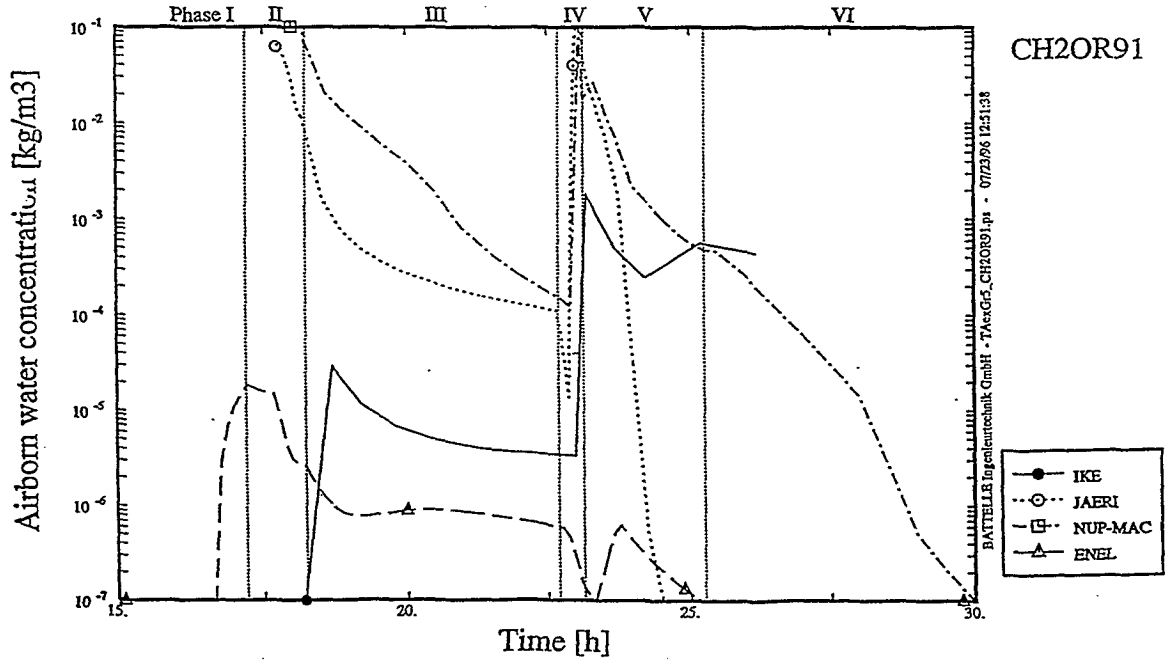

Fig. 4.21e Airborne Water (Stand Alone Codes and ECART)

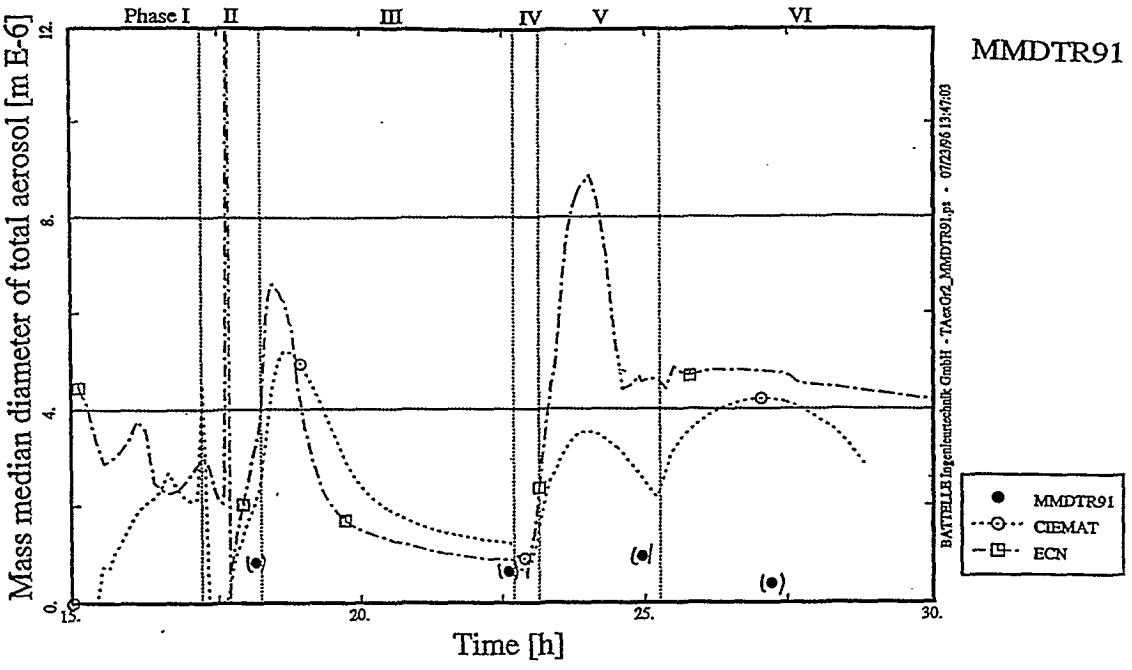

Fig. 4.22a Mass Median Diameter, Dome (CONTAIN)

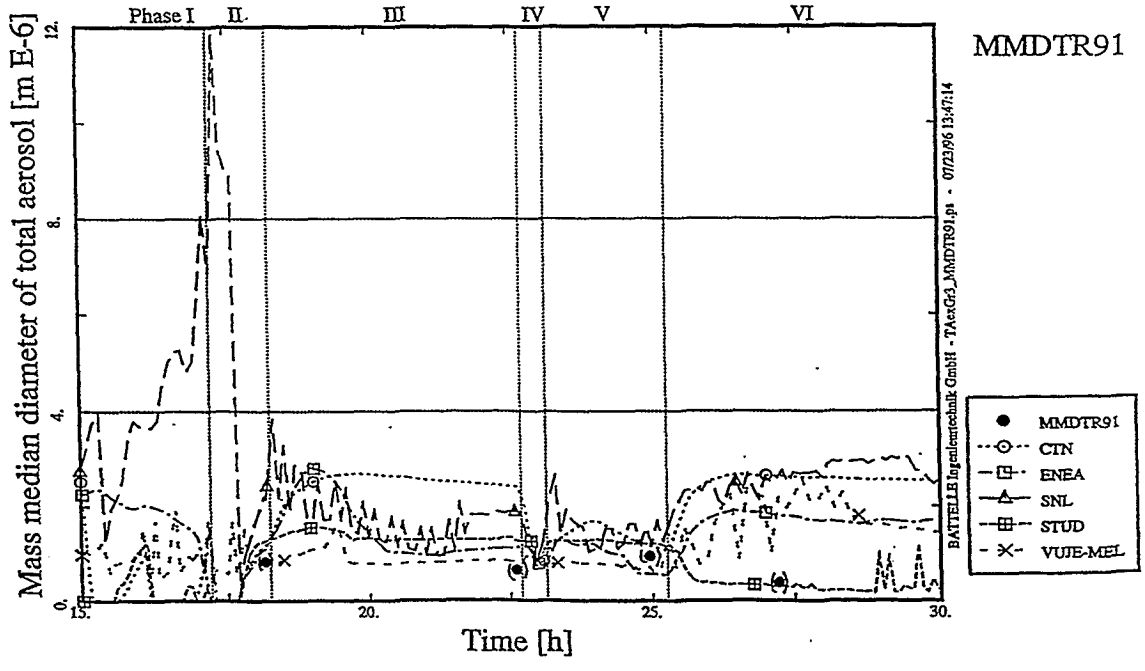

Fig. 4.22b Mass Median Diameter, Dome (MELCOR, part I)

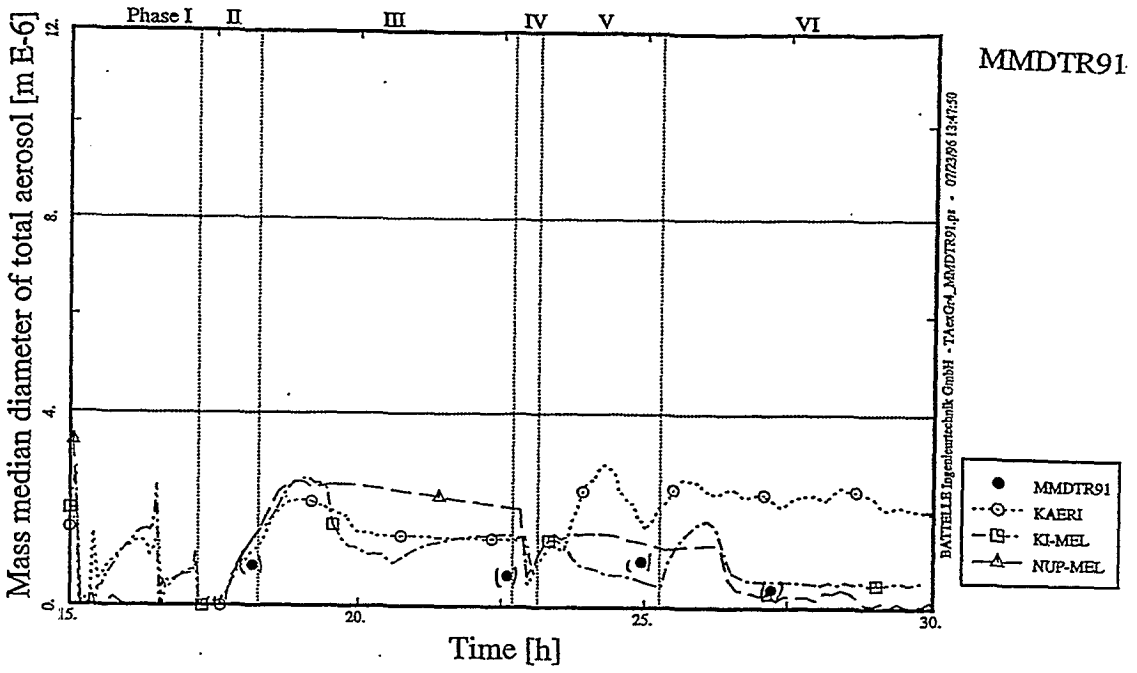

Fig. 4.22c Mass Median Diameter, Dome (MELCOR, part II)

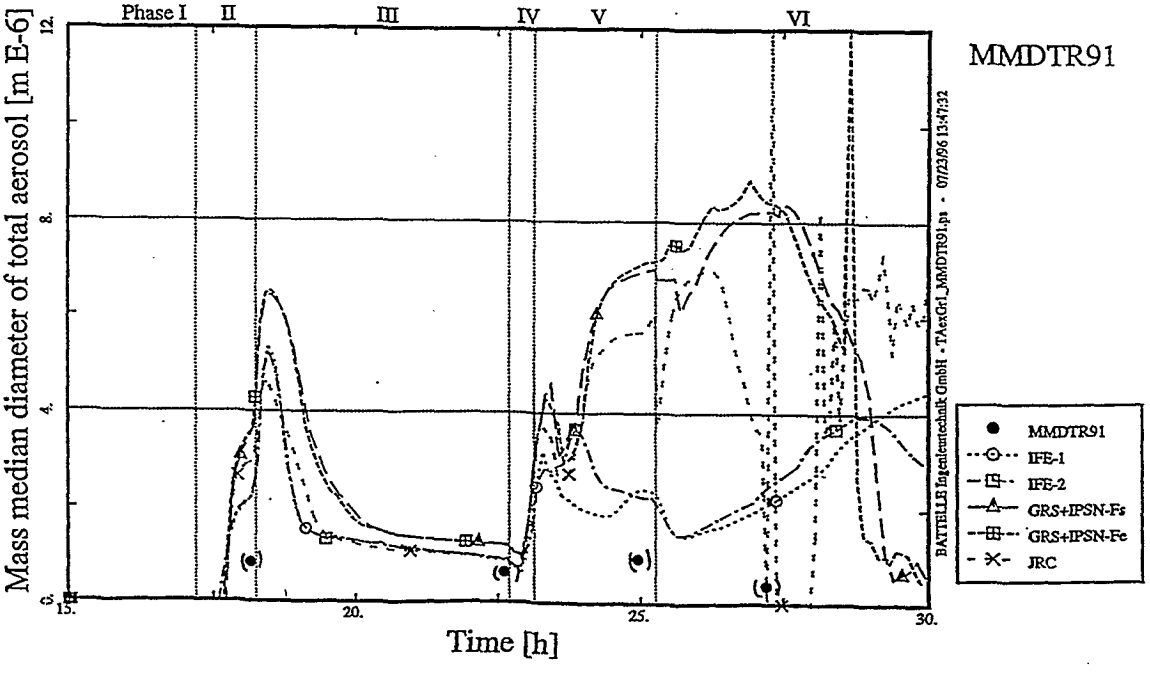

Fig. 4.22d Mass Median Diameter, Dome (FIPLOC)

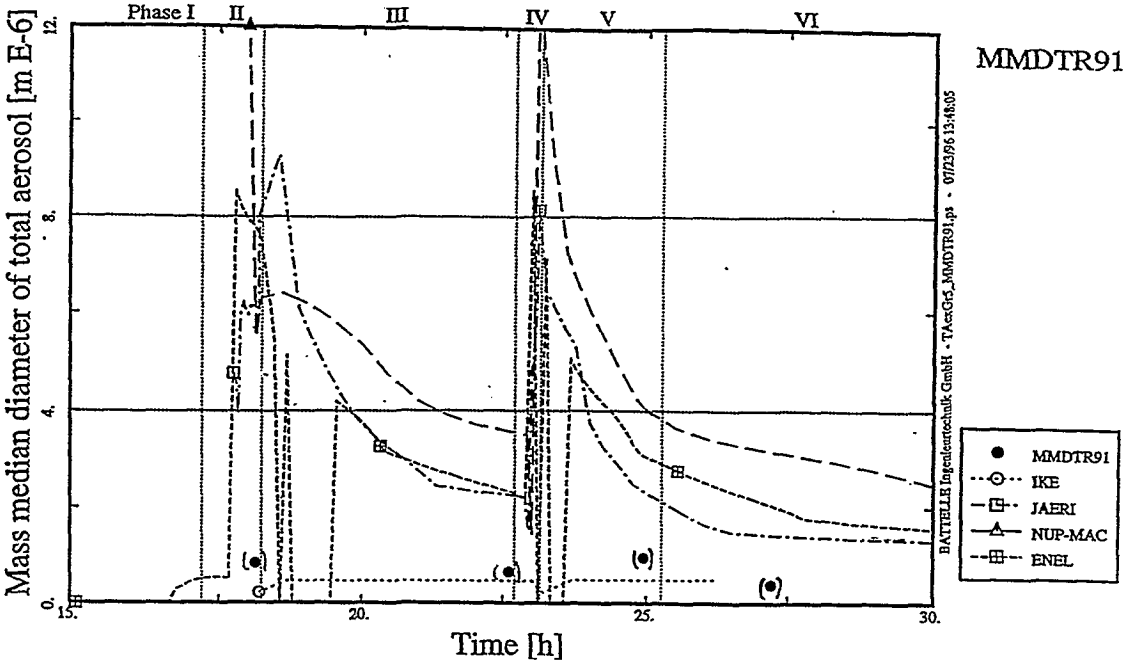

Fig. 4.22e Mass Median Diameter, Dome (Stand Alone Codes and ECART)

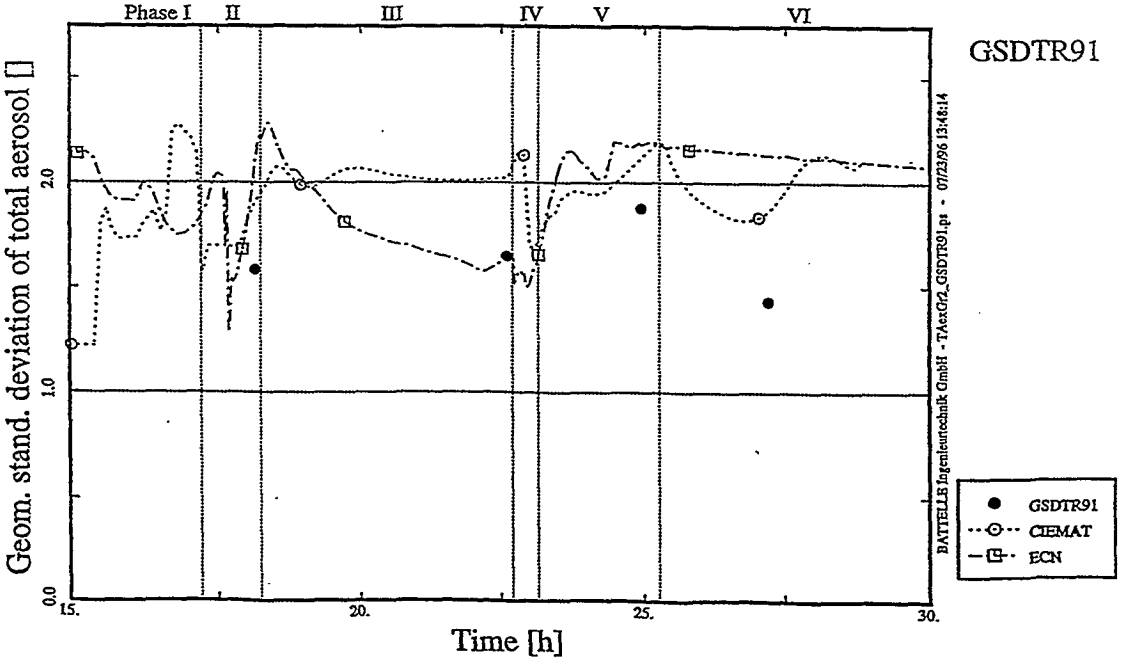

Fig. 4.23a Geometric Standard Deviation, Dome (CONTAIN)

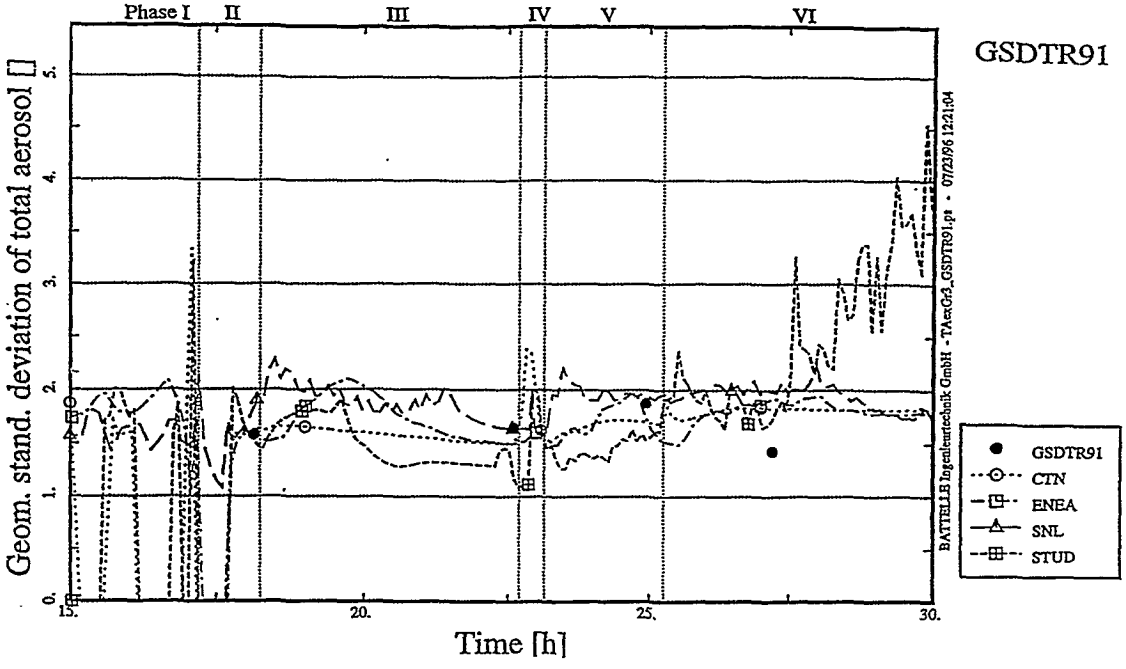

Fig. 4.23b Geometric Standard Deviation, Dome (MELCOR, part I)

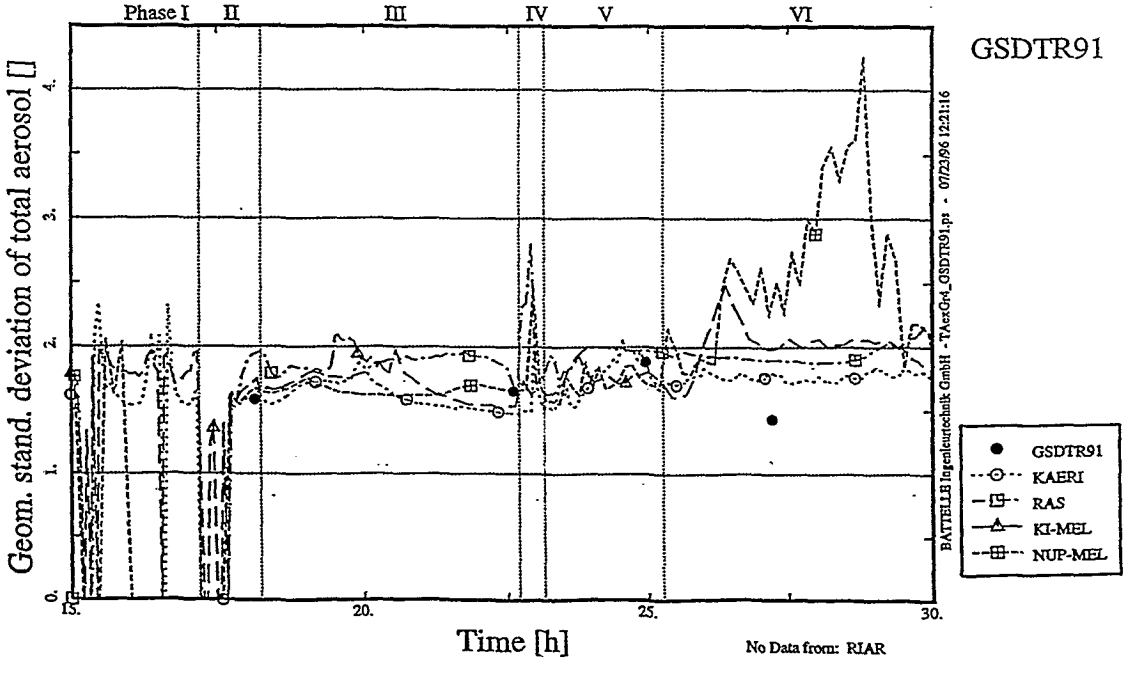

Fig. 4.23c Geometric Standard Deviation, Dome (MELCOR, part II)

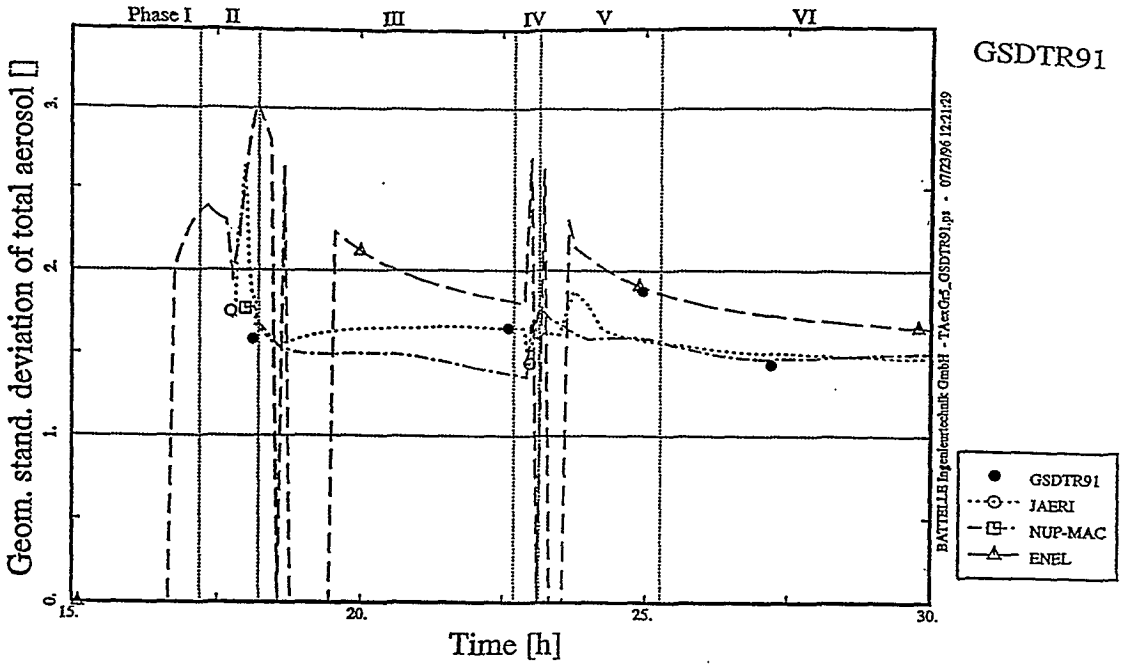

Fig. 4.23d Geometric Standard Deviation, Dome (Stand Alone Codes and ECART)

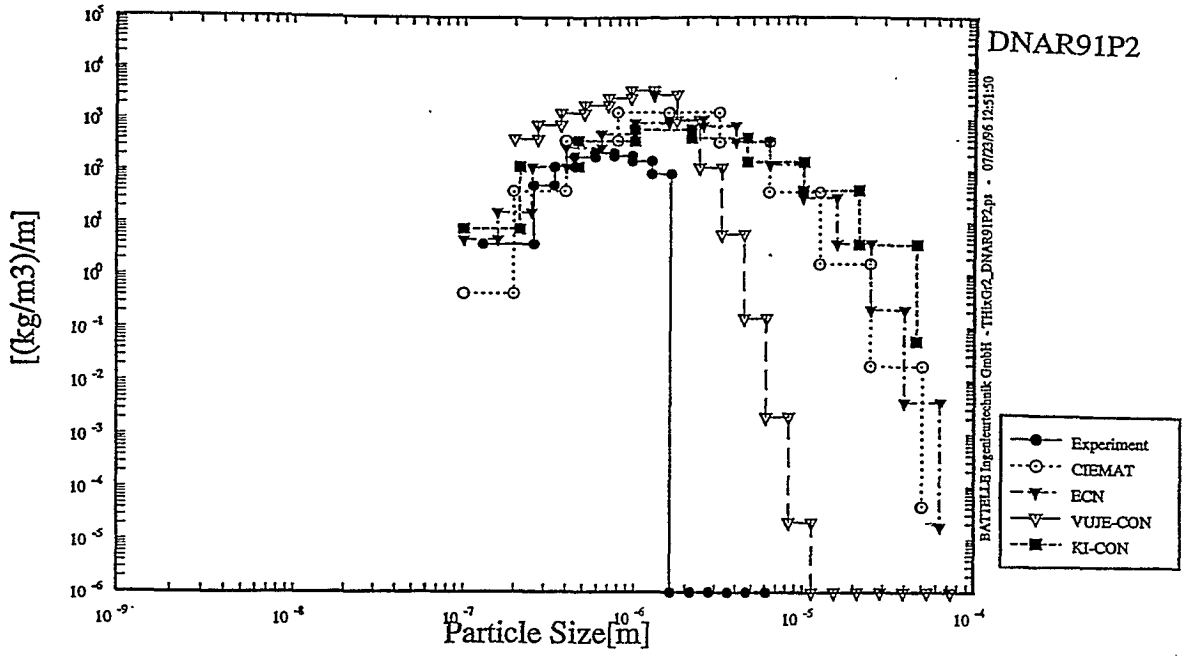

Fig. 4.24a Particle Size Distribution in the Dome at t=18.14 h (CONTAIN)

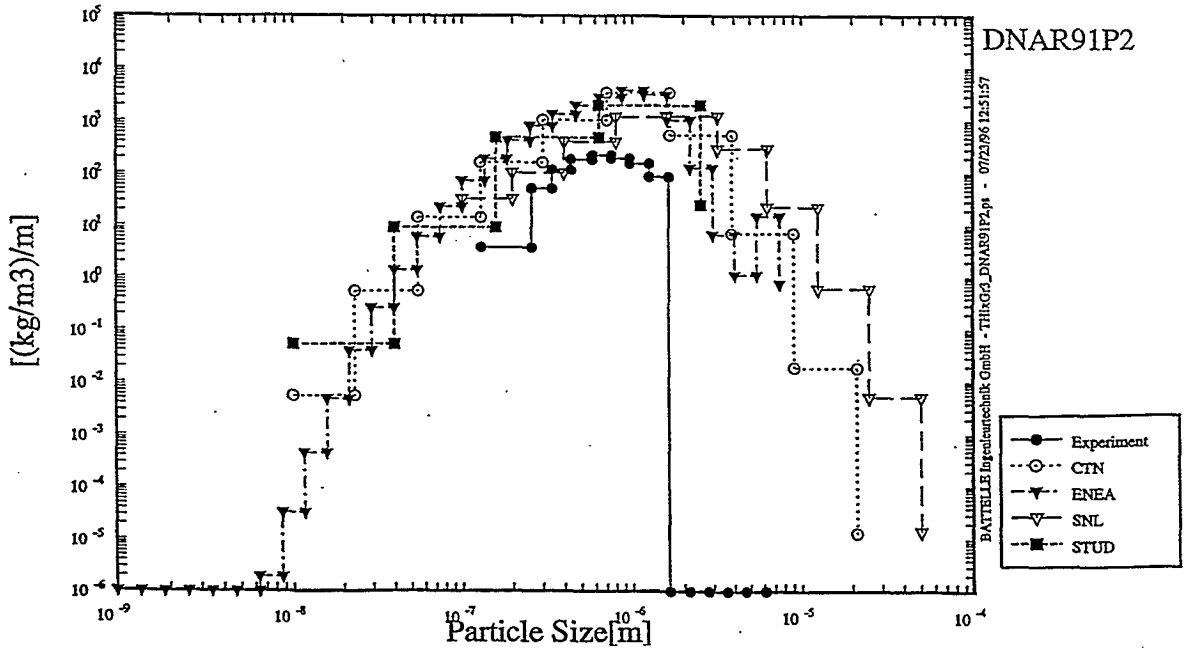

Fig. 4.24b Particle Size Distribution in the Dome at t=18.14 h (MELCOR, part I)

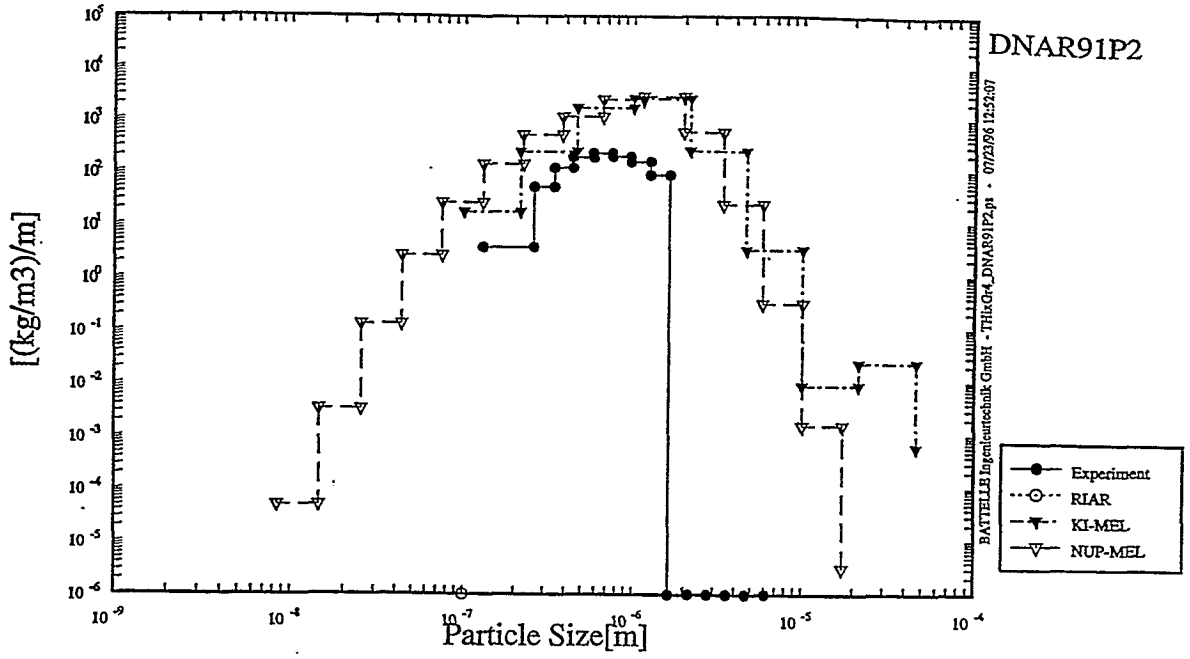

Fig. 4.24c Particle Size Distribution in the Dome at t=18.14 h (MELCOR, part II)

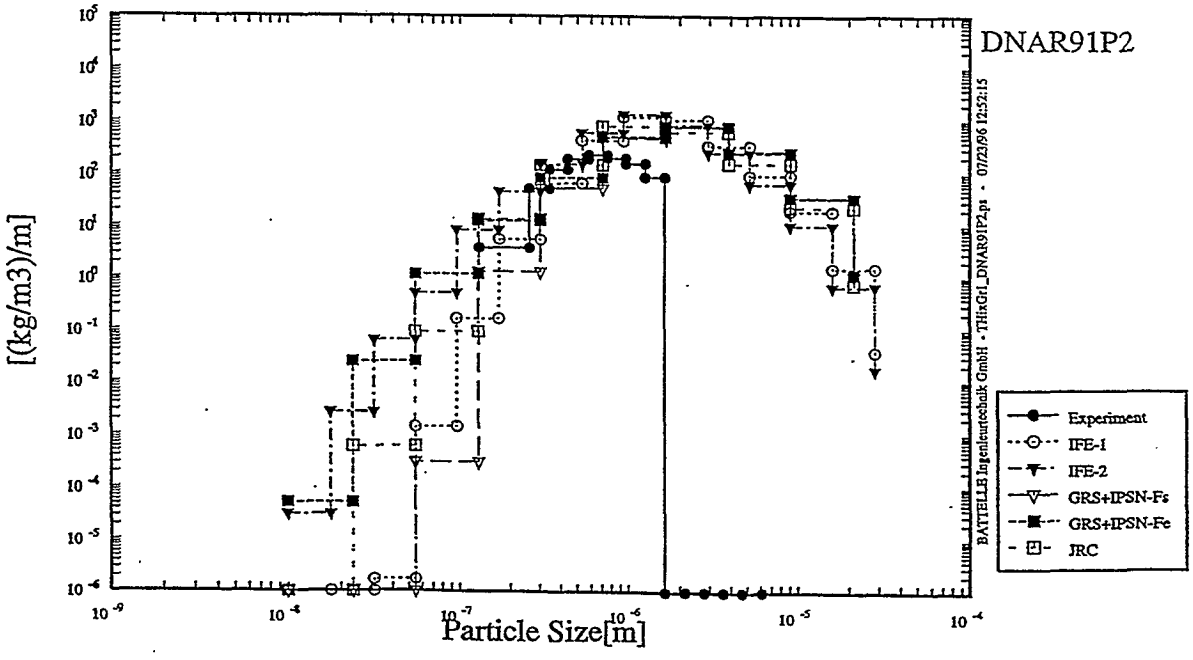

Fig. 4.24d Particle Size Distribution in the Dome at t=18.14 h (FIPLOC)

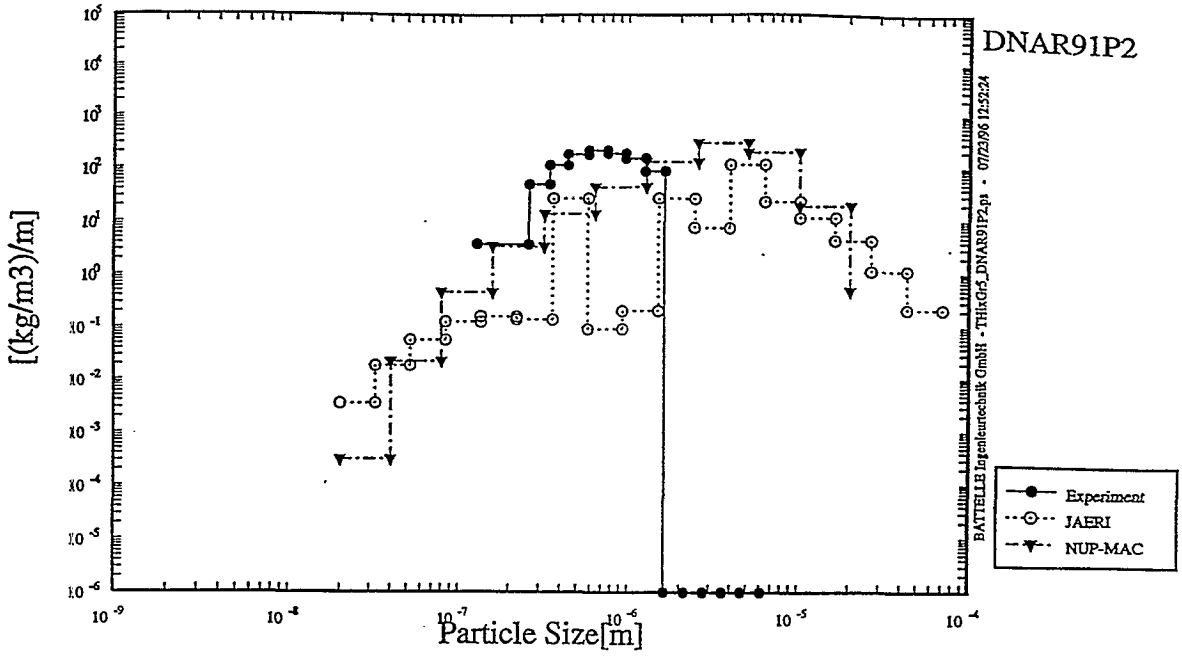

Fig. 4.24e Particle Size Distribution in the Dome at t=18.14 h (Stand Alone Codes)

Gesellschaft für Anlagen- und Reaktorsicherheit (GRS) mbH

Schwertnergasse 1
50667 Köln
Telefon (02 21) 20 68-0
Telefax (02 21) 20 68-888

Forschungsgelände
85748 Garching b. München
Telefon (0 89) 3 20 04-0
Telefax (0 89) 3 20 04-599

Kurfürstendamm 200
10719 Berlin
Telefon (0 30) 88 589-0
Telefax (0 30) 88 589-111

Theodor-Heuss-Straße 4
38122 Braunschweig
Telefon (0531) 80 12-0
Telefax (0531) 80 12-200

ISBN 3-923875-90-8